Gravity Base Foundations for Offshore Wind Turbines

Thesis for the degree MSc. in Civil Engineering

Rutger Koekkoek

Delft University of Technology
Department of Civil Engineering and Geosciences

9 April 2015

TU Delft Delft University of Technology

CFE

Gravity Base Foundations
for
Offshore Wind Turbines

Master Thesis

Author	Rutger Koekkoek
Student number	1354043
E-Mail address	R.T.Koekkoek@student.tudelft.nl
University	Delft University of Technology
Faculty	Civil Engineering and Geosciences
Department	Structural Engineering
Section	Structural and Building Engineering
	Concrete Structures
Assessment committee	
Chairman	Prof.dr.ir. D.A. Hordijk
Supervisors	Dr.ir. C. van der Veen
	Dr.ir. W. Broere
Supervisor CFE Nederland	ing. H. Mortier PMSE
Coordinator	Ir. L.J.M. Houben

Faculty of Civil Engineering and Geosciences
Stevinweg 1
2628 CN Delft

Phone: +31 (0)015-27 89802
Fax: +31 (0)15-27 87966

www.citg.tudelft.nl

CFE Nederland B.V.
Kilkade 2
3316 BC Dordrecht

Phone: +31 (0)78-632 10 20
Fax: +31 (0)78-632 10 55

www.cfe.nl

Abstract

For the last years the energy market share of offshore wind energy is growing rapidly. With the plans from various governments and the European Union[1] to invest in offshore wind energy this trend will continue. The market for offshore wind turbines foundations is currently dominated by monopile (74%) and Gravity Base Foundations (16%) according to 2012 data. From the projects constructed until today it can be seen that the application of Gravity Base Foundations (GBF's) is mainly for shallow water in the Scandinavian region. The current application of GBF's is primarily for water depths ranging from 4 to 15m. Since it is thought that GBF's are having some advantages over other types of foundations it is investigated what the possibilities are for applying GBF's at larger water depths. This is done by investigating the influence of various parameters involving the design of offshore wind turbines such as environmental parameters and construction dimensions.

The input for the calculations for the forces on the turbine and foundation consists of both physical parameters such as tower heights and diameters but also of environmental parameters such as wind speed and wave heights. To be able to input realistic parameters for the environmental conditions an analysis is made for the environmental parameters for several offshore locations in Europe. Since this study is primarily focussing on the foundation of the wind turbine an assumption is made for a standard turbine structure. This standard turbine is based on a Repower 5MW wind turbine and has a height of 87,6m and a rotor diameter of 128m. The reference water depth is set to 25m and is varied from 15 to 35m.

The calculations performed to determine the forces on the foundation are based on the guidelines presented in the Norwegian Code DNV-OS-J101. With the aid of this code a calculation sheet is created which is able to calculate the influence of the variation in various structural and environmental parameters.
In first instance the wind speed and water depth are varied. It is found that the magnitude of the horizontal forces due to wind loads on the turbine structure and wave loads on the foundation are of the same order. Because of the high lever arm of the turbine blades with respect to the foundation base the bending moments on the foundation are dominated, up to 90%, by the wind forces acting on the turbine structure. It is stated that a variation in the wind speed and the tower height are having the largest influence on the bending moments acting on the foundation. Regarding the horizontal forces it is found that an increase of water depth decreases the horizontal forces. This is due to the decrease of the forces acting on the foundation base. The bending moments are still increasing for an increasing water depth due to the high lever arm of the foundation shaft.

Using the design conditions presented in the DNV it is found that the governing load condition is a parked situation with extreme wave heights. For this load combination and a water depth of 25m the governing bending moment in SLS is 177MNm and the governing horizontal force in SLS is 7516kN. With these calculated forces the bending moment capacity for the foundation shaft is calculated. It is found that a reinforcement ratio of $2 \cdot \varnothing 32 - 150$ is sufficient to withstand the occurring bending moment. Also the crack width is limited to $w = 0{,}18mm$ which is sufficient according to the design rules. For the self weight of the turbine and foundation it is found that the mass needed for stability of the foundation is 5951 tonnes.

[1] DIRECTIVE 2009/28/EC OF THE EUROPEAN PARLIAMENT AND OF THE COUNCIL of 23 April 2009 on the promotion of the use of energy from renewable sources

With these forces, dimensions and weights calculated the influence of the foundation subsoil is determined. In first instance the influence of various soil parameters on the bearing capacity is investigated by hand calculations using the formulas of Brinch Hansen. It is concluded that a variation in the angle of internal friction of the sub soil has by far the most influence on the bearing capacity, far more than the specific weight and the cohesion of the soil.

For the hand calculations it is found that the bearing capacity of a normal sand sub soil is not sufficient. Therefore it is investigated what measurements are effective to increase the bearing capacity. Three measurements are investigated: An increase in foundation diameter, an increase in the overburden depth and an increase in the angle of internal friction of the soil. Since the latter option is not possible without changing locations or applying soil improvements the other two options are weighted. It is concluded that an increase of the foundation diameter leads to an increase of the self weight of the foundation. Since the maximum weight of the foundation is a limiting factor for the application of GBF’s it is chosen to apply an overburden depth at the foundation. By applying an overburden depth of 3,1m the bearing capacity will be sufficient. This overburden depth is applied by means of application of skirts.

Besides the bearing capacity of uniform soils also the bearing capacity of multi layered soils in investigated. It is calculated using the geotechnical software Plaxis 3D what the influence is of the presence of a weaker clay layer within a sand soil stratum. It is found that shallow clay layers are strongly influencing the bearing capacity of the soil up to reducing the bearing capacity with 70%. It is found that for shallow clay layers an increase of the clay layer thickness has a larger influence than for deeper situated clay layers. This is explained by the location of the slip circles whether or not it is located within the clay layer.

After the static calculations it is also tried to calculate the influence of weaker clay layers on the bearing capacity for conditions simulating a dynamic behaviour. This is done by setting the soil parameters to undrained and calculating a dynamic load based on a percentage of the ULS bending moment. Although the use of two different software packages and multiple attempts it is not managed to obtain sophisticating results in which clear phenomena’s are observed. Therefore some interesting patterns are observed, but no hard conclusions are made.

To answer the question what the possibilities are for applying GBF’s at larger water depths it is found that for an increasing water depth the increase of the forces on the foundation base is within acceptable proportions. For the design of the foundation the increase of the forces is not leading to large design problems. What could be a limiting factor is the increase of the foundation weight because the number of suitable heavy lifting vessels is limited.
When the bearing capacity of the foundation is regarded it is found that the use of specialized geotechnical software leads to higher bearing capacities than hand calculations for similar soil properties. With these programs it is found that the presence of a weaker clay layer within a stronger sand stratum has a significant influence on the bearing capacity of the foundation. This influence is larger for shallow layers as well as for thicker clay layers.
Regarding the performed variance study and geotechnical study it is concluded that it is technically possible to construct concrete Gravity Base Foundations for larger water depths, but due to the increase of the foundation weight the handling of the foundations and the bearing capacity of the sub soil are the aspects that are determining the applicability to a large extend.

Acknowledgements

I hereby want to greatly thank all the persons who made it possible for me to graduate for my MSc. degree. I know that without their help, advice and patience it would not be possible to present this thesis.

First I want to thank my professor Prof.dr.ir. D.A. Hordijk and first supervisor Dr.ir. C. van der Veen for helping me during my graduation with both substantive issues as guiding and advising me during the preparation of my thesis. I highly appreciate the confidence and patience shown despite of the sometimes slow progression of my graduation.

Furthermore I want to show my sincere appreciation to my second supervisor Dr. Ir. W. Broere for helping me with the geotechnical part of this study. Since this is not my area of expertise I highly appreciate the help with both creating and evaluating the models used in this thesis as well as evaluating the contents of the geotechnical study.

A special word of thanks to H. Mortier who has served as my daily supervisor at the company CFE. I am really grateful for the offered graduation place at the company CFE. I also want to thank him for the endless effort and support he has shown by helping me during my graduation.
My thanks are also for the contractor CFE who gave me the opportunity and facilities to graduate and the employees of this company who have greatly supported me during my graduation period. I specially want to name M. de Graaf for helping me when needed.

I also want to thank R. Foekema from Siemens for providing me with the data for various wind turbines which helped me a lot during this graduation.

Last but of equal importance are the persons around me who supported me unconditionally. Specially my parents and brother who had to suffer of the long duration of my graduation.

All my love goes to my girlfriend Renée who has done everything within her power by supporting me during my graduation period.

Finally, I want to emphasize that my graduation would not have been possible without the support and trust of everybody that helped me both directly and indirect.

- This page is intentionally left blank –

Preface

This master thesis is written as part of the graduation for the MSc. degree in Civil Engineering. This thesis consists of two distinct parts.

In the first part, the variance study it is attempted to investigate the influence of a variation in the design parameters on the resulting forces on a Gravity Base Foundation for offshore wind turbine. It is tried to highlight the governing loadings on the foundation due to structure dimensions and environmental conditions.

The second part, the geotechnical study, aims to investigate the influence of the soil parameters on the bearing conditions of the GBF. Also the influence of weaker layers within a soil stratum is investigated.

These two parts together are aiming to investigate the points of interest for the design of a GBF when it is located at larger water depths where environmental conditions are more severe.

I wish you a pleasant reading of this thesis,

Rutger Koekkoek

- This page is intentionally left blank –

Table of contents

Part 1 – Variance Study

1. Introduction

1.1 Current state of offshore wind turbine foundations

For the last years the energy market share of offshore wind energy is growing rapidly. With the plans from various governments and the European Union[2] to invest in offshore wind energy this trend will continue. When analyzing the offshore wind market of today it can be noticed that it is dominated by monopile founded wind turbines. According to the European Wind Energy Association[3], see the given figures below, the total share in Europe of monopile founded wind turbines is 74% at the end of 2012. As can be seen the share of Gravity Based Foundations (GBF) is only 16% of the total market share. The data for erected foundations in 2012 sketches the same market share for monopile foundations, but a different one for GBF's. An impression of a Gravity Base foundation is placed in the figure besides.

Figure 1, Impression of a GBF

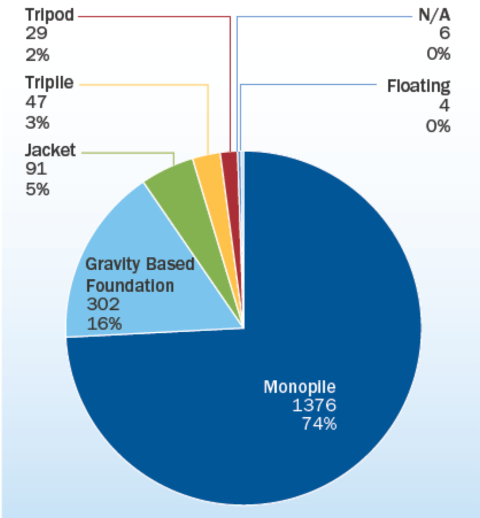

Figure 2, Share of foundations up to 2012

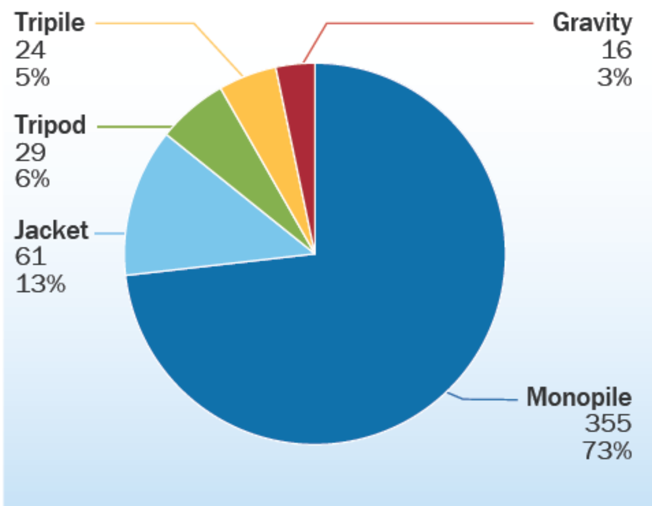

Figure 3, Share of foundations installed in 2012

1.1.1 Share of Gravity Base Foundations

Besides the observation that the Gravity Base Foundation is the second most used foundation type up to 2012 it is also investigated what the current application is for GBF's. According to online statistics projects using GBF's as a foundation are mainly located in the Scandinavian waters. Also the water depth at which the GBF's are applied is limited to 4-15m. This also holds for the GBF presented in the figure above. This GBF is placed at the Rødsand 2 project in Denmark at a water depth of 7,5 to 12,5m.

Until today only one project exists where a GBF is applied at larger depths. The Thornthonbank Wind Farm located in the Belgian part of the North Sea applies GBF's at an average water depth of 25m.

[2] DIRECTIVE 2009/28/EC OF THE EUROPEAN PARLIAMENT AND OF THE COUNCIL of 23 April 2009 on the promotion of the use of energy from renewable sources

[3] The European offshore wind industry -key trends and statistics 2012

1.2 Characteristics monopile foundation

Monopiles are constructed in fabrics and are build up from several steel circular sections welded to one tube. One monopile can have a weight of up to 700 tonnes of steel. With high and varying steel prices the material costs are an important part of the total structure costs. The total construction costs are around €1500 per tonne [4] of monopile foundation.
The questions that rises is why the offshore wind turbine market is dominated by monopile foundations. One of the main reasons for that is that the used monopile technique is derived from the offshore oil and gas industry. In this industry there is a lot of experience with the use of steel tubular foundations. Also the offshore equipment needed for drilling the monopiles into the seabed is widely available. This makes that the monopile foundation is the most obvious solution for the foundation of the wind turbines for today.

Figure 4, An offshore monopile foundation

1.3 Characteristics Gravity Base Foundation

The second most used type of offshore wind turbine foundation up to 2012 is the GBF. The GBF's are usually made of concrete and construction takes place onshore. Construction of the foundations needs a large construction field, for example a harbour where the foundations can be constructed and from where they can be transported to the intended location. Due to the low material costs the construction of the concrete GBF is around €200 per tonne which is cheaper when compared to a steel monopile. Even if the difference in weight is regarded the total construction costs will be lower for a GBF. The GBF's can have a mass up to 3000 tonnes which makes them harder to transport on sea.
The GBF is not as widely used as the monopile, but together with the monopile these two types of foundations cover 90% of the total installed foundation market up to 2012.
One of the reasons why GBF's are not the main foundation for offshore wind turbines is the relatively long construction time and complexity of constructing the foundations. Also the relatively high mass of the structure makes it more difficult to transport. Because of the increasing depth for offshore wind farms the foundation lengths are increasing as well. For the GBF's this means they are getting more heavy and lifting and shipping of the foundations will get more difficult.

1.4 Comparing monopile and GBF foundations

When comparing the two most used foundation types some significant differences can be indicated. Since the GBF is placed on the seabed no drilling or hammering is required. When the soil conditions allow the use of GBF's the soil often only needs some preparation and levelling before the GBF can be lowered on the sea bed. This makes the GBF more suitable for locations with harder subsoil than monopiles. Furthermore the dynamic properties of the GBF are advantageous when compared to those of the monopiles[5]. Because of the greater mass of the GBF the overall stiffness of the structure increases. The concrete structure has a lower natural period and better dynamic performance compared to steel monopiles.
When costs are regarded the GBF's have an advantage compared to steel monopiles. Since the material costs for a steel monopile are much higher than the costs for a concrete GBF the construction costs of GBF's are lower. (Steel: €1500/tonne concrete: €200/tonne). The total costs for a 700 tonnes monopile and a 3000 tonnes GBF then are respectively €1,05mln and €,06mln.

[4] Concrete is the Future for Offshore Foundations - Per Vølund
[5] Concrete Towers for Onshore and Offshore Wind Farms, Concrete Center and Gifford

When installation is regarded monopiles are in advantage over GBF’s. Because of the lower lifting weight and high degree of experience for the offshore monopile foundation the installation costs are lower when compared to GBF’s. This has also to do with the higher risk involved with the placing of GBF’s. Since the placing of heavy GBF is more sensitive to environmental influences such as wind speed and wave height more costs are involved with placing GBF’s.
Also the amount of offshore construction work differs for the two foundation types. For the monopile the construction consist of hammering the pile, placing and grouting the transition piece and connecting the turbine tower. Offshore construction for the GBF only consists of lowering the GBF and connecting the turbine tower. The offshore construction work thus is less for GBF’s than for a monopile foundation. On the other hand if the upper soil layer doesn’t meet the requirements for directly placing the GBF the preparation time needed for the GBF is larger than for the monopiles. The seabed of the location of the GBF’s needs to be dredged to remove the loose upper layer and improved with a foundation layer.
Regarding the application possibilities GBF can be placed on locations with various soil conditions. Only at locations with too soft soils or soils with a risk for liquefaction it is necessary to apply a different kind of foundation.

1.5 Scope of thesis

As indicated the Gravity Base Foundation is the second most applied foundation type for offshore wind turbines although its share is much smaller when compared to the steel monopile foundation. Because it is thought that GBF’s could have some benefits over other types of foundations such as lower costs, less offshore work and a longer life time it is investigated what the possibilities are for applying GBF’s at larger water depths. This is because there is a tendency to place offshore wind turbines further from the coast because of higher wind speeds and less visual impact. This is done by investigating the influence of various parameters involving the design of offshore wind turbines such as environmental parameters and construction dimensions.

2. Purpose and outline of variance study

2.1 Purpose of variance study

When designing an offshore wind turbine foundation the forces acting on the foundation have a large influence on the final design. To gain an insight on the influence of these forces this variance study is executed. With the aid of mathematical programs and a spreadsheet containing the calculations for the foundation the variance in the forces acting on the foundations is explained for different foundation sizes. The foundations examined are placed in three different water depths, being 15, 25 and 35 metres as can be seen in the figure below. The total height of the foundations is 3,5 meter larger than the water depth, because a part of the foundation is above the water level. For the comparability of the different outcomes of the study the turbine size, type and diameter are held constant. In this way only the influence of the difference in the foundation dimension is accounted for.

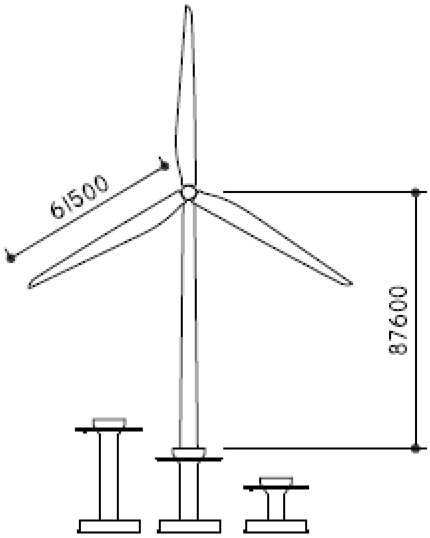

Figure 5, Overview total turbine size

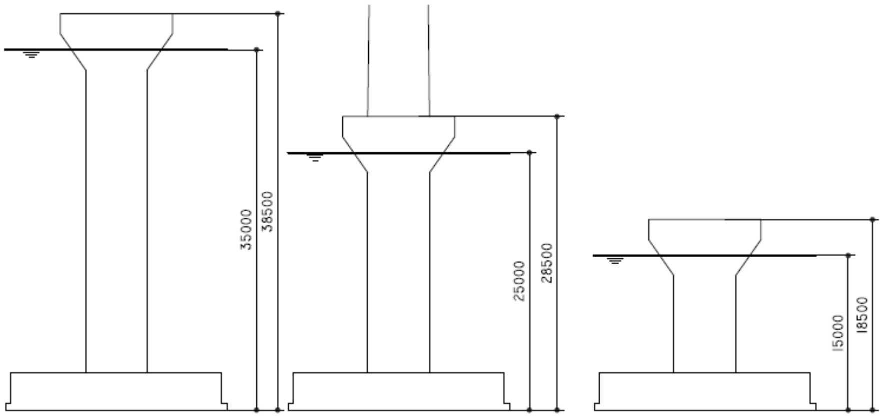

Figure 6, Different foundation heights used in variance study

2.2 Assumptions made

For this project a wind turbine structure is chosen to be representative for the design of the foundation structure. For the forces acting on the foundation use is made of a design turbine based on the Repower 5M turbine. According to documents of the manufacturer[6] and a scientific document of a 5MW reference wind turbine[7] the following data is obtained:

REpower 5 MW design wind turbine

Turbine	
Turbine capacity:	5 MW
Rotor weight	120 tonne
Nacelle weight	290 tonne

[6] REpower 5M Prospekt de - 5m_de

[7] http://offshore-windport.de/fileadmin/downloads/unternehmen/REpower/5m_de.pdf
Definition of a 5-MW Wind Turbine for Offshore System Development.pdf

Blades	
Blade surface	183 m^2
Blade length	61.5 m
Blade maximum thickness	4.1 m
Blade weight	17.74 tonne

Tower	
Length	87.6 m
Tower weight	347.46 tonne
Mass point	38.234 m from bottom
Base diameter and thickness wall	6 m / 0.027 m
Top diameter and thickness wall	3.87 m / 0.019 m

Total weight	657 tonne

Table 1, 5MW design wind turbine parameters

The design of the foundation is based on the standard design often used for a Gravity Base Foundation. It consists of a square or hexagonal base plate with a cylinder from the base plate till the required foundation level. Depending on the environment it can be necessary to place an ice cone to withstand ice loads on the foundation.

Figure 7, Standard design GBF with ice cone

2.3 Design codes and methods used

For the design of the foundations use is made of the codes available for offshore wind turbine design. Since the Norwegian classification society Det Norske Veritas (DNV) has several widely accepted and applied norms on the construction of offshore wind turbine structures these norms are used as a guideline for the design of the wind turbine foundation. These norms state design rules, calculation methods and determination and calculation of environmental loads. The most relevant norms are listed below.

DNV-OS-J101	DESIGN OF OFFSHORE WIND TURBINE STRUCTURES
DNV-OS-C502	OFFSHORE CONCRETE STRUCTURES
DNV-RP-C205	ENVIRONMENTAL CONDITIONS AND ENVIRONMENTAL LOADS
NEN-EN-IEC 61400	WIND TURBINES

Table 2, Used codes and norms for calculations

These norms for offshore wind turbine structures have a high similarity to the IEC61400 norm. On some fields there are differences between the IEC 61400 and the DNV. Sometimes the DNV refers to the IEC 61400 for specific formulas or calculation methods.

For determining the forces on the foundation use is made of a document based on the DNV norms: Guidelines for Design of Wind Turbines by DNV and Risø[8]. In this document design rules and methods are clearly indicated.

[8] Guidelines for Design of Wind Turbines, DNV/Risø, 2nd edition 2004, ISBN 87-550-2870-5

2.4 Approach used

To determine the forces acting on the foundation a depth of 25m is assumed as a basis for the calculations. This depth is held constant and the parameters for wind, waves and other loadings are varied and the resulting forces acting on the foundation are noted. This is also done for a foundation at a lower depth of 15 m, and a higher depth of 35 m. For all these variances in loadings and dimensions of the foundation the results are collected and compared. With the results of these calculations the relations between forces and dimensions are ought to explained and revealed which parameter changes will have a large influence on the forces acting on the structure.

2.5 Limit states and their characteristics

A limit state is a condition beyond which a structure or structural component will no longer satisfy the design requirements[9]. For different situations different requirements hold. For the design of the offshore wind turbine foundation four different limit states are regarded which are listed below. According to DNV-OS-J101:

- Ultimate limit states (ULS)
    - loss of structural resistance (excessive yielding and buckling)
    - failure of components due to brittle fracture
    - loss of static equilibrium of the structure, or of a part of the structure, considered as a rigid body, e.g. overturning or capsizing
    - failure of critical components of the structure caused by exceeding the ultimate resistance (which in some cases is reduced due to repetitive loading) or the ultimate deformation of the components
    - transformation of the structure into a mechanism (collapse or excessive deformation).

Fatigue limit states (FLS)
- cumulative damage due to repeated loads.

Accidental limit states (ALS)
- accidental conditions such as structural damage caused by accidental loads and resistance of damaged structures.

Serviceability limit states (SLS)
- deflections that may alter the effect of the acting forces
- deformations that may change the distribution of loads between supported rigid objects and the supporting structure
- excessive vibrations producing discomfort or affecting non-structural components
- motions that exceed the limitation of equipment
- differential settlements of foundations soils causing intolerable tilt of the wind turbine
- temperature-induced deformations.

[9] DNV-OS-J101 Section 2 Item D101

3. Calculation of wind forces

3.1 Determination wind parameters

To determine the wind forces acting on the turbine structure first the wind parameters need to be defined. The wind climate for normal wind conditions is represented by the 10-minute mean wind speed U_{10} at 10m height and the standard deviation of the wind speed σ_U. The wind speed is often characterised by a recurrence period of either 1 or 50 years.

3.2 Frøja offshore wind speed profile

The wind speed offshore is not constant over the height. Because of the resistance and roughness of the sea the wind speed close to the water level is lower than the speed at greater heights. For determination of the offshore wind speed profile the DNV norm advises to use the Frøja offshore wind speed profile.

For extreme mean wind speeds corresponding to specified return periods in excess of approximately 50 years, the Frøja expression can be used for conversion of the one-hour mean wind speed U at height h above sea level to the mean wind speed U with averaging period T at height z above sea level. The formula for the Frøja wind speed presented by the DNV-RP-C205 is:

$$U(T,z) = U_0 \cdot \left\{1 + C \cdot \ln\frac{z}{H}\right\} \cdot \left\{1 - 0.41 \cdot I_u(z) \cdot \ln\frac{T}{T_0}\right\}$$

where $H = 10\text{m},\ T_0 = 1\text{h},\ T < T_0$

$$C = 5.73 \cdot 10^{-2}\sqrt{1 + 0.148U_0}$$

$U_0 =$ One hour mean reference wind speed at 10 m height with a recurrence period of 50 years

and

$$I_u = 0.06 \cdot (1 + 0.043U_0) \cdot \left(\frac{z}{H}\right)^{-0.22}$$

This formula for the Frøja wind speed is calibrated for use for Norwegian sea and North Sea locations and thus should only be used for these locations.

Because the wind speed used for the Frøja wind speed profile has a recurrence period of 50 years this model is usable for the conversion of extreme mean wind speeds from an hourly value to a value with a shorter period.

For a location with an average wind speed of 7,04m/s at 10m height the wind speed profile according to the Frøja calculations will look like:

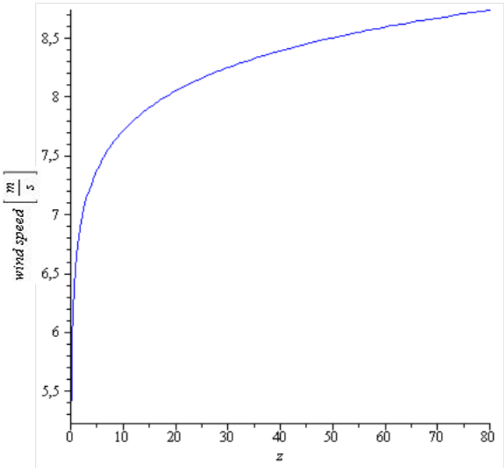

Figure 8, Frøja wind profile for U=7,04m/s

Another method for determination of the wind speed profile is to use the normal wind profile model (NWP) as stated in IEC61400-3 and DNV-OS-J101. This profile is described by

$$V(z) = V_{hub}\left(\frac{z}{z_{hub}}\right)^{\alpha}$$

with the power law exponent $\alpha = 0.14$ for offshore locations

Compared to the Frøja method this normal wind profile method results in higher wind speeds at larger heights for a low average wind speed at 10m height. . For higher average wind speeds the Frøja method results in higher wind speeds at larger heights.
A comparison of the Frøja and normal wind profile model for a low wind speed of 7.04m/s and a high wind speed of 30m/s at 10 m height is presented in the figures below.

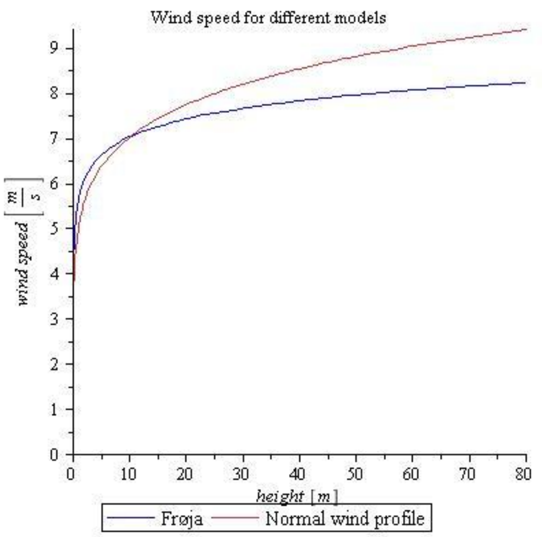

Figure 9, Comparison Frøja and Normal wind profile for low average wind speeds

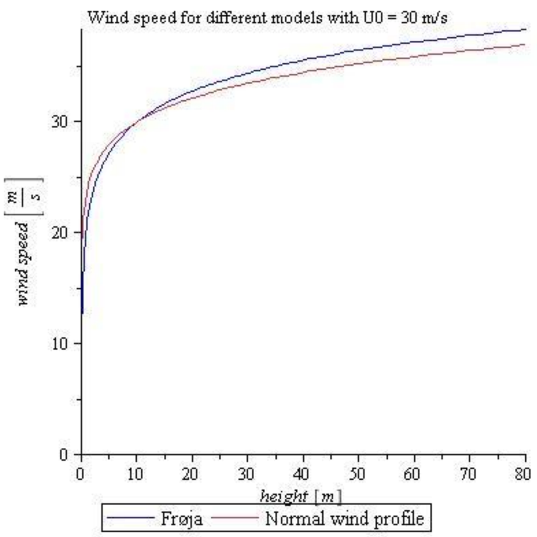

Figure 10, Comparison Frøja and Normal wind profile for high average wind speed

3.3 Wind models and calculation prescriptions

When the wind forces are regarded several wind models are investigated. These models are used for the different load combinations prescribed by the DNV-OS-J101. The models are representing a specific wind state or wind activity and are used for evaluating the forces during different design situations. Some models only apply on the RNA (Rotor Nacelle Assembly) and not or less on the foundation. The design conditions that are prescribed by the DNV are discussed further in this study. For wind conditions the following models and wind events are regarded according to DNV:

Normal wind profile (NWP)
Normal turbulence model (NTM)
Extreme wind speed model (EWM)
Extreme operating gust (EOG)
Extreme turbulence model (ETM)
Extreme direction change (EDC)
Extreme coherent gust with direction change (ECD)
Extreme wind shear model (EWS)
Reduced wind speed model (RWM)

A description and associated formulas for the listed wind profiles and models is placed in the appendix of this document.

4. Calculation of wave forces,

4.1 Determination of wave parameters

The wave climate is represented by the significant wave height H_s and the spectral peak period T_p. In the short term, i.e. over a 3-hour or 6-hour period, stationary wave conditions with constant H_s and constant T_p are assumed to prevail. The significant wave height H_s is defined as four times the standard deviation of the sea elevation process. The significant wave height is a measure of the intensity of the wave climate as well as of the variability in the arbitrary wave heights. Next to the significant wave height the wave climate is also described by the extreme wave conditions. For the extreme conditions the extreme significant wave height and an associated wave period is determined. The extreme significant wave height is determined with a return period of 1 or 50 years. Between the wave height and the wave period a positive relation holds: for larger wave heights the wave period becomes also larger. This relation is further discussed by the variation of the wave parameters.
A sea state is defined by a significant wave height and its wave period. But real wave behaviour is not described by one wave and period. Site specific densities of the sea elevation process can be determined from available wave data. For modelling the site specific spectral densities of the sea elevation process the JONSWAP (Joint North Sea Wave Project) spectrum can be used which is described in the appendix.

4.2 Wave models and calculation prescriptions

As for the wind loadings the DNV norm also describes different wave models. All the models below are describing different situations that could occur during the lifetime of an offshore wind turbine. A description of the different states and formulas is placed in the appendix.

Normal sea state (NSS)
Normal wave height (NWH)
Severe sea state (SSS)
Severe wave height (SWH)

Extreme sea state (ESS)
Extreme wave height (EWH)
Reduced wave height (RWH)

4.3 Calculation of current loading

When detailed field measurements are not available, the variation in current velocity with depth may be taken as: $v(z) = v_{tide}(z) + v_{wind}(z)$ where

$v_{tide}(z) = v_{tide0}\left(\frac{h+z}{h}\right)^{1/7}$ for $z \leq 0$ and $v_{wind}(z) = v_{wind0}\left(\frac{h_0+z}{h_0}\right)$ for $-h_0 \leq z \leq 0$ in which

$v(z)$ = total current velocity at level z
z = distance from still water level, positive upwards
v_{tide0} = tidal current at still water level
v_{wind0} = wind-generated current at still water level
h = water depth from still water level (taken as positive)
h_0 = reference depth for wind-generated current; $h_0 = 50\ m$

Unless data indicate otherwise, the wind-generated current at still water level may be estimated as: $v_{wind0} = 0,01 \cdot U_0$ where U_0 is the 1-hour mean wind speed at 10m height.

5. Turbine properties for Siemens wind turbines

From the Siemens engineer R. Foekema the following parameters and resulting moments of three types Siemens wind turbines are obtained. For the three turbines resulting moments on the tower-foundation interface are given for different tower heights and extreme wind speeds. The data obtained from Siemens is used to validate the calculations for the forces on the turbine structure.

Type	Interface hub height	Extreme mean wind speed	Moment interface	Moment torsion interface
2.3-93	64m	41m/s	111.000kNm (ULS), 17.000kNm (FLS, m=3,5, N=1^{e}7)	6.200kNm
3.0-113	80m	31m/s	78.000kNm (ULS), 14.000kNm (FLS, m=3,5, N=1^{e}7)	8.000kNm
6.0-154	90m	43m/s	200.000kNm (ULS), 40.000kNm (FLS, m=3,5, N=1^{e}7)	25.000kNm

Table 3, Turbine properties for three types Siemens wind turbines

For the dimensions and other properties of a 5MW wind turbine use is made of a document about a RePower 5MW wind turbine as mentioned before. Some parameters from this document are listed below. In combination with the data obtained from Siemens these parameters are used for further calculations of the forces acting on the offshore wind turbine.

Normative capacity	5,0 MW
Cut-in wind speed	3,5 m/s
Normative power wind speed	13 m/s
Cut-off wind speed	30 m/s Offshore 25 m/s Onshore
Diameter rotor	126 m
Speed range normal operation	6,9 – 12,1 rotations/min
Rotor mass	120 t
Nacelle mass (excluding rotor)	290 t
Length wing	61.5 m
Area wing	183 m2

Table 4, Parameters used for validation Siemens data

5.1 Calculations for tower loadings, determine dimensions of turbine and tower

With the calculation methods and guidelines presented in the DNV norm a calculation sheetsis build which calculates the bending moment for a wind turbine. This sheet is added in the appendix. To check the validity of this calculation sheet it is tried to reproduce the bending moments received from Siemens.

For the bending moment calculation the turbine structure is split up in three parts: the blades, the nacelle and the tower. For all these parts the effective bending moment is calculated.

For the calculation of the environmental loads use is made of a gust factor provided by the DNV. This gust factor incorporates high wind gusts with a duration of 3 seconds. The gust factor for the mean winds speed is 1,2 according to DNV. Also an ULS environmental load factor is used with a value of 1,35 which is also provided by the DNV-OS-J101.

The calculation for the basic wind pressure can be done with the following formula presented by the DNV-RP-C205: $q = \frac{1}{2}\rho_a U_{T,z}^2$ where ρ_a is the density of the air and $U_{T,z}^2$ is the wind speed.

The blade surface for the three different turbine types is calculated with the aid of the known blade surface of the Repower 5WM turbine. The surface is linearly extrapolated to the blade length of the turbine types. This gives a surface of :

$$\frac{\frac{93}{2}\cdot 183}{61,5} = 138,4m^2 \text{ per blade for 2,3 MW turbine}$$

$$\frac{\frac{133}{2}\cdot 183}{61,5} = 168,1m^2 \text{ per blade for 3,0 MW turbine}$$

$$\frac{\frac{154}{2}\cdot 183}{61,5} = 229,1m^2 \text{ per blade for 6,0 MW turbine}$$

To calculate the surface of the tower structure an integral is solved over the height of the turbine. This integral is:

$\int_0^h 3,87 + \frac{2,13}{H_{tower}} \cdot hdz$ where h is the height of the tower and $3,87$ is the top tower diameter and $3,87 + 2,13 = 6m$ is the bottom tower diameter.

This gives an tower surface for the three turbines of:

$$H_{tower} = 64m, A = 315,8m^2 \text{ for 2,3MW turbine}$$

$$H_{tower} = 80m, A = 394,8m^2 \text{ for 3,0MW turbine}$$

$$H_{tower} = 90m, A = 444,2m^2 \text{ for 6,0MW turbine}$$

5.1.1 Validation for the effective moments on the foundation for Siemens wind turbines

With the determined dimensions of the turbine and the calculation sheet created before the effective moments on the interface between the tower and foundation are calculated. The calculations are split up in three parts, namely the rotor, the nacelle and the tower. The exact calculation of the forces is placed in the appendix. The results of the calculation are discussed in the next paragraph.

5.2 Comparison calculated values and values given by Siemens

When the results of the calculations are compared with the values obtained from Siemens some differences can be remarked:

Type	Calculated moment [kNm]	Given moment [kNm]	Calculated / Given
2,3-93 2,3 MW	79.099	111.000	71,3%
3,0-113 3 MW	68.650	78.000	88,0%
6,0-154 6 MW	191.652	200.000	95,8%

Table 5, Comparison calculated moments and given moments by Siemens

When the results of the calculations are compared with the forces obtained from Siemens it can be noticed that there are some significant differences. The first turbine type has a difference of almost 30%. This is not within an acceptable range. The second turbine type has a difference of 12% with the given value which is significantly smaller than the 30% from the first turbine type. The largest turbine type has the smallest difference of only 4,2%. This is close enough to the given value to be acceptable, also when it is mentioned that the reference turbine is a 5MW model which is close to the 6MW of the evaluated model. With the increase of the rotor diameter the difference between the calculated moments and the moments given decreases. An explanation for this can be that for smaller rotor diameters other forces have more influence on the total moment than is accounted for. A second explanation can be that the linear interpolation for the rotor diameters is not correct.

6. Environmental properties

For calculating the forces acting on an offshore wind turbine structure it is investigated what environmental conditions are governing at offshore locations in different areas of the North-West European seas. When it comes to the loading of the turbine structure and the foundation the parameters of most importance for this variance study are:

- Mean wind speed
- Extreme wind speed
- Maximum significant wave height and corresponding wave period
- Current speed
- Minimum and maximum water level
- Sea ice

A detailed overview with related notations of the environmental parameters is placed in the appendix.

6.1 Location specific environmental parameters

To investigate the environmental parameters for different locations in North - West Europe the major parameters discussed before are listed. This is done for various locations where wind farms are constructed and areas where new wind farms are planned.

The locations for which the environmental parameters are investigated are:
1) Baltic sea
2) German and Danish part of North sea
3) Dutch part of North sea
4) English part of North sea
5) English channel
6) Celtic sea

In the map presented below the six offshore locations are indicated.

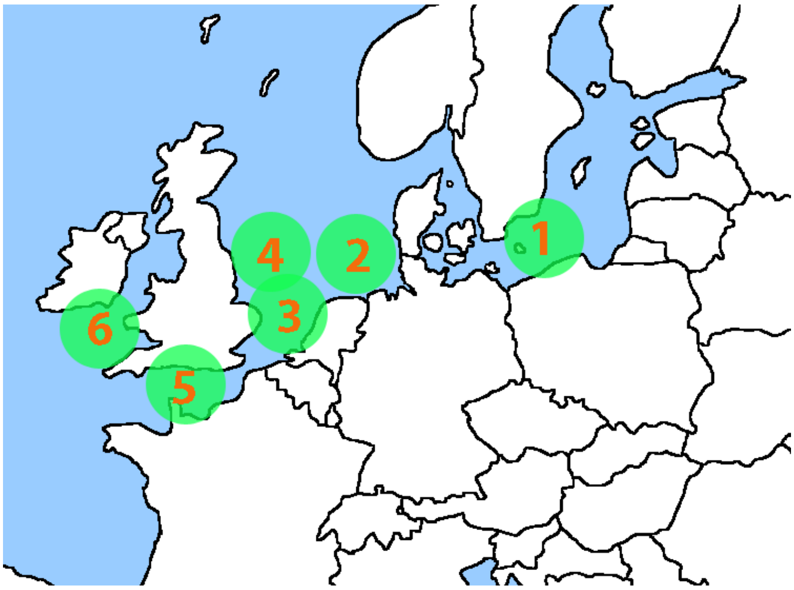

Figure 11, Locations for environmental parameter investigation

For these 6 locations the major environmental parameters are investigated. An overview of the major parameters for the various locations is given in the following table.

	Baltic sea	North sea DE/DK	North sea Netherlands	North sea England	English channel	Celtic sea
	1	2	3	4	5	6
Mean wind speed [m/s]	8,8 (at 80 m)	9,5 (at 10 m)	7 – 9 (at 10 m)	9,1 – 9,5 (at 100m)	9,1 – 10 (at 100m)	9,6 – 10 (at 100 m)
Maximum wind speed [m/s]	37,5 (at 80 m)	26,7 (at 70 m)	31,1 (at 78,8 m)			31 (1h mean) (at 103m)
Maximum significant wave height [m]	5,2	7,4	7 m	5,9	8	10
Icing [Y/N]	Yes	No	No	No	No	No

Table 6, Environmental data for various locations

As can be seen in the table given above there are various differences in wind speed and maximum significant wave height between different locations. Especially the wave height shows remarkable differences between the locations.

For two locations detailed information is available. These are the projects Kriegers Flak in the Baltic sea and Horns Rev in the German part of the North sea. For these locations extended environmental parameter studies are performed and are public accessible. The datasheets for these projects can be reviewed in the appendix.

7. Cyclic loading and fatigue

Because wind turbines are subjected to cyclic loads it should be verified that the first natural frequency of the tower does not coincide with the rotor frequency and blade-passing frequencies, i.e. the 1P and 3P frequencies respectively. The 1P and 3P frequencies are visible in the figure below for a soft-stiff response (black line) and stiff-stiff response (grey line). If it is confirmed that the tower frequency is kept outside the ranges defined as the rotor frequency (+-10%) and the blade passing frequency (+- 10%), respectively, there normally will be no problems due to load amplification arising from vibrations at or near the natural frequency[10].

Special attention should be given to variable-speed turbines, in which cases the turbine should not be allowed to operate in a frequency interval defined as the eigenfrequency of the tower (+-10%). For this project the dynamic behaviour of the structure itself is out of scope, but the influence of the dynamic loads on the subsoil of the turbine foundation is evaluated in the second part of this document. More information about the fatigue loading on wind turbines and guidelines presented by DNV/Risø can be found in the appendix.

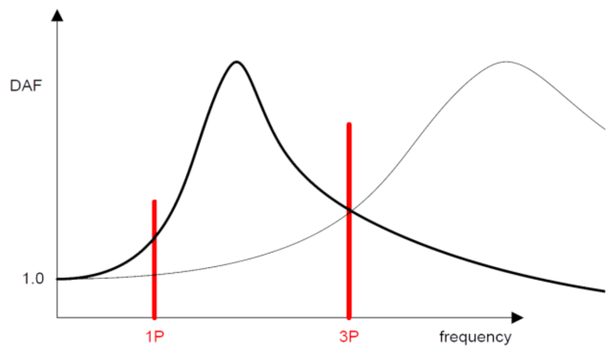

Figure 12, 1P and 3P frequencies for different responses

The data of the turbines provided by Siemens also contains information on the fatigue loading of the turbine. The fatigue data provided by Siemens is summarized in the table beside. The complete table is presented before.

Turbine size	Moment interface
2,3 MW ø93m	17.000kNm, m=3,5, N=1e7
3,0 MW ø113m	14.000kNm, m=3,5, N=1e7
6,0 MW ø154m	40.000kNm, m=3,5, N=1e7

Table 7, Fatigue loading for various turbine types, data presented by Siemens

Modelling all the different load conditions prescribed for a dynamic load analysis is a laborious and time consuming process. Therefore for this study use is made of the known fatigue loadings and load cycles as shown in the table above. It is assumed that the ratio between the maximum bending moment and the fatigue moment from the given data can be used to determine the fatigue loading for other configurations. The ratios for the data given by Siemens are displayed in the following table.

Turbine	Bending moment	Fatigue moment	Ratio
2,3 MW	111.000 kNm	17.000 kNm	0,15 [-]
3,0 MW	78.000 kNm	14.000 kNm	0,18 [-]
6,0 MW	200.000 kNm	40.000 kNm	0,20 [-]

Table 8, Ratios between bending moment and fatigue moment for given data

As can be seen in the table the ratio increases for an increasing turbine size and hub height. Therefore it can be assumed that the turbine size and thus the hub height are positively related to the fatigue loading. What should be remarked for the table above is that the bending moments are determined at interface level and not at foundation base level. The latter turbine from the table above has the most similarity, when turbine height and diameter are regarded, with the 5MW design turbine as described before. Therefore the ratio of 0,20 between the extreme bending moment and the fatigue moment is also found applicable for the 5MW design turbine.

[10] Guidelines for Design of Wind Turbines – DNV/Risø P71

8. Accidental loading

For the accidental loading on offshore structures the DNV-OS-A101 is regarded. This norm entitled Safety Principles and Arrangements contains a paragraph over collision loads.
When accidental loading is concerned the major accidental loading to be regarded is a ship collision. There is a chance that a ship gets out of control at sea and floats towards an offshore wind turbine. Assumed is that the ship has a drift velocity of $2m/s$ [11] [12]. This assumption is based on the speed drafting ships will have. Here no account is taken for ships colliding on full speed, this is done because the wind farms will not be on the shipping routes but besides them.
The expression to calculate the collision forces according to the paper Ship Impacts: Bow Collisions are used to calculate the collision forces for vessels between 500 DWT (Deadweight Tonnage) and 300.000 DWT. The exact expression and calculations are placed in the appendix.

Figure 13, 270.000 DWT vessel Maersk Hayama

For a large vessel with a Deadweight Tonnage of 270.000 tonne and a length of 330m (see figure above) the following collision forces are calculated:

using:

$m_x = 312.384$ tonnes

$V_0 = 2m/s$

$L_{pp} = 330m$

The calculation for P_{bow} becomes:

$$P_{bow} = 2,24 \cdot P_0 [\bar{E}_{imp} \bar{L}]^{0,5} = 341MN$$

The force of the ship collision is exerted on the foundation. Depending on the shape of the ship and the presence of an ice cone the force is exerted around the water level. As can be seen from the calculation the bow force is immense. Therefore it may be concluded that the foundation of the wind turbine cannot withstand the collision force of such a large ship.

[11] DNV-OS-A101
[12] Ship impacts: Bow collisions, P. Pedersen, S. Valsgard, D Olsen and S. Spangenberg, 10-1992

9. Calculation outcomes for parameter variance

9.1 Outcomes calculations forces and moments for varying wind speeds and water depths

To determine the influence of the design parameters on the overall forces on the structure several different calculations are made. In these calculations major parameters are varied so it becomes visible what the influence is. The parameters that will be varied are listed below, in brackets the standard value that is used for the parameter are mentioned.

- Wind speed (Varied)
- Water depth (Varied)
- Wave height (8m)
- Wave period (9,7m)
- Turbine size (5mw, 90m tower height, 154m rotor diameter)
- Shaft diameter (4,78m)
- Base diameter (19m)
- Base height (3m)
- Ice thickness (0,38m)

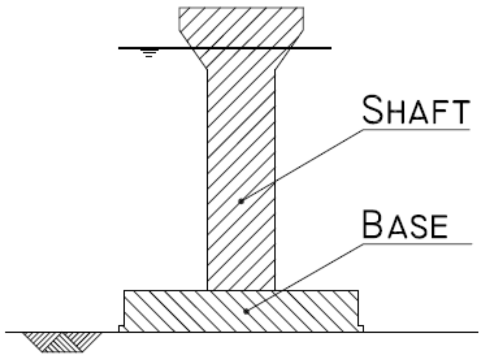

Figure 14, Indication shaft and base of foundation

During the evaluation of the calculations a distinction is made for the wave forces acting on the shaft and the wave forces acting on the base of the foundation. In the adjacent figure it can be seen which part of the foundation is indicated as the shaft and which part is indicated as the base.
In the second figure on this page the profiles for the wind and wave loads can be viewed. It can be seen that the largest wave forces are acting near the water surface and that the highest wind loads are acting on the height of the blades. The effect on the forces for these profile shapes is discussed later on.

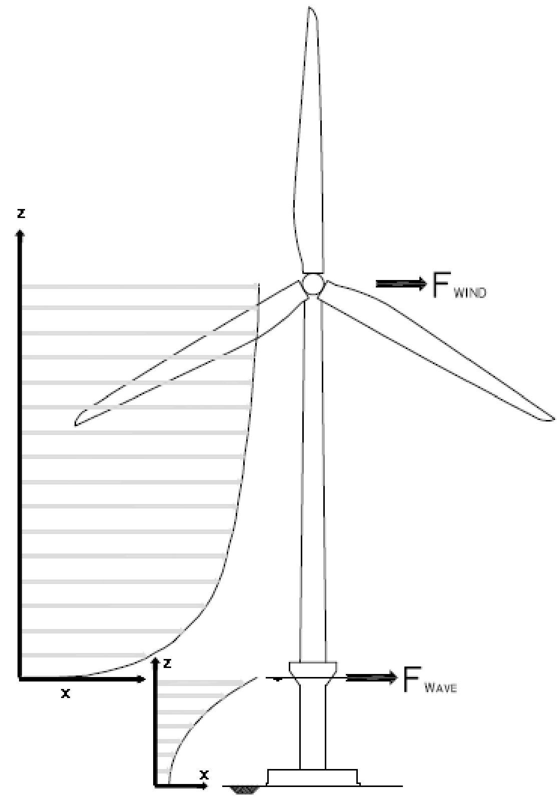

Figure 15, Wind and wave profile

9.2 Variation in water depth and wind speed

For the first calculation sequence only the depth and the wind speed are varied since it is most likely that these parameters will have the largest influence on the total forces on the structure. The depth is varied in three steps: 15, 25 and 35 meters and the 10 minute average extreme wind speed in four steps: 30, 35, 40 and 45 m/s.

The results from these calculations are summarized below. All the detailed outcomes are placed in the appendix. The results are sorted on the water depth first. The moment on the footing is taken at the interface of the foundation foot and the soil. It is mentioned that the obtained horizontal forces are in the SLS and the bending moments are noted in the ULS.

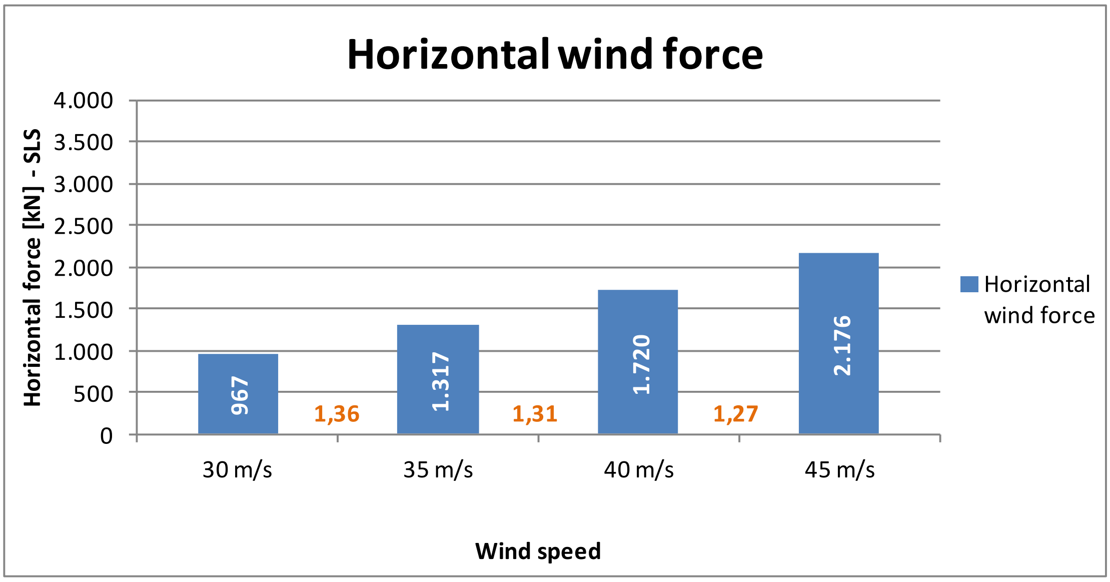

Figure 16, Horizontal wind force and ratio for various wind speeds

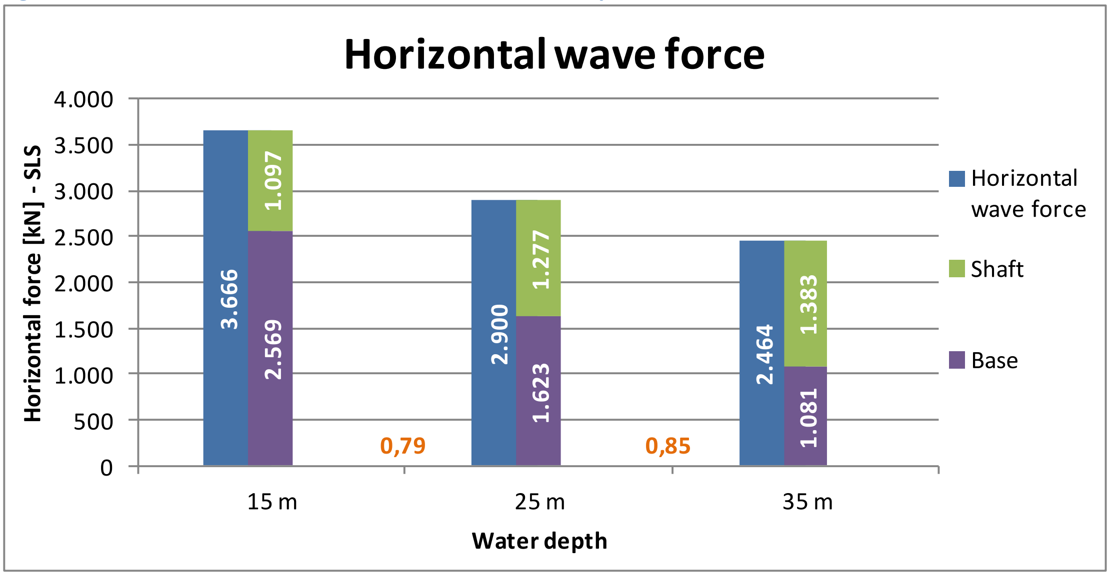

Figure 17, Horizontal wave force for various water depths

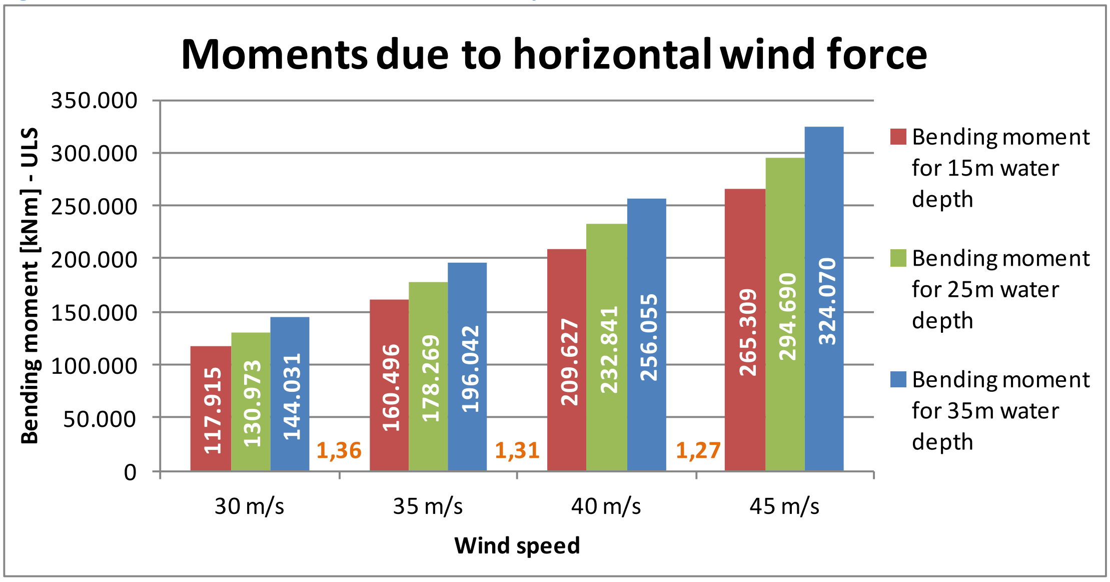

Figure 18, Bending moments due to horizontal wind force for varying water depth and wind speeds

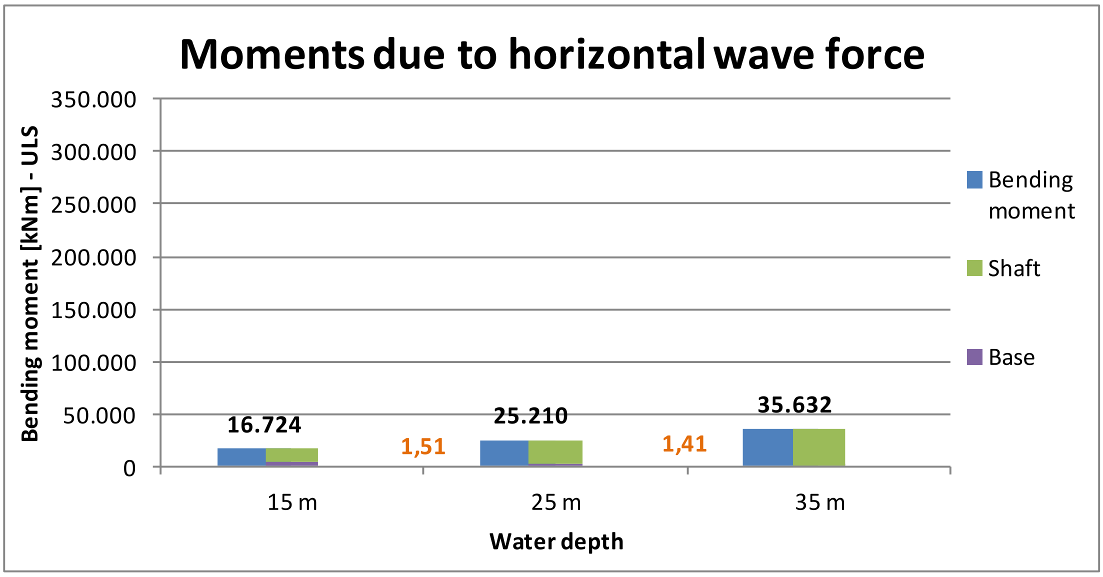

Figure 19, Bending moments due to horizontal wave for various water depths

As can be seen in the graphs above the horizontal wave forces are of a greater order than the horizontal wind forces. But when the moments are regarded the wind forces are of much greater order than the wave forces. This is mainly due to the height of the tower and thus the high lever arm of the forces acting on the blades and tower.

Also remarkable is the decrease of the horizontal wave forces with increasing depth. This can be explained by the fact that for deeper waters the wave forces on larger depths become smaller. Since the base of the foundation has a larger diameter and thus a larger surface the force on the base decreases more than the force on the slender shaft increases. When the moments due to wave forces are regarded the decreasing force with increasing depth is not visible. This is again due to the higher lever arm of the forces acting on the shaft of the foundation.

When the forces due to the wind loading are analyzed the ratio between the horizontal forces can be calculated for different wind speeds and water depths. This can also be done for the moments acting on the foundation. In the graphs presented before the ratio between the forces or moments are added in orange. The scale of the vertical axis is equal for both horizontal forces and bending moments. Therefore also the absolute differences in forces can be evaluated.

For the horizontal wind loadings it can be seen that the water depth has no influence on the horizontal force as could be expected. For the ratios between the different wind speeds it can be seen that the ratio is around 1,3. The same ratios are also visible between the moments for various wind speeds. The ratio between the moments for one wind speed is 1,1. What can be concluded from the graphs is that the wind speed has a large influence on the total force and thus the bending moment. When the wind speed is increased from 30m/s to 45m/s the forces and moments are more than doubled. This can be explained by the quadratic relation between the wind pressure and wind speed

Regarding the horizontal forces and moments due to the wave loadings other ratios between forces and depth occur. Since the wave force is build up of two parts, being the force on the shaft and the force on the base of the foundation, the total force and moment are also split up in two parts as can be seen in the graphs. As also can be seen in the data in the appendix the wind speed has no influence on the wave force on the foundation.

Analyzing the graphs of the wave forces it is noticeable that the total horizontal force decreases for an increasing water depth. As can be seen this is due to the decrease of the force on the base of the foundation. What can be seen is that the share of the force on the shaft increases for increasing water depths. When the horizontal loads due to wind and to waves are compared it can be seen that they are of the same order and that the wave forces are slightly higher. But when the moments are regarded the moment due to wind forces is a factor 9 higher than the moment due to wave forces. The share of the moment on the shaft is also very large compared to the share of the base. Although the ratio between the moments due to wave force is quite high (1,5) this total moment is still small compared to the wind moment.

9.3 Relation water depth, wind speed and wave height

For the next variance of parameters a variance is made in the water depth, wind speed and wave height. This is done to view the influence of the significant wave height on the forces acting on the foundation. Since the wave height has no influence on the turbine structure this part is not regarded in this section. The basic results from this parameter variance are listed in the graphs below. In the first two graphs the horizontal forces on the foundation are drawn. In the last two graphs the moments on the foundation are presented. A complete table with all the outcomes is presented in the appendix.

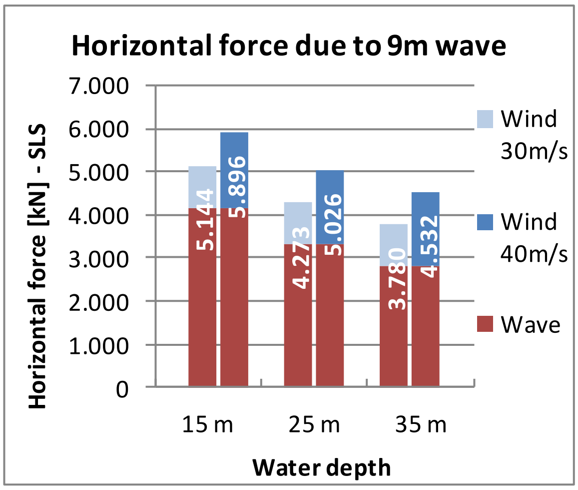

Figure 20, Horizontal force for 9m wave

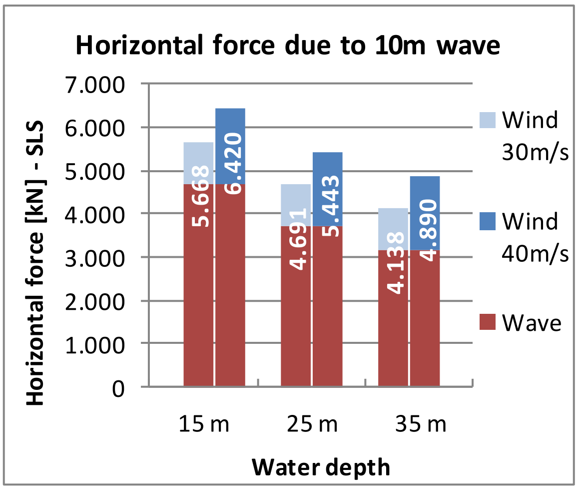

Figure 21, Horizontal force for 10m wave

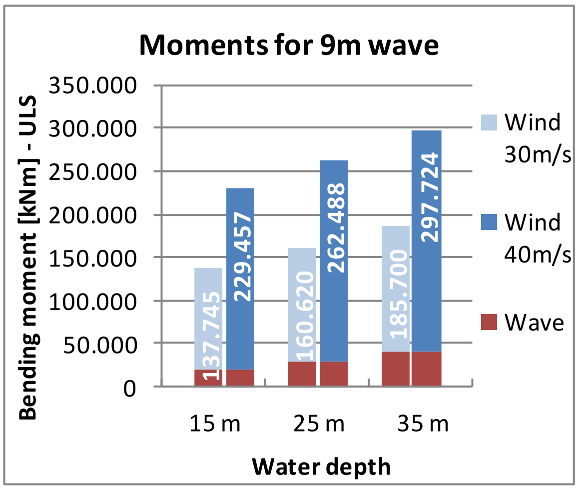

Figure 22, Moment for 9m wave

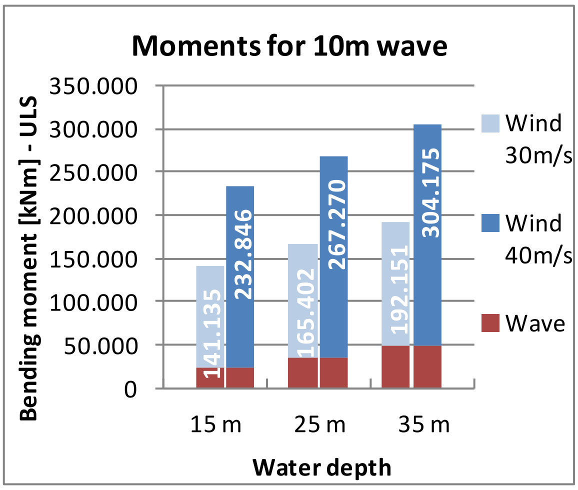

Figure 23, Moment for 10m wave

For all the situations the wave force and wind force are displayed. Since the wind speed has no influence on the wave force the wave force is equal for both 30m/s and 40m/s wind speed. In the graph bars the total value of the wind plus wave force is placed.

As mentioned before the variance in wave height has no influence on the wind forces on the structure. Also the wind speed has no influence on the wave forces as can be seen in the figures. When the outcomes for the horizontal forces are regarded the same behaviour as before can be mentioned; the total horizontal force decreases with increasing depth.

When the horizontal forces are analyzed it can be seen that the wave force is still dominating the total horizontal force. Comparing to the wave forces for a 8m high wave presented before, the wave force has increased relatively much. The share of the wave forces in the total moment is also slightly increased. Still it is visible that the total bending moment is dominated by the moment due to wind loadings.

The ratios between the wave height and water depth are investigated below. For the graphs below the ratio between the forces is displayed in orange. In the first graph the ratios between the total horizontal forces is shown. The second graph shows the ratios between the total moments for various water depths and wind speeds. The ratios are the same for the variation in wave height, therefore this variation is not visible in the graphs below. The detailed data for the ratios is visible in the appendix.

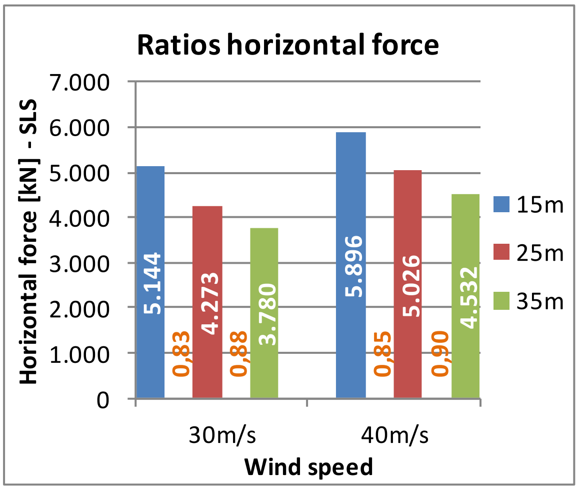

Figure 24, Ratios for horizontal forces for varying depths

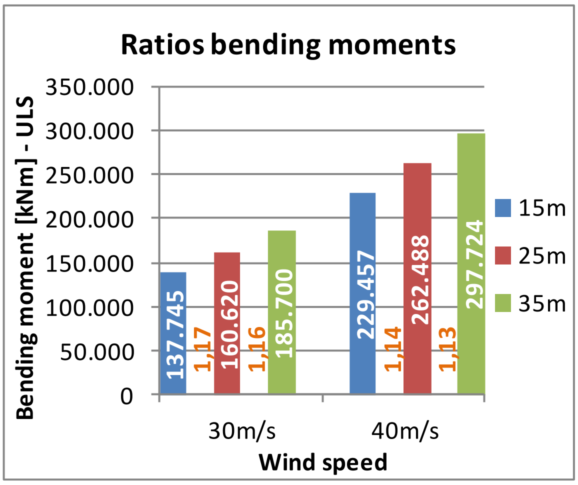

Figure 25, Ratios for bending moments for varying depths

When the graphs are studied more in detail it can be seen that the ratios for the horizontal force are lower than 1, which indicates the declination of the horizontal force for larger water depths as discussed before. The ratios are increasing for increasing water depths.

The ratios for the moments are larger than 1, as can be seen in the second graph. This means that the moments are increasing for an increasing water depth. For a larger wind speed the ratios become smaller.

For both the horizontal force and the moment the difference in ratios is small for the different wind speeds.

9.3.1 Resume

With the graphs and calculation outcomes presented in this chapter it is concluded that there is a large difference in influence between the wind and wave loads. The wave loadings are the major horizontal force acting on the turbine structure, but due to the small lever arm the resulting bending moment is low compared with the bending moment due to wind loads. For the wind loads this is the other way around, the wind leads to small horizontal forces but results in high bending moments due to the high lever arm. Therefore an increase in wind speed and water depth leads to higher bending moments and an increase of the wave height leads to an increase in the horizontal forces.

10. Calculation and representation wave loadings

In the previous chapters calculations are made for situations with varying environmental parameters. In this way the influence of the governing environmental parameters is found. To be able to better investigate the change of forces when environmental parameters are changed graphical plots are made for varying parameters. When making plots only one parameter at a time is varied. It is noted that by accident all horizontal forces are in SLS and the presented bending moments are in ULS.

10.1 Declaration of parameters

To calculate the wave force use is made of a formula presented in the DNV norm. The formula consists of two force components, being an inertia force and a drag force. The formula, also known as the Morison Equation, is presented below. As can be seen in the formula the inertia part of the formula is depending on the acceleration $(\ddot{x})$ of the waves where the drag force is depending on the speed $(\dot{x})$ of the waves.

$$dF = dF_m + dF_d = \underbrace{C_M \rho \pi \frac{D^2}{4} \ddot{x} dz}_{\text{inertia force}} + \underbrace{C_D \rho \frac{D}{2} |\dot{x}| \dot{x} dz}_{\text{drag force}}$$

As can be seen several parameters are needed as input for the Morison Equation. The declaration and calculation of these parameters is placed in the appendix.

10.2 Standard parameters used

A standard situation is used as a basis for generating the graphical representation of the variation in the wave parameters. The parameters belonging to the standard situation are:

Water depth:	25m
Significant wave height:	6m
Wave period:	9,7s
Diameter shaft:	6m
Diameter base:	15m
Height base:	2m
Tower height:	95m
Rotor diameter:	154m

In the following sections several parameters relating to the wave forces are varied and the results are shown in the presented plots. The most significant wave parameters are displayed in the figure below. A parameter not visible in this graph is the wave period. The wave period is defined as the time between two wave crests.

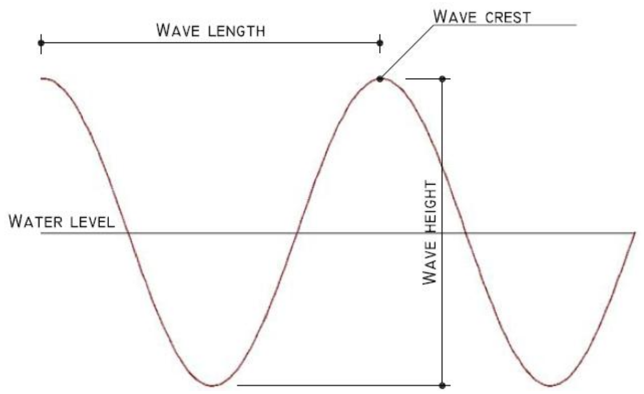

Figure 26, Indictation of the wave paramters wave length, wave height and wave crest

10.3 Calculation and variation of wave loadings, drag and inertia forces

When the Morison Equation which is used to determine the wave forces is integrated over the total water depth the forces acting on the foundation are obtained. When the forces acting at the water level are regarded the following graph with horizontal forces on the foundation is obtained:

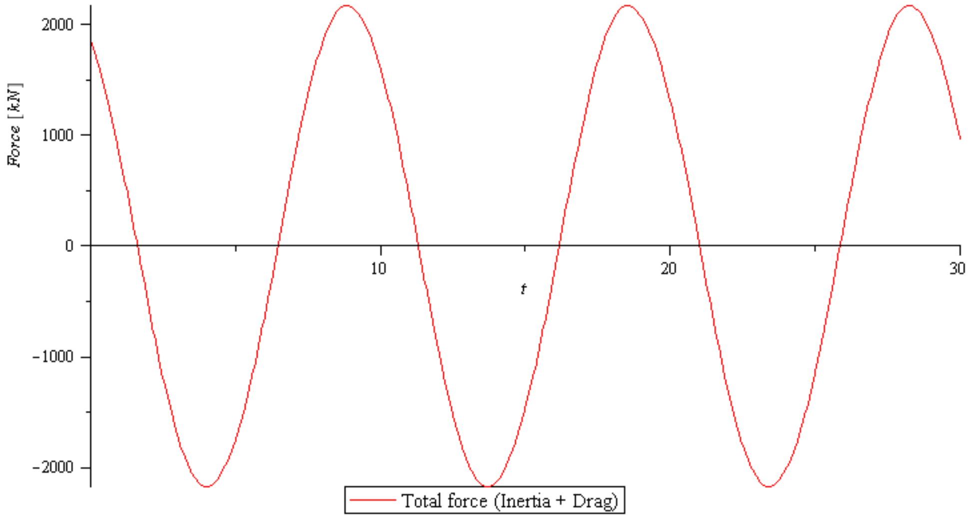

Figure 27, Horizontal forces at water level according to Morisons Equation

This total force consists of both the inertia and the drag force on the foundation. When these forces are plotted separated it can be seen that the drag force has a negligible influence on the total force on the foundation.

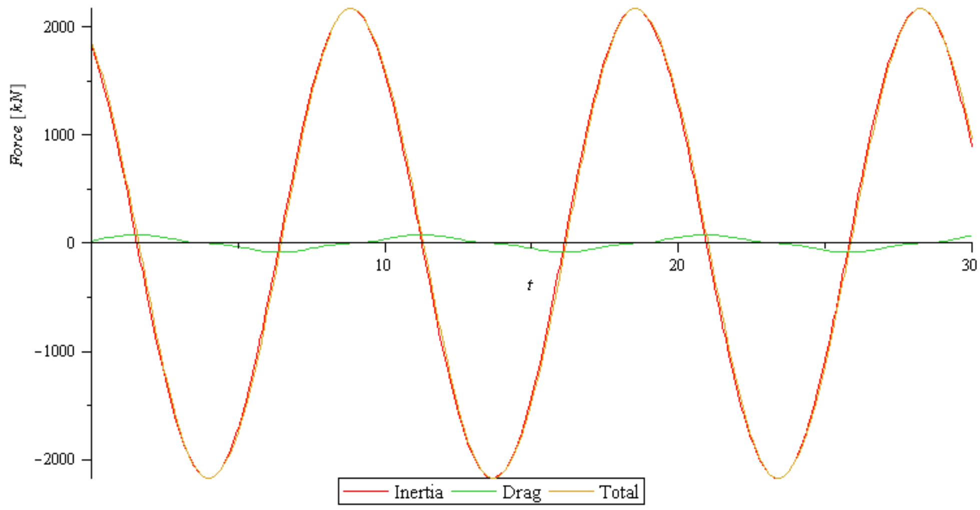

Figure 28, Inertia and drag components for Morisons Equation

Therefore it can be concluded that the inertia force is dominating the forces on the foundation. This means that the acceleration of the wave forces results in the largest loading on the foundation. What is found is that the drag force cannot be dominating the total horizontal force on the foundation when Morison's equation is used according to the calculations made. Only an unfavourable combination of loads such as a low wave period and large wave height or an extreme wave height (>40m) can make the drag force dominating. Since these combinations are not realistic these are not considered.

10.4 Calculation and variation of wave loadings, shaft and base loadings

When the total force is used for further force calculations insight can be obtained on the forces on the foundation for different conditions.

For this variance study the relation between different wave parameters is investigated. First the relation between the horizontal force and the water depth is regarded. From this the resulting moments due to wave loadings on the foundation are regarded. The force is split up between the shaft and the base of the foundation. The results for the horizontal forces on the foundation are shown below.

To calculate the values used for this graphs an approximation is made for the wave length. For this use is made of a fitted formula on validated data points. This formula is valid for the domain between 10 and 45m water depth. Therefore all graphs have this range on the horizontal axis. This range also covers the range for this study and is therefore usable for the calculations made in this report.

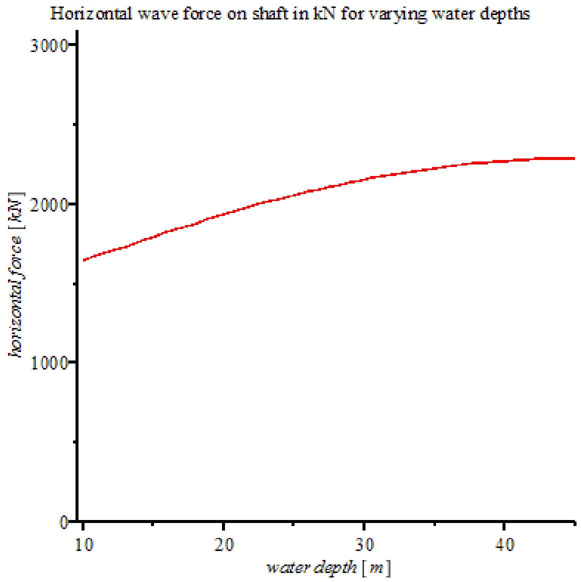

Figure 29, Horizontal wave force on shaft

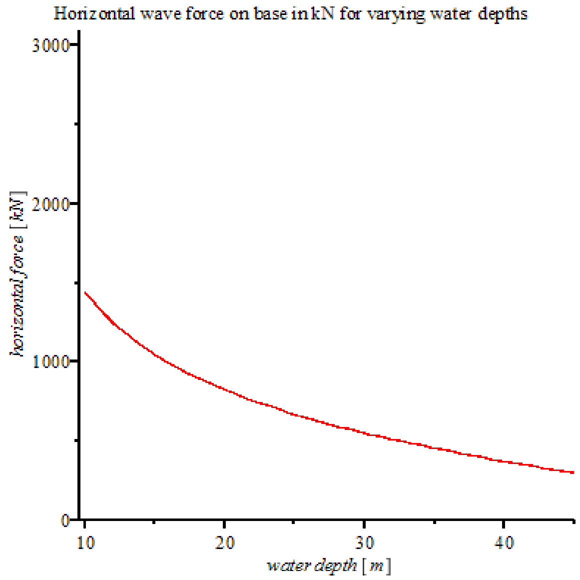

Figure 30, Horizontal wave force on base

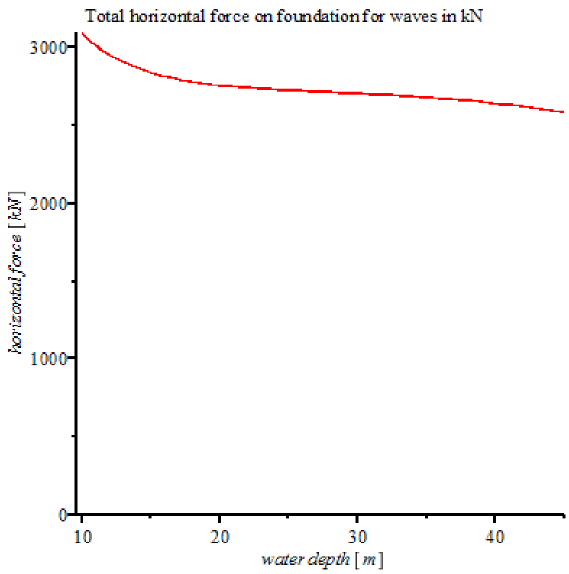

Figure 31, Total horizontal force on foundation

As can be seen from the first graph the horizontal force on the foundation shaft increases with increasing water depth. The increase declines for larger water depths. This is because of the non linear force profile over the water depth as can be seen in the figure below. Because the force per meter on large water depths decreases, the influence of the larger water depth also decreases.

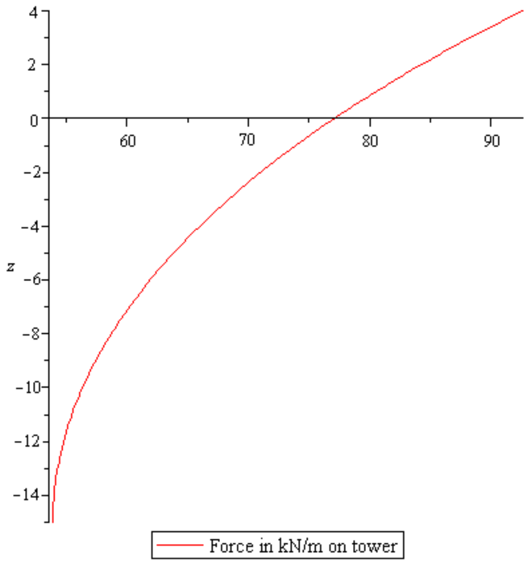

Figure 32, Force on shaft for various water depths, on the vertical axis is the water depth from +4m to -15m

In the second graph the horizontal force on the base can be regarded for different water depths. When compared to the first graph it can be noticed that the force on the base decreases with an increasing water depth. This is again due to the decrease of the horizontal force when the water depth increases. Because the large diameter of the base and thus the high surface that is exposed to the water loadings this decrease of horizontal load is highly noticeable in the force on the base of the foundation.

When both the horizontal force on the shaft and on the base are summed up the result shows some particularities. First it can be noticed that the total horizontal force decreases when the water depth increases. This is thus mainly because the high surface of the base and the decrease of horizontal force on greater water depths. The second remarkable feature is that the decrease is not linear but has a s-shape which means that the decrease is not linear.

From these graphs it can be concluded that for the investigated situation the water depth has an positive effect on the total horizontal force, although the absolute decrease of the force is small. This is mainly due to the reduced effect of the wide base of the foundation.

10.5 Calculation and variation of wave loadings, water depth

On the other hand there are the bending moments on the foundation foot. For these calculations the effect of the foundation base is less remarkable because of the small lever arm to the foundation foot. The graphs for the moments on the foundation are listed below.

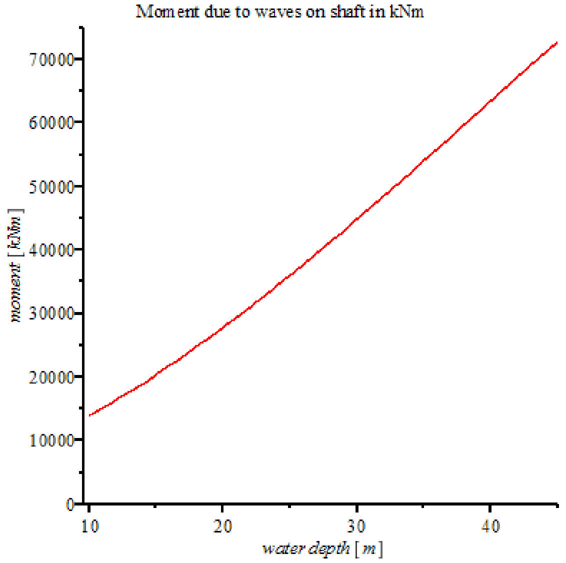

Figure 33, Bending moment for force on shaft

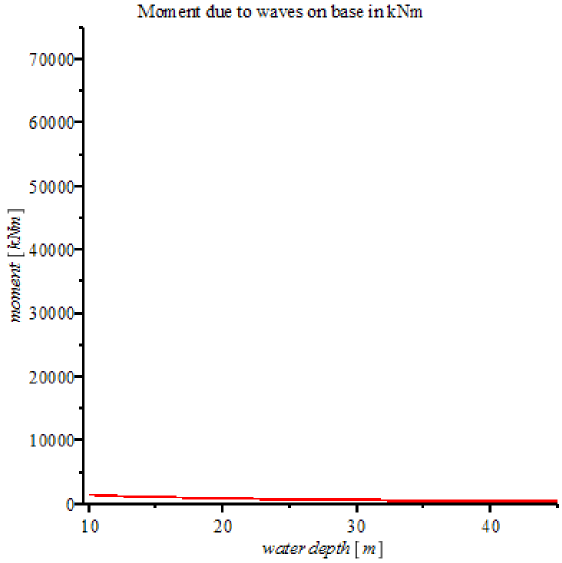

Figure 34, Bending moment for force on base

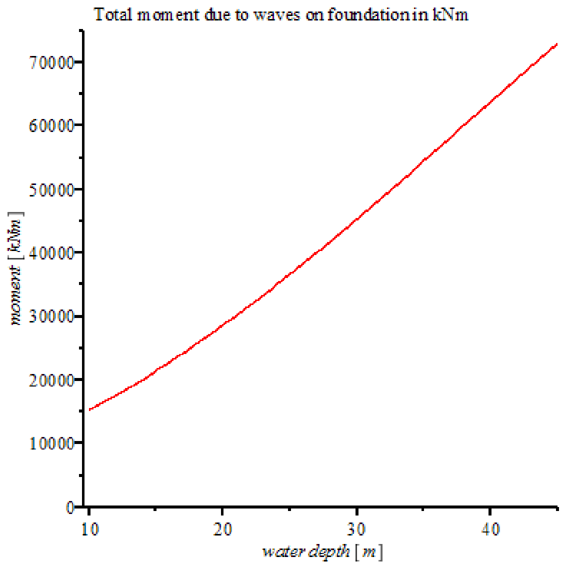

Figure 35, Total bending moment and moment for shaft

Form the first graph it can be seen that the moment on the foundation foot due to the loadings on the foundation shaft increases for increasing water depths. This relation is not linear but increases slightly for an increasing water depth. It is worth mentioning that the total bending moment increases from 15.000kNm for a 10m water depth to 70.000kNm for 45m water depth.
For the moment on the foot due to the forces on the foundation base the relation between moment and water depth is opposite to the relation of the shaft, with an increasing water depth the force decreases as already mentioned. A large difference is the magnitude of the moment. For the shaft the moment is at least an order 10 larger than for the moment for the base. This because of the small lever arm for the base. This difference in magnitude can also be seen in the graph for the total bending moment on the foundation foot. The total bending moment on the foundation due to water loading is almost equal to the moment due to only the shaft, as can be seen in the figure.

When regarding the figure it is noticed that only for small water depths the bending moment due to forces on the base are having influence on the total bending moment.

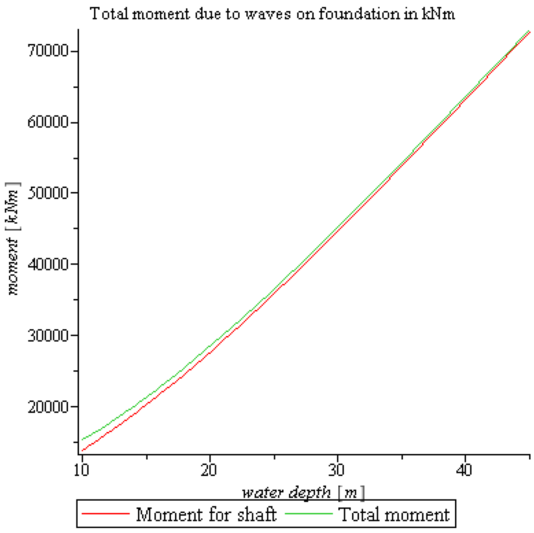

Figure 36, Moment on shaft and total moment

10.6 Calculation and variation of wave loadings, H_S, T_P and foundation diameter

The presented graphs in the previous paragraph are giving an insight in the relation between the forces on the foundation and the water depth. Beside this relation there are more conceivable relations to investigate. These relations primary concern the forces exited on the structure since this is the dominant aspect for the design. Three parameters regarded here are the wave height H, the wave period Tp and the shaft and base diameter. The results for the relation between the parameter and the force on the foundation are presented in the following graphs. The layout and calculation method of these graphs differs from the previous ones because for these parameters it did not work to graph the results using the software Maple.

10.6.1 Variation of shaft diameter

First the relation between the shaft diameter and forces on the foundation are highlighted. As can be seen in the presented graphs the relation between the forces and the shaft diameter is not linear. This holds for both the horizontal force and the moment on the foundation. The horizontal force increases from 660 kN for a ø2m shaft to 4560 kN for a ø10m shaft. For the moment the increase is from 3.200 kNm for a ø2m shaft to 68.500 kNm for a ø10m shaft which is a factor 21 higher for a factor 5 increase in diameter. Realistically seen a diameter of 2m is not feasable, but the relations for the shaft diameter give a clear image of the influence of the shaft diameter.

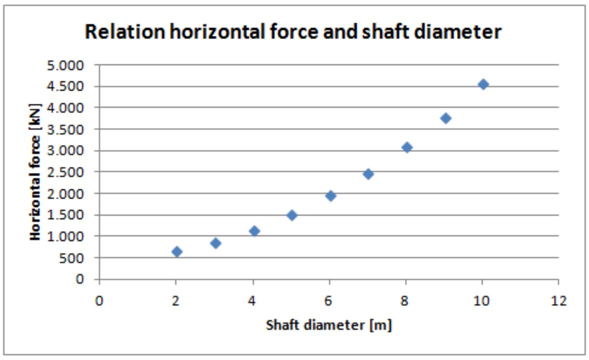

Figure 37, Relation shaft diameter and horizontal force

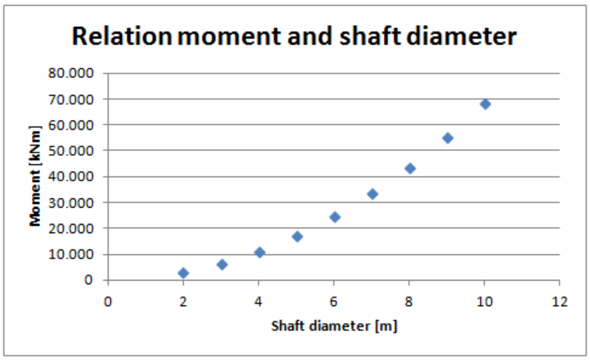

Figure 38, Relation shaft diameter and moment

The explanation for this high factors is that the calculation outcome is inertia dominated. As can be seen in the formula for the calculation of the wave forces below, the inertia part of the wave force formula contains the foundation diameter quadratic. This results in a large influence of the foundation diameter on the horizontal force.

$$dF = dF_m + dF_d = \underbrace{C_M \rho \pi \frac{D^2}{4} \ddot{x} dz}_{\text{inertia force}} + \underbrace{C_D \rho \frac{D}{2} |\dot{x}| \dot{x} dz}_{\text{drag force}}$$

10.6.2 Variation of base diameter

For the relation between the base diameter and the total forces on the foundation a somehow different relation can be found. Still the relation is not linear as it is not for the shaft diameter, but the difference in total forces is smaller than it is for the variance in shaft diameter. As can be seen in the graphs the difference in the total horizontal force for a base with ø12m and ø28m is only a factor 1,8 and for the total bending moment a factor 1,1. This small change in horizontal force and moment is again because of the small influence of the base diameter on the total forces for the foundation.

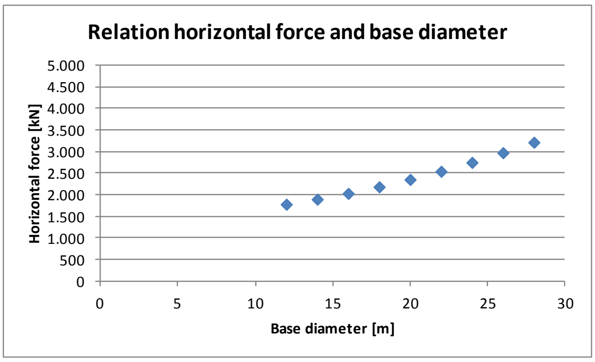

Figure 39, Relation base diameter and horizontal force

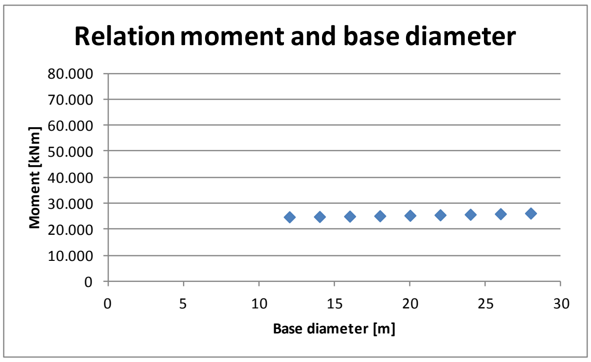

Figure 40, Relation base diameter and bending moment

What can be concluded from the previous graphs for the variation in the diameter of the shaft and base is that the influence of a variance in the shaft diameter is significantly higher than a variance in the base diameter. This holds both for the horizontal force as for the bending moment.

10.6.3 Variation in wave height

Besides the relation between the foundation dimensions and the wave forces also the relation between wave parameters and the wave forces is investigated. For this the wave height and the wave period are varied. Since there is a relation between the wave height and the wave period the results from these variances cannot be investigated separately. For the Norht Sea it holds that when the waves are higher the wave period is also higher[13]. Therefore load calculations with a large wave height and short wave period are not governing since this combination will not occur on sea. Because for the calculations of the graphs the wave period or wave height is held constant the graphs do not describe the real behaviour and are only considerable for investigating the relations.

First the relation between the wave height and the forces acting on the foundation are presented in the graphs below.

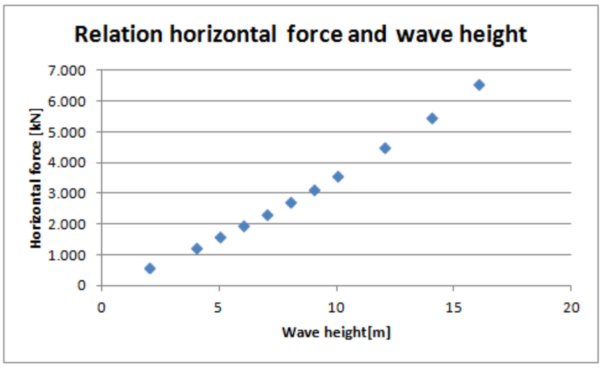

Figure 41, Relation wave height and horizontal force

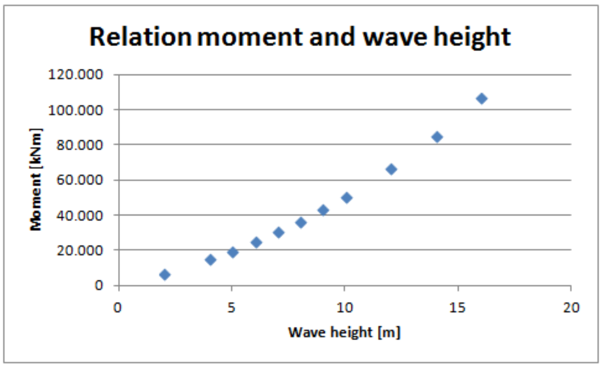

Figure 42, Relation wave height and moment

[13] Wave loads on offshore wind turbines, Feasibility study using results of wave experiments executed by Electricitié de France (EDF), J.M. Peeringa, april 2004.

The graphs for the relation between the wave height and the forces on the foundation show a clear relation between the wave height and the horizontal force and moment on the structure. Both for the horizontal force and the moment the factor between a wave height of 2 meters and a wave height of 16 meters is significant. For the horizontal force the factor between 2 and 16 meters is 11 and for the moment the factor is 15. As can be seen from the graph for the moment on the foundation the increase of wave height has a significant increase of the moment as result. For larger wave heights the total moment reaches 100.000 kNm which is in the same order as the wind loads on a wind turbine.

10.6.4 Variation in wave period

The other wave parameter investigated is the wave period. The time between two waves has significantly less influence on the total force than the wave height. It can also be remarked that a higher wave period results in lower forces on the foundation. Taking in mind the relation between the wave height and the wave period it can be remarked that the total horizontal force and moment will be lower than presented by the variance in wave height. This because the associated larger wave period reduces the total force.

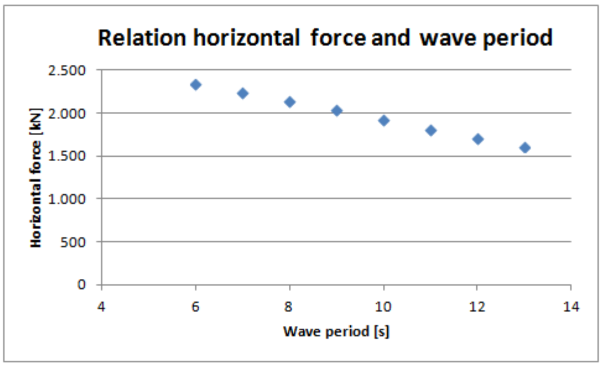

Figure 43, Relation wave period and horizontal force

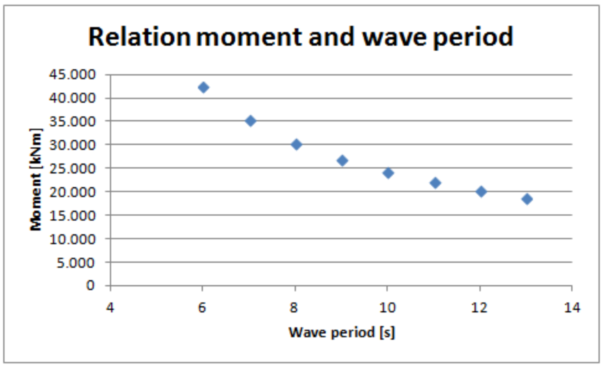

Figure 44, Relation wave period and moment

10.7 Calculation and variation of wave loadings, wave height and wave period for location IJmuiden

To implement and evaluate the relation between the wave height and the wave period calculations are made using measured data. This data coming from measurements from the location IJmuiden Munitiestortplaats[14] in the North Sea represents the wave height and wave period for extreme events with a return period of 10, 100 1000 and 10000 years. The values for this location are here presented. It should be mentioned that the wave heights are significant wave heights and the relation between the significant wave height and maximum wave height is: $H \approx 1{,}8 \cdot H_{m0}$.

return period [year]	10	100	1000	10000
wave height H_{m0} [m]	6,71	7,64	8,42	9,10
peak wave period T_p [s]	12,4	13,7	14,7	15,7

When the parameters from this table are inserted into the calculation sheets the following graph is obtained. It should be remarked that the origin of the graphs is not located at zero.

[14] Wave loads on offshore wind turbines, Feasibility study using results of wave experiments executed by Electricitié de France (EDF), J.M. Peeringa, april 2004.

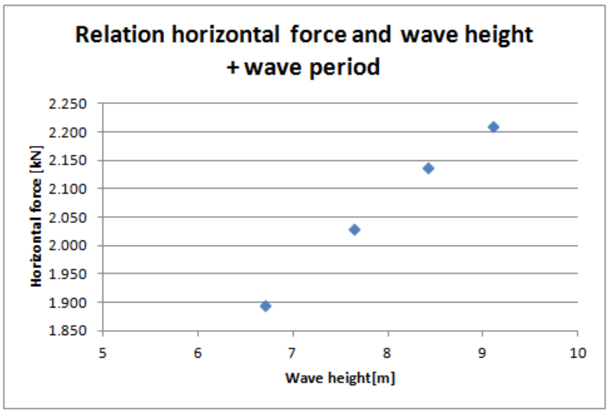

Figure 45, Relation wave height + wave period and horizotal force for location IJmuiden

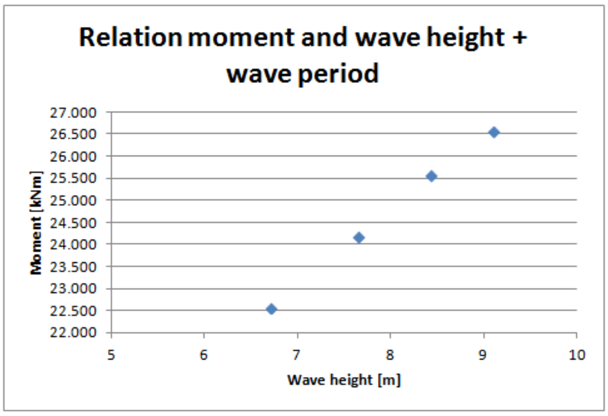

Figure 46, Relation wave height + wave period and moment for location IJmuiden

When the graphs for the moment on the foundation for varying wave height are regarded it can be seen that the total bending moment is lower when the wave height and its associated wave period are used. This can be indicated with the following outcomes. When the wave period is held constant at 9,7s and the wave height is varied the outcome of the moment calculation for a 9m high wave is 43.300 kNm. When the wave period associated to the wave height is used the outcome of the calculation for a wave height of 9,1m with a wave period of 15,1s is 26.500 kNm. This is lower than the previous calculated moment of 43.300 kNm.

10.8 Calculation and variation wave loadings, current loadings

Besides the loadings by wave forces the foundation is also loaded by current loadings. The currents in the water can have different origins. The most prominent currents are wind generated currents and tidal currents. The wind generated currents are generated by the wind blowing over the water surface. In case of a storm with an extreme wind speed of 40m/s the wind generated current becomes 40cm/s. The tidal currents are generated by the tides on the sea. For the North Sea these tidal currents are in the order of 60-100cm/s.
The constant current speed only results in drag forces. Since the water related forces on the foundation are inertia dominated the constant speed of the wind and tidal currents will not have a large influence on the total loading. When the current loadings are calculated using the formulas presented in the appendix it is found that the current loadings for the current speeds aforementioned are:

$$F_{\text{wind current}} = 12{,}15kN$$

$$F_{\text{tidal current}} = 75{,}95kN$$

As can be seen from these results the horizontal forces and thus the resulting moments are very small compared to the wave loadings (>1000kN). This is because the water loading of the foundation is inertia dominated as mentioned before. From these results it may be concluded that for small foundation diameters compared to the wave length the currents loadings have minimal influence on the total loadings of the foundation.

10.9 Resume

Regarding the wave loadings on the foundation it can be concluded from the previous considerations that the forces exited on the foundation shaft are the dominating forces for the total moments on the foundation. This is mainly because of the higher lever arm of the shaft and because of the effect that wave loadings are higher close to the water level than they are close to the soil level.
Furthermore the effects of a greater wave height are reduced due to an associated increase in the wave period. It is also concluded that the currents existing in open waters are not having a large influence on the loads on the foundation

11. Calculation and representation wind loadings

Concerning the wind loadings on the offshore wind turbine the major parameters that can be investigated are mostly of a structural nature such as tower height, turbine diameter and tower diameter. The only environmental property to investigate is the wind speed. It is mentioned that the horizontal forces are noted in SLS and the bending moments in ULS.

11.1 Calculation and variation of wind loadings, wind speed

The first parameter to be varied and investigated is the wind speed. The wind speed at hub height is varied from 30m/s to 45 m/s. This wind speed entered in the model is an 10-minute average extreme wind speed. In the model using this average extreme wind speed the extreme wind gust is calculated using a gust factor of 1,2. This makes that the investigated extreme wind gusts are varied from 36m/s to 54m/s. The results for the variance in wind speed are added below.

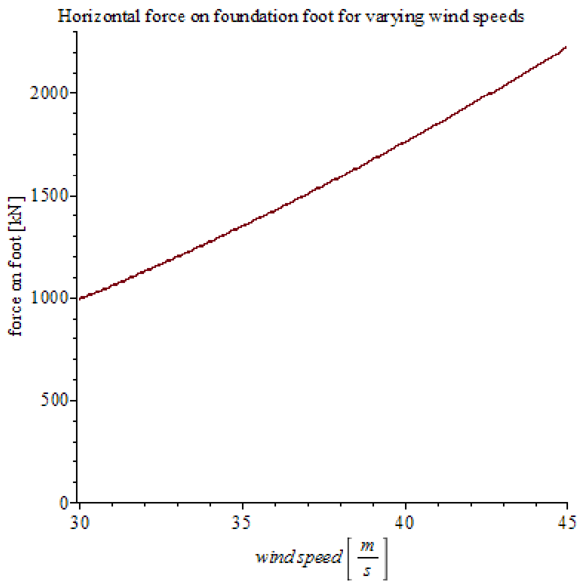

Figure 47, Relation wind speed and horizontal force

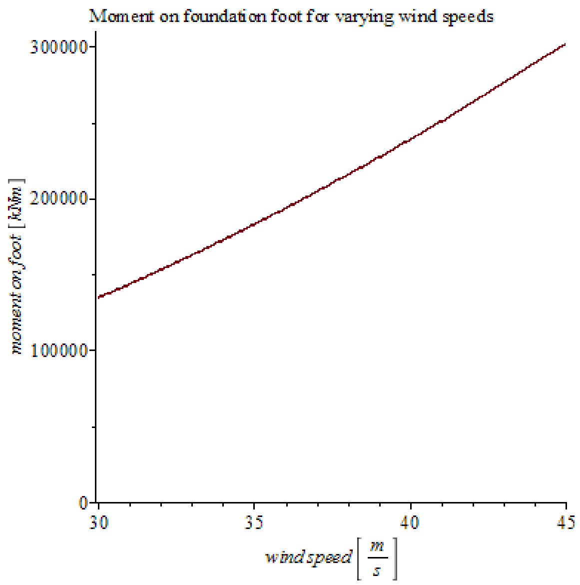

Figure 48, Relation wind speed and moment

As can be seen on the graph for the horizontal force the relation between an increase in wind speed gives an increase in the horizontal force. This relation is not linear but slightly parabolic. The horizontal force increases from 1000 kN for 30m/s wind speed to 2200 kN for 45m/s 10-minute extreme wind speed. In this increase the quadratic relation of the wind speed and the horizontal force is observed. This same relation holds for the wind speed and the moment on the foundation. Here the moment on the foundation increases from 135.000 kNm for 30m/s to 300.000 kNm for 45m/s 10-minute extreme wind speed.
Because the wind is the dominating load component of a wind turbine the magnitude of the moment increases relatively much from 135 MNm to 300 MNm. This magnitude of the wind moment indicates that the wind force is the dominating force on the foundation.

11.2 Calculation and variation of wind loadings, tower height

A structural parameter that can be varied is the tower height of the wind turbine. By increasing the tower height the wind speed on the blades will be higher. Therefore the power output of the turbine can be increased or the blades can be smaller to generate the same power. On the other hand increasing the tower height also increases the lever arm of the rotor force and thus results in a higher bending moment.

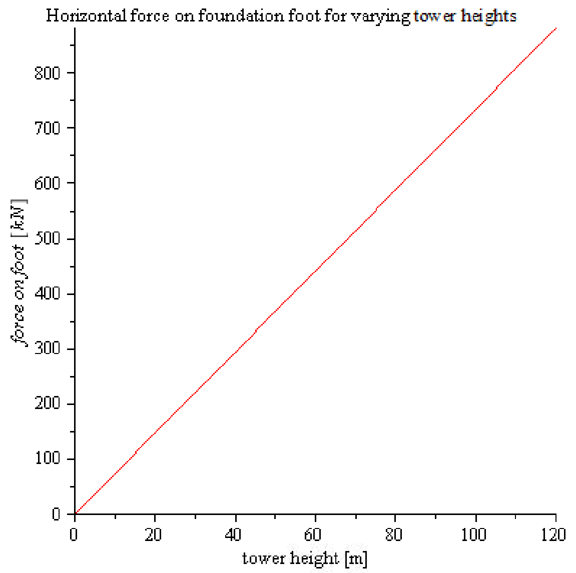

Figure 49, Horizontal force on tower only for varying tower height

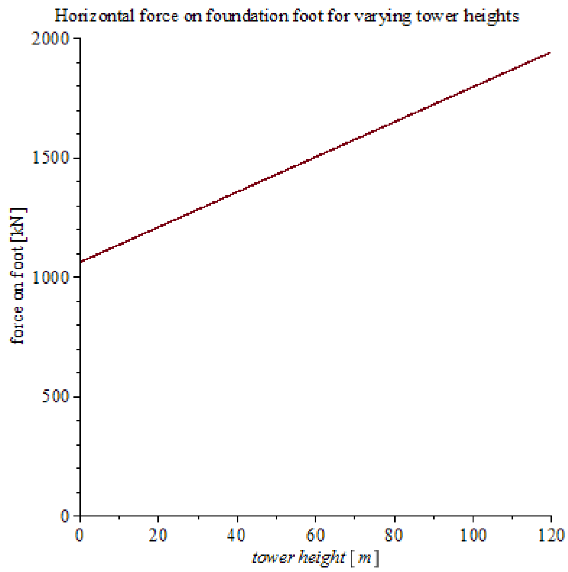

Figure 50, Relation tower height and total horizontal force

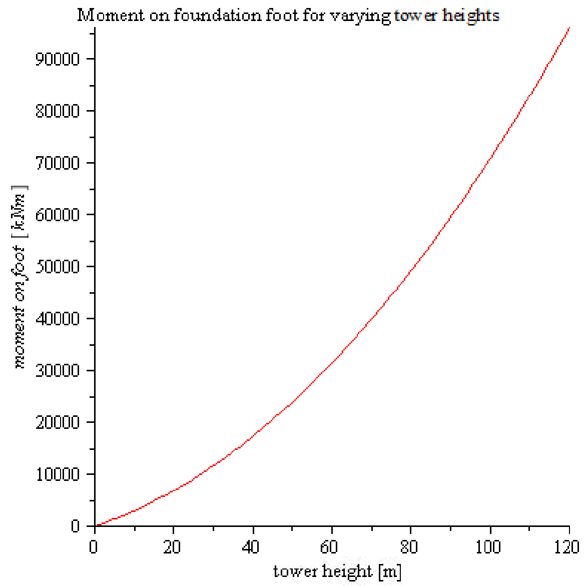

Figure 51, Moment on tower only for varying tower height

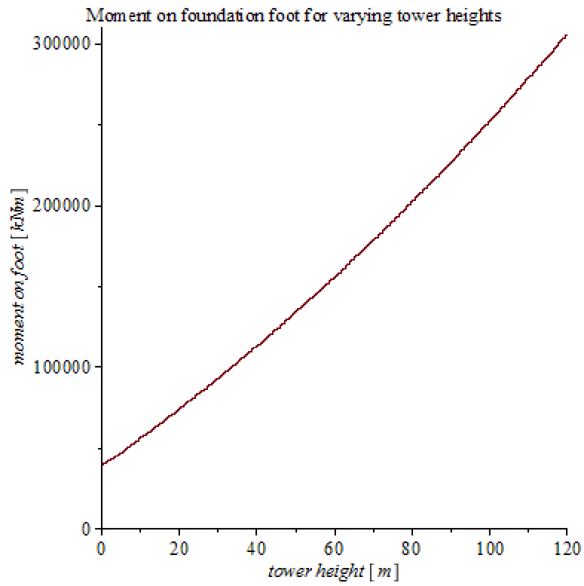

Figure 52, Relation tower height and total moment

The results of the variation in tower height are visible in the graphs presented above. In the first column the force only acting on the tower are presented. In the second column the total forces on the structure are presented. From the graphs for both the horizontal forces it can be noticed that the horizontal force increases for an increasing tower height. The increase of the horizontal force declines a little for larger tower heights, but this is barely visible.
This behaviour is not observed for the bending moments. For the bending moments it can be seen that the increase of the moment is growing for larger tower heights. The increase of the moment is larger for the moments due to the forces on the tower only. This is because the height has a quadratic effect on the moment calculation. For the total bending moments on the structure it can be noticed that the increase ratio between the tower height and the moment is smaller and the graph is more linear. This can be explained by remarking that the moment due to the forces on the tower only is roughly 1/4th for low towers to 1/3th of the total bending moment for higher towers.

11.3 Calculation and variation of wind loadings, rotor diameter

Finally the relation between the rotor diameter and the forces on the turbine is investigated. The effect of a larger rotor diameter is that the swept area of the turbine blades increases. Therefore the turbine is able to increase the power output for the same wind conditions.
As can be seen from the graphs there is a practically linear relation between the increase in rotor diameter and the increase in both horizontal force and moment. This may be explained by the assumption made in the calculation sheet for a linear behaviour between the length of a rotor blade and the surface of the blade. When the rotor diameter is increased from 100 to 160 meter the horizontal force increases from respectively 1400 kN to 1800 kN. The moment increases for the same range from 180.000 kNm to 245.000 kNm.

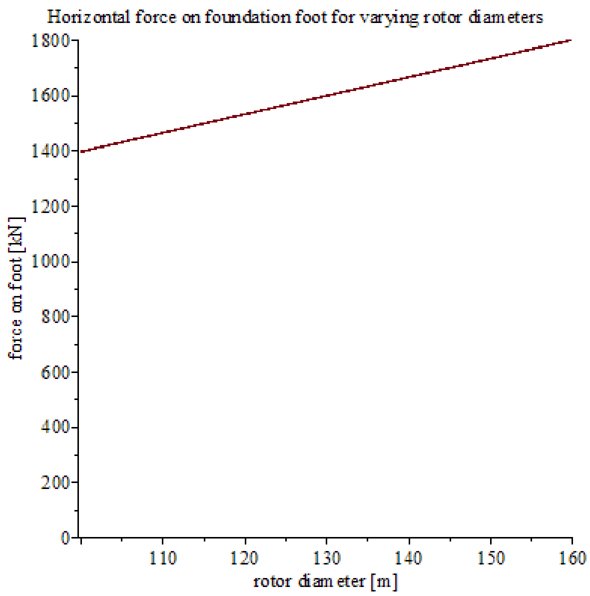

Figure 53, Relation rotor diameter and horizontal force

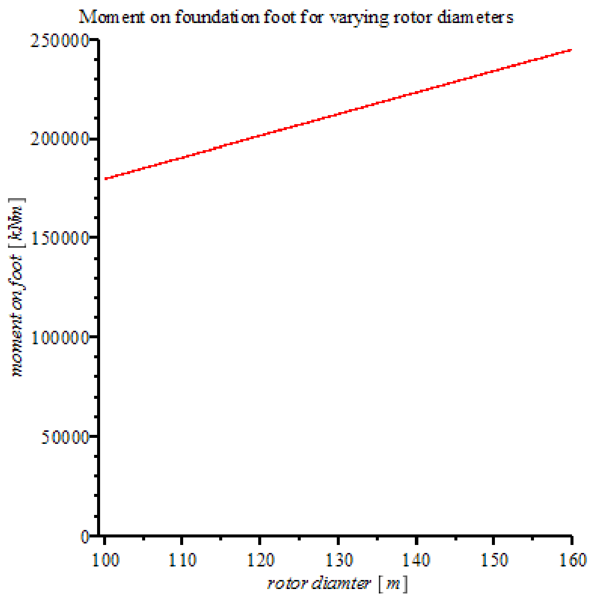

Figure 54, Relation rotor diameter and moment

11.4 Resumé

From the presented graphs and calculations in this chapter it is concluded that the wind speed at the location of the wind turbine is resulting in the largest variation in forces on the wind turbine. The wind forces are largely responsible for the magnitude of the bending moments due to the high lever arm. The reason that a variation in the wind speed has a high influence on the bending moment is the quadratic relation between the wind speed and the load on the wind turbine.
Besides the wind speed a variation in the tower height has the most influence on the calculation outcomes. Because an increase in the tower height results in a larger lever arm and thus directly in an increase of the bending moment.
The least influence on the forces has the rotor diameter. This is because an increase of the rotor diameter causes a relative small increase in the horizontal forces and thus a small increase of the bending moments. It is also mentioned that an increase of the rotor diameter often also means an increase of the tower heights because a minimum clearance between water level and the rotor tip is required.

12. Calculation and representation ice loadings

An environmental loading that is very site specific is ice loading. For locations on the North Sea no account has to be taken for ice loadings. For locations such as the seas around Denmark and the Baltic Sea ice loadings do have to be taken into account. According to the calculations presented in the DNV the variables that influences the ice loading on a foundation with ice cone are the ice sheet thickness, flexural strength and cone diameter which is related to the cone angle.
The results of the forces on the foundation consist of three components being the horizontal force, the moment and a vertical force due to the breaking of the ice on the cone. Since the ice sheet thickness is the major ice parameter only this parameter is varied. The cone diameter and thus the angle should be adjusted according to the ice force on the foundation to let it be smaller than the design wave load.
The results for the variance in ice sheet thickness are included below. For all the three forces the relation between the ice sheet thickness and the force is parabolic. What can be seen Is that the horizontal and vertical force increase rapidly for thick ice sheets. The moment on the foundation for an ice sheet thickness of 3m is almost 400.000 kNm. It may be clear that locations with such harsh ice conditions should be avoided to construct wind farms. When locations are chosen with a maximum ice sheet thickness of 1m the moment on the foundation foot will be around 50.000 kNm which is a more reasonable force to withstand. For example the Kriegers Flak wind farm is designed using a 0,38m thick ice sheet. This gives moments around 10.000 kNm.

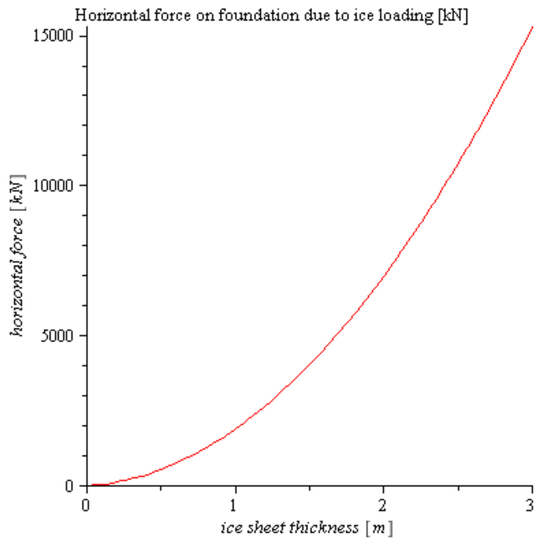

Figure 55, Relation ice sheet thcikness and horizontal force

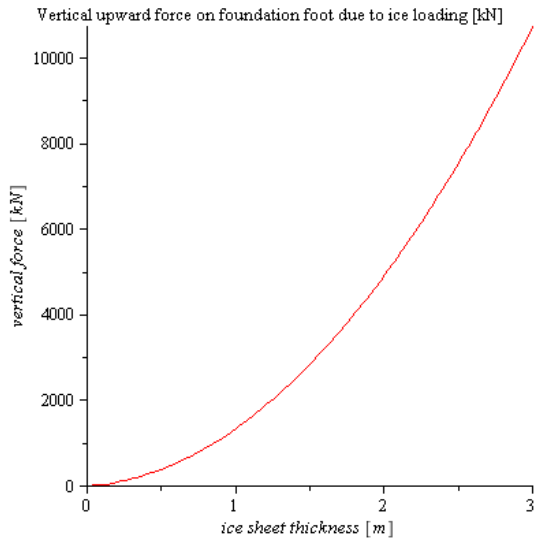

Figure 56, Relation ice sheet thickness and vertical force

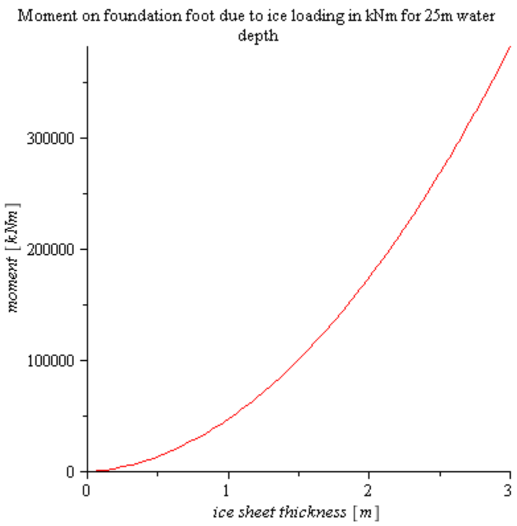

Figure 57, Relation ice sheet thickness and moment

13. DNV load combinations

The Norwegian norm DNV-OS-J101 describes for the environmental loads several load combinations. The DNV says:

> For design of the support structure and the foundation, a number of load cases for wind turbine loads due to wind load on the rotor and on the tower shall be considered, corresponding to different design situations for the wind turbine. Different design situations may govern the designs of different parts of the support structure and the foundation.
>
> The load cases shall be defined such that it is ensured that they capture the 50-year load or load effect, as applicable, for each structural part to be designed in the ULS. Likewise, the load cases shall be defined such that it is ensured that they capture all contributions to fatigue damage for design in the FLS. Finally, the load cases shall include load cases to adequately capture abnormal conditions associated with severe fault situations for the wind turbine in the ULS.

13.1 Design conditions and design situations

As mentioned there are in total 31 design conditions proposed to evaluate by designing an offshore wind turbine foundation. All these load cases refer to designs made for ULS and FLS. The table containing all the 31 design conditions is added in the appendix.
For the 31 design conditions in total 8 different design situations are specified. The 8 design situations are:

- Power production
- Power production plus occurrence of fault
- Start up
- Normal shutdown
- Emergency shutdown
- Parked (standing still or idling)
- Parked and fault conditions
- Transport, assembly, maintenance and repair

All these points describe different situations that could occur during the lifetime of the wind turbine. Each situation has is specific demands for the environmental loading parameters determined using specific models. These models are mentioned before in the chapter Calculation of wind forces. Since some of the design conditions certainly won't be governing for the loads on the foundation not all design combinations are investigated. Form the 31 design conditions only the conditions with an extreme wind speed or wave height are investigated. This are the load cases 2.3, 6.1a, 6.1b, 6.1c, 6.3b, 7.1b and 8.2a. These design situations are described as can be seen in the table below. The abbreviations of the wind and sea states can be found in the chapters for the calculation of wind and wave forces.

Design situation	Description
2.3	Power production plus occurrence of fault, EOG and NSS
6.1a	Parked, EWM with turbulent wind, ESS, 50-yr current and water level
6.1b	Parked, EWMl with steady wind, RWH, 50-yr current and water level
6.1c	Parked, RWM with EWH, 50-yr current and water level
6.3b	Parked, EWM with steady wind, RHW, 1-y current and water level
7.1b	Parked and fault condition, EWM with turbulent wind, ESS, 1-yr current and water level
8.2a	Transport, assembly, maintenance and repair, EWM, RWH, 1-yr current and water level

Table 9, Description of design situations used for calculations

For these 8 design situations three different water depths are evaluated, being 15, 25 and 35m. For the other load combinations it can be assumed that they will not be governing since they describe situations such as power production and start up conditions. For these conditions the parameters will not have their maximum value and thus won't result in the largest forces on the foundation but are more related to the turbine structure than to the foundation. The design situation with the highest environmental conditions for the foundation is the parked situation.

13.2 Environmental parameters used for design conditions

To be able to evaluate the design conditions which will have the most influence on the forces on the foundation three basic parameters have to be defined. From these parameters the parameters for the calculations for the design conditions can be derived using the formulas presented before. The basic parameters needed for calculation are:

- Wind speed with a return period of 50 years
- Significant wave height
- Spectral peak period

With these parameters the parameters needed for the design conditions can be derived. An overview of the parameters is presented in the following table.

$U_{10,1-yr}$	$0,8 \cdot H_{s,50-yr} = 28 m/s$
$U_{10,50-yr}$	$35 m/s$
$H_{S,1-yr} = E[H_S \mid U_{10,hub}]$	$6m$
T_{1-yr}	$8,7s$
$H_{S,50-yr}$	$7,2m$
T_{50-yr}	$9,5s$
1-yr water level	$\pm 1m$
50-yr water level	$\pm 2m$
1-yr current	$0,5 m/s$
50-yr current	$0,7 m/s$

Table 10, Parameters used for calculating design combinations

Most of the values presented are derived from graphs found in the document Wind and Wave Conditions from DOWEC[15] and the Offshore Wind Atlas by ECN[16]. The graphs used to determine the values presented above can be found in the appendix.

With the values above the previous mentioned design conditions are evaluated. The results are presented in the next paragraph.

[15] Wind and wave conditons, DOWEC Dutch Offshore Wind Energy Converter Project, Wim Bierbooms ed, Section wind energy, Delft University of Technology. DOWEC 47 rev. 2.

[16] Offshore Wind Atlas of the Dutch Part of the North Sea, J.A.J. Donkers, A.J. Brand and P.J. Eecen, Energy research Center Netherlands, march 2011

13.3 Results evaluation design conditions

With the use of the software maple and the calculation sheet for all the loadings involved on the structure the calculations are made for the different design conditions. Below the final results for the different water depths are presented. For a more detailed overview of the different contributions of the wind, wave and ice loadings reference is made to the appendix. For all the calculations made the ice loadings are included. Since the ice force is constant for a constant water depth the relation between the different design conditions is not changed if the ice loadings are not included.

Design conditions for 15m water depth

	2.3	6.1a	6.1b	6.1c	6.2a	6.3b	7.1b	8.2a
F_H [kN]	3959,12	4606,93	6434,70	8620,46	4606,93	4484,62	5759,16	6225,58
M [MNm]	63,60	89,51	144,20	129,85	89,51	94,35	105,62	120,66

Table 11, Design conditions for 15m water depth

Design conditions for 25m water depth

	2.3	6.1a	6.1b	6.1c	6.2a	6.3b	7.1b	8.2a
F_H [kN]	3360,41	4074,41	5716,72	7515,724	4074,41	3661,47	4670,58	5456,322
M [MNm]	81,0844	111,868	176,933	168,279	111,868	118,289	135,49	149,863

Table 12, Design conditions for 25m water depth

Design conditions for 35m water depth

	2.3	6.1a	6.1b	6.1c	6.2a	6.3b	7.1b	8.2a
F_H [kN]	3015,31	3753,13	5288,18	6869,988	3753,13	3257,37	4141,05	5009,423
M [MNm]	100,749	136,484	212,685	211,4023	136,484	144,763	168,847	182,2152

Table 13, Design conditions for 35m water depth

As can be seen from the tables above the range between the maximum and minimum force per design condition is quite significant. For all the three heights the relation between the design conditions is constant. For all the three water depths the first calculated design condition, condition 2.3 has the lowest resulting force on the foundation. This condition describes an extreme operating gust with a normal sea state during power production.
The design condition with the highest resulting forces on the foundation is also the same condition for all three water depths. This condition, condition 6.1b, describes the wind turbine during a parked situation. The wind speed during this situation is described by the extreme wind model and the wave height by the reduced wave model. This does not gives the highest wave heights, but in combination with the extreme wind speed the resulting forces are the largest for this combination.

Also the ratios between the horizontal forces and moments are investigated. As can be seen on the graphs on the next page the bending moment is the highest for design case 6,1b for the three evaluated water depths. This is not the case for the horizontal force. Here the largest horizontal force is for the load case 6,1c which represents a parked situation with a steady wind for the Reduced Wind Model. The wave height is an Extreme Wave Height with a recurrence period of 50 years.
The horizontal force for this design condition is higher because of the larger wave height that is used for the calculation. Since this higher wave force does not influences the bending moment that much the largest bending moment occurs for a different design condition.

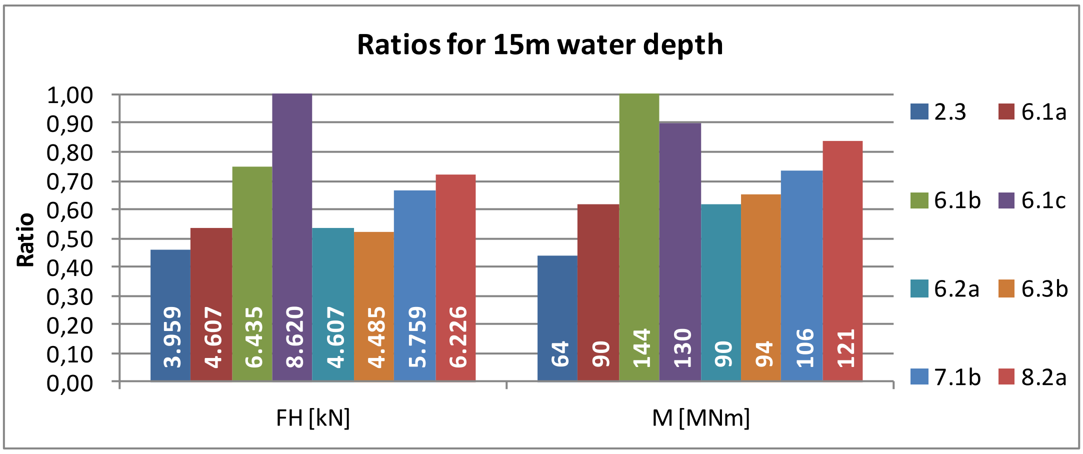

Figure 58, Ratios for different design conditions for 15m water depth

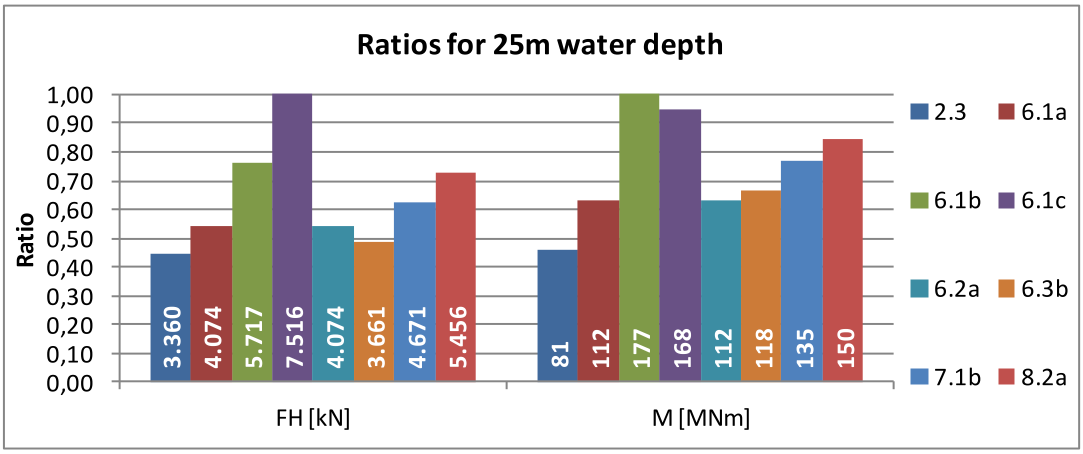

Figure 59, Ratios for different design conditions for 25m water depth

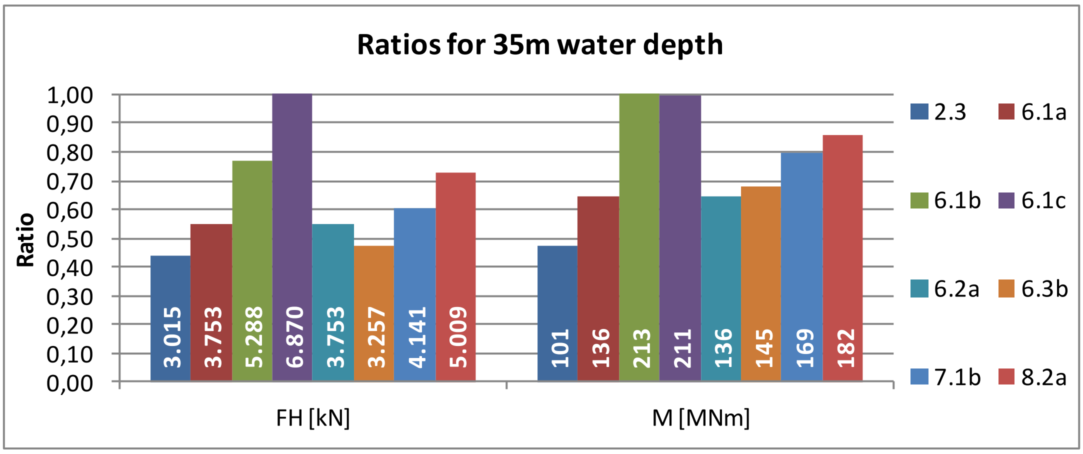

Figure 60, Ratios for different design conditions for 35m water depth

14. Determine force resistances and foundation dimensions

14.1 Input calculation

The governing calculation outcomes of the DNV Design Conditions evaluation are used as the input forces acting on the gravity base foundation. The governing bending moment and horizontal force are taken and a load factor of 1,35 is applied to obtain the ULS forces.
For the determination of the bending moment resistance of the foundation shaft also the bending moment at the interface between the foundation shaft and base is calculated. This is done because the interface between the shaft and base is the governing location for the bending moment resistance of the shaft. At larger depths the bending moment will be slightly higher, but due to the foundation base the bending moment resistance will also be larger.

For the dimensions of the foundation the following assumptions are made. The chosen dimensions are based on the Lillgrund wind farm foundation. The dimensions of this foundation are scaled to this study. Since for this part of the study the soil parameters are not investigated intensively a sea bed consisting of loose sand is assumed as seabed for the foundation.
Below the input for the calculations and the soil parameters are presented.

Parameter	Value	Unit
Water depth	25.000	mm
Effective bending moment in ULS at base	2,39E+11	Nmm
Effective bending moment in ULS at interface	2.13E+11	Nmm
Horizontal force in ULS at base	1,01E+07	N
Height shaft above water	3500	mm
Total height shaft	28.500	mm
Diameter shaft foundation	6.000	mm
Wall thickness shaft	750	mm
Diameter base foundation	19.000	mm
Thickness base slab	800	mm
Concrete used	C45/55	N/mm²
Reinforcement used	S500	N/mm²
Reinforcement bar diameter	Ø32	mm
Elasticity modulus steel	210.000	N/mm²
Elasticity modulus concrete un-cracked	32.500	N/mm²
Elasticity modulus concrete cracked		
$\alpha_e = E_s / E_c$ (un-cracked)	6,46	[-]

Table 14, Input parameters for design calculations

Parameter	Value	Unit
Internal angle of friction	35	°
Cohesion of soil	0	kN/m²

Table 15, Soil parameters for foundation

With these parameters calculations are executed for the bending moment resistance of the foundation, the crack width in the shaft, the turning over resistance of the foundation, the buckling of the shaft and the compressive strength.

For the turning over resistance of the foundation it is calculated what the mass of the foundation should be and how much ballast weight has to be added to the self weight of the foundation.

The results of this dimensioning of the foundation are the input for the following part of this study, a geotechnical study. The dimensions and weights of the finally designed foundation are the important input parameters for the geotechnical part since the focus for this part lies on the behaviour and bearing capacity of the soil where the foundation is installed on.

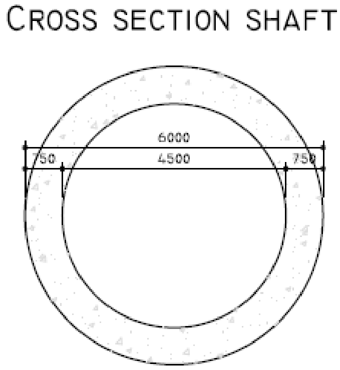

Figure 61, Cross section of foundation shaft

14.2 Calculation ultimate bending capacity

As stated in the table presented the ULS bending moment at the governing interface between the foundation shaft and base is $M_{ED} = 2.13 \cdot 10^{11}\,Nmm$. For the calculation of the bending moment resistance the self weight of the structure is not regarded which is a conservative assumption.

To determine the surface and lever arms with respect to the centre of gravity of the foundation shaft use is made of the following formula[17]: $A_a = \frac{1}{2}\frac{D^2}{4}(\theta_1 - \sin\theta_1) - \frac{1}{2}\frac{d^2}{4}(\theta_2 - \sin\theta_2)$ where

$\theta_1 = 2\tan^{-1}\left(\frac{\sqrt{\frac{D^2}{4} - y^2}}{y}\right)$ and $\theta_1 = 2\tan^{-1}\left(\frac{\sqrt{\frac{d^2}{4} - y^2}}{y}\right)$. All notations are also visible in the figure below.

The bending moment capacity is calculated by first estimating a reinforcement ratio based on a rough calculation and subsequently calculating the needed concrete compressive zone to resist the bending moment. Because of the circumferential reinforcement the area of the foundation shaft where the reinforcement yields is equal to the concrete compressive zone. This only holds when the concrete compressive zone is smaller than $\frac{1}{2} \cdot D$ which is expected to be the case.

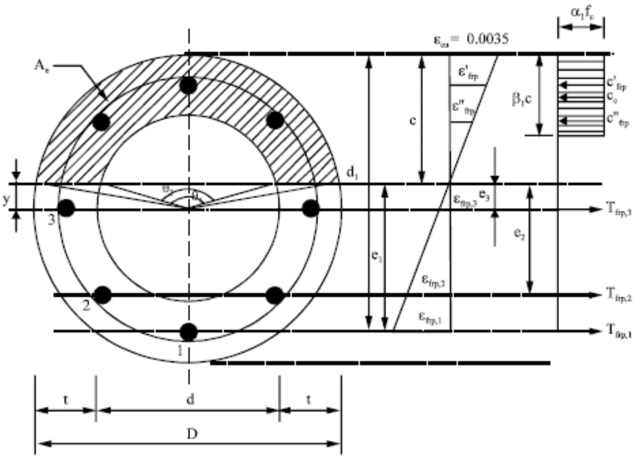

Figure 62, Concrete hollow section under bending

14.2.1 Calculation of needed reinforcement

As a first estimate of the needed reinforcement a rough calculation is performed. From this calculation it follows that an estimate for the needed reinforcement is $A_s = 10850 mm^2 / m'$. When a double reinforcement layer of $\varnothing 32 - 150$ is chosen the amount of reinforcement is

[17] N. Taranu, G. Oprisan, M. Budescu and I. Gosav, 2009. Hollow Concrete Poles with Polymeric Composite Reinforcement. *Journal of Applied Sciences, 9: 2584-2591.*

$A_s = 10723 mm^2 / m'$. With this amount of reinforcement the needed compression zone is calculated which is needed to withstand the bending moment. As mentioned before the amount of reinforcement that yields is related to the concrete compression depth. When this is assumed a conservative calculation is performed since the area unde tension could be larger in practice.The calculations performed with Maple are visible in the appendix.
For the concrete compression zone it is assumed that one half of the concrete compression zone is stressed past the linear strain and has a stress of $f_{cd} = \frac{45}{15} = 30 N / mm^2$. The other half of the concrete compression zone is loaded within the linear elastic domain and has an average stress of $\frac{f_{cd}}{2} = 15 N / mm^2$. With these stresses and the weighted surface the distance to the centre of gravity is calculated. Since it is assumed that the reinforcing steel is yielding over the full tension area the distance to the centre of gravity is calculated as the weighted centre of the shaft area in tension.

Using the calculation sheet is it found that a concrete compressive depth of $1136mm$ is needed to withstand the bending moments. The resulting concrete compressive force and steel yield force are: $N_c = 6.63 \cdot 10^7 N$, $N_s = 1.91 \cdot 10^7 N$ with the corresponding distance to the centre of gravity: $d_c = 2533mm$, $d_s = 2384mm$. These forces and distances to the centroidal axis are resulting in an bending moment resistance of $M_{RD} = 2.13 \cdot 10^7 Nmm$ which is equal to the M_{ED}. All forces and distances can be viewed in the figure besides.
It is noticed that the distance to the centroidal axis for the compressive zone d_c is not equal to d_s because the zone is half under plastic loading and half under linear elastic loading.

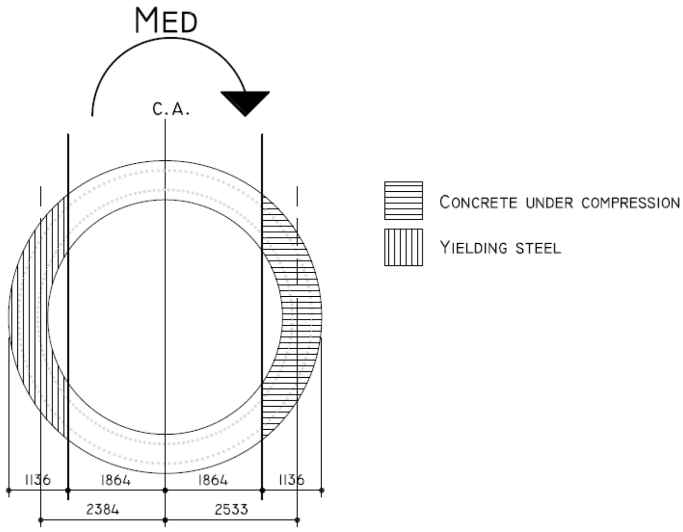

Figure 63, Cross section shaft under bending moment

14.3 Calculation of maximum crack width

With the calculated reinforcement and forces the crack width for the critical section in the foundation shaft can be calculated. This is done using the following formula for the stabilized cracking stage:

$w_{max} = \frac{1}{4} \frac{f_{ctm}}{\tau_{bm}} \frac{ø}{\rho} \frac{1}{E_s} (\sigma_s - \sigma_{sr})$ where $\frac{f_{ctm}}{\tau_{bm}} = 0,5$, $ø = 32mm$, $\rho = \frac{A_s}{A_c} = \frac{2 \cdot 804}{750 \cdot 150} = 1,43\%$,

$E_s = 210.000 N / mm^2$, $\sigma_s = \frac{M_{ED}}{A_s \cdot z}$ and $\sigma_{sr} = \frac{f_{ctm}}{\rho}(1 + \alpha_e \cdot \rho) = 290 N / mm^2$.

For the force the SLS value is taken since the crack width is a SLS requirement. The effective moment for the SLS is: $M_{ED} = 1,58 \cdot 10^{11}$.

Since the turbine foundation is subjected to dynamic loads in an aggressive environment it is advised to limit the crack width to $0,1mm$ if possible. It was calculated that with the designed reinforcement it is not possible to obtain a maximum crack width of max $0,1mm$. For the calculated reinforcement of $2{\cdot}\varnothing 32-150$ the smallest obtainable crack width is $0,18mm$, which also meets the requirements in the Eurocode for construction in an aggressive environment.The calculated crack width is determined with an average steel stress. When the extreme steel stress in the outer fiber is calculated the crack width may be higher and tend towards 0,20mm. To obtain a smaller crack width the reinforcement bar diameter should be reduced and the amount of reinforcement increased.

14.4 Calculation compressive force resistance of concrete shaft

As calculated before the bending moment exerted on the foundation is resisted by a force couple in the shaft of the foundation. This couple causes tensile force on one side, resisted by the reinforcement, and a compressive force on the opposite side that is resisted by the concrete under compression. Therefore a calculation is done to determine the compressive force resistance of the part of the shaft that is under compression. Since a concrete is used with class C45/55 the design compressive strength of the concrete is $f_{cd} = \frac{f_{ck}}{\gamma_m} = \frac{45}{1,5} = 30N/mm^2$. The compressive force calculated in the SLS has a magnitude of $F_R = 5,13{\cdot}10^7\,N$. The area under compression during loading in de SLS was calculated as $A_c = 4,57{\cdot}10^6\,mm^2$. With the given force F_R the average loading of the concrete cross section is $\sigma_c = \frac{5,13{\cdot}10^7}{4.57{\cdot}10^6} = 11,2N/mm^2$. Since the maximum allowable stress is $30N/mm^2$ it is concluded that the foundation shaft is able to withstand the compression force. The perimeter length of the area under compression is calculated as: $L_{compr} = 6093mm$.

14.5 Calculation of turning over resistance and ballast needed

For the calculation of the turning over resistance and the ballast needed to prevent turning overuse is made of the ULS bending moment on the foundation base. This moment $M_{ED} = 2,39{\cdot}10^{11}\,Nmm$ is resisted by the mass of the foundation since the foundation is a gravity base foundation. The mass of the concrete part of the foundation is deducted from the calculations made for the Lillgrund foundation. For the turbine the data for the 5MW reference turbine is used. The total mass of the foundation is 1.261 tonnes without an ice cone and 1.836 tonnes with an ice cone. The total mass for the reference turbine structure Is 757 tonnes. This makes a total dead weight of the foundation without ballast of 2.018 tonnes for a foundation without ice cone and 2.593 tonnes for a foundation with an ice cone.

With the given bending moment it is calculated what the bending moment resistance should be to prevent turning over. The bending moment resistance comes from the mass of the foundation. To be able to calculate the bending moment resistance it is needed to determine the point of rotation for the foundation. At first it can be estimated that the point of rotation is the most outer point of the foundation, but this is not expected to be the practice. The resultant force of the soil under compression is taken as the point of rotation. To find the final ballast weight needed some iteration has to be done for the rotation point and the needed mass for the foundation.

To determine the point of rotation a stress analysis is made for the self weight of the foundation and the bending moment. By doing so the location of the resulting force and thus the point of rotation is determined. As a first attempt this is done with assuming that the point of rotation is the most outer point of the foundation. For the self weight F_{DW} and the moment M_{ED} a stress diagram is drawn and the needed self weight is calculated. With the stress diagram it is determined what the point of rotation is. Because of the change of the point of rotation the needed self weight changes and the calculation is repreated with the new point of rotation. After some iteration steps the equilibrium between self weight and point of rotation is found. These final values are presented in the table on the next page. The final value that is found for the self weight is divided by 0,9 to obtain the ULS value. This is because the self weight has a positive effect on the force resistance.

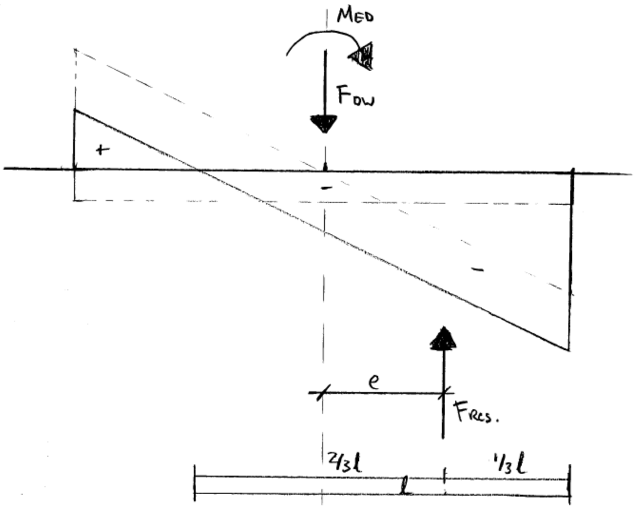

Figure 64, Stress in subsoil foundation

Parameter	Value	Unit
Bending moment	2,39E+11	Nmm
Point of rotation measured from centre	4.460	mm
Self weight needed in ULS	5.951	Tonnes

Table 16, Outcomes for calculation turning over resistance

With the previous calculated self weight of the concrete foundation and the turbine structure it can be seen that ballast has to be added to the foundation in order to meet the total needed self weight. The ballast weight needed for the foundation without ice cone and with ice cone is visible in the table below.

Foundation	Self weight concrete + turbine	Needed self weight	Ballast needed
Foundation without ice cone	2.018	5.951	3.933
Foundation with ice cone	2.593	5.951	3.358

Table 17, ballast needed for foundation, all weights in tonnes

Now that the ballast needed is determined it is calculated what the volume of ballast is needed. For ballast material iron ore is chosen. This ballast material is widely available and has a self weight of 3,2 tonnes per m^3[18]. With this ballast material it can be calculated that the ballast volume needed for the foundations is:

Foundation	Weight ballast needed [t]	Volume ballast needed [m^3]
Foundation without ice cone	3.933	1.229
Foundation with ice cone	3.358	1.049

Table 18, Volume of ballast needed

Since this volume is larger than the volume that is available in the foundation the design of the foundation needs to be adapted. It is calculated that an increase of the foundation with 1,5 meters

[18] http://www.debinnenvaart.nl/binnenvaarttaal/lijsten/sd-ladingen.html

gives enough volume to put the ballast. Because of the increase in diameter the ballast needed is also decreased to 1.099 and 919 m³.

14.6 Calculation of horizontal sliding resistance

The foundation is besides the bending moment also loaded with a horizontal force. This horizontal force can cause sliding of the foundation over the sea bed. To determine if the sliding resistance is sufficient calculation provided by the DNV are done. Since it is assumed that the soil underneath the foundation consists of cohesion-less sand the following soil parameters can be assumed:

$C \quad = \quad 0 \qquad$ (Cohesion factor)

$\varphi \quad = \quad 35° \qquad$ (Angle of internal friction)

With these values and the formula for the horizontal resistance $H_R = A_{c,eff} C + V \tan(\varphi) = A_{C,eff}\, 0 + 5{,}36 \cdot 10^7 \tan(35°) = 3{,}75 \cdot 10^7\, N$. Since the effective horizontal force has a magnitude of $1{,}01 \cdot 10^7\, N$ the unity check for the horizontal sliding resistance becomes:

$UC = \dfrac{F_{ED}}{F_R} = \dfrac{1{,}01 \cdot 10^7}{3{,}75 \cdot 10^7} = 0{,}27$. As can be seen the unity check is below zero and thus the foundation is able to resist the horizontal force for the sliding capacity.

14.7 Calculation of ice cone dimensions

To determine the dimensions of the ice cone on the top of the foundation it is needed to know the parameters of the sea ice and the differences in sea level. For locations where sea ice can occur, such as the Baltic sea the differences in water levels during the winter period are 2,1m (+1,09 and -1,03m)[19].This means that the sea level where the sea ice can occur differs with 2,1 meters and thus the ice cone should have a inclined height that is larger than this variance in water level. The centre of the inclined part of the ice cone should thereby be placed around the Mean Sea Level.

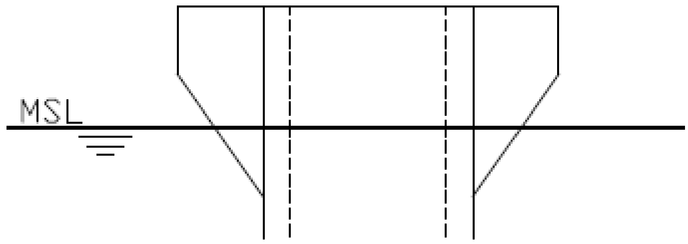

Figure 65, Ice cone layout for foundation

The inclination angle of the ice cone needs to be determined on basis of the design wave load and the design ice load. The DNV-OS-J101 advises to adjust the inclination angle of the ice cone such that the design ice load is just less than the design wave load. Following from the calculations made for the DNV Design Conditions it holds that the design ice force is much lower than the design wave force. (respectively 3.333kNm and 53.328kNm).

14.8 Calculation dimensions gravity base foundation

With the calculated forces and ballast needed the needed dimensions of the gravity base foundation can be determined. As shown before the diameter of the base is adjusted to provide space for the needed ballast storage. The diameter of the shaft is fitted to the diameter of the reference turbine tower diameter. This diameter is set to 6m. The diameter of the base becomes 20,5m as calculated before. The height of the base walls is 3m. An eventual ice cone has a width of around 2,5m and a height of 5,5m. The layout of the foundation is visible in the figure below. In the appendix the drawing is visible on larger scale.

[19] Kriegers Flak Offshore Wind Farm, Site Assessment

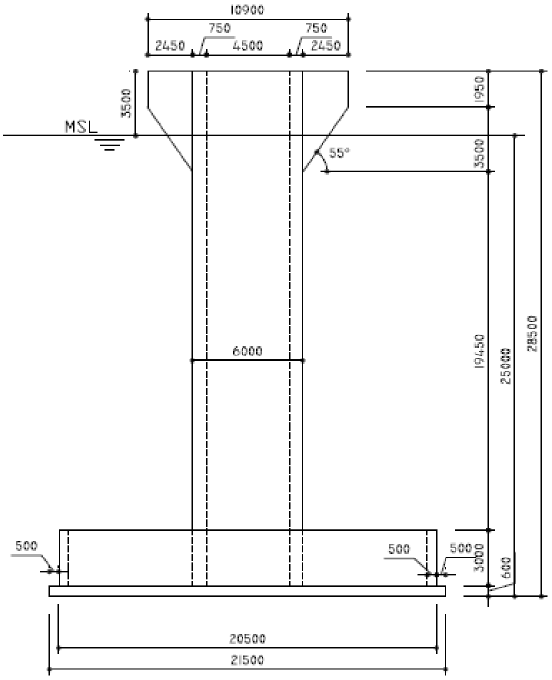

Figure 66, Sketch of foundation with dimensions

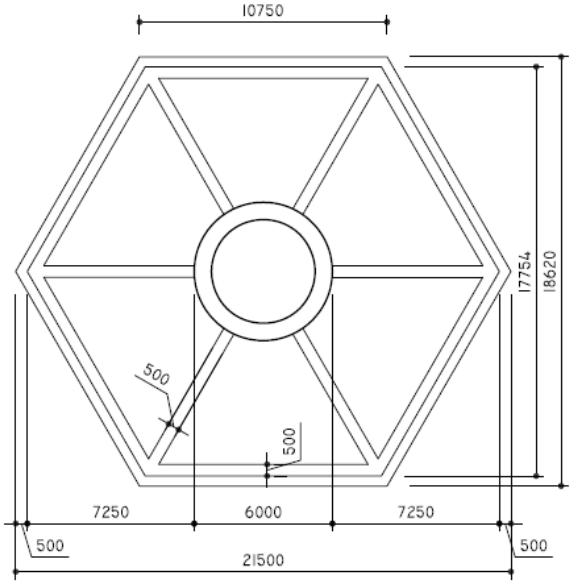

Figure 67, Top view of foundation base

For this foundation the final volumes and weight of the different components are determined and listed in the table on the next page. As can be seen in the table the volumes and thus weights of the foundation differ slightly with the assumed values. But since these differences are quite small these differences are accepted.

Part		Volume [m³]	Mass [tonnes]
1	Base plate	180	450
2	Outer wall base plate	92	231
3	Inner walls base plate	80	200
4	Shaft	185	462
5	Ice cone	224	560
	Total with ice cone:	**761 m³**	**1.903 tonnes**
	Total without ice cone:	**537 m³**	**1.343 tonnes**

Table 19, Volume and weight of different parts of foundation

15. Conclusions

This variance study has the aim to get an insight in the influence of the forces acting on the wind turbine structure. This is done by defining a standard turbine which is used for the calculations and by investigating the different calculation rules.
Based on the formula's for the different wind and wave conditions formula's it can be concluded that a wide range of aspects has to be taken into account. All the design conditions relate to dynamic loadings or specific parts of the turbine structure. Since this study mainly focuses on the static loadings on foundation of the turbine structure not all the design conditions are relevant for this study. The design cases involving extreme wind speeds, wave heights or sea states have the most impact on the foundation and thus these cases are primarily focussed on.

At the evening lecture Designing a Wind Turbine from the Concrete Association (Avondcollege Windmolenontwerpen) indicative data for the moments on a turbine structure are obtained from a Siemens engineer. With the aid of this data it is checked if the calculations made resemble with the indicative data provided by Siemens. From this comparison it can be seen that for the smaller and lower turbines the difference between calculated and given forces is quite significant with a difference of almost 30%. For the data of the largest turbine the difference between the given and calculated data is only 5%. It can be concluded that for smaller turbines it is likely that other loads have a relative large influence on the total forces when compared to larger and higher turbine structures.

Since the major loadings on the offshore turbine structures are wind and/or wave related it is investigated what the significant and extreme values of these parameters are for various locations in the seas in the North-West part of Europe. Evaluating these data it is shown that there are significant differences in wind speed and wave height for the various locations. Moreover it is found that the significant maximum wave heights are lower for seas surrounded by land. For the mean wind speeds it also holds that for locations where the governing wind speed direction is not obstructed by near land the mean winds speeds are slightly higher. Thereby it should be remarked that the differences in wind speeds are smaller than for the wave heights.

An aspect that also is regarded is the accidental loading. For this accidental loading a ship impact is regarded. When the bow force of a colliding ship is calculated it is found that the force for a large 270.000 tonnes vessel is larger than 300MN. This is a factor 100 higher than the horizontal forces from the environmental loadings. Therefore it is stated that the turbine structure probably will not withstand these high loadings. Therefore the collision with a ship should be prevented.

To get an insight into the influence of different environmental and turbine properties on the forces on the structure an analysis is made. Therefore the parameters are changed and the outcomes of the calculations with the changed parameters are compared. From these analyses it can be seen what the major force components are and what the influence is on the force when a parameter is changed. The most significant outcome of this analyse is the ratio between the forces due to wind and due to wave loadings. For the horizontal force the wave loading is the dominating part of the total force. But when the bending moment is regarded it can be seen that the moment due to wind loading is an order 10 larger than the moment due to wave loading. This is due to the fact that the wind forces are having a high point of action compared to the wave forces. This thus results in higher moments for the wind loadings. Also the relation between the wave forces on the foundation shaft and base are investigated and it is found that the shaft forces are almost solely dominating the moments due to wave loadings. This is due to the dimensions of the foundation and the

hydrodynamic principles involved with this foundation dimension. Because of the relative small shaft diameter the loading on the foundation is inertia dominated.
Also the individual influence of the environmental and structural parameters is investigated. This is done by a graphical representation of the forces for varying parameters. One remarkable outcome is the fact that the horizontal wave forces decrease for an increasing water depth. This is due to the geometry of the foundation. When the water depth is larger the loadings on the large diameter of the base decrease. This decrease is larger than the increase of the forces on the shaft and thus the total horizontal force decreases for constant geometry of the foundation.

What is mentioned in the analysis is the relation between the wave height and the wave period. Since the increase of solely the wave height has a large influence on the forces on the foundation it is noticed that an increase of the wave height is coupled with an increase of the wave period. This larger wave period causes for a decrease of the forces on the foundation. Therefore it is mentioned that for the wave calculations always the wave height with its associated wave period should be used.

Since the foundation is dominated by inertial wave forces it is calculated that the currents do not have a large influence on the foundation loadings. Since the current has a constant speed this flow of water only induces drag forces which are very small.
When the wind forces are investigated it can be seen that the wind speed has a large influence on the total loadings. Since the wind force is the major load component for the bending moment an increase in the wind speed causes a large increase in the forces on the foundation. Also the structural parameters involved with the wind speed have significant influence on the total forces. Specific the tower height and the rotor diameter have a large influence.

A very location specific loading is the environmental ice loading. This loading only occurs on locations where an ice layer on the sea can arise. The horizontal forces of this ice sheet can be reduced by an ice cone. This cone breaks the ice downwards and so reduces the horizontal load of the ice. Even though this ice cone reduces the horizontal force and thus the moment still large forces can be exerted by the ice when the ice sheet thickness is large. The bending moment for increasing ice forces increases very rapidly. Therefore it is advised to not apply wind turbines on locations with large ice sheet thicknesses.

In the DNV-OS-J101 in total 31 design conditions are described. These design conditions make use of the earlier mentioned wind and wave models. Since not all the design conditions are related to the foundation some specific design cases with high wind and/or wave loads are evaluated. As can be seen from the results for de different design conditions the design conditions with the highest horizontal force is not the same as the design condition with the highest bending moment. For all the three evaluated water depth the maximal horizontal force and bending moment Both the maximum horizontal force and the bending moment occur for parked conditions. In these conditions the turbine is standing in parked mode and not producing electricity. This is often due to high wind speeds.

With the results from the design situations a study is done for the dimensions of the gravity base foundation of an offshore wind turbine. It is found that for a shaft with an amount of reinforcement of $2 \cdot \varnothing 32 - 150$ is sufficient to withstand the governing bending moment at the interface between the foundation shaft and base. Furthermore it is calculated that the maximum crack with for this amount of reinforcement is $w = 0{,}18mm$. This crack width is sufficient according to the Eurocode, although a crack width of $w = 0{,}1mm$ is more desirable due to the fatigue properties of the foundation.

15.1 Resume

In brief it is found that the major force influencing the design of the Gravity Base Foundation is the wind force. This is mainly due to the high lever arm of the forces with respect to the foundation base. An increase of the wind speed and the seize of the rotor are thus highly influencing the bending moments on the foundation. The bending moments due to wave forces are of an order 10 smaller than the bending moments caused by wind loads. Because the wave loads are inertia dominated only the wave height is influencing the wave loads and that current loadings are having a negligible contribution.

When the design conditions of the DNV are evaluated it is found that the parked situations are leading to the highest forces on the foundation. When these forces have to be resisted by the foundation a reinforcement of $2 \cdot \varnothing 32 - 150$ is needed. This reinforcement leads to a mean crack width of 0,18mm which is just within the limits stated in the Eurocode. For fatigue properties it is more desirable to limit the crack width to 0,10mm which should result in an increase of the reinforcement.

Part 2 – Geotechnical study

16. Introduction

The second part of this graduation study for Gravity Base Foundations is related to the subsoil of the foundation. Since a GBF is placed on top of the subsoil all the forces acting on the turbine and foundation are transferred to the subsoil by the GBF and soil interface. Due to the heavy weight of the total structure and both high static and dynamic loadings of the GBF structure the properties of the subsoil are of major importance for the applicability of GBF's for offshore locations.

The first part of this study has calculated the bearing capacity of the soil using the formulas presented by the DNV. These hand calculation formula's are very conservative when it comes to calculating the bearing capacity of the subsoil. Since these formula's do not incorporate the stress increase in the subsoil during loading the calculated bearing capacity is lower than it is in reality. To calculate the bearing capacity more accurate use is made of geotechnical software. This software incorporates the stress increases in the subsoil and thus is giving more realistic results. It is expected that the bearing capacity of the soil models will increase due to the use of the geotechnical software.

On the other hand the DNV formulas and the used software are only dealing with static loads and do not take dynamic loadings into account If this dynamic behaviour of the loads is incorporated it will reduce the bearing capacity of the foundation calculated using the static forces. At the end, when the bearing capacity is calculated with the use of the geotechnical software for both static and dynamic loads it is expected that a safety factor is obtained that has a comparable magnitude when compared to the safety factors obtained by hand calculations. In this geotechnical study it is presented what the safety factors will be for both the static and dynamic calculation methods.

16.1 Elements discussed in this geotechnical study

In this part of the study it is aimed to present a study on the influence of various soil parameters on the bearing capacity of the Gravity Base Foundation. This geotechnical study will involve different aspects of the bearing capacity of an offshore foundation.

As discussed in the first part of this thesis the bearing capacity of sand only is not sufficient to bear the GBF under extreme loadings. Therefore an analysis is made on the influence of three different parameters on the bearing capacity. These parameters are the base diameter of the GBF, the overburden depth and the internal angle of friction of the sand.

Secondly the bearing capacity of different types of soil is investigated. By applying the formula's of Brinch Hansen presented in the DNV for the bearing capacity of uniform soil layers it is calculated what the bearing capacity is for three different types of clay soils.

All these investigations of the bearing capacity of the foundation are done for uniform soils. Since in the field not all soils will be uniform a major part of this geotechnical study relates to multi layered soils. This means that more than one type of soil is present. Since the formula's of Brinch Hansen are only applicable for uniform soil layouts use is made of specialized geotechnical software. With the help of this software the influence of clay layers in the sand soil stratum is investigated.

The last part of this geotechnical study will discuss the bearing capacity during dynamic loading. Since the behaviour of the soil is different between static and dynamic loading also the dynamic properties of the subsoil are investigated.

17. Calculating bearing capacity of subsoil

For calculating the bearing capacity of the soil use is made of the bearing capacity formula's from the DNV. The bearing capacity of the subsoil is calculated for the stability of the foundation under extreme loads. Due to the combined loading of the vertical force and the bending moment an eccentricity is created for the resulting bearing capacity and the centre of the foundation.

This eccentricity reduces the effective bearing area of the foundation and thus reduces the total bearing capacity. The DNV-OS-J101 has added in Appendix G calculations for the bearing capacity for gravity base foundation. The annex distinguishes three different aspects for the calculation of the bearing capacity. First the forces and resulting from these forces the eccentricity has to be calculated. With this eccentricity and the dimensions of the foundation the effective foundation area can be calculated. When this area is known and the specific soil parameters are known the bearing capacity of the soil underneath the foundation can be calculated.

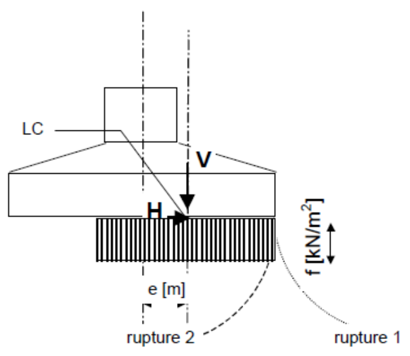

Figure 68, Eccentricity of load centre for combined loading

17.1 Parameters used for calculation of bearing capacity

To be able to calculate the bearing capacity of the soil some parameters have to be set. These are the forces acting on the foundation that are obtained previously and also the soil properties of the seabed. For the calculations it is assumed that the soil type is sand. The assumed parameters are listed below. All the soil parameters used in this geotechnical study are obtained from the NEN6740, table 1. This table is added in the appendix at the end of this document.

Parameter	Value
Effective bending moment M_d	2,40e10 Nmm
Effective vertical force V_d	74.670 kN
Effective horizontal force H_d	10.891 kN
Type of soil	Medium sand[20]
Unit weight γ of soil type	18 kN/m³
Unit weight γ_w of water	9.81 kN/m³
Angle of internal friction ϕ	32,5°
Cohesion c of soil	0 kN/m²
Overburden layer thickness h	0 m
Overburden pressure p_0'	0 kN/m²
Outer radius of foundation	21,5 m
Inner radius of foundation	18,6 m

Table 20, Parameters used for bearing capacity calculations

[20] Soil reference values obtained from NEN6470, table 1

17.2 Foundation loading and effective foundation area

The formula's presented in the DNV-OS-J101 are based on the calculation method of Brinch Hansen. To use the formulas presented by Brinch Hansen the eccentricity of the load and the effective foundation dimensions have to be calculated. For Gravity Base Foundation presented in the previous table the eccentricity of the force becomes $e = \frac{M_d}{V_d} = \frac{2,40 \cdot 10^{11}}{7,647 \cdot 10^{7}} = 3134mm$.

With this eccentricity also the effective foundation area of the GBF is calculated. The resulting effective dimensions of the GBF are an effective width of $b_{eff} = 10,5m$ and an effective length of $l_{eff} = 15,0m$ which results in an effective foundation area of $A_{eff} = 157,8m^2$. The exact calculation of the eccentricity and the effective foundation area can be found in the appendix at the end of this document.

17.3 Calculation bearing capacity of foundation soil for drained conditions

With the calculated effective foundation area and the known vertical load of the foundation the bearing capacity of the foundation subsoil can be calculated. The formulas used in this paragraph are only valid for drained conditions for the subsoil.

The formula used is a variation on the Prandtl formula by Brinch Hansen. The formula consists of three parts. The first part incorporates the bearing capacity of the soil itself, the second the bearing capacity due to an effective overburden pressure by the adjacent soil and the last part incorporates the bearing capacity due to the cohesion of the soil. The formula also takes into account a possible inclination of the load and the shape of the loaded area. The total formula stated by Brinch Hansen is: $q_d = \frac{1}{2}\gamma' b_{eff} N_\gamma s_\gamma i_\gamma + p_0^{'} N_q s_q i_q + c_d N_c s_c i_c$

where $N = \text{bearing capacity factor, } s = \text{shape factor and } i = \text{inclination factor}$.

With the calculated eccentricity and effective foundation dimensions the various factors can be calculated. Since the soil used to perform the drained soil calculations is cohesionless and no overburden depth is applied only the first component of the Brinch Hansen formula results in effective bearing capacity.

The result of the performed calculation for q_d results in a bearing capacity of $q_d = 209kN/m^2$. When this value for q_d is multiplied with the effective foundation area the bearing capacity of the total bearing capacity of the GBF is calculated: $R_d = q_d \cdot A_{eff} = 209 \cdot 157,8 = 32.944kN$. This is smaller than the effective vertical force of $V_d = 76.470kN$ and thus the soil is not able to bear the foundation with the given foundation diameter. A full calculation is placed in the appendix.

17.4 Increase the bearing capacity of the foundation

Because the insufficient bearing capacity of the subsoil of the foundation it is necessary to increase the bearing capacity of the foundation. This can be done in two ways if it is assumed that the soil conditions are held constant.

The first possibility to increase the bearing capacity is to embed the foundation in the soil. By doing so an overburden pressure is created. This overburden pressure is denoted in the bearing capacity formula as p_o'. The overburden pressure by the soil can be calculated as $\gamma' \cdot h$ where γ' = effective soil weight and h =thickness of soil layer above foundation foot as can be seen in the figure. To increase the bearing capacity of the soil to such an extent that it is capable of bearing the total vertical load the overburden layer should have a thickness of at least 3,1m.

A second way to create an overburden pressure is to apply skirts for the foundation. When skirts are applied they penetrate into the seabed and are confining a block of soil. Applying these skirts has the same effect as embedding the foundation if the distance between the skirts is designed in such a way that it is ensured that the confined soil displaces as a rigid body during plastic failure of the foundation[21]. This is illustrated in the figure below.

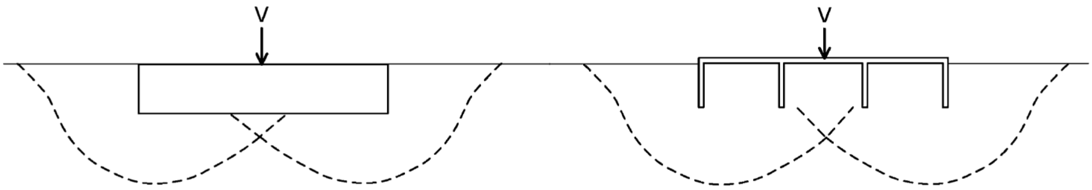

Figure 69, Slip circles for solid foundation (left) and skirted foundation (right)

An overview of a foundation with an overburden and a foundation with skirts is visible in the figures on the next page.

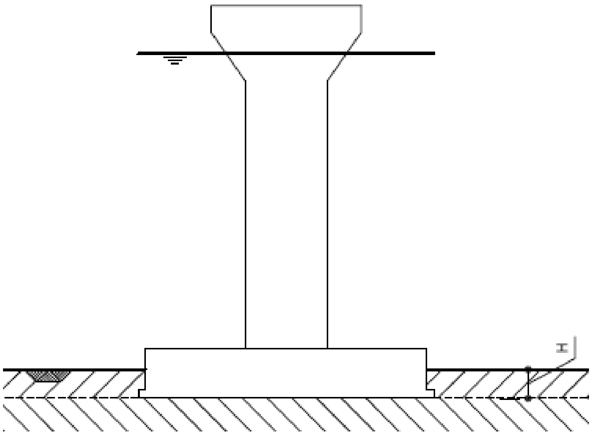

Figure 70, Overburden height H to increase bearing capacity

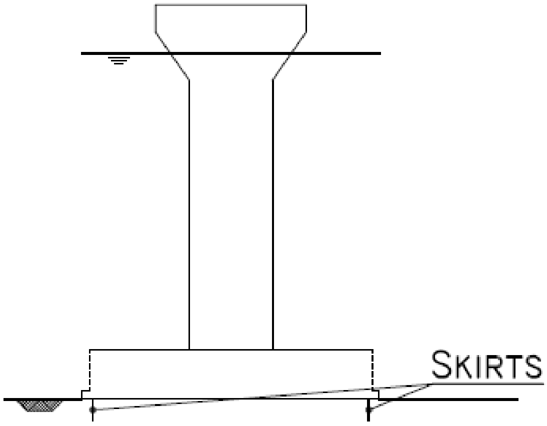

Figure 71, Skirts for foundation to increase bearing capacity

The second possibility to increase the bearing capacity of the foundation is to increase the foundation diameters such that the effective foundation area increases. Therefore the total bearing capacity increases as well. To obtain a sufficient bearing capacity to be able to withstand the effective vertical force calculated the radius of the foundation should be at least 26,7m instead of the previously assumed 21,5m.

Both increasing the overburden depth and the foundation diameter will have effect on the loadings on the foundation. When the foundation is embedded in soil the foundation height should be increased to keep the same height above the sea bed. Therefore also the bending moments on the foundation foot will increase as well as the total weight of the foundation. The horizontal forces on the base of the foundation will decrease since the height of the base above the soil bed decreases.

[21] Mana, Divya SK, Susan Gourvenec, and Christopher M. Martin. "Critical skirt spacing for shallow foundations under general loading." Journal of Geotechnical and Geoenvironmental Engineering 139.9 (2012): 1554-1566.

Increasing the foundation diameter results in a higher horizontal loading on the foundation base due to the increased surface of the foundation base. The larger surface will result in a higher horizontal force. Also the mass of the foundation will increase. The effect on the bending moment is limited due to the small lever arm. When one of these two options is used increasing the bearing capacity it should be noticed that this will require a recalculation of the design forces acting on the foundation.

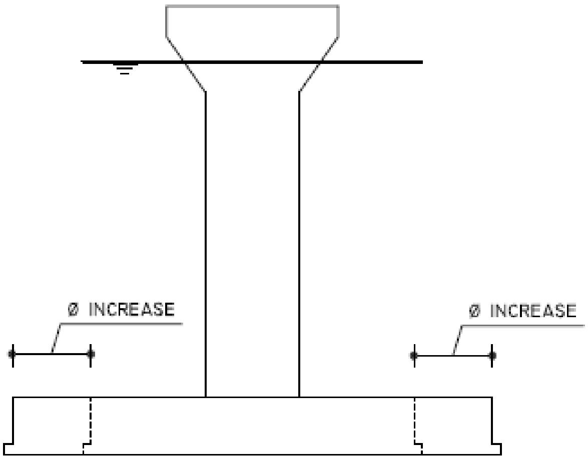

Figure 72, Increase of diameter to increase bearing capacity

Another option to obtain a higher bearing capacity of the foundation is to choose or create a location with other soil parameters. The parameter that has a large influence on the bearing capacity is the angle of internal friction of the soil material. When a soil material with a high density is chosen both the internal angle of friction as the unit weight of the soil are increased. An increase in those two parameters (γ and ϕ) also results in an increase of the total bearing capacity of the soil. For the case used in this study it is calculated that when sand with an internal angle of friction of $\phi = 38,3^o$ is used as subsoil for the foundation the total bearing capacity is large enough to withstand the effective vertical loading. This means that highly dense sand is needed to bear the foundation. This high dense sand can be obtained by searching to a location with better soil conditions or by applying soil improvements. This latter option is discussed later in this chapter.

17.5 Sensitivity analysis for various measurements

As described before there are several options to increase the bearing capacity of the foundation subsoil. In this chapter it is aimed to investigate the sensitivity of the bearing capacity formulae to a change in the soil parameters. For this sensitivity analysis the following soil parameters are varied: The angle of internal friction of the subsoil, the diameter of the foundation base and the overburden depth of the foundation.

17.5.1 Varying the angle of internal friction

For this variation the angle of internal friction is varied within the limits that are expected to be prevailing on the North Sea. This range is from 30° to 42°. This is the range for normally packed soil to highly dense packed soil. The results for the calculations are placed in the graph beside. From this graph it can be seen that the bearing capacity increases exponential when the internal angle of friction is increased. As mentioned before two options to increase the internal angle of friction of the subsoil is by changing the foundation location or by soil improvement. Possibilities for offshore soil improvement are the application of sand compaction piles and grouting of the subsoil[22]. These measurements will result in an

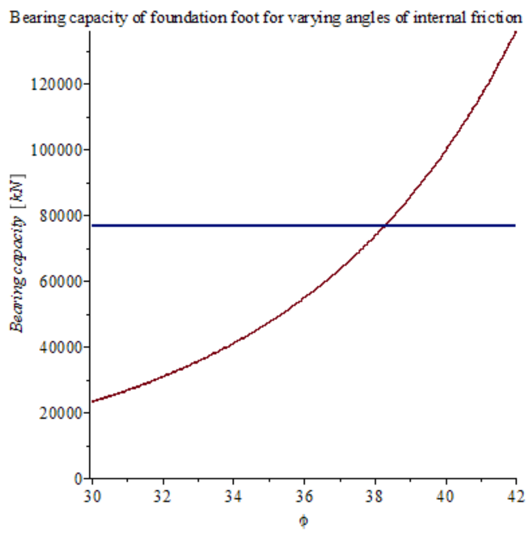

Figure 73, Bearing capacity for varying angle of internal friction

[22] Raju, V. R., and Sridhar Valluri. "Practical Application Of Ground Improvement." Symposium on Engineering of Ground & Environmental Geotechnics, Hyderabad, india 29th Feb–1st March. 2008.

increase of the shear strength and/or an increase in the bearing capacity of the foundation subsoil[23]. On the other hand these methods can result in an increase of the foundation costs due to the extra offshore work needed.

17.5.2 Varying the foundation diameter

The second parameter that is varied to increase the bearing capacity is the foundation diameter. By increasing this diameter the effective area and thus the bearing capacity is increased. The results for the varying diameter calculations are visible in the graph below. The graph has an non linear curve since the bearing capacity is depending on the area of the foundation which is in turn quadratic related with the diameter of the foundation.

It can be seen from the graph that an increase in the foundation diameter has a large increase in the bearing capacity as a result. The result of the increase in the base parameter is that the self weight of the structure increases. The increase of the dimension also results in more construction space needed for the foundation. These factors will increase the cost of the foundation.

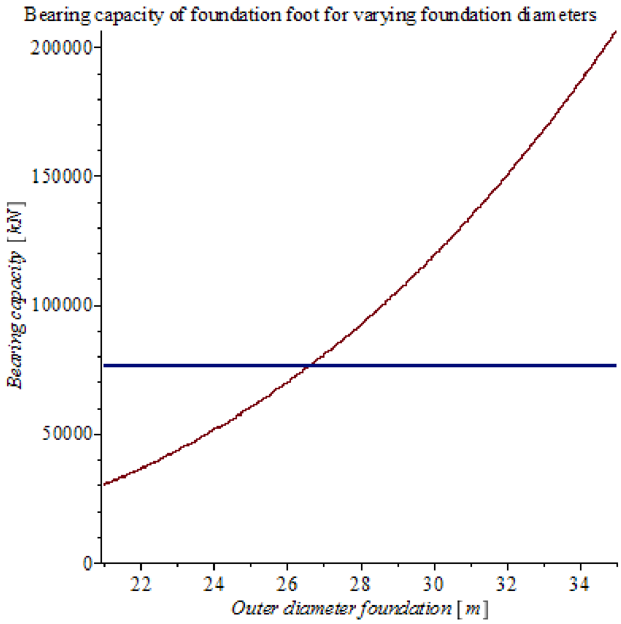

Figure 75, Bearing capacity for varying foundation diameter

17.5.3 Varying the overburden depth

The last variation made to increase the bearing capacity is to increase the foundation depth. This can be done in two ways as described before: by embedding the foundation in soil or by applying skirts that penetrate into the soil. Increasing the overburden depth by applying skirts is an effective but complicated measurement to increase the bearing capacity. Skirts can be constructed by means of pile sheets that are applied in the subsoil on which the foundation is placed an grouted or during the construction of the foundation large concrete skirts have to be constructed. Both construction methods are difficult to execute. The results for the variation of the overburden depth are placed in the graph besides. From this graph it can be seen that the relation between the overburden depth increase and the increase of the bearing capacity is linear. This is because the bearing capacity is only linear depending on the overburden depth. Despite this linear relation the increase of the overburden depth is an effective measurement to increase the bearing capacity of the foundation.

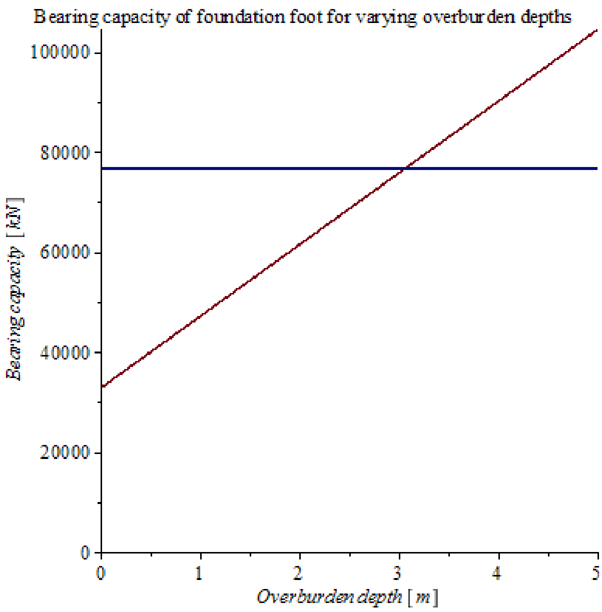

Figure 74, Bearing capacity for varying overburden depths

[23] "Facts About Soil Improvement" An Information Update from the IADC – Number 5 – 2008

When the overburden depth is created by embedding the foundation in the soil the total bending moment on the foundation foot will increase. As concluded in the variance study an increase of the foundation height has a large influence on the total bending moments.

17.6 Measurement taken to increase the bearing capacity

To increase the bearing capacity of the foundation foot one of the three described measurements is taken. One of the options was an increase in the internal angle of friction of the soil. As mentioned before this parameter can be influenced by changing the location or by applying soil improvements at the desired location. Because the change of the foundation location is not a convincing measurement the only option to increase the bearing capacity is by means of soil improvements.
Out of the three options described (soil improvement, increase of foundation diameter and increase overburden depth) it is chosen to increase the overburden depth by applying skirts for the foundation. This measurement is an effective way to increase the foundation and will not result in extra forces exerted on the foundation. To obtain the desired bearing capacity the skirt length should be 3,1m as calculated before.
The motivation to choose for the application of skirts instead of enlarging the foundation diameter is that the application of skirts will not cause a significant increase in dimensions of the foundation. Since the availability of heavy lifting equipment is limited it should be avoided that the foundations are becoming too heavy. As calculated before the base plate is one of the heaviest components of the foundation. When the diameter of the foundation is increased from 21,5m to the required 26,7m the increase of the surface and thus the weight of the base plate is a factor 1,5.
The application of the skirts is a point of attention for this solution. Because of the needed length (3,1m) it is needed that the skirts are having sufficient thickness to prevent buckling of the skirt. This can be done by building in thick skirts during the construction of the foundation or by applying sheet piles in the foundation subsoil. Subsequently the foundation could be placed on these sheet piles and connected by means of grouting or locks. Since the latter option, applying sheet piles, results in more offshore works it is preferred to apply the skirts during the construction process.

18. Foundation capacity for different soil types

With the outcomes from the design for an offshore wind turbine an analysis is made for the bearing capacity of different soil types. In the previous part of the study the bearing capacity was calculated with a sub soil consisting of cohesionless sand with an internal angle of friction of 32,5° and a unit weight of 18kN/m³.

18.1 Outcomes calculations for foundation dimensions

In the previous part of this study the dimensions for a gravity base foundation are calculated. The results for this calculations will serve as input for the calculations for the second part of this study which is related to the bearing capacity of the sub soil. The forces on and dimensions of the foundation calculated in the first part are summarized in the table below.

Description	Value
Effective bending moment	2,40E+05 kNm
Effective horizontal force	1,09E+04 kN
Effective vertical force	7,65E+04 kN
Water depth	25 m
Diameter foundation shaft	6 m
Diameter foundation base	21,5 m
Length skirts	3,1m
Self weight foundation with ice cone	2.128 tonnes
Self weight foundation without ice cone	1.568 tonnes
Bearing capacity for cohesionless sand	77.352 kN

Table 21, Forces and dimensions for foundation

These parameters will function as the input for the further calculations of this second part. When parameters are changed to increase calculation outcomes this will be indicated in the text.

18.2 Set parameters for different soil types

To investigate the bearing capacity for other types of sub soils a study is done for three different types of clay sub soils. The calculated values for these three types of clay soil are compared with the values obtained with the cohesionless sand. The values for the soil types are presented in the table below.

Soil type		Unit weight [kN/m³]	Angle of int. friction [°]	Cohesion [kN/m²]
Sand	Clean	18	32,5	0
Clay	Clean	17	17,5	10
Clay	Moderate sandy	18	22,5	10
Clay	Strong sandy	18	27,5	2

Table 22, Parameters for different soil types

It is chosen to only evaluate the materials mentioned in the previous table to calculate the bearing capacities. This is done to be able to investigate the influence of strong and weaker sub soils for the foundation. This does not imply that these materials are the only soil materials suitable for the application of a Gravity Base Foundation. Other soil materials such as rock, gravel or loam could also be suitable for as foundation subsoil, but are not regarded during this study.

When the parameters as described in the table above are used for the calculation of the bearing capacity of the foundation different outcomes are expected. Because the angle of internal friction for a clay subsoil is lower than for sand the bearing capacity for the clay subsoil will become lower. The cohesion of the clay soil will cause an increase of the bearing capacity, although this will be smaller than the decrease by the reduction of the angle of internal friction.

18.3 Calculation of the bearing capacity for different types of soil

With the parameters of the clay soil calculations are made for the bearing capacity of the foundation as described in the first part of this chapter. These calculations are done in the same way as it was done for the sand soil. The results for the calculations are presented in the table and graph below. In the first graph the bearing capacity for the four different evaluated types of soil are shown. In the second graph the bearing capacity for the four different soil types is plotted for a varying angle of internal friction. In this way it can be seen what the influence the variation in the angle of internal friction is on the evaluated types of soil.

Soil type		Bearing capacity [kN]	Ratio with sand [-]
Sand	Clean	77.352	100%
Clay	Clean	27.691	36%
Clay	Moderate sandy	43.748	57%
Clay	Strong sandy	48.782	63%

Table 23, Bearing capacity for various soil types

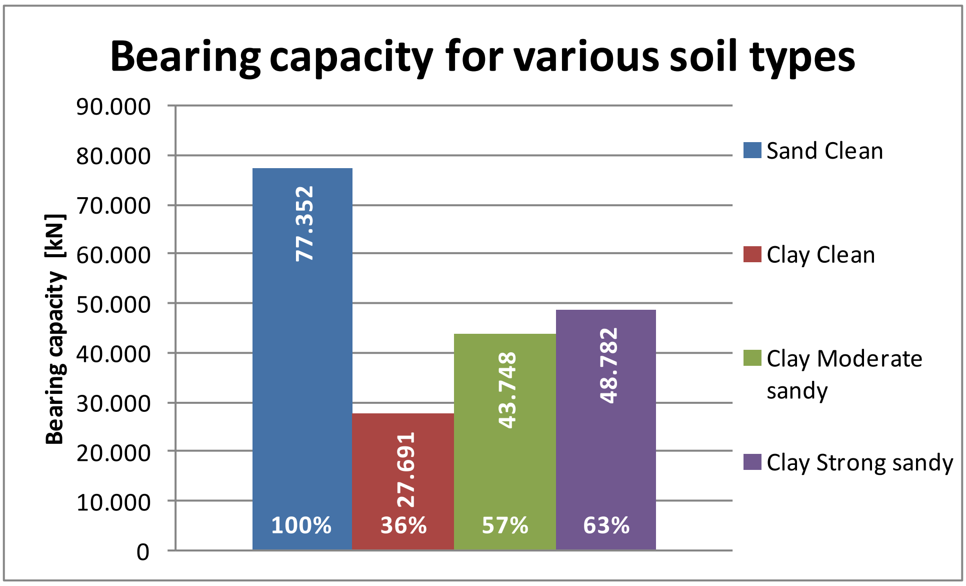

Figure 76, Bearing capacity for various soil types

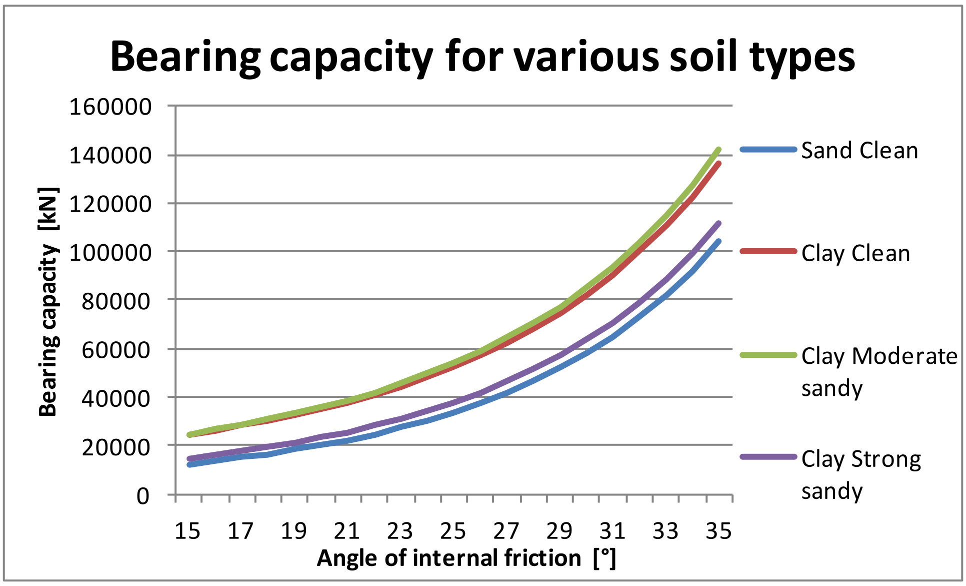

Figure 77, Bearing capacity for various soil types with varying angles of internal friction

From the calculations it can be concluded that for soil types with a smaller angle of internal friction the bearing capacity extremely reduces. For the clean clay soil the bearing capacity is only 36% of the bearing capacity for sand. For the other types of clay the bearing capacity increases mainly due to an increase in the internal angle of friction. In the graph above it is seen that for equal angles of internal friction only the cohesion of the clay soils is influencing the bearing capacity.
The most sandy type of clay has only 63% of the bearing capacity when compared to the sand sub soil while the angle of internal friction is only differing 5°. From the calculations above it thus can be concluded that the clay based soil types are reducing the bearing capacity significantly.

19. Calculations for multi layered sub soils using Deltares D-Geo Stability

Because in practice sub soils in are not consisting of one type of soil only it is investigated what the influence is of a clay layer in the sand soil stratum. It is chosen to only evaluate one type of sand soil and one type of clay soil to keep the calculations simple and comparable. Although the sand has a relative low angle of internal friction compared to stiff soil types the sand is chosen as a stronger soil material and the clay as a weaker soil material. In this way it is aimed to create models where it is possible to determine the influence of weaker soil layers within a stronger soil layer.

For the calculations made the depth and the thickness of the clay layer existing in the sand stratum are varied because it is indicated that the weaker the clay layer, the larger the depth up to which the clay has an adverse effect on the bearing capacity of a footing[24]. In the first instance the software D-Geo Stability produced by Deltares was used. When it was found that this program was not able to perform the calculations as desired the switch is made to a different program named Plaxis 3D. In the following chapter the use and the outcomes of the program D-Geo Stability are explained. Also the possible limitations for the program, making this software not usable for this study, are described.

19.1 Deltares D-Geo Stability

To perform calculations for the stability for different soil types use is made of the Deltares software D-Geo Stability. This program is developed for the design and control for stability for embankments on weak subsoil[25].

With this program the stability of the soil is modelled by the input of a soil layout and external forces. With this input the program calculates the slip circles for the model and gives the slip circle with the lowest safety factor as output. These results can be evaluated in both graphical and in text representation. The model that is made with this program is 2D. Therefore the forces acting on the soil are also represented as 2D loadings. The surface loads of the self weight and the external forces are modelled as line loads in the D-Stability model. How this is done is explained later.

By modelling the foundation as a strip instead of a circular footing the bearing capacity of the foundation will be slightly higher due to the increase of the shape factor in the Brinch Hansen formula.

19.2 Conversion external forces to loads usable for D-Geo Stability model

The top structure of the wind turbine is loaded by horizontal forces and bending moments. Since it is not possible to insert bending moments in the program D-Geo Stability the bending moment is transferred to a vertical force with a lever arm with respect to the centre of the foundation. Subsequently this calculated vertical force is combined with the external horizontal force to a resulting force acting under an angle with respect to the horizontal axis of the foundation. This procedure is briefly explained in the following sections.

[24] Bearing capacity of footings over two-layer foundation soils, R.L. Michalowski and L. Shi, ASCE, Journal of Geotechnical engineering may 1995

[25] http://www.deltaressystems.nl/geo/product/618724/d-geo-stability1

19.2.1 Converting bending moment to vertical force

When the governing bending moment acting on the foundation $M_{ED} = 239.640kNm$ is combined with the self weight of the turbine structure a resulting vertical force F_v with eccentricity $e = \frac{M_D}{SW} = \frac{239.640}{76.470} = 3{,}13m$ can be calculated. This eccentric force F_v ,which is visible in the figure below, is applied at the top of the modelled foundation slab in D-Geo Stability.

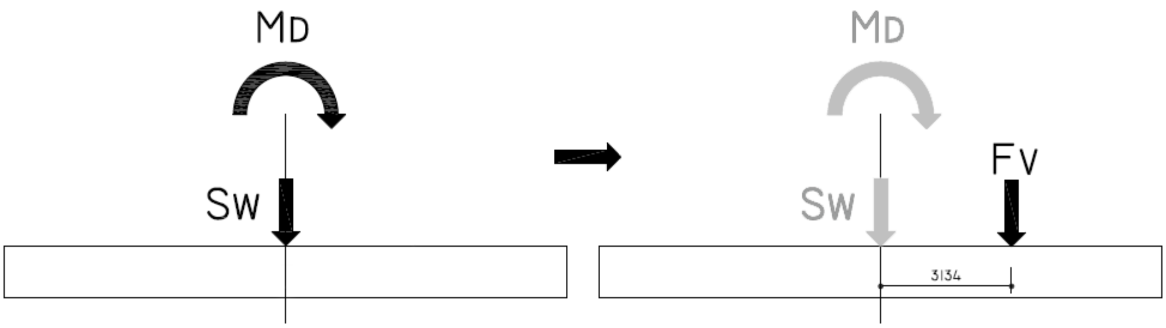

Figure 78, Conversion of bending moment and self weight in force Fv

19.2.2 Combining horizontal force and bending moment

Besides the bending moment also an external horizontal force is working on the foundation. This horizontal force H_D has been calculated in the first part and has a magnitude of $H_D = 10.890kN$. This force is now named F_H and applied at the same location as the force F_V as can be seen in the figure. With the ratio between the forces the resulting force acting under an angle with respect to the horizontal axis can be calculated.

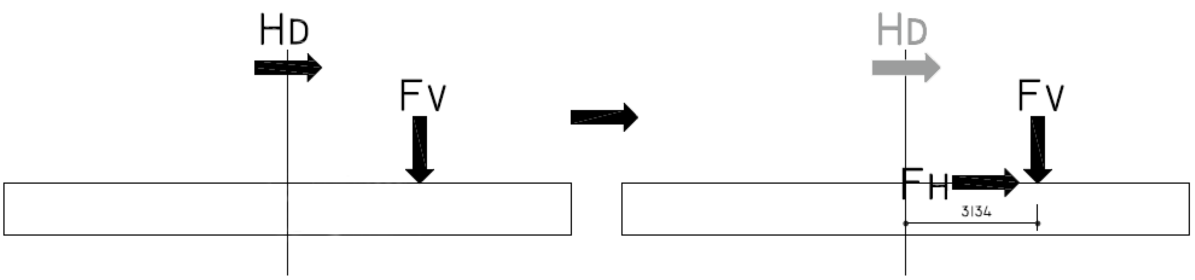

Figure 79, Combining horizontal force and bending moment

This resulting force, named F_{RES} is calculated as follows:

$F_{res} = \sqrt{F_H^2 + F_V^2} = \sqrt{10.890^2 + 76.470^2} = 77.242kN$. The angle with respect to the horizontal axis is calculated as follows: $\alpha_{F_{RES}} = \tan^{-1}\left(\frac{76.470}{10.890}\right) = 81{,}90^o$.

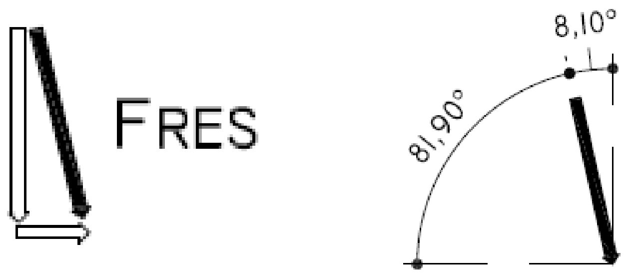

Figure 80, Fesulting force Fres

19.2.3 Converting force from circle foundation to strip foundation

The forces calculated before and used to determine the resulting force F_{RES} are calculated for a circular foundation. Since the forces inputted in the model are line loads the forces have to be converted from kN to kN/m'. This is done by dividing the force by the diameter of the circle. The result of this calculation is the external force acting on the soil per unit length. This value is calculated as follows: $F_{RES}' = \frac{F_{RES}}{A_{circle}} \cdot D_{circle} = \frac{77.242}{0,25 \cdot \pi \cdot 21,5^2} \cdot 21,5 = 4.574,31 kN/m'$. This resulting force is the input for the D-Geo Stability model line load.

19.3 Creating the D-Geo Stability model

To be sure that the model boundaries are not influencing the calculation results the model dimensions should not be too small. It is useful to use a model size of at least 6-8 times the foundation diameter. Due to experience gained by using D-Geo Stability it was decided to use model dimensions even larger than 8 times the foundation diameter resulting in a model with the dimensions of 400m x 50m.

19.3.1 Material input

In the program D-Geo Stability the model material properties are inserted by hand. As shown before the soil material properties are obtained from the NEN6740 code, table 1. In the sand only model used the only soil material present is foundation sand. The overburden depth existing for the foundation foot has to be modelled using a plate simulation. Since the GBF structure is not modelled itself a weightless stiff plate is modelled as the GBF. The stiffness of the plate is modelled by giving the plate material properties with a very large cohesion and angle of internal friction. On this stiff plate the forces from the GBF are applied. Both the stiff plate properties as the input of the forces is visible in the appendix.

19.3.2 Calculation modules, Bishop and Uplift Van

With D-Geo Stability the soil stability can be calculated using different theoretical modules. The two modules used in this study are the Bishop module and the Uplift Van module. Since the Bishop method only uses 1 slip circle to determine the safety of the soil it is possible that the influence of multiple soil layers is not properly taken into account.
To take these multiple soil layers properly into account use is made of the Uplift Van method. Van's method assumes that the total slip plane is composed of a horizontal part bounded by two circular parts. The safety factor is determined using equilibrium of the horizontal forces acting on the compressed area between the active and passive slip circles. The method becomes equal to Bishop's method if the length of the horizontal part reduces to zero.
In the D-Geo Stability the existence of two slip circles is modelled by inputting the location of two slip circle centre grids and the location of the horizontal tangent line. The software creates multiple slip circles according to the data inserted.

19.4 Evaluation and validation of Uplift Van calculations

Using the D-Geo Stability program with the Uplift Van calculation module resulted in calculation outcomes for multiple soil configurations. In total 5 different soil configurations are evaluated where the clay layer thickness and depth is varied. In the following table the situation 5-2,5 means a clay layer starting at a depth of 5m with a thickness of 2,5m.

Situation	Safety factor
5-2,5	0,59
5-5,0	0,59
5-7,5	0,59
10-2,5	1,09
10-5,0	1,09

Table 24, Results for variations in soil layout

As can be seen from the results presented in the table above the thickness of the clay layer has no influence on the safety factor. The results are found not correct because it is quite remarkable that the safety factor is not changing when the layer thickness is increased. It is namely expected that the thickness should have an influence on the safety of the model.
Because of this remarked behaviour and it is decided to perform a validation to check whether the program D-Geo Stability is able to calculate the models as described before. This is done by checking with the aid of calculations if the stress increment in the soil by the point loads is correctly incorporated in the model calculations. If this is not the case the program is not able to calculate the correct safety factors and thus not usable for this study.

19.4.1 Validation of D-Geo Stability Uplift Van calculations

To check whether the D-Geo Stability program takes the increase of the stress in the subsoil due to the point loads adequately into account two different models are evaluated. The first model uses a weightless foundation plate and has the combined force (Horizontal, bending moment and self-weight) applied at a distance of 3,13m from the centre of the foundation. The second model has placed the combined force at 8,75m from the centre of the foundation. Because by doing so not all the vertical force of the foundation is incorporated also a mass is given to the stiff foundation plate. For both the models only the forces and on the plate and the mass and thickness of the plate are varied. The calculation grid and other model parameters are held constant.
When the two calculations are performed it is found that the calculation outcomes are showing significant differences where it is expected that no or small differences should occur. Because of this it is stated that the program used, D-Geo Stability, is not sufficiently capable in incorporating the stress increases in the soil due to point loads and thus unsuitable for performing the calculations for the Gravity Base Foundation models.
Besides this explanation a second possible explanation for the differences in the calculation outcomes is the modelling of the stiff plate performed. The foundation plates are namely modelled as a very stiff material. It could be that when the modelled plate is not acting completely stiff, differences in the thickness of the plate could result in differences in the calculation outcomes. When this is true indeed it is also an indication that the program D-Geo Stability is not suitable for performing the calculations for the Gravity Base Foundation, since there are no other possibilities found in the software to model a stiff plate.
Taking the possible shortcomings of the D-Geo Stability program into account it was justified to make a switch to a different geotechnical software package, which will be discussed in the next chapter.
The entire evaluation and validation of the D-Geo Stability can be found in the appendix at the end of this document.

20. Soil safety calculated using Plaxis 3D

As discussed in the previous chapter it was found that the use of the software D-Geo Stability was not suitable for calculating the problems modelled for this study. To perform calculations for the stability for different soil types the switch is made of the finite element program Plaxis 3D. In this program the foundation dimensions, the soil layout and the external forces are the input for the model. With this input the program calculates and evaluates the bearing capacity of the model and gives the governing safety factor as output. Within the program the calculation results can be viewed in multiple forms.

Plaxis 3D is a finite element calculation program for three-dimensional analysis of deformation and stability in geotechnical engineering[26]. For this graduation study a consideration is made between using Plaxis 2D or Plaxis 3D. Since it is not possible to precisely model the asymmetric loading problem for the loading of the foundation with the 2D program it is decided to use the Plaxis 3D environment. When the 2D environment was used it is only possible to model the foundation as a strip footing. Since the foundation in reality has a circular footing the results of the 2D calculation for a strip foundation will lead to higher bearing capacities as for a circular foundation. The input of the model is more complicated for this 3D environment but the interpretation of the results of the 3D calculations will be easier.
The outcomes of the safety factor calculations will give more realistic safety factors for the bearing capacity of the foundation than those that are found using hand calculations. This is because the program Plaxis 3D incorporates phenomena that are not incorporated with the hand calculations. Therefore the safety factors obtained with the Plaxis 3D software are higher compared to the simple hand calculations made before.

20.1 Modelling the foundation and soil layout

As a first step to use Plaxis 3D a general model is made which is used for this study. The dimensions of the foundation are the same as indicated in the first part of this study. The foundation foot is a hexagonal with an external diameter of 21,5m. All the dimensions of the foundation base can be found in the figure besides. In the model only the dimensions of the foundation base are modelled. The self weight and the external force of the foundation are modelled later.
In the first part of this study it was calculated, using the formula's of Brinch Hanssen that an overburden depth of 3,1m is needed for the foundation. In the Plaxis 3D model this overburden depth is also modelled.

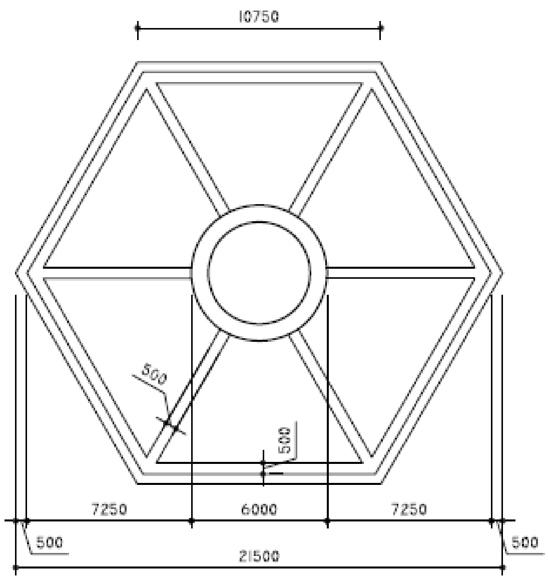

Figure 81, Dimensions of foundation base

[26] http://www.plaxis.nl/plaxis3d/

20.1.1 Modelling the soil

When modelling the foundation subsoil it is needed to create a stratum that is large enough so that the boundaries of the model will not affect the calculation results. The diameter of the foundation is 21,5m as stated before. Therefore the width and length of the soil stratum are chosen as 180m x 180m; roughly eight times the diameter of the foundation. For the depth of the soil stratum a distance of 50m is modelled which is around 2x the foundation diameter plus the overburden depth. This makes that the dimensions of the soil model are 180m x 180m x 50m (length x width x depth).

The purpose of the study made in this chapter is to investigate the influence of weaker clay layers in a stronger sand subsoil, as mentioned before. By using only two different soil types the complexity of the models is small even though the possibility to study the effect of weak soil layers is maintained. For both soil materials the physical properties as entered in the Plaxis 3D model are based on the clean sand and clean clay material presented in the NEN6740 table 1. The major parameters are the self weight ($\gamma_{sat/unsat}$), the stiffness (E_{50}), cohesion (c'_{ref}) and the internal angle of friction (φ'). In the tables below the used strength and stiffness properties are listed. For both the sand and clay soil material the Hardening Soil model is selected which has some advantages over the Mohr-Coulomb model. Since the Hardening Soil model also requires stiffness parameters of the soil they are also listed.

	Sand	**Clay**
$\gamma_{unsat}\,[kN/m^3]$	18	17
$\gamma_{sat}\,[kN/m^3]$	20	17
$c'_{ref}\,[kN/m^2]$	0,1	10
φ' [°]	32,5	17,5
ψ [°]	2,5	0

Table 25, General and strength properties sand and clay

	Sand	**Clay**
$E_{50}^{ref}\,[kN/m^2]$	43.000	10.000
$E_{oed}^{ref}\,[kN/m^2]$	43.000	10.000
$E_{ur}^{ref}\,[kN/m^2]$	129.000	30.000
Power (m)	0,5	0,9

Table 26, Stiffness properties for Hardening Soil model

The material properties are used for Plaxis 3D and the determination of the soil strength and stiffness properties are visible in the appendix of this document.

20.1.2 Phreatic level

The phreatic level for the model is stated at 10m above the soil level. Since the total height of the water level should not influence the bearing capacity of the soil the height of the phreatic level is arbitrary when it is assured the level is above the soil level. An illustration of the soil model and the phreatic level as modelled in Plaxis 3D is added in the appendix.

20.1.3 Modelling the foundation

In the centre of the soil layout the foot of the foundation is placed which is modelled as a weightless ($\gamma = 0,00 kN/m^3$) very stiff ($E_1 = 100 \cdot 10^9 kN/m^2$) plate with a thickness of 0,3m. The fact that the foundation is embedded 3,1m into the soil is modelled by applying walls at the outer perimeter of the foundation foot. These walls are having the same physical properties as the foot plate of the foundation. The modelled foundation foot is visible in the figure besides.

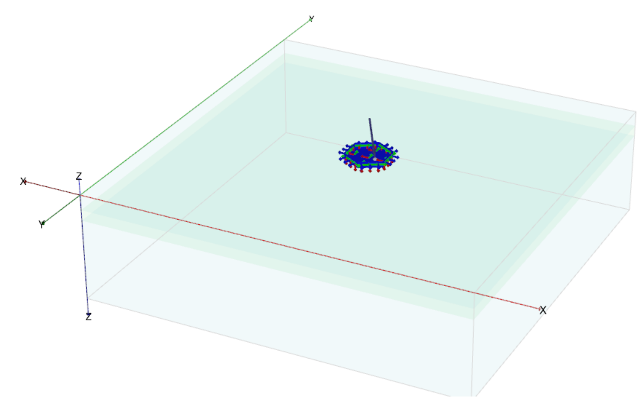

Figure 82, Modelling of the foundation foot

20.2 Applying the loads

After the modelling of the soil and the foundation the loads are applied. As indicated before the foundation plate is modelled weightless. Therefore the self weight is modelled as a load on the foundation base.
The top structure of the wind turbine is loaded by horizontal forces and bending moments. Since it is not possible to insert bending moments in the program Plaxis 3D the bending moment is transferred into a vertical force with a lever arm with respect to the centre of the foundation. Subsequently this calculated vertical force is combined with the external horizontal force to a resulting force acting on the foundation under an angle with respect to the vertical axis. The calculation of the forces and eccentricities has already been performed in the chapter for the calculations using D-Geo Stability.
The same vertical force F_v with magnitude $F_v = 76.470kN$ with an eccentricity of 3,13m and horizontal force H_D with magnitude $H_D = 10.890kN$ are inserted into the Plaxis 3D model. The angle under which the forces are acting is calculated by the program itself. The exact input of the forces in the program Plaxis 3D can be viewed in the appendix.

20.3 Meshing of the model

Before the program Plaxis 3D can perform the calculations a mesh is created for both the soil and the foundation structure. The mesh properties are set to medium in order to obtain a mesh fine enough for the modelled situation. As a result of this medium mesh the calculation time of the model increase to 10-30 minutes per model. The program Plaxis 3D meshes the model automatically. At the interface between the stiff plate and the soil the mesh is more dense, and on larger depths the mesh becomes more coarse. The result of the mesh for a situation where a clay layer is present is visible in the figure besides.

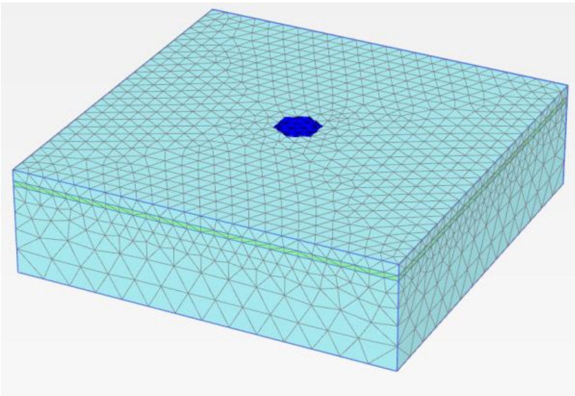
Figure 83, Meshed model for soil with clay layer

20.4 Calculation approach

In the program Plaxis 3D the calculations are done by so called calculation phases. In those phases it is indicated which objects, soil layers and forces in the model should be activated or deactivated. The model as used for this study consists of four calculation phases. In the first (initial) phase all the soil layers are activated and the phreatic layer is applied. All the structures and forces are deactivated in this first phase. In the second phase (Phase_1) the area of the soil is excavated to -3,1m, the calculated overburden depth, and the stiff foundation plate is activated. The third phase (Phase_2) activates the applied extreme load. Finally in the fourth phase (Phase_3) a load 10x higher than the extreme load is applied which will be discussed in the next paragraph. By applying the foundation plate and the external extreme forces in two different phases it is intended to eliminate numerical distortions in the model that could occur if all phases were combined to one action.

As can be seen in the figure besides the both the Load phase (Phase_2) and the phase Load_10 are calculated with the stiff plate (Phase_1) as preceding phase. In this way both the Load phase (Phase 2) and the Load_10 phase (Phase 3) are comparable since they are starting from the same initial calculation conditions.

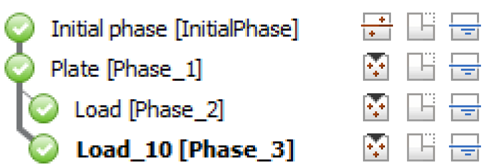

Figure 84, Phases in Plaxis 3D

20.4.1 Determination of the safety factor using calculation phase Load_10

To determine the bearing capacity of the model layout a special method is used to determine the bearing capacity. First the model is made according to the models presented before. Then, in the fourth calculation phase a load is applied with a value of 10 times the magnitude of the extreme design load as calculated in the first part of this study. This multiplied loads ($F_V = 764.700kN$ and $F_H = 108.906kN$) are applied in the model as a point load at a distance of 3,13m from the centre of the foundation. This large force is chosen in such a way that it is likely that the soil will collapse. By both multiplying the horizontal and vertical forces by a factor 10 the self weight of the foundation is also increased by a factor 10. This is an optimistic approach since for the determination of the safety factor normally only the extreme loads has to be increased.

After finishing the fourth calculation step in which the Load_10 is applied the results are consulted and it can be seen if, and at which load step the soil collapses. The program increases the load step by step which is visible in the value for ΣM_{stage}. The value ΣM_{stage} represents the percentage of the force applied, which is defined in the corresponding phase, that has been applied before the soil body of the model collapses. A value smaller than 1 indicates that the soil collapses. Because the load defined in the Load_10 stage has a magnitude of 10 times the calculated design load it follows that an obtained value for $\Sigma M_{stage} = 0,52$ indicates that 52% of the load defined in the Load_10 phase and thus the safety factor of the model with Load_10 is 5,2.

20.4.2 Variation in soil layout

The purpose of this part of the study is to investigate the influence of weaker soil layers in the foundation subsoil. This is done by varying the Plaxis 3D model in clay layer depth and thickness. In total 15 different clay layer configurations are evaluated The depth of the clay layer starts at 2m below the foundation and is increased with 5 steps of 2m to a maximum of 10m. The thickness of the clay layer is varied in three steps: 2,5m 5,0m and 7,5m thick. An overview of the layer depths ant thicknesses is placed in the appendix.

20.5 Calculation outcomes

All the 15 models representing the 15 variations in the soil layout are calculated using Plaxis 3D. From the calculation outcomes the load step ΣM_{stage} is converted to the safety factor. This is also done for a sand only model and a clay only model as a reference for the 15 models. The safety factors for all 15 models are inserted in an Excel sheet which processes the values into the graphs and tables presented below and in the appendix. In the graphs for the individual layer depths the actual values are displayed as well as the relation between the layer thicknesses.

Since this study mainly focuses on the safety of the model, the settlements and displacements of the foundation are of minor importance. Although some remarkable phenomena can be observed in the displacement contour plots the plots are placed in the appendix, as well as the principal stresses and settlements of the soil where it can be observed that a credible failure mechanism is developing.

The key results of the performed calculations are the safety factors for the 15 calculated models. In the table besides these safety factors are listed. It can be seen that some interesting patterns and differences can be observed in the safety factor outcomes which will be discussed in the following paragraphs. It is mentioned that the obtained safety factor for a sand only model is 12x higher than that was

		Thickness [m]		
		2,50	5,00	7,50
	Clay only	1,861	1,861	1,861
Depth [m]	2,00	5,105	3,591	3,552
	4,00	6,211	4,352	4,144
	6,00	7,366	6,338	5,769
	8,00	8,474	6,905	6,382
	10,00	9,034	8,446	8,014
	Sand only	12,209	12,209	12,209

Table 27, , Safety factors for 15 soil variations calculated by hand calculations. Therefore it is stated that specialized calculations such as Plaxis 3D calculations are having a high added value. The graphs for the safety factors set per layer depth are visible in the appendix.

20.5.1 Analysis of clay layer thickness calculation outcomes

At all the layer depths the clay layer thickness is varied between three thicknesses 2,5m, 5,0m and 7,5m. The safety factor calculations for these variations are visible in the graphs presented below. For all layer depths it can be seen that the increase in thickness from 2,5m to 5,0m has more influence on the safety factor than the increase from 5,0m to 7,5m thickness.
For the shallower layers it can be seen that the increase in layer thickness from 5,0 to 7,5m has little influence on the safety factor when compared to the layer increase from 2,5m to 5,0m. For the deeper layers this relation between the layer thicknesses is more constant. This behaviour is also clearly visible in the graph safety factor for various layer depths. Here it can be seen that the difference between the safety factor for a 2,5m and 5,0m thick clay layer is larger than for the difference between the 5,0m and 7,5m thick layer.

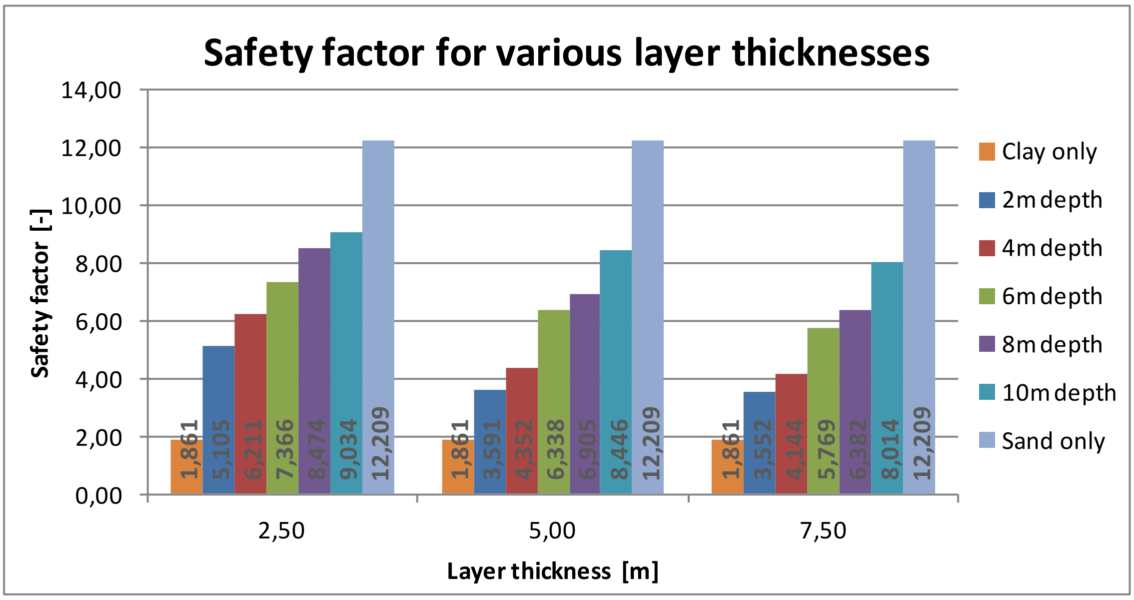

Figure 85, Combined safety factors for various layer thicknesses

When the plots of the principal stress plots for the calculations are observed in the appendix it is noticed that the thickness of the clay layer influences the depth of the formed slip circle. When trying to explain the influence of the clay layer thickness on the depth of the slip circle, denoted z_f in the figure besides, use is made of existing hand calculations to determine depths of slip circles, the page containing the formula's is visible in the appendix. With these formula's it is found that the depth of the formed slip circle is only influenced by the angle of internal friction. It is noticed that the angle of internal friction for both the sand and clay material is held constant. When the formula's are used to calculate the slip circle depth for a sand only $(\varphi = 32,5^o)$ and a clay only soil $(\varphi = 17,5^o)$, the reached depths of the slip circles are found to be 20,5m for sand only and 13,7m for a clay only soil.

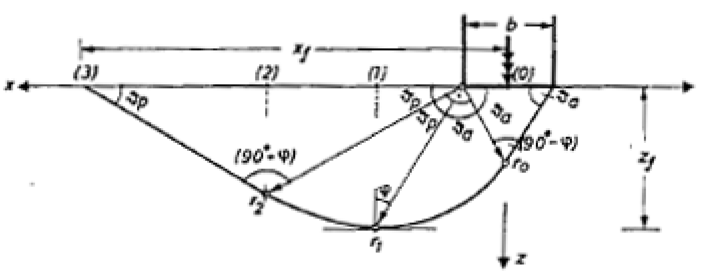

Figure 86, Example slip circle depth for 30° angle of internal friction

Because the clay layer has a lower angle of internal friction, an increase in the clay layer thickness has as a result that the combined angle of internal friction for the model is decreasing. This means that for an increasing clay layer thickness the average angle of internal friction is decreasing and thus the depth of the slip circle is decreasing, which is also visible in the principal stress plots.

Why this reduction in the average angle of internal friction for the model is having a greater influence on the safety factor for the deeper layers than it has for the more shallow layers could possibly be explained by the observation that the slope of the slip circle is very steep close to the foundation and less steep at the bottom of the slip circle as can be seen in the figure presented above. An increase of the clay layer thickness for the shallow layer does decreases the combined angle of internal friction and thus decreases the slip circle depth, but because the less steep parts of the slip circle are still located well below the clay layer the influence on the safety factors is limited. This behaviour changes when the clay layers are located at greater depths. When for the greater depths the clay layer thickness is increased the bottom of the slip circle also shifts upward, but is now closer located to the clay layer and thus results in a larger influence on the safety factor.

20.5.2 Analysis of clay layer depth calculation outcomes

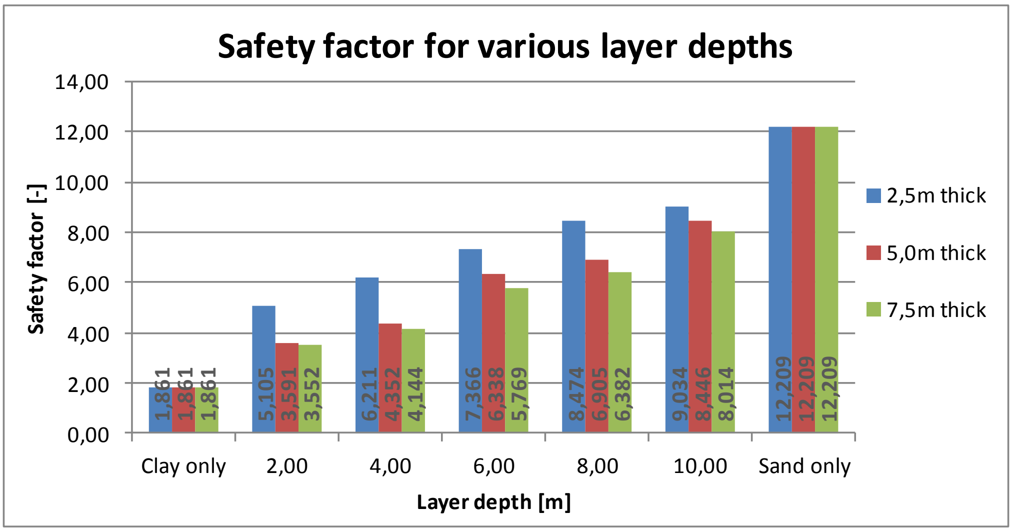

Figure 87, Combined safety factors for various layer depths

From the presented data it can be seen that the depth of the clay layer has a positive influence on the bearing capacity of the foundation. When the safety factor graph for various layer depths placed below is regarded it can be seen that an increase of the clay layer dept results in significant increases of the safety factor. Since all loadings and foundation dimensions are held constant this directly means that the bearing capacity of the foundation increases for an increasing clay layer depth.

In the appendix graphs and an analysis of the ratio's for the increment of the safety factors are placed. When regarding these graphs it is stated that the thickness of the clay layers is significantly influencing the safety factors for the shallow clay layers, but that the influence of the clay layer thickness reduces when the layer is located at larger depths. On the larger depths the thickness of the layer is of minor importance and the proximity of the slip circle is having a larger influence. This change from the safety factor sensitivity from the clay layer thickness to the clay layer depth may possible explain the inconsistent behaviour of the safety factors for the thicker clay layers.

It should be noticed that the findings presented are partly based on the slip circle theory and partly on the principal stress plots presented in this appendix. The exact location and shape of the slip circles is not known and it is thus mentioned that the findings are not based on the exact slip circles. When plots could be created of the exact shape and location of the slip circles it is possible to validate the findings presented.

20.5.3 Comparison with sand only and clay only model calculations

Besides the calculations with layered soil two calculations for a sand only and a clay only model are executed as can be seen in the graphs presented before. When the calculation for a sand only model is compared to the layered calculations with the highest safety factor, a layer with a thickness of 2,5m at 10m depth, it is found that the presence of a thin clay layer at a relative large depth already reduces the safety factor significantly with 26% (12,209 to 9,034).
When the clay only model is compared with the most severe model calculation, a clay layer of7,5m thick at a depth of 2m, it can be seen that the safety value of a clay only model still (1,861) is almost half the safety factor for the severe layered calculation (3,552).
Therefore it is concluded that the presence of a clay layer has a significant influence on the bearing capacity of the foundation model, even though the clay layer is situated at larger depths. On the other hand a thick clay layer being present near the surface of the foundation still has significant more bearing capacity than a clay only situation.

20.6 Parameter variation for soft clay layer

Besides the influence of the clay layer depths and thicknesses the influence of the soil parameters for the weak clay layer is investigated. This is done by varying the soil parameters for the cohesion of the clay $[c]$, the specific soil weight $[\gamma]$ and the angle of internal friction $[\varphi]$ of the clay material within realistic boundaries. All the calculations and determination of the safety factors are performed at the same way as it was done for the clay layer depth and thickness variation calculations presented before.
For the calculations use is made of one reference model which served as the basis of the clay parameter variation calculations. This model is the previously used model for a 5,0m thick clay layer at a depth of 6m with cohesion $c = 10kN/m^2$, soil weight $\gamma = 17kN/m^3$ and internal angle of friction of $\varphi = 17,5°$.
In total 7 models with different clay parameters are evaluated, which are differing in only one parameter with respect to the reference model. The 7 calculated models are resulting in the following safety factors as can be seen in the graph below.

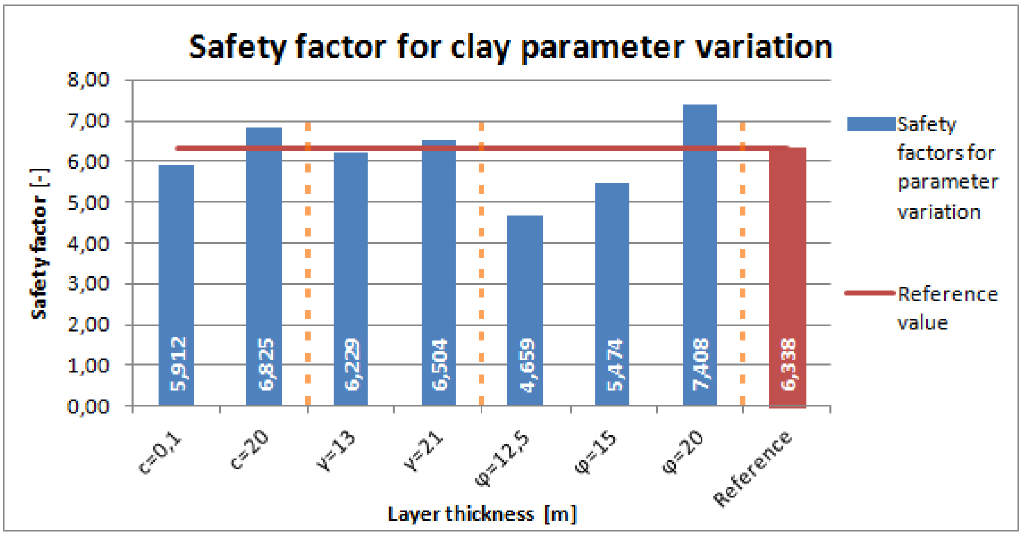

Figure 88, Graphical representation of safety factors for clay parameter variation

From this graph it can be seen that the difference between the safety factors and the reference value is the largest for the variations of the internal angle of friction. For the other parameter variations the differences are much smaller where the difference for specific soil weight has the least influence on the safety factor. It is concluded that a variation in the angle of internal friction has the largest influence on the bearing capacity, followed by a variation in the cohesion. The least influence has a variation of the specific soil weight. More details can be found in the appendix.

21. Dynamic loadings in Plaxis 3D

Until now only the safety factors for static forces are evaluated in this study because they are having the largest magnitude. But besides the static forces discussed the offshore wind turbine are also very suspected to dynamic loadings. Since the forces acting on the turbine are mainly dynamic (wind, wave, blade passing forces etc.) these forces can have a large influence on the bearing capacity when the soil is sensitive for liquefaction problems from the stress increase due to the dynamic loads.

Due to the fluctuations in the forces exerted on the foundation and subsoil stress fluctuations are occurring in the soil. These fluctuations can lead to excess pore pressures in the subsoil which are reducing the strength of the soil and thus reducing the bearing capacity of the soil. For the sand soils the fluctuating load can cause the grain skeleton to distort and rearrange. In this way pore pressure can be build up which will lead to a reduction in the effective stress and eventually liquefaction of the soil and thus a reduction of the bearing capacity of the sand soil material.
For clay sub soils the fluctuations of the loads will lead to building up of pore pressure due to the restriction in the runoff of the pore water. Due to the low consolidation of the clay material this increase in pore pressure will lead to a reduction of the bearing capacity of the soil material.

To determine the sensitivity to the dynamic forces first the dynamic load has to be determined. This is done by relating the dynamic force by a specified ratio to the extreme static force.
Secondly it is discussed what soil parameters are used for the dynamic analyses since the soil properties for dynamic loaded soils are differing from the soil conditions used for the static loadings. With the dynamic loads and the soil parameters the calculated safety factor of the model for dynamic loading are evaluated.

21.1 Determination of the dynamic force

The dynamic force is determined as a fixed percentage of the extreme static load. For this study it is assumed that the dynamic force used for fatigue calculations is 20% of the extreme static force. This percentage is discussed in the first part of this study and originates from the data obtained by Siemens. Since the static force has a magnitude of $239.640kNm$ the dynamic force used to calculate the bearing capacity under dynamic loading is $0,2 \cdot 230.640kNm = 47.928kNm$.
The vertical force of the turbine structure, the self weight is still constant. Therefore the arm with respect to the centre of the foundation changes. The eccentricity for the external forces now becomes $e = \frac{47.928kNm}{74.640kN} = 0,627m$.

21.2 Soil properties for dynamic analysis

The load fluctuations by for example the waves with a frequency of 0,2-0,1Hz (5-10sec per period) and the wind with a frequency of 1-2Hz (0,5-1sec per period) can cause the build up of internal stresses in the soil stratum as explained before. A representation of the load fluctuations for an offshore wind turbine is placed in the appendix.
For this study two types of soil are regarded, namely sand and clay. The sand material has a high pore ratio and an open structure. When the sand is modelled as an undrained material the fluctuating forces can lead to excess pore pressures in the soil. These excess pore pressures are reducing the strength of the soil material.
For the clay material the fluctuations in loading can also lead to increased water pressure in the soil material if the water is not able to runoff. Therefore also the clay material is modelled as an undrained material. It is considered safe to model both the sand and clay soil material as undrained soil materials.

21.2.1 Material properties for sand

For the undrained sand material the same base parameters are taken as for the drained soil analyses. For the drainage type of this soil Undrained (A) is chose. For the two undrained types A and B it is chosen to take the Undrained (A) type since this is the type mostly used in calculation methods like these. For the undrained analysis only the following parameters are different compared to the drained analysis:

- Skempton-B	0,9866 (Standard value)
- ν_u	0,4950 (Standard value)
- $K_{w,ref} / n$	1,229E6 (Standard value)
- R_{inter}	0,900 (Standard value = 1,000)

The values for the undrained behaviour are the standard values presented by the software. These values are found suitable for this calculations and are therefore not changed. The values for the interface strength are set from 1 to 0,9 to reduce the strength between the modelled interface between the stiff plate and the soil material.

21.2.2 Material properties for clay

The clay material is also assumed as undrained. In the software Plaxis 3D this is done by defining the drainage type as Undrained (A). This is done for the same reason as discussed for the sand properties. The additional parameters needed for the undrained material properties are taken equal to the values chosen for the sand material. For both the clay and sand soil material the soil properties are added in the appendix at the end of this document.

21.3 Model properties and calculation method

Just like the model used for the drained calculations the dimensions of the undrained models are having the following dimensions: 180m x 180m x 50m (Length x Width x Depth). Also the modelling of the stiff plate and the water level conditions are identical for both the drained and undrained calculations. The mesh size for the undrained analysis is set to a coarse mesh.
For the undrained calculations the same 15 soil configurations for clay layer depth and thickness as used for the drained calculations are evaluated.

21.3.1 Calculation phases

The calculation phases for the undrained 3D calculations are defined in a similar way as for the drained 3D calculations. The calculation phases consists of four different phases. The only difference between the drained and the undrained calculation phases is that for the undrained phase the magnitude and the eccentricity of the applied force has changed. The application of a force with a magnitude of 10x the initial force to determine the safety factor is also true for the undrained calculations.

21.4 Calculation outcomes for undrained soil calculations

For the 15 calculated undrained models the calculation outcomes are placed in the appendix. The calculation result related to the safety factor is again the value for M_{stage} obtained for the calculations with an applied load with a factor 10 times the calculated design load (named Load10 in Plaxis). The value for M_{stage} is multiplied with 10 to obtain the safety value for the calculated model. These calculated safety factors for the models are placed in the table on the next page.

From this table it is noticed that the calculated safety factors are not showing any corresponding ratios with the safety factors calculated for the drained models. For some models the calculation outcomes are based on model outcomes with unfinished calculations or insufficient load steps. If this is the case for a calculation outcome this is written at the remarks of the model.
The ratios observed at the drained calculations, a decreasing safety factor when the clay layer thickness is increased and an increasing safety factor when the depth of the clay layer is increased, is not observed in the calculation outcomes from the table below.

Layer depth [m]	Layer thickness [m]	Safety factor [-]	Remarks
2	2,5	0,2334	
	5	1,926	
	7,5	1,038	
4	2,5	1,831	Not enough load steps
	5	1,225	
	7,5	1,331	
6	2,5	1,33	
	5	???	Calculation not finished
	7,5	1,742	Calculation not finished
8	2,5	3,797	Not enough load steps
	5	2,901	
	7,5	4,519	Not enough load steps
10	2,5	1,897	
	5	1,396	
	7,5	5,342	Not enough load steps

Table 28, Calculation outcomes for undrained calculations using Plaxis 3D

21.4.1 Possible sources of errors in calculation outcomes

Since the outcomes for the safety factors are not showing any expected patterns it is asked why this happens. Therefore a search to possible errors in the model is executed. During this process multiple model properties are changed. Below these changes are summed up and it is described what their influence is.

- Increase mesh fineness around foundation

A possible explanation of the inconsistent calculation outcomes could be that the mesh for the model is modelled too coarse and causing errors. For several models the mesh was refined around the foundation foot, but the effect of this refinement is not directly visible in the calculation outcomes.

- Apply interface between foundation plate elements and soil material

To increase the reliability for the model it is suggested to apply an interface between the modelled foundation plate and the soil material. For all the models this is done by applying positive and negative interfaces for both the horizontal and vertical plate elements. The interface elements are extended in both horizontal and vertical direction to exclude the influence of concentrated forces at the corners of the foundations. The interface elements are not having any physical contribution to the model, they only influence the calculation of the model. An image of the applied interface elements is placed below.
The influence of the applied interfaces is recognizable in the calculation outcomes. With the interfaces being present the calculation of the model costs less time. Also the application of the interfaces results in lower outcomes for the safety factors.

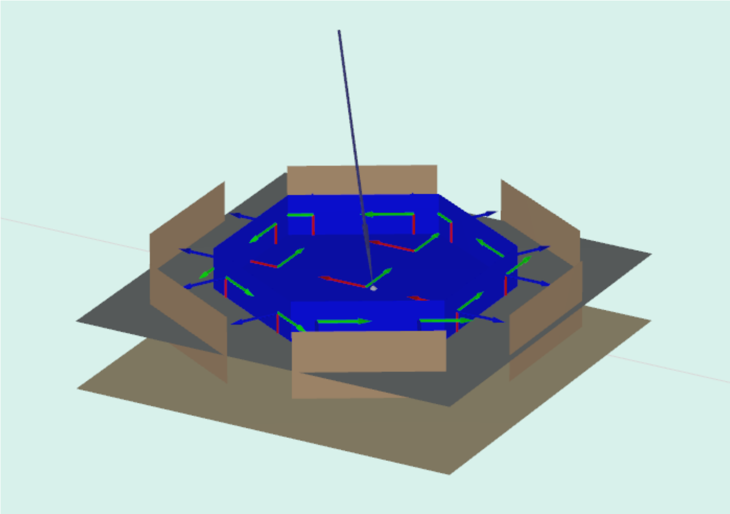

Figure 89, Interface elements as modelled in Plaxis 3D

<u>- Reduce dimensions of model</u>
Some of the models calculation outcomes are giving errors involving insufficient load steps or the calculation time is too large to finish. The reason for these errors may be sought in de direction of the model dimensions. Because the dimension of the model is much larger than the dimensions of the foundation the number of elements in the meshed model often reaches a value of around 20.000 elements, even with a coarse mesh. If the mesh is refined the number of elements even increases more. Due to this number of elements the calculation time increases elaborately and due to the coarse mesh elements errors could occur like the error “Not enough load steps”. When the model size is reduced it is possible to reduce the number of elements and thus increase the calculation speed or to reduce the size of the mesh elements to reduce possible errors due to a large mesh and as result a possible increase in the reliability of the calculation outcomes, although it should be said that an reduction of the mesh elements will not automatically result in more reliable calculation outcomes.

The first two options, refine the mesh around the foundation and apply interfaces, did not result in better calculation outcomes for the undrained 3D calculations. Therefore it is suggested to used the software Plaxis 2D to perform the undrained calculations. How this is done is described in the following chapter.

22. Dynamic loadings in Plaxis 2D

As mentioned before the calculation outcomes for the undrained calculations using Plaxis 3D are not leading to satisfying calculation outcomes for the safety factors. Therefore it is suggested to use the software Plaxis 2D to perform the undrained calculations.

22.1 Why use Plaxis 2D

Since the results for the undrained Plaxis 3D calculations are not showing any consistency it is decided to use the software Plaxis 2D which is less complicated than the 3D program. Therefore it may be less likely that errors will occur during making the models. The second advantage is that the calculation speed for the Plaxis 2D environment is much faster than it is for the 3D models which makes it possible to calculate models with a more dens mesh structure.
A disadvantage of the 2D software is that it is unable to directly model radial non-symmetric structures like the foundation used for this study. When using the Plaxis 2D software the foundation will be modelled as a strip foundation. By doing so the calculation outcomes of the 2D analysis will result in lower safety factors than when the same situation using the real foundation dimensions was modelled using the 3D software.

22.1.1 Relate Plaxis 2D outcomes to Plaxis 3D outcomes

The aim of the undrained 3D calculations was to compare the already obtained drained 3D calculations with the to be calculated undrained 3D values to investigate the influence of the dynamic loads. Due to the switch to Plaxis 2D software it is no longer possible to directly compare the drained 3D calculations with the to be performed 2D calculations because of the different model layouts.
Therefore drained 2D calculation are performed and the ratios between the drained 2D and 3D safety factors are calculated. Subsequently undrained 2D calculations are performed and the ratios for the drained safety factors are used to produce 3D safety factors representing the undrained 3D calculation outcomes. A scheme illustrating the latter procedure is visible in the figure below.

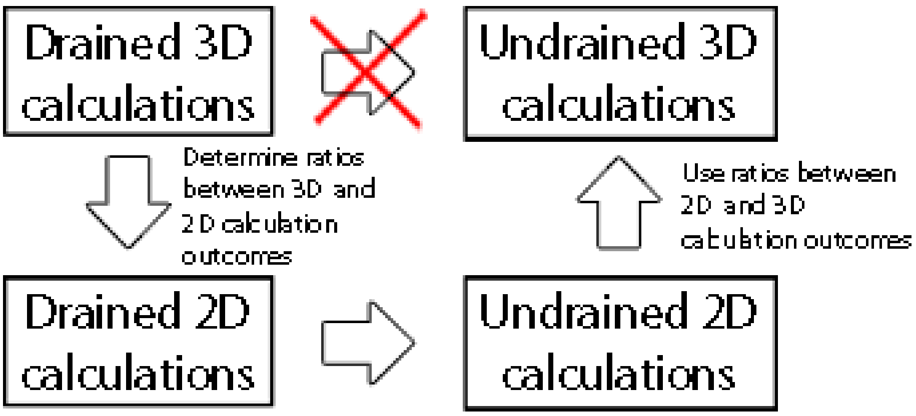

Figure 90, Procedure to determine safety factors for undrained 3D models using relation drained 3D and 2D models

22.2 Model properties for drained Plaxis 2D models

Since a different program is used the properties for the 2D models are briefly explained. It is tried to create the same circumstances for both the 2D and 3D models as much as possible.

22.2.1 Forces magnitudes and model dimensions for Plaxis 2D model

Since the strip foundation used for this Plaxis 2D analysis has a large resemblance with the models created for the Deltares D-Geo Stability the forces calculated for this D-Geo Stability models can also be applied in the Plaxis 2D software. Therefore the forces used in the Plaxis 2D calculation are also existing of two components, being a horizontal and vertical force component.

The magnitude of the horizontal component is $F_H = \frac{H_D}{l_{eff}} = \frac{10.890}{18,62} = 584,9kN$ and for the vertical component the force magnitude is $F_V = \frac{S_w}{l_{eff}} = \frac{76.470}{18,62} = 4107kN$ acting downwards. How the forces S_w and H_D are calculated can be viewed in the Deltares D-Geo Stability part of this report.

The dimensions of the strip footing are also calculated at a similar way as has been done for the D-Geo Stability models. This results in a strip footing with a width of 18,62m and a depth of 3,1m, which is the overburden depth calculated before. For the width and depth of the model the same dimensions as used for the 3D analysis are applied resulting in a model width of 180m and a height of 50m. The phreatic level is applied at 10m above the soil level, identical to the 3D models.

22.2.2 Material properties for 2D models

It is tried to model the same material properties for both the 2D and 3D soil analyses. The major difference between the 2D and 3D soil properties is that the stiffness parameter for the 2D plate has the thickness of the 0,3m thick stiff plate incorporated. Therefore the stiffness is denoted as EA [kNm²/m²] in the Plaxis 2D soil properties.

When creating the models for the 2D analysis also interface elements are incorporated in the model to increase the reliability of the models. This is done by setting an outer interface at all the plate elements. For these 2D models the interfaces are also being extended beyond the corners of the foundation. This is to reduce the influence of the edges of the foundation plates.

An overview of the Plaxis 2D model, including the applied forces, soil layers, stiff plates and interface elements can be seen in the figure presented below.

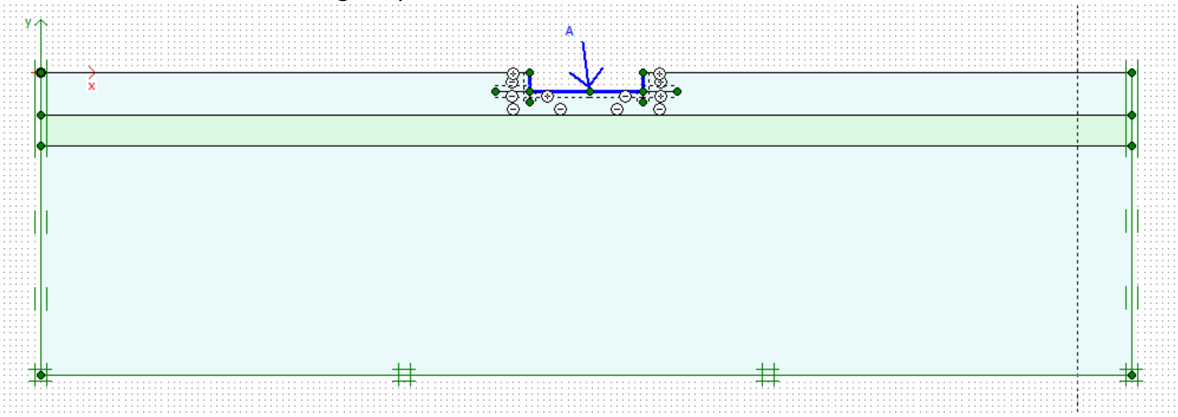

Figure 91, Layout for Plaxis 2D model with interfaces

22.2.3 Calculation phases used for drained 2D calculations

To calculate the safety factor of the models the same procedure is applied as it is for the Plaxis 3D models. This means that four different calculation phases are applied and the calculated value for M_{stage} in the Load10 calculation phase is used to determine the safety factor of the model.

22.3 Calculation outcomes for drained 2D calculations using Plaxis 2D

As stated before two types of 2D calculations are done, namely a drained and an undrained 2D calculation, to be able to relate the calculated 2d analyses to the 3D analyses. Therefore first the drained safety factors for the Plaxis 2D models are calculated.

22.3.1 Calculation outcomes for activated interface elements

When the models with the activated interface elements are calculated it is noticed that some calculation outcomes are presenting calculation errors. This is an unexpected behaviour since it is thought that the application of the interface elements is leading to more reliable calculation outcomes. Also the relation between the calculation outcomes is not as expected and therefore questioned. All the calculation outcomes and analysis is placed in the appendix since the usability of the outcome is questioned.

22.3.2 Calculation outcomes for inactive interface elements

Because of these errors and questioned values for the calculated safety factors with interface it is decided to perform a calculation of the drained 2D models with the interfaces turned off which resulted in no errors.
The safety factor calculation outcomes are showing a strange pattern. It is noticed that all the safety factors for the 2,5m thick clay layers are showing a remarkable pattern, first the safety factor decreases and at a depth of 10m it increases. The only other safety factor that does not meet the expected behaviour is the value for the 10-7,5 model. All the other calculation outcomes are of the same order as was found for the drained calculation with the active interfaces elements.
Since the calculation outcomes for the models with the interface active and inactive are showing both questionable outcomes it is concluded that it is not possible to make a reliable comparison between the drained 2D and 3D calculation outcomes. Because the obtained results are not usable to make a reliable comparison anevaluation of the calculation outcomes can be found in the appendix.

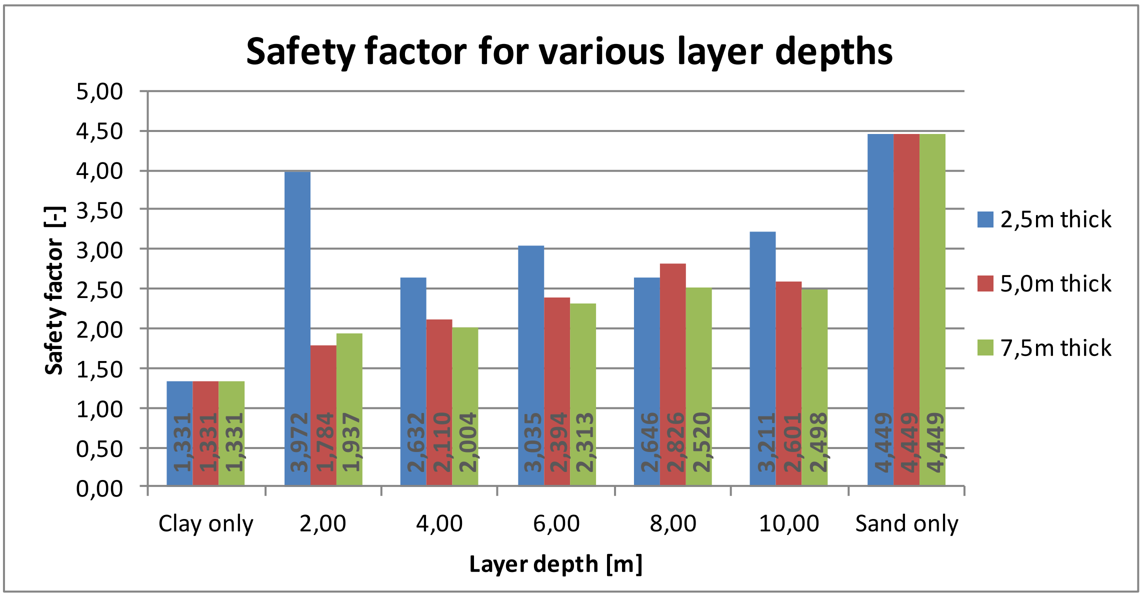

Figure 92, Graph safety factors for drained calculations without interface

22.3.3 Reliability of Plaxis 2D calculation outcomes

When performing the drained 2D calculations it is expected that the safety values obtained will not have the same value as the 3D models because the models are physically not equal. On the other hand it is expected that the ratios and relations between the safety factors for the 2D and 3D calculations will be comparable because it is expected that the failure mechanism will be equal for both the 2D and 3D models.

Since the ratios and relations between the 2D and 3D safety factors are not corresponding it is concluded that the obtained 2D safety factors are not usable to find a reliable ratio between the drained 2D and 3D calculations. A brief analysis can be found in the appendix.

22.3.4 Possible explanations for relations not meeting expectations

Regarding the undrained calculation outcomes without interface it is noted that the most shallow and most deepest layer calculation outcomes are questioned. In the mesh plots it is found that the number of mesh elements between the foundation and the top of the clay layer is only 1. This may cause problems during the calculation of the 2m deep clay layer models. Since the mesh size cannot be further refined and thus no solution is found to increase the number of mesh elements between the foundation and the clay layer. For the 10m deep clay layers there is no possible explanation found since the number of mesh elements is sufficient and the boundaries are wide enough.
f
When the calculation outcomes of the models without interface are regarded it is seen that the calculation outcomes for the models with a clay layer of 2,5m thick are questioned. It looks like the program is not able to accurately calculate the influence of thin clay layers. It is seen that the lower the clay layer is located the more the safety factors for the 2,5m thick layer are decreasing to a more expected value. From the values for the 8m deep layer it is noticed that the calculated safety factors are more meeting the expected values as obtained at the 3D calculations.

22.4 Model properties for undrained Plaxis 2D models

Although it is not possible to define reliable relations between the drained outcomes for the Plaxis 2D and 3D models, the results of the undrained 2D model calculations are nevertheless presented. Though it should be taken in mind that the presented safety factors are not comparable with the ones obtained with the drained 3D calculations.
The design and calculation method of the undrained models as well as the properties of the stiff plate are identical to the drained models as explained before. Therefore this part of the modelling is not further discussed for the undrained models. The only differences in the models are found in the material properties for the sand and clay soil material for which reference is made to the material properties presented at the undrained Plaxis 3D calculations. All the undrained soil material properties for sand and clay using Plaxis 2D can be viewed in the Appendix.

22.5 Calculation outcomes for undrained 2D calculations using Plaxis 2D

Calculations for the undrained 2D calculations are performed at the same way as the drained 2D calculations. Also for the undrained 2D models calculations are performed with and without interface elements. This was done because the undrained 2D calculations with the interfaces active were giving inconsistent calculation outcomes.

22.5.1 Calculation outcomes for undrained 2D calculations with interfaces

During the calculation it turned out that the safety factor of the calculated models was not exceeding 1 for both the calculation phases using a load factor 1 (Load1) and load factor 10 (Load10). Therefore the calculation outcomes for both the safety factors of Load1 and Load 10 are presented.

In the calculation outcomes in the appendix some values are marked green. These marked values are indicating calculation outcomes where the soil collapsed. For all the other safety factors the soil body did not collapse before the end of the calculation.

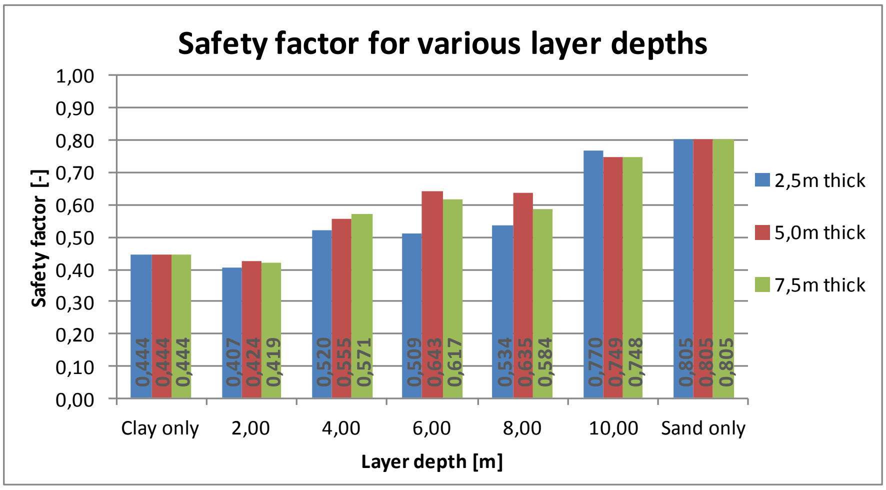

Figure 93, Load1 graph safety factors for undrained calculations with interface

What can be seen from the presented graphs is that the relations between the obtained safety factors are not as expected since it is expected that the safety factor would increase for deeper clay layers and that the safety factor would decrease if the clay layer becomes thicker.

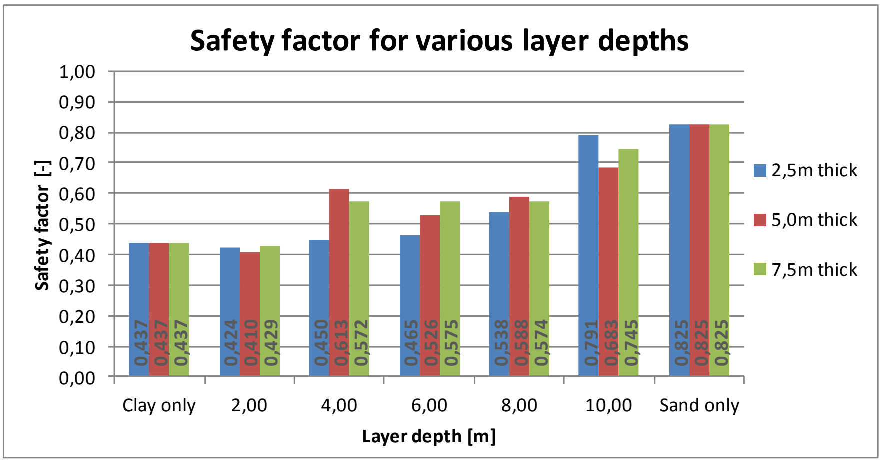

Figure 94, Load10 graph safety factors for drained calculations with interface

For both the Load1 and Load10 graphs it can be seen that the safety factor of the clay only model is higher than for the models with a clay layer at 2m depth which is remarkable because it is expected that the clay only layer would have the lowest safety factor of all models.

What is also noticeable is that for some safety factors the difference between the Load1 and Load10 value is very small, but for other values the difference is quite high. For example the difference between the 10-7,5 safety factors is very small (0,748 for Load1 and 0,745 for Load10) but for the 6-5,0 safety factor the difference is very large (0,643 for Load1 and 0,526 for Load10). Why the differences between the safety factors for the same model are fluctuating so much is not clear. Since they are using the same model with the same parameters it is expected that the safety factors would be equal between the Load1 and Load10 calculation phase.

22.5.2 Calculation outcomes for undrained 2D calculations without interfaces

Because of the unsatisfying calculation results in the previous paragraph it is also attempted to calculate the safety factors of the models with the interface turned off. These calculation outcomes are presented in the graph below. Also for these calculations some values are questioned, namely the safety factors for the 4-2,5, 6-5,0 and 8-5,0 models.
The number of doubtful outcomes is quite low for the undrained models without interface. When these doubtful outcomes are not regarded it can be seen in the graphs presented below that the pattern present for the calculated outcomes are showing some consistency, both for the thickness and depth of the layer. All the graphs for the undrained 2D safety factors for models without interface are added in the appendix at the end of this document.

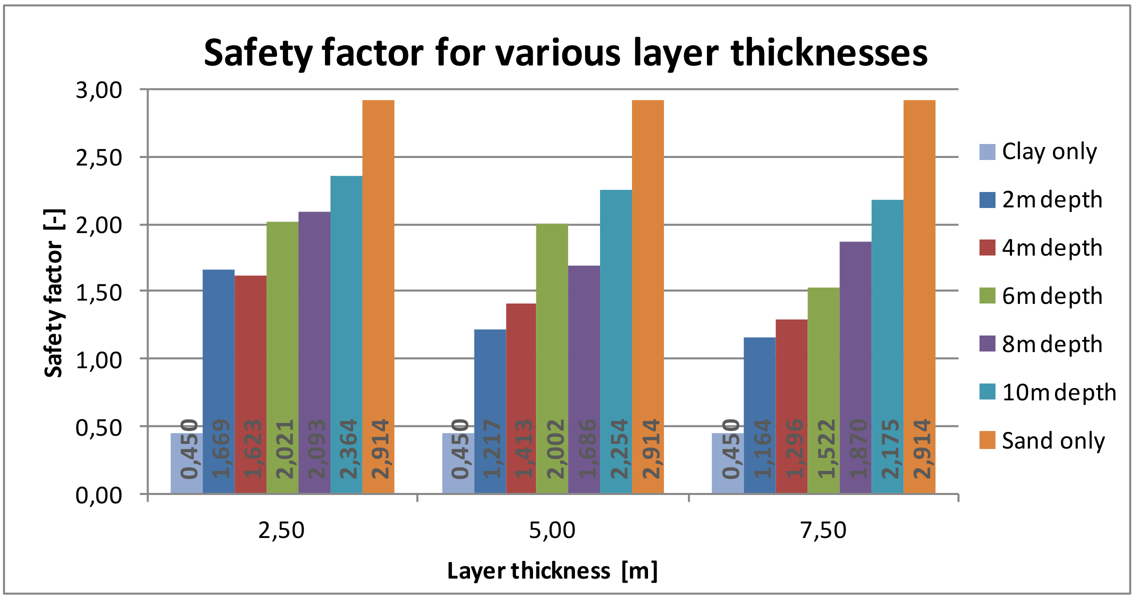

Figure 95, Undrained safety factors for various layer thicknesses for 2D models without interface

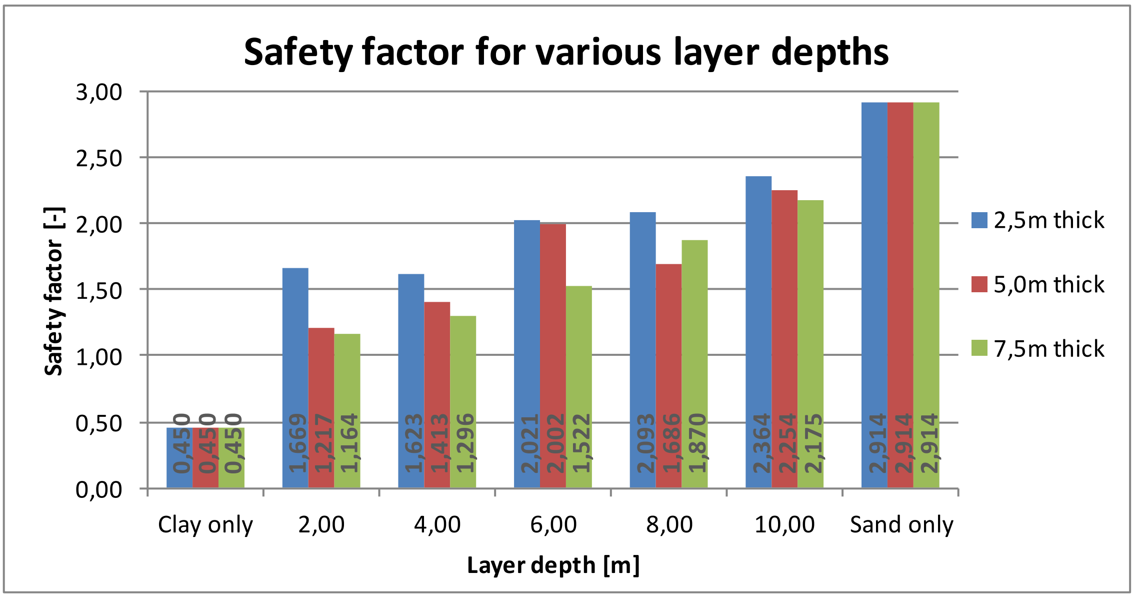

Figure 96, Undrained safety factors for various layer depths for 2D models without interface

Since it was not possible to obtain a reliable relationship between the 3D and 2D calculation outcomes it is not possible to compare the static (drained calculations) and dynamic (undrained calculations) safety factors. Because the obtained safety factors for the undrained 2D models without interface are found the most reliable of all the undrained safety factor calculations it is attempted to describe the quantitative behaviour of the soil with these calculated values.

22.5.3 Relation between undrained safety factors for 2D models without interface

From the previous presented graph for the relationship between the safety factors for various layer depths it can be seen that the safety factor for a clay only model is much lower than for the clay layer model with the lowest safety factor. In the graph presented below it can be seen that for the 7,5m thick layers, where no questioned values are present, the safety factor increases with a ratio of 1,11 for the shallow clay layers to a ratio of 1,23 for the clay layer at 8m depth which indicates a positive effect on the safety factor for an increasing clay layer depth. Since for the 2,5m and 5m thick clay layers thicknesses the results are not reliable it cannot be justified if this same relation also holds for these layer thicknesses.

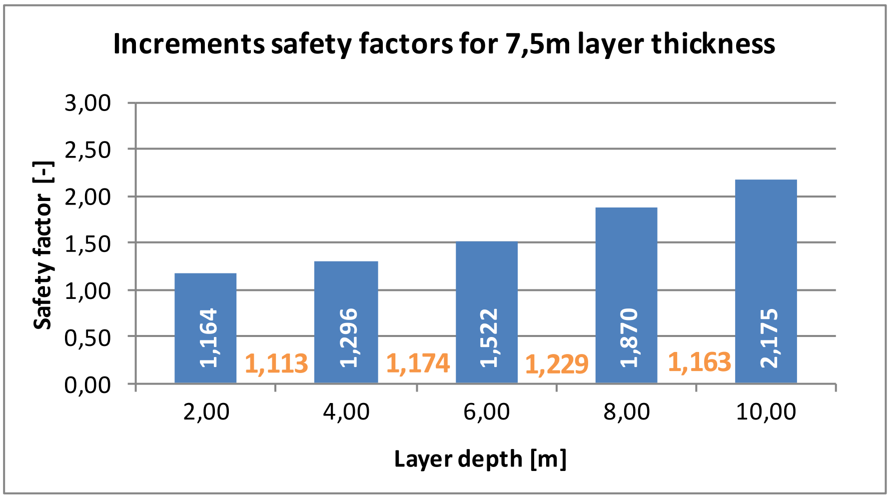

Figure 97, Relation safety factors for 7,5m thick layers for 2D models without interface

When regarding the graph for the safety factors for various layer depths it is noticed that for the deeper layers the ratio between the safety factors is much smaller than it is for the shallow clay layers. This indicates that for shallow layers an increase of the layer depth has more influence on the safety factors than it has for deeper located clay layers.
If there is made a small comparison between the drained 3D and undrained 2D calculations it is noticed that for the undrained calculations the difference between safety factors of the deeper clay layers and the sand only model is smaller that it is found for the drained 3D models. This indicates that the presence of a clay layer has less influence on the safety factor for undrained models than it has for the drained models, although it should be mentioned that a 1:1 comparison between the drained 3D models and undrained 2D models cannot be fully justified.

22.6 Résumé

Since it was not possible to determine correct safety factors for different soil models using Deltares D-Geo Stability software the program switch is made to Plaxis 3D. With the aid of this software it is tried to determine the safety factor for the designed wind turbine foundation on different sub soils. The determination of the safety factors is done for two type of drainage conditions. The first is a drained condition which should represent the static safety of the soil. The second drainage condition is undrained soil. By using this drainage type it is attempted to determine the safety factor of the soil under dynamic loadings.
Since the modelling of the undrained soil models is not leading to reliable calculation outcomes the switch is made to Plaxis 2D. It is aimed to use the ratios between the drained 2D and 3D calculations to determine the undrained 3D safety factors using the calculated 2D safety factors for undrained models. But also the calculation of the safety factors for the drained 2D models is not leading to reliable outcomes. Therefore it is found that it is not directly possible to compare the safety factors of drained and undrained soil conditions by using the calculations made for this study. This has as a result that it is not possible to say whether the static loading or the dynamic loading on the wind turbine foundation is leading to the lowest safety factors for the different soil models.
The only quantative analyses that can be made are for either only the relations between the drained 3D models or only the relation between the undrained 2D models, although the undrained 2D models are also showing some questionable outcomes.

23. Conclusion and findings

The scope of this study is to investigate the possibilities for applying Gravity Base Foundations at larger water depths. To do so the influence of various parameters for the foundation and turbine are investigated as well as the properties of the sub soil.
From the variance study it is found that the wind forces acting on the wind turbine are causing the major part of the bending moments acting on the foundation. Compared with the wave forces the bending moments due to wind forces are a factor 10 larger. When the horizontal forces are regarded both the wind and wave forces are having the same order of magnitude.
With the forces found for a foundation at 25m depth a design is made for a hexagonal foundation. It is calculated that the reinforcement as well as the needed self weight of the foundation are within acceptable and practical limits.
In the calculation outcomes it can be seen that an increase from 25 to 35m water depth leads to an increase of 13% of the bending moment. For the design of the foundation it is stated that such a relative small increase in bending moments will not lead to problems for designing a foundation for 35m deep waters.

In the second part the bearing capacity of the foundation is regarded. Here it is found that the use of specialized 3D geotechnical software leads to significant higher bearing capacities, a factor 12 higher than hand calculations. On the other hand it is found that the presence of weaker clay layers within a stronger sand stratum is significantly influencing the bearing capacity. This effect is higher for shallow layers but also for thicker clay layers. In this study it is found that the presence of a clay layer is reducing the bearing capacity with 25 to70% depending on depth and thickness of the clay layer. Almost similar behaviour is found for models which model dynamic bearing capacity. Only the obtained safety factors are not comparable because a different calculation method is used.

With the calculations and conclusions found in this thesis it is stated that the application of GBF at larger depths is a viable application. When forces are regarded the wind forces are dominating the design of the foundation and therefore the size of the turbine and the governing wind conditions are important parameters. The up scaling of the foundation size is limited by the increasing weight of the concrete foundation. This because there are limited suitable heavy lift vessels and offshore handling becomes more difficult.
Also the bearing capacity of the foundation can be the limiting factor for the application of GBF´s at larger depths. Because the weight of the foundation and the forces on the foundation are increasing a higher bearing capacity is needed. When weaker layers are present at an intended offshore location the bearing capacity is highly influenced and can become a limiting factor.

In brief it is concluded that it is technically possible to construct concrete Gravity Base Foundations for larger water depths, but due to the increase of the foundation weight the handling of the foundations and the bearing capacity of the sub soil are the aspects that are determining the applicability to a large extend.

Appendix

1. Calculation of wind speeds

Different wind profiles and models

Normal wind profile (NWP)

This profile represents the average wind speed as a function of heights above sea level. This profile is explained before. The formula for the normal speed wind model is

$$V(z) = V_{hub}\left(\frac{z}{z_{hub}}\right)^{\alpha}$$

with the power law exponent $\alpha = 0.14$ for offshore locations

Normal turbulence model (NTM)

The Normal turbulence model represents turbulent wind speed in terms of a characteristic standard deviation of wind speed, $\sigma_{U,c}$. The value for σ_1 can be calculated with the following formula:

$$\sigma_{U,c} = I_{ref}(0,75V_{hub} + b); \quad b = 5,6 \text{ m/s}.$$

The value for I_{ref} can be found in the following table for the standard wind turbine classes:

Wind turbine class		I	II	III	S
V_{ref}	(m/s)	50	42,5	37,5	Values
A	I_{ref} (-)		0,16		specified
B	I_{ref} (-)		0,14		by the
C	I_{ref} (-)		0,12		designer

Table 29, Standard wind turbine classes

Extreme wind speed model (EWM)

The Extreme wind speed model is used to represent extreme wind conditions with a specified return period, usually either one year of 50 years. It shall be either a steady wind model or a turbulent wind model. In case of a steady wind mode, the extreme wind speed (U_{EWM}) at the hub height with a return period of 50 years shall be calculated as: $U_{hub,50-yr} = 1,4 \cdot U_{10,hub,50-yr}$ where $U_{10,hub,50-yr}$ denotes the 10-minute mean wind speed at hub height with a return period of 50 years.

The extreme wind speed (U_{EWM}) at the hub height with a return period of one year shall be calculated as $U_{hub,1-yr} = 0,8 \cdot U_{hub,50-yr}$.

The quantities $U_{hub,1-yr}$ and $U_{hub,50-yr}$ refer to wind speed averaged over three seconds.

The 10-minute mean wind speed at hub height with a return period of one year shall be calculated as $U_{10,hub,1-yr} = 0,8 \cdot U_{10,hub,50-yr}$. Further the turbulent extreme wind model makes use of a characteristic standard deviation of the wind speed. The characteristic standard deviation of the wind speed shall be calculated as: $\sigma_{U,c} = 0,11 \cdot U_{10,hub}$.

Extreme operating gust(EOG)

The Extreme operating gust at hub height has a magnitude which shall be calculated as:

$$V_{gust} = \min\left\{1,35(U_{hub,1-yr} - U_{10,hub}); \frac{3,3\sigma_{U,c}}{1+0,1D/\Lambda_1}\right\}$$ in which

$\sigma_{U,c}$ = Characteristic standard deviation of wind speed

Λ_1 = Longitudal turbulence scale parameter $(L_k = 8{,}1\Lambda_1)$ where $\Lambda = \begin{cases} 0{,}7z & z \le 60m \\ 42m & z \ge 60m \end{cases}$

D = Rotor diameter

The wind speed V as a function of height z and time t shall be defined as follows:

$$V(z,t) = \begin{cases} u(z) - 0{,}37V_{gust}\sin(\frac{3\pi \cdot t}{T})(1-\cos(\frac{2\pi \cot t}{T})) & for 0 \le t \le T \\ u(z) & \text{otherwise} \end{cases}$$

Where $T = 10{,}5$ sec and $u(z)$ is defined by the Normal wind profile.
In the figure below an example of a Extreme Operating Gust is shown with a recurrence period of 1 year and a wind speed at hub height of $V_{hub} = 25m/s$.

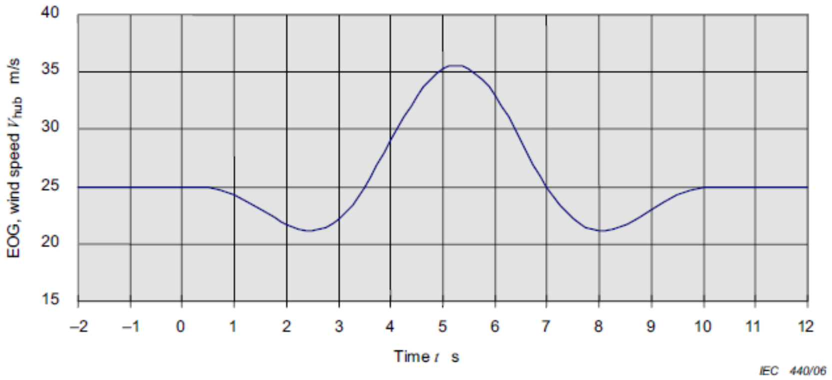

Figure 98, Example of extreme operating gust with vhub=25m/s

Extreme turbulence model (ETM)

The Extreme turbulence model combines the normal wind profile model with a turbulent wind speed whose characteristic standard deviation is given by:

$$\sigma_{U,c} = c \cdot I_{ref} \cdot \left(0{,}072 \cdot \left(\frac{U_{average}}{c} + 3\right) \cdot \left(\frac{U_{hub}}{c} - 4\right) + 10\right)$$

In which

c = 2 m/s

U_{hub} = Wind speed at hub height

$U_{average}$ = Long-term average wind speed at hub height

I_{ref} = Expected value of turbulence intensity at hub height at $U_{10,hub}$ = 15 m/s

Extreme direction change (EDC)

The extreme direction change has a magnitude whose value shall be calculated according to the following expression:

$\theta_e = \pm 4 \cdot \arctan \dfrac{\sigma_{U,c}}{U_{10,hub}(1+0{,}1D/\Lambda_1)}$. θ_e is limited to the range $\pm 180^\circ$.

The extreme direction change transient, $\theta(t)$, as a function of time t shall be given by:

$$\theta(t) = \begin{cases} 0 & for\ t < 0 \\ 0{,}5\theta_e(1-\cos(\pi \cdot t/T)) & for\ 0 \le t \le T \\ 0 & for\ t \ge T \end{cases}$$

where $T = 6$ sec is the duration of the extreme direction change.

Extreme coherent gust with direction change (ECD)

The extreme coherent gust with direction change shall have a magnitude of $V_{cg} = 15 \text{ m/s}$.

The wind speed V as a function of height z and time t shall be defined as follows:

$$V(z,t) = \begin{cases} u(z) & for \quad t < 0 \\ u(z) + 0,5V_{cg}(1 - \cos(\pi \cdot t / T)) & for \quad 0 \le t \le T \\ u(z) + V_{cg} & for \quad t > T \end{cases}$$

Where $T = 10 \text{ sec}$ is the rise time and $u(z)$ is the wind speed from the normal wind profile.

The rise in wind speed shall be assumed to occur simultaneously with the direction change θ from 0 degrees up to an d including θ_{cg}, where θ_{cg} is defined by:

$$\theta_{cg}(U_{10,hub}) = \begin{cases} 180^{\circ} & for \quad U_{10,hub} \le 4m/s \\ \dfrac{720^{\circ} m/s}{U_{10,hub}} & for \quad U_{10,hub} > 4m/s \end{cases}$$

The direction change which takes place simultaneously as the wind speed rises is given by:

$$\sigma(t) = \begin{cases} 0^{\circ} & for \quad t < 0 \\ \pm 0,5\theta_{cg}(1 - cos(\pi \cot t / T)) & for \quad 0 \le t \le T \\ \pm \theta_{cg} & for \quad t > T \end{cases}$$

Where $T = 10 \text{ sec}$ is the rise time.

Extreme wind shear model (EWS)

The Extreme wind shear model is used to account for extreme transient wind shear events. It consists of a transient vertical wind shear and a transient horizontal wind shear. The extreme transient positive and negative vertical shear shall be calculated as:

$$V(z,t) = \begin{cases} U_{10}(z) \pm \dfrac{z - z_{hub}}{D} \cdot \left(2,5 + 0,2\beta\sigma_{U,c} \left(\dfrac{D}{\Lambda_1} \right)^{1/4} \right) \cdot \left(1 - \cos(\dfrac{2\pi \cdot t}{T}) \right) & for\ 0 \le t \le T \\ U_{10}(z) & \text{otherwise} \end{cases}$$

The extreme transient horizontal shear shall be calculated as:

$$V(y,z,t) = \begin{cases} U_{10}(z) \pm \dfrac{y}{D} \cdot \left(2,5 + 0,2\beta\sigma_{U,c} \left(\dfrac{D}{\Lambda_1} \right)^{1/4} \right) \cdot \left(1 - \cos(\dfrac{2\pi \cdot t}{T}) \right) & for\ 0 \le t \le T \\ U_{10}(z) & \text{otherwise} \end{cases}$$

With $\beta = 6,4$ and $T = 12 \text{ sec}$.

Reduced wind speed model (RWM)

The Reduced wind speed model defines a companion wind speed U_{RWM} to be used in combination with the extreme wave height (EWH) for definition of an extreme event with a specified return period. The reduced wind speed can be expressed as a fraction of the extreme wind speed, $U_{RWM} = \psi \cdot U_{EWM}$, $\psi < 1$. The reduced wind speed is used for definition of events with return periods of 50 years and 1 year, and the corresponding reduced wind speeds are denoted $U_{Red,50-yr}$ and $U_{Red,1-yr}$ respectively. The value for $\psi = 0,79$ can be assumed.

2. Calculation of wave forces

Description JONSWAP

The JONSWAP spectrum is presented below:

$$S(f)=\frac{\alpha g^2}{(2\pi)^4}f^{-5}\exp\left(-\frac{5}{4}\left(\frac{f}{f_p}\right)^{-4}\right)\gamma^{\exp\left(-0,5\left(\frac{f-f_p}{\sigma\cdot f_p}\right)^2\right)}$$

Where:

f = wave frequency, f=1/T

T = wave period

f_p = spectralpeakfrequency, $f_p=1/T_p$

T_p = peak period

g = acceleration of gravity

α = generalised Philips′ constant

= $5\cdot(H_S^2 f_p^4/g^2)\cdot(1\text{-}0,287\ln\gamma)\cdot\pi^4$

σ = spectral width parameter

= 0,07 for f $\leq f_p$ and σ=0,09 for f $\geq f_p$

γ = peak-enhancement factor

The peak-enhancement factor is:

$$\gamma=\begin{cases}5 & for \quad \frac{T_p}{\sqrt{H_S}}\leq 3,6\\ \exp(5,75-1,15\frac{T_p}{\sqrt{H_S}} & for \quad 3,6<\frac{T_p}{\sqrt{H_S}}\leq 5\\ 1 & for \quad 5<\frac{T_p}{\sqrt{H_S}}\end{cases}$$

Where T_p is in seconds and H_S is in meters.

The significant wave height with return period T_R in units of years is defined as the $(1-1/T_R)$ quantile in the distribution of the annual maximum significant wave height, i.e. it is the significant wave height whose probability of exceedance in one year is $1/T_R$. It is denoted H_{S,T_R} and is expressed as:

$H_{S,T_R}=F_{H_{S,max,1year}}{}^{-1}(1-\frac{1}{T_R})$ in which $T_R>1$ year .

TU Delft Delft University of Technology CFE

Different wave models presented in DNV norm

Normal sea state (NSS)

The Normal sea state is characterised by a significant wave height, a peak period and a wave direction. It is associated with a concurrent mean wind speed. The significant wave height $H_{S,NSS}$ of the normal sea state is defined as the expected value of the significant wave height conditioned on the concurrent 10-minute mean wind speed. The normal sea state is used for calculation of ultimate loads and fatigue loads. For fatigue load calculations a series of normal sea states have to be considered, associated with different mean wind speeds. The range of peak periods T_p appropriate to each significant wave height shall be considered. Design calculations shall be based on values of the peak period which result in the highest loads of load effects in the structure.

Normal wave height (NWH)

The Normal wave height is defined as the expected value of the significant wave height conditioned on the concurrent 10-minute mean wind speed, i.e. $H_{NWH} = H_{S,NSS}$. In deep waters the wave periods T to be used with H_{NWH} may be assumed to be within the range given by:

$$11,1\sqrt{H_{S,NSS}(U_{10})/g} \leq T \leq 14,3\sqrt{H_{S,NSS}(U_{10})/g}$$

Severe sea state (SSS)

The Severe sea state is characterised by a significant wave height, a peak period and a wave direction. It is associated with a concurrent mean wind speed. The significant wave height of the severe sea state $H_{S,SSS}$ is defined by extrapolation of appropriate site-specific MetOcean data such that the load effect from the combination of the significant wave height $H_{S,SSS}$ and the 10-minute mean wind speed U_{10} has a return period of 50 years. For all 10-minute wind speeds U_{10} during power production, the unconditional extreme significant wave height, $H_{S,50-yr}$ with a return period of 50 years may be used as a conservative estimate for $H_{S,SSS}(U_{10})$.

Severe wave height (SWH)

For the Severe wave height the same wave height holds as for the Severe sea state. In deep waters, the wave periods T to be used with H_{SWH} may be assumed to be within the range given by:

$$11,1\sqrt{H_{S,SSS}(U_{10})/g} \leq T \leq 14,3\sqrt{H_{S,SSS}(U_{10})/g}$$

Extreme sea state (ESS)

The Extreme sea state is characterised by a significant wave height, a peak period and a wave direction. The significant wave height $H_{S,ESS}$ is the unconditional significant wave height with a specified return period, determined from the distribution of the annual maximum significant wave height.

Extreme wave height (EWH)

The extreme deterministic design wave shall be considered for both the extreme wave height, H_{50} , with a recurrence period of 50 years and the extreme wave height, H_1, with a recurrence period of 1 year. The values of H_{50} , H_1, and the associated wave periods may be determined from analysis of appropriate measurements at the offshore wind turbine site.

Alternatively, assuming a Rayleigh distribution of wave heights, it may be assumed that: $H_{50-yr} = 1,86 \cdot H_{S,50-yr}$ and $H_{1-yr} = 1,86 \cdot H_{S,1-yr}$ where $H_{S,50-yr}$ and $H_{S,1-yr}$ are values for a 3-hour reference period.

Reduced wave height (RWH)

The Reduced wave height is a companion wave height to be used in combination with the extreme wind speed (EWS) for definition of an extreme event with a specified return period. The reduced wave height can be expressed as a fraction of the extreme wave height, $H_{RWH} = \psi \cdot H_{EWH}, \psi < 1$.

The reduced wave height is used for definition of events with return periods of 50 years and 1 year, and the corresponding reduced wave heights are denoted $H_{Red,50-yr}$ and $H_{Red,1-yr}$ respectively.

According to IEC61400-3 the values for $H_{Red,50-yr}$ and $H_{Red,1-yr}$ are:

$H_{Red,50-yr} = 1,3 \cdot H_{S,50-yr}$ and $H_{Red,1-yr} = 1,3 \cdot H_{S,1-yr}$

3. Turbine properties for Siemens wind turbine

Below the calculations are placed for the 3 different wind turbine types provided by R. Foekema from Siemens.

2,3-93 2,3MW turbine:

The wind pressure on the turbine is:

$$q = \frac{1}{2} \cdot 1,293 \cdot (41 \cdot 1,2)^2 = 1,565 kN/m^2$$

The force and moment on the blades becomes:

$$F_{blades} = 3 \cdot A_{blades} \cdot q = 3 \cdot 138,4 \cdot 1,565 = 649,6 kN$$

$$M_{blades} = F_{blades} \cdot h = 371,6 \cdot 64 = 41.575 kNm$$

In the ULS this becomes: $M_{blades} \cdot 1,35 = 56.126 kNm$

The lever arm of the forces on the tower is calculated with the following formula:

$$H_{moment} = \frac{3,87 H_{tower} \cdot \frac{1}{2} H_{tower} + \frac{1}{2} 2,13 H_{tower} \cdot \frac{1}{3} H_{tower}}{3,87 H_{tower} + \frac{1}{2} 2,13 H_{tower}}.$$

For this turbine with a tower height of 64 meter the lever arm of the resulting moment is: $29,7m$.

$$F_{tower} = A_{tower} \cdot q = 315,8 \cdot 1,565 = 494,3 kN$$

$$M_{tower} = F_{tower} \cdot H_{tower} = 270,4 \cdot 29,7 = 14.679 kNm$$

In the ULS this becomes: $M_{tower} \cdot 1,35 = 19.817 kNm$

For the nacelle the front surface of the nacelle is taken. For all the turbine types the front radius is taken as 5,4m. This gives a surface of $23m^2$. With the lever arm of 64 meter for this turbine type the moment due to the wind forces on the nacelle becomes:

$$M_{nacelle} = 23 \cdot 1,595 \cdot 64 = 2.338 kNm$$

$M_{nacelle}$ for the ULS becomes: $M_{nacelle} \cdot 1,35 = 3.156 kNm$

When there three moments are summed up the resulting bending moment on the tower foot is:

$$M_{blades} + M_{tower} + M_{nacelle} = 56.126 + 19.817 + 3.156 = 79.099 kNm$$

According to the data of Siemens it can be seen that the moment on the interface is 110.000kNm.

3,0-113 3MW wind turbine

The wind pressure on the turbine is:

$$q = \frac{1}{2} \cdot 1,293 \cdot (31 \cdot 1,2)^2 = 0,895 kN/m^2$$

The force and moment on the blades becomes:

$F_{blades} = 3 \cdot A_{blades} \cdot q = 3 \cdot 168,1 \cdot 10,895 = 451,2kN$

$M_{blades} = F_{blades} \cdot h = 451,2 \cdot 80 = 36.099kNm$

In the ULS this becomes: $M_{blades} \cdot 1,35 = 48.733kNm$

The lever arm of the forces on the tower is calculated with the following formula:

$$H_{moment} = \frac{3,87H_{tower} \cdot \frac{1}{2}H_{tower} + \frac{1}{2}2,13H_{tower} \cdot \frac{1}{3}H_{tower}}{3,87H_{tower} + \frac{1}{2}2,13H_{tower}}.$$

For this turbine with a tower height of 80 meter the lever arm of the resulting moment is: $37,1m$.

$F_{tower} = A_{tower} \cdot q = 394,8 \cdot 0,895 = 353,2kN$

$M_{tower} = F_{tower} \cdot H_{tower} = 353,2 \cdot 37,1 = 13.112kNm$

In the ULS this becomes: $M_{tower} \cdot 1,35 = 17.701kNm$

For the nacelle the front surface of the nacelle is taken. For all the turbine types the front diameter is taken as 5,4m. This gives a surface of $23m^2$. With the lever arm of 80 meter for this turbine type the moment due to the nacelle becomes:

$M_{nacelle} = 23 \cdot 1,595 \cdot 80 = 1.642kNm$

$M_{nacelle}$ for the ULS becomes: $M_{nacelle} \cdot 1,35 = 2.216kNm$

When there three moments are summed up the resulting bending moment on the tower foot is:

$M_{blades} + M_{tower} + M_{nacelle} = 48.733 + 17.701 + 2.216 = 68.650kNm$

According to the data of Siemens it can be seen that the moment on the interface is 78.000 kNm.

6,0-154 6MW wind turbine

The wind pressure on the turbine is:

$q = \frac{1}{2} \cdot 1,293 \cdot (43 \cdot 1,2)^2 = 1,721kN/m^2$

The force and moment on the blades becomes:

$F_{blades} = 3 \cdot A_{blades} \cdot q = 3 \cdot 229,1 \cdot 1,721 = 1.183,2kN$

$M_{blades} = F_{blades} \cdot h = 1.183,2 \cdot 90 = 106.487kNm$

In the ULS this becomes: $M_{blades} \cdot 1,35 = 143.758kNm$

The lever arm of the forces on the tower is calculated with the following formula:

$$H_{moment} = \frac{3,87H_{tower} \cdot \frac{1}{2}H_{tower} + \frac{1}{2}2,13H_{tower} \cdot \frac{1}{3}H_{tower}}{3,87H_{tower} + \frac{1}{2}2,13H_{tower}}.$$

For this turbine with a tower height of 90 meter the lever arm of the resulting moment is: $41,8m$.

$F_{tower} = A_{tower} \cdot q = 444,2 \cdot 1,721 = 764,5kN$

$M_{tower} = F_{tower} \cdot H_{tower} = 764,5 \cdot 41,8 = 31.929kNm$

In the ULS this becomes: $M_{tower} \cdot 1,35 = 43.104kNm$

For the nacelle the front surface of the nacelle is taken. For all the turbine types the front diameter is taken as 5,4m. This gives a surface of $23m^2$. With the lever arm of 80 meter for this turbine type the moment due to the nacelle becomes:

$M_{nacelle} = 23 \cdot 1,595 \cdot 90 = 3.548kNm$

$M_{nacelle}$ for the ULS becomes: $M_{nacelle} \cdot 1,35 = 4.790kNm$

When there three moments are summed up the resulting bending moment on the tower foot is:

$M_{blades} + M_{tower} + M_{nacelle} = 143.758 + 43.104 + 4.790 = 191.652kNm$

According to the data of Siemens it can be seen that the moment on the interface is 200.000kNm.

4. Location specific environmental parameters

Major environmental parameters

- Wind
  - Normal wind conditions at 10m height (U_{10})
  - Normal wind conditions at hub height ($U_{10,hub}$)
  - Extreme wind conditions with 1 year return period
    - 10 min extreme wind
    - 3 sec extreme gust
  - Extreme wind conditions with 50 year return period
    - 10 min extreme wind
    - 3 sec extreme gust

- Water
  - Average water depth
  - Extreme wave conditions with 1 year return period
    - Significant wave height ($H_{s,1-yr}$)
    - Wave period ($T_{p,1-yr}$)
    - Maximum wave height ($H_{max,1-yr}$)
    - Current
  - Extreme wave conditions with 50 year return period
    - Significant wave height ($H_{s,50-yr}$)
    - Wave period ($T_{p,50-yr}$)
    - Maximum wave height ($H_{max,50-yr}$)
    - Current
  - Maximum and minimum water level with return period of 1 year
  - Maximum and minimum water level with return period of 50 years
  - Maximum and minimum water level with ice conditions

Snow and ice
  - Sea ice load
    - Ice thickness (h)
    - Bending strength (σ_f)

5. Graphs from parameters for wave and wind properties for K13A platform on the north sea.

Figure 99, Location K13A platform

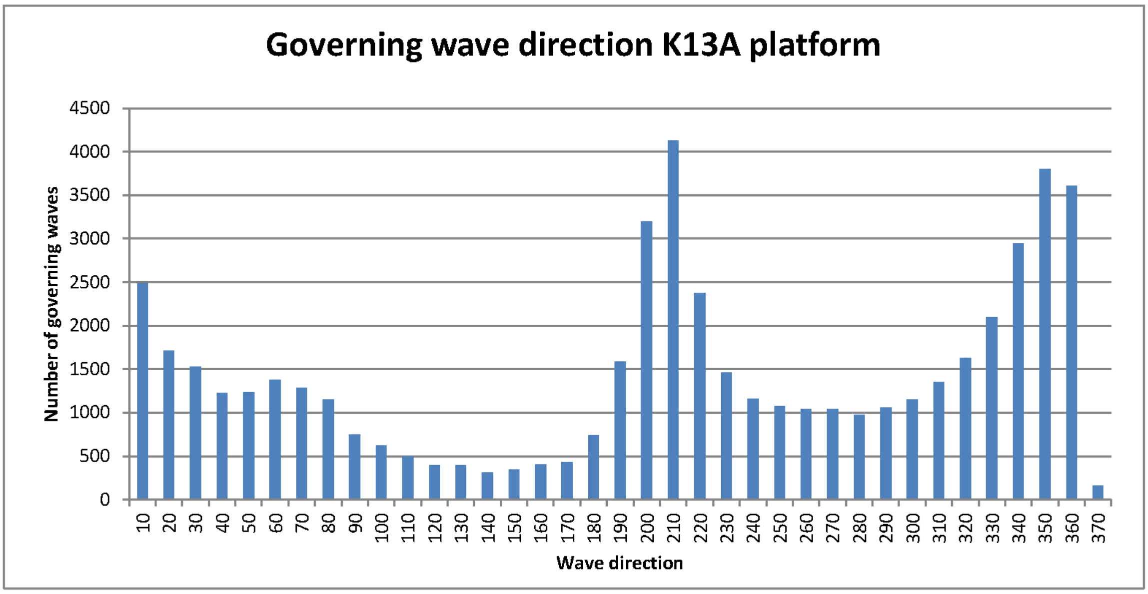

Figure 100, Governing wave directions for K13A platform

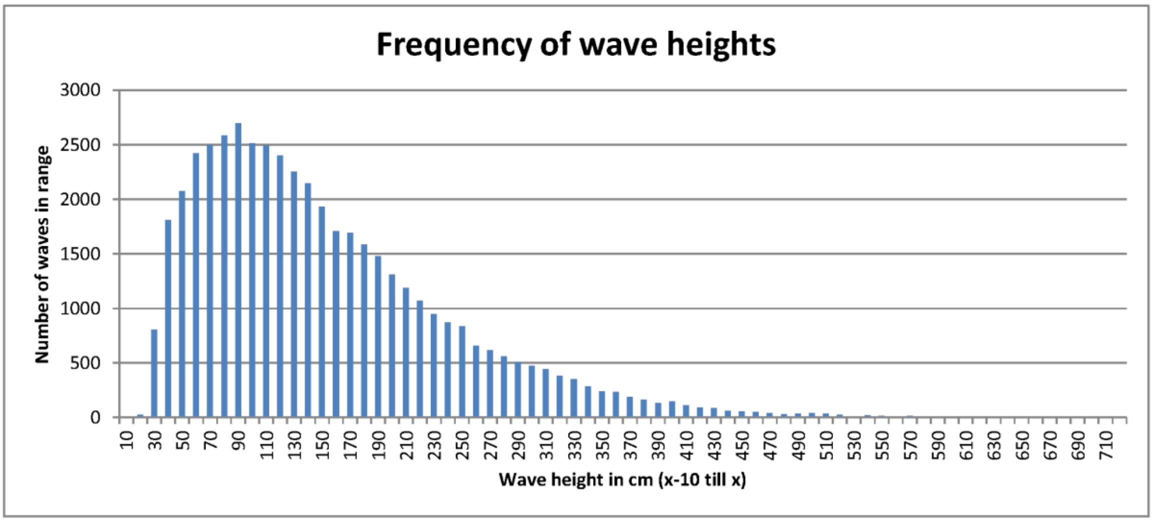

Figure 101, Frequency of wave heights for K13A platform

Relation Hs and Hmax = Hmax = 1.85*Hs

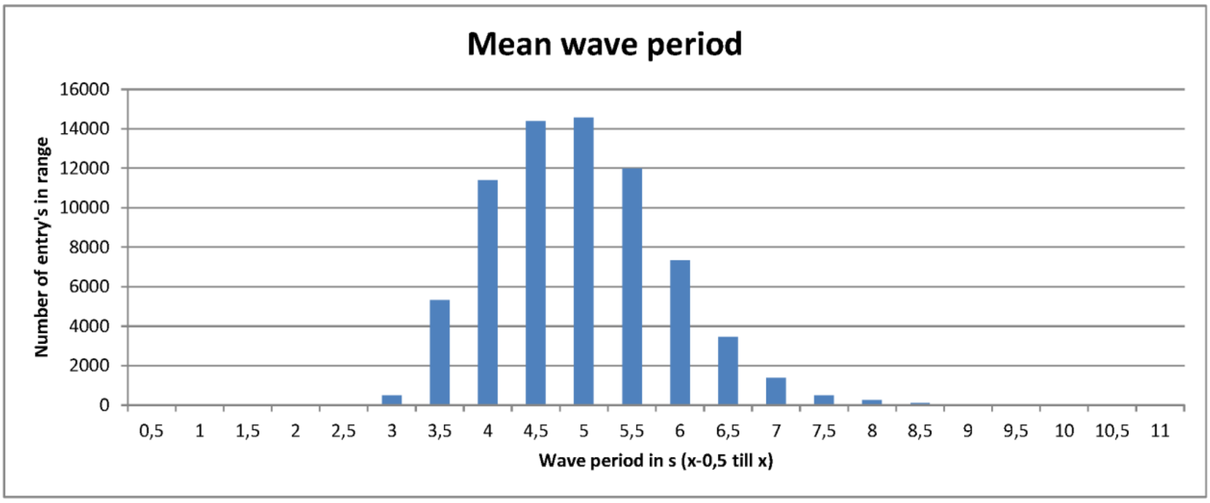

Figure 102, Mean wave period for K13A platrofm

Datasheet for kriegers flak

Kriegers Flak						
Turbine size	5	MW				
Maximum water depth	35	m				
Wind conditions						
Normal wind conditions at 10m height						
Mean wind speed	7,04	m/s				
Normal wind conditions at hub height						
Mean wind speed	8,8	m/s				
at heigth	80	m				
Wind shear exponent	0,11	-				
Extreme wind conditions 1 year return period						
10 min extreme wind	28,3	m/s				
3 sec extreme gust	37,4	m/s				
at height	80	m				
Extreme wind conditions 50 year return period						
10 min extreme wind	37,5	m/s				
3 sec extreme gust	49,6	m/s				
at height	80	m				
Wave conditions						
Extreme wave conditons 1y return period						
Hs	3,6	m				
Tp	8	s				
Hmax	-	m				
Crest elevation η	-	m				
Particle velocity	-	m/s				
Current	-	m/s				
Extreme wave conditons 50y return period						
Hs	5,2	m				
Tp	9,7	s				
Hmax	9,6	m				
Crest elevation η	6	m				
Particle velocity	6	m/s				
Current	0,3	m/s				
Water level conditions						
Max water level 1y	0,85	m				
Max water level 50y	1,33	m				

Min water level 1y	-0,81	m				
Min water level 50y	-1,25	m				
Max water level with ice	1,09	m				
Min water level with ice	-1,03	m				
Snow and ice						
Ice from sea spray						
Thickness	5	mm				
Density	850	kg/m^3				
Wet snow						
Thickness	40	mm				
Density	500	kg/m^3				
Sea ice loads						
Ice thickness	0,38	m				
Crushing strength	1,9	N/mm^2				
Bending strength	0,5	N/mm^2				
Ice floe size	1	km				
Ice floe velocity	0,6	m/s				

6. Datasheet for Hons Rev 3

Horns Rev 3							
Turbine size		MW		HR3-TR-020 Metocean.pdf			
Maximum water depth	20	m					
Wind conditions							
Normal wind conditions at 10m height							
Mean wind speed	9,5	m/s					
Normal wind conditions							
Mean wind speed	9,5	m/s					
at heigth	10	m					
Wind shear exponent	0,09	-					
Extreme wind conditions 1 year return period							
10 min extreme wind	23,2	m/s					
3 sec extreme gust		m/s					
at height	10	m					
Extreme wind conditions 1 year return period							
10 min extreme wind	26,7	m/s					
3 sec extreme gust		m/s					
at height	70	m					
Extreme wind conditions 50 year return period							
10 min extreme wind	29,3	m/s					
3 sec extreme gust		m/s					
at height	10	m					
Extreme wind conditions 50 year return period							
10 min extreme wind	34,7	m/s					
3 sec extreme gust		m/s					
at height	70	m					
Wave conditions							
Normal wave conditions							
Significant wave height	1,85	m					
Current	0,25	m/s					
Extreme wave conditons 1y return period							

Hs	5,9-6,9	m				
Tp	9	s				
Hmax	7	m				
Crest elevation η		m				
Particle velocity		m/s				
Current	1	m/s				
Extreme wave conditons 50y return period						
Hs	6,1-7,4	m				
Tp	8,9	s				
Hmax		m				
Crest elevation η		m				
Particle velocity		m/s				
Current	1,3	m/s				
Water level conditions						
Max water level 1y		m				
Max water level 50y		m				
Min water level 1y		m				
Min water level 50y		m				
Max water level with ice		m				
Min water level with ice		m				
Snow and ice						
Ice from sea spray						
Thickness		mm				
Density		kg/m³				
Wet snow						
Thickness		mm				
Density		kg/m³				
Sea ice loads						
Ice thickness	-	m				
Crushing strength	-	N/mm²				
Bending strength	-	N/mm²				
Ice floe size	-	km				
Ice floe velocity	-	m/s				

7. Cyclic loading and fatigue

A turbine structure is exposed to fatigue loadings because fluctuating loads are exerted on the turbine structure. Varying states of the turbine are resulting in different force fluctuations. To be able to determine the fatigue loading numerous simulations have to be executed. The Danish Energy Agency advises to execute at least 5 simulations to determine the fatigue loading, but this may even be insufficient in many cases[27].
The lifetime fatigue loading can be simulated for a structure. Therefore all the fatigue contributions of the forces on the turbine structure have to be investigated. As can be seen in the Guideline for Design of Wind Turbines the load combinations involved with normal power production are governing the total fatigue loading. 96% of the total fatigue loading is due to loads that occur during normal power production. The result of the modelling of the fatigue loading is the equivalent fatigue load for the turbine structure with a coefficient of variation and an equivalent number of load cycles, which is mostly taken as 10^7 cycles.
According to an example presented in the Guidelines for Design of Wind Turbines it is shown that the equivalent fatigue load is dependent on the wind speed and the turbulence. For an increasing wind speed and/or turbulence the damage equivalent increases. It can also be seen that the uncertainty of the calculations increases with an increasing wind speed and/or turbulence. These results for the fatigue loads on a 1,5 MW wind turbine are shown in the figure below.

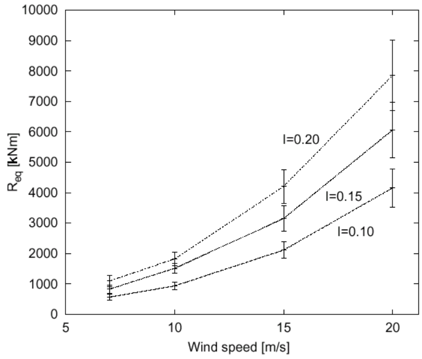

Figure 103, Sensitivity of fatigue load to wind speed and turbulence

[27] Guidelines for Design of Wind Turbines – DNV/Risø

8. Accidental loading

The expression presented in the paper Ship Impacts: Bow Collisions is placed below:

$$P_{bow} = \begin{cases} P_0 \cdot \overline{L}[\overline{E} + (5,0 - \overline{L})\overline{L}^{1,6}]^{0,5} & \text{for } \overline{E}_{imp} \geq \overline{L}^{2,6} \\ 2,24 \cdot P_0[\overline{E}_{imp}\overline{L}]^{0,5} & \text{for } \overline{E}_{imp} < \overline{L}^{2,6} \end{cases}$$

Where

$$\overline{L} = L_{pp} / 275m$$

$$\overline{E}_{imp} = E_{imp} / 1425MNm$$

$$E_{imp} = \frac{1}{2} m_x V_0^2$$

and

P_{bow} = maximum bow collision load [MN];

P_0 = reference collision load equal to 210 MN;

E_{imp} = energy to be absorbed by plastic deformations;

L_{pp} = length of vessel [m];

m_x = mass plus added mass (5%) with respect to longitudinal motion [$10^6 kg$];

V_0 = initial speed of vessel [m s^{-1}];

When calculating the collision force for a ship with a DWT of 270.000 the following calculation outcomes are obtained:

using:

$m_x = 312.384$ tonnes

$V_0 = 2m/s$

$L_{pp} = 330m$

The calculation for P_{bow} becomes:

$$P_{bow} = 2,24 \cdot P_0[\overline{E}_{imp}\overline{L}]^{0,5} = 341MN$$

9. Maple calculation sheets

Maple wind loadings sheet

```
> restart;
```

Explanation parameters:

Abg = Given area of known blade

Lbg = Given length of known blade

DiamRotor = The diameter of the rotor blades

Lbc = Lenght of blades to be calculated

Ht = Height of tower

Hub = Height of hub above tower

Twb = Tower width at the bottom of the tower

> $Abg := 183;$

$$Abg := 183;$$
$$Lbg := 61.5;$$
$$DiamRotor := 154;$$
$$Lbc := \frac{DiamRotor}{2};$$
$$Ht := 95;$$
$$Hub := 1.5;$$
$$Twb := 6;$$
$$Twt := 3.87;$$
$$Rn := 5.4;$$
$$U := 43;$$
$$GustFac := 1.2;$$
$$\mathrm{rho} := 1.293;$$
$$ULSFac := 1.35;$$

$$Abg := 183$$

$$Lbg := 61.5$$

$$DiamRotor := 154$$

$$Lbc := 77$$

$$Ht := 95$$

$$Hub := 1.5$$

$$Twb := 6$$

$$Twt := 3.87$$

$$Rn := 5.4$$

$$U := 43$$
$$GustFac := 1.2$$
$$\rho := 1.293$$
$$ULSFac := 1.35$$

Calculation of blade surface [m2]

$> \quad Ab := \frac{Lbc}{Lbg} \cdot Abg;$

$$Ab := 229.121951\text{:}$$

Calculation of tower surface [m2]

$> \quad At := \int_0^{Ht} Twb - \frac{(Twb - Twt)}{Ht} \cdot h \, \mathrm{d}h;$

$$At := 468.825000\text{(}$$

Calculation of wind pressure [n/m2]

$> \quad q := \frac{1}{2} \cdot \mathrm{rho} \cdot (U \cdot GustFac)^2;$

$$q := 1721.34504\text{(}$$

Force on the blades [kN]

$> \quad Fblades := \frac{3 \cdot Ab \cdot q}{1000};$

$$Fblades := 1183.19380\text{:}$$

Moment on tower feet due to forces on blades (ULS) [kNm]

$> \quad Mblades := Fblades \cdot (Ht + Hub);$
$\quad MbladesULS := Mblades \cdot ULSFac;$

$$Mblades := 1.141782020\,10^5$$
$$MbladesULS := 1.541405727\,10^5$$

Force on the tower [kN]

$> \quad Ftower := \frac{At \cdot q}{1000};$

$$Ftower := 807.009588\text{·}$$

Level arm of forces on tower structure [m]

$> \quad HtArm := \frac{Twt \cdot Ht \cdot \frac{1}{2} \cdot Ht + \frac{1}{2} \cdot (Twb - Twt) \cdot Ht \cdot \frac{1}{3} \cdot Ht}{Twt \cdot Ht + \frac{1}{2} \cdot (Twb - Twt) \cdot Ht};$

$$HtArm := 44.0830800\text{·}$$

Moment on tower feet due to forces on tower (ULS) [kNm]

> $Mtower := Ftower \cdot HtArm;\ MtowerULS := Mtower \cdot ULSFac;$

$$Mtower := 35575.4682$$

$$MtowerULS := 48026.8821$$

Force on the Nacelle [kN]

> $Fnacelle := evalf\left(\frac{1}{4} \cdot \frac{\pi \cdot Rn^2}{1000} \cdot q\right);$

$$Fnacelle := 39.4226063$$

Moment ont tower feet due to forces on nacelle (USL) [kNm]

> $Mnacelle := Fnacelle \cdot (Ht + Hub);$
> $MnacelleULS := Mnacelle \cdot ULSFac;$

$$Mnacelle := 3804.28151$$

$$MnacelleULS := 5135.78004$$

Total horizontal forces on tower due to wind loadings[kN]

> $Ftotal := Fblades + Ftower + Fnacelle;$

$$Ftotal := 2029.62599$$

Total bending moment on tower foot due to wind loadings (ULS) [kNm]

> $Mtotal := Mblades + Mtower + Mnacelle;$
> $MtotalUSL := MbladesULS + MtowerULS + MnacelleULS;$

$$Mtotal := 1.535579518 10^5$$

$$MtotalUSL := 2.073032349 10^5$$

>

Maple wave loadings sheet

```
> restart;

> "

d  = Depth of water [m]

Di = Diameter shaft [m]

Hb = Height base [m]

Db = Diameter base [m]

Tp = Wave period [s]

y  = Height of point of evaluation (seabed=-d, sealevel=0, wave =
H/2) [m]

t  = Time of evaluation [s]

x  = Horizontal position of point of evaluation [m]

lambda = Wave length [m]

H  = Wave height [m]

Cd = Drag coefficient [-]

Cm = Inertia coefficient [-]

rho = Seawater density [kg/m3]

":

>
```

$d := 25;$
$Di := 6;$
$Hb := 2;$
$Db := 15;$
$Tp := 9;$
$y := y;$
$t := t;$
$x := 0.16 \cdot \text{lambda};$
$\text{lambda} := \text{lambda};$
$H := 6;$
$Cd := 0.5639;$
$Cm := 1.7822;$
$\text{rho} := 1027;$
$\text{omega} := \frac{2 \cdot \pi}{Tp};$
$k := \frac{2 \cdot \pi}{\text{lambda}};$
$\text{theta} := k \cdot x - \text{omega} \cdot t;$
$s := y + d;$

$$d := 25$$
$$Di := 6$$
$$Hb := 2$$
$$Db := 15$$
$$Tp := 9$$
$$y := y$$
$$t := t$$
$$x := 0.16\,\lambda$$
$$\lambda := \lambda$$
$$H := 6$$
$$Cd := 0.5639$$
$$Cm := 1.7822$$
$$\rho := 1027$$
$$\omega := \frac{2}{9}\,\pi$$
$$k := \frac{2\,\pi}{\lambda}$$
$$\theta := 0.32\,\pi - \frac{2}{9}\,\pi\,t$$
$$s := y + 25$$

Inital estimation for Lambda for deep water: [m]

```
> lambda := evalf(9.81*Tp^2/(2*Pi));
```

$$\lambda := 126.466109$$

Iteration to determine lambda for intermediate water: [m]

```
> for n from 1 to 100 do
  lambda := 9.81/(2*Pi)*9^2*tanh((2*Pi*5)/lambda)
  end do:
  lambda := evalf(lambda);
```

$$\lambda := 60.4139502$$

Morisons equation valid if:

```
> Di < 0.2*lambda;
```

$$6 < 12.0827900$$

Intermediate depth assumption valid if:

```
> 0.05 < d/lambda; d/lambda < 0.5;
```

$$0.05 < 0.413811708$$
$$0.4138117089 < 0.5$$

Insert formula's for particle speed and particle velocity

$$> xdot := \frac{\pi \cdot H}{Tp} \cdot \frac{\cosh(k \cdot s)}{\sinh(k \cdot d)} \cdot \cos(\text{theta});$$

$$xdotdot := \frac{2\,\pi^2 H}{Tp^2} \cdot \frac{\cosh(k \cdot s)}{\sinh(k \cdot d)} \sin(\text{theta});$$

$$xdot := \frac{2}{3} \frac{\pi \cosh(0.03310493672\pi\,(y+25)) \cos\left(-0.32\,\pi + \frac{2}{9}\,\pi\,t\right)}{\sinh(0.8276234180\pi)}$$

$$xdotdot := -\frac{4}{27} \frac{1}{\sinh(0.8276234180\pi)} \left(\pi^2 \cosh(0.03310493672\pi\,(y + 25)) \sin\left(-0.32\,\pi + \frac{2}{9}\,\pi\,t\right)\right)$$

Formula's for wave forces on the shaft and on the base

$$> dFs := Cm \cdot \text{rho} \cdot \pi \cdot \frac{Di^2}{4} \cdot xdotdot + Cd \cdot \text{rho} \cdot \frac{Di}{2} |xdot| \cdot xdot;$$

$$dFb := Cm \cdot \text{rho} \cdot \pi \cdot \frac{Db^2}{4} \cdot xdotdot + Cd \cdot \text{rho} \cdot \frac{Db}{2} |xdot| \cdot xdot;$$

$$dFs := -\frac{1}{\sinh(0.8276234180\pi)} \left(2440.425867\pi^3 \cosh(0.03310493672\pi\,(y + 25)) \sin\left(-0.32\,\pi + \frac{2}{9}\,\pi\,t\right)\right) + \frac{1}{\sinh(0.8276234180\pi)^2} \left(772.1670665\pi^2 \left|\cosh(0.0331049367\!\!:\pi\,(y + 25)) \cos\left(-0.32\,\pi + \frac{2}{9}\,\pi\,t\right)\right| \cosh(0.03310493672\pi\,(y + 25)) \cos\left(-0.32\,\pi + \frac{2}{9}\,\pi\,t\right)\right)$$

$$dFb := -\frac{1}{\sinh(0.8276234180\pi)} \left(15252.66167\pi^3 \cosh(0.03310493672\pi\,(y + 25)) \sin\left(-0.32\,\pi + \frac{2}{9}\,\pi\,t\right)\right) + \frac{1}{\sinh(0.8276234180\pi)^2} \left(1930.417666\pi^2 \left|\cosh(0.0331049367\!\!:\pi\,(y + 25)) \cos\left(-0.32\,\pi + \frac{2}{9}\,\pi\,t\right)\right| \cosh(0.03310493672\pi\,(y + 25)) \cos\left(-0.32\,\pi + \frac{2}{9}\,\pi\,t\right)\right)$$

Integrate formula to obtain maximum force in time

> $y := 0;\ diffF := \frac{\mathrm{d}}{\mathrm{d}\,t}\ dFs;$

$$y := 0$$

$$diffF := -\frac{542.3168593\pi^4 \cosh(0.8276234180\pi)\cos\left(-0.32\,\pi + \frac{2}{9}\,\pi\,t\right)}{\sinh(0.8276234180\pi)} - \frac{1}{\sinh(0.8276234180\pi)^2}\Big(171.5926814\pi^3 \cosh(0.8276234180\pi)^2\ \mathrm{abs}\left(1, \cos\left(-0.32\,\pi + \frac{2}{9}\,\pi\,t\right)\right) \sin\left(-0.32\,\pi + \frac{2}{9}\,\pi\,t\right) \cos\left(-0.32\,\pi + \frac{2}{9}\,\pi\,t\right)\Big) - \frac{1}{\sinh(0.8276234180\pi)^2}\Big(171.5926814\pi^3 \cosh(0.8276234180\pi)^2 \left|\cos\left(-0.32\,\pi + \frac{2}{9}\,\pi\,t\right)\right| \sin\left(-0.32\,\pi + \frac{2}{9}\,\pi\,t\right)\Big)$$

Solve the equation to find the value for t where the force maximises [s]

> $\mathrm{maxtime} := fsolve\,(\mathrm{diffF} = 0, \mathrm{t}) + Tp;$

$$maxtime := 8.19000000($$

Plot the graph for the function for F and its derivative, Set t to the found time and y to the variable z (height)

> $plots[multiple](plot, [diffF, t = 0 ..2\ Tp, color = blue], [dFs, t = 0 ..2\ Tp]);\ t := maxtime;\ y := z;$

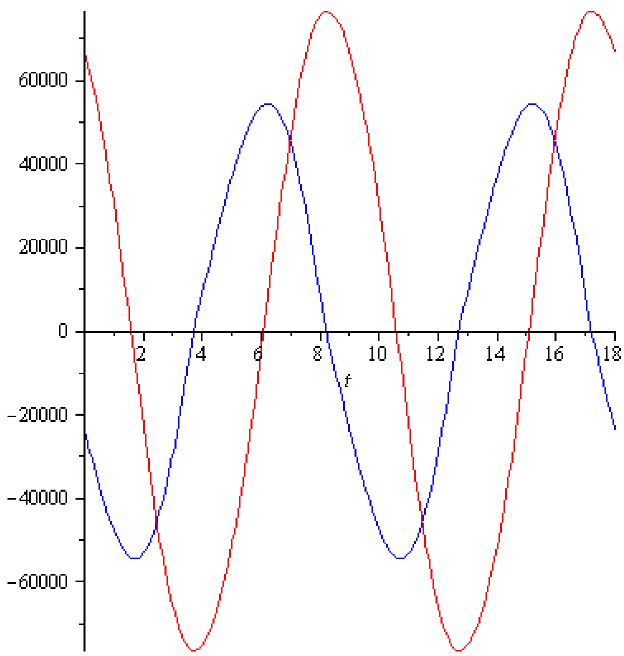

$$t := 8.19000000($$

$$y := z$$

Integrate the functions to find the forces on the shaft and the base of the foundation [kN]

$$> \quad Fshaft := \frac{\int_{-d+Hb}^{\frac{H}{2}} dFs \, dz}{1000};$$

$$Fbase := \frac{\int_{-d}^{-d+Hb} dFb \, dz}{1000};$$

$$Ftotal := Fshaft + Fbase;$$

$$Fshaft := 973.766596'$$

$$Fbase := 142.296686($$

$$Ftotal := 1116.06328$$

Plot the graph for the function Fs This gives the force on the foundation shaft over the height

$$> \quad plot\left(\frac{dFs}{1000}, z=-d..\frac{H}{2}\right);$$

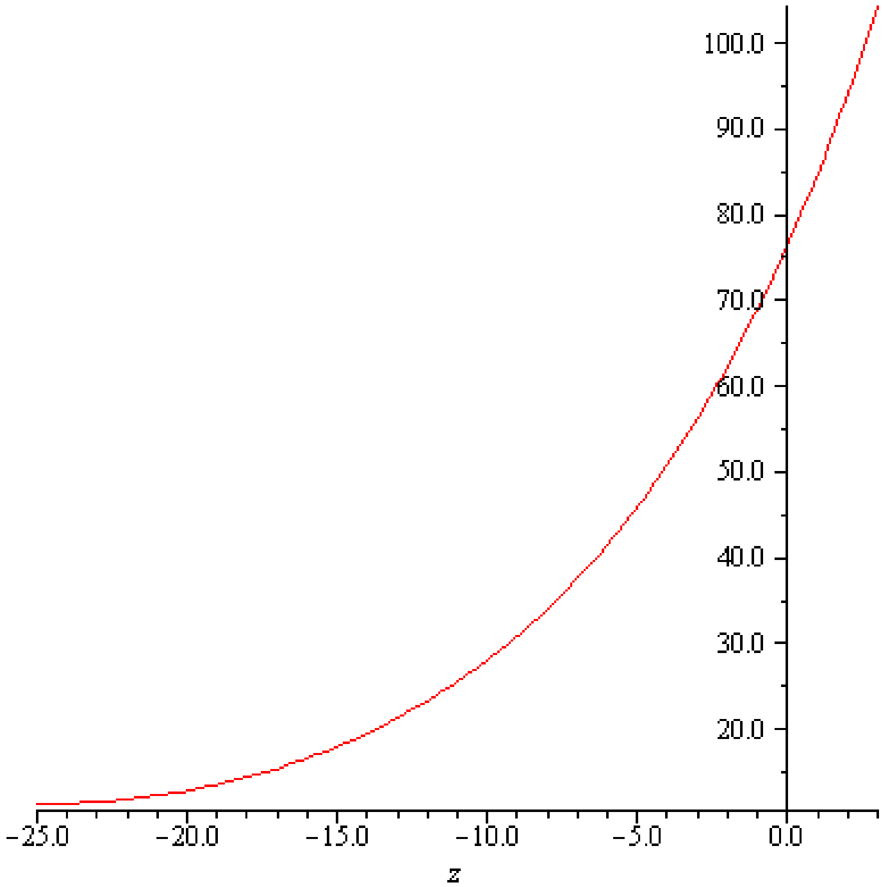

Determine the location for the masspoint of the functions. The result is the lever arm for the force. [m]

>
$$masspointshaft := \frac{\int_{-d+Hb}^{\frac{H}{2}} z \cdot dFs \, dz}{\int_{-d+Hb}^{\frac{H}{2}} dFs \, dz};$$

$$masspointbase := \frac{\int_{-d}^{-d+Hb} z \cdot dFb \, dz}{\int_{-d}^{-d+Hb} dFb \, dz};$$

$$masspointshaft := -5.19408184$$

$$masspointbase := -23.9964100$$

Calculate the moments on the footing for the wave loadings on the shaft and base [kNm]

>
$$momentshaft := (d + masspointshaft) \cdot Fshaft;$$
$$momentbase := (d + masspointbase) \cdot Fbase;$$
$$momenttotal := momentshaft + momentbase;$$

$$momentshaft := 19286.3415$$

$$momentbase := 142.807525$$

$$momenttotal := 19429.1490$$

>

Maple calculation of accidental loadings sheet

```
> restart;
```

Explanation of used parameters:

V = Collision speed of vessel [m/s]

P0 = Referencce collision load (=equal to 210MN)

Lpp = Length of vessel [m]

DWT = Deadweight tonnage [10^3 kg]

Mx = mass plus added mass with respect to longitudinal motion [10^6 kg]

> $V := 2;\ P0 := 210;\ Lpp := 330;\ DWT := 270000;\ Mx := \frac{312384}{1000};$

$$V := 2$$

$$P0 := 210$$

$$Lpp := 330$$

$$DWT := 270000$$

$$Mx := \frac{39048}{125}$$

Calculate impact energy

> $Eimp := evalf\left(\frac{1}{2} \cdot Mx \cdot V^2\right);$

$$Eimp := 624.7680000$$

Calculation of factors Ē and L

> $EBimp := evalf\left(\frac{Eimp}{1425}\right);\ LB := evalf\left(\frac{Lpp}{275}\right);$

$$EBimp := 0.4384336842$$

$$LB := 1.200000000$$

Determine which formula to use and calculate Pbow [MN]

> **if** $EBimp \geq LB^{2.6}$ **then** $Pbow := P0 \cdot LB \cdot \left(EBimp + (5.0 - LB)\, LB^{1.6}\right)^{0.5}$ **else** $Pbow := 2.24 \cdot P0 \cdot (EBimp \cdot LB)^{0.5}$ **end if**;

$$Pbow := 341.2006833$$

>

Maple sheet of ice loadings on ice cone

```
> restart;
```

Explanation variables

sigmaF = Flexural strength of ice [N/mm2]

gammaW = specific weight of seatwer (1027 kg/m3 for 10°C seawate) [kN/m3]

H = Ice sheet thickness [m]

Bwl = Cone diameter at water level [m]

Bt = Cone diameter at top of cone (smallest diameter under waterlevel) [m]

>

$$sigmaF := 1.9 \cdot 1000;$$
$$gammaW := \frac{1027}{9.81};$$
$$H := 0.38;$$
$$Bwl := 7;$$
$$Bt := 4;$$
$$k := \frac{gammaW \cdot Bwl^2}{9 \cdot sigmaF \cdot H};$$
$$\mathrm{alpha} := 30;$$

$$sigmaF := 1900.0$$
$$gammaW := 104.689092$$
$$H := 0.38$$
$$Bwl := 7$$
$$Bt := 4$$
$$k := 0.789437603$$
$$\alpha := 30$$

Horizontal axis value needed to determine A1 and A2 [-]

$$> HorizontalValue = \frac{gammaW \cdot Bwl^2}{sigmaF \cdot H};$$

$$HorizontalValue = 7.10493843$$

Input of parameters A1, A2, A3, A4, B1 and B2 [-]

>

$$A1 := 1.73;$$
$$A2 := 0.16;$$
$$A3 := 0.26;$$
$$A4 := 0.75;$$
$$B1 := 1.7;$$
$$B2 := 0.043;$$

$$A1 := 1.73$$
$$A2 := 0.16$$
$$A3 := 0.26$$

$$A4 := 0.75$$

$$B1 := 1.7$$

$$B2 := 0.043$$

Calculation of the horizotal force on the cone for downward breaking cones [kN]

> $$Rh := \left(A1 \cdot sigmaF \cdot H^2 + \frac{1}{9} \cdot B2 \cdot gammaW \cdot H \cdot Bwl^2 + \frac{1}{9} \cdot A3 \cdot gammaW \cdot H \cdot \left(Bwl^2 - Bt^2\right)\right) \cdot A4;$$

$$Rh := 391.411157\!\!\!\!\text{'}$$

Calculation of vertical force on the ice cone [kN]

> $$Rv := B1 \cdot Rh + \frac{1}{9} \cdot B2 \cdot gammaW \cdot H \cdot \left(Bwl^2 - Bt^2\right);$$

$$Rv := 671.671239\!\!\!\!\text{'}$$

>

Maple sheet for calculation of bearing capacity

```
> restart;
```

Explanation parameters

Drained = [y]: drained conditions, [n]: undrained conditions

Md = Design bending moment on foundation [kNm]

Vd = Design vertical force on foundation [kN]

Hd = Design horizontal force on foundation [kN]

e = Eccentricity of foundation center and vertical force [m]

R = Radius of foundation footing. If it is for example hexagonal take inner diameter [m]

Soil parameters

phi = Internal angle of friction of soil [°]

qd = Design bearing capacity [kN/m2]

gamma' = Effective (submerged) unit weight of soil [kN/m3]

p'0 = Effective overburden pressure at the level of the foundation-soil interface [kN/m2]

cd = Design cohesion or design undrained shear strength [kN/m2]

Ny,Nq,Nc = Bearing capacity factor [-]

sy,sq,sc = Shape factors [-]

iy, iq, ic = Inclination factor [-]

gammac = Material factor effective cohesion [-]

gammaphi = Material factor angle of internal friction [-]

\>

$drained := y;$
$Md := 200000;$
$Vd := 50000;$
$Hd := 5000;$
$e := \frac{Md}{Vd};$
$R := 15;$
$\text{phi} := 35;$
$cd := 0;$
$gammac := 1.5;$
$gammaphi := 1.2;$
$gammaacc := 24;$
$P0 := 10;$

$$drained := y$$

$$Md := 200000$$

$$Vd := 50000$$

$$Hd := 5000$$

$$e := 4$$

$$R := 15$$

$$\phi := 35$$

$$cd := 0$$

$$gammac := 1.5$$

$$gammaphi := 1.2$$

$$gammaacc := 24$$

$$P0 := 10$$

Bearing capacity, shape and inclination factors (page 129 DNV-OS-J101) [-]

\>
if *drained* = *y* **then**

$Nq := e(\mathrm{pi}\cdot\tan(phid))\cdot\dfrac{1+\sin(phid)}{1-\sin(phid)};$

$Nc := (Nq-1)\cdot\cot(phid);$

$Ny := 2(Nq-1)\tan(phid);$

$sy := 1-0.4\left(\dfrac{Beff}{Leff}\right);$

$sq := +\,0.2\cdot\left(\dfrac{Beff}{Leff}\right);$

$sc := sq;$

$iq := \left(1-\dfrac{Hd}{Vd+Aeff\cdot cd\cdot\cot(phid)}\right)^2;$

$ic := iq;$

$iy := iq^2;$

elif *drained* = *n* **then**

$Nc0 := \pi+2;$

$sc0 := 0.2\cdot\left(\dfrac{Beff}{Leff}\right);$

$ic0 := 0.5+0.5\cdot\mathrm{sqrt}\left(1-\dfrac{Hd}{Aeff\cdot cud}\right);$

end if

$$Nq := \frac{4\,(1+\sin(phid))}{1-\sin(phid)}$$

$$Nc := \left(\frac{4\,(1+\sin(phid))}{1-\sin(phid)}-1\right)\cot(phid)$$

$$Ny := 2\left(\frac{4\,(1+\sin(phid))}{1-\sin(phid)}-1\right)\tan(phid)$$

$$sy := 1-\frac{0.4\,Beff}{Leff}$$

$$sq := \frac{0.2\,Beff}{Leff}$$

$$sc := \frac{0.2\,Beff}{Leff}$$

$$iq := \frac{81}{100}$$

$$ic := \frac{81}{100}$$

$$iy := \frac{6561}{10000}$$

Calculation of the design shear parameters

\> $cud := \dfrac{cd}{gammac};\ phid := evalf\left(\arctan\left(\dfrac{\tan(\mathrm{phi})}{gammaphi}\right)\right);$

$$cud := 0.$$

$$phid := 0.376055046'$$

Calculation of effective dimensions of circular footing wit raduis R

> $Aeff := evalf\left(2\cdot\left(R^2\cdot \arccos\left(\frac{e}{R}\right) - e\cdot \mathrm{sqrt}\left(R^2 - e^2\right)\right)\right);$
$Be := evalf(2\cdot(R - e));$
$Le := evalf\left(2\cdot R\cdot \mathrm{sqrt}\left(1 - \left(1 - \frac{Be}{2\cdot R}\right)^2\right)\right);$

$$Aeff := 469.733930'$$
$$Be := 22.$$
$$Le := 28.9136646($$

The effective area Aeff can be represented by a rectangle with dimensions [m]

> $Leff := \mathrm{sqrt}\left(Aeff\cdot\frac{Le}{Be}\right);\ Beff := evalf\left(\frac{Leff}{Le}\cdot Be\right);$

$$Leff := 24.8465557!$$
$$Beff := 18.9053941!$$

Calculation of the bearing capacity for fully drained conditions [kN/m2]

> **if** $drained = y$ **then** $qdrained := \left(\frac{1}{2}\cdot gammaacc\cdot Beff\cdot Ny\cdot sy\cdot iy + P0\cdot Nq\cdot sq\cdot iq + cd\cdot Nc\cdot sc\cdot ic\right)$ **end if**;

$$qdrained := 635.630381!$$

Calculation of the bearing capacity for undrained conditions [kN/m2]

> **if** $drained = n$ **then** $qundrained := evalf(cud\cdot Nc0\cdot sc0\cdot ic0 + P0)$
end if;

Calculation of sliding resistance for drained conditions [kN]

> **if** $drained = y$ **then** $Hdrained := evalf(Aeff\cdot cud + Vd\cdot \tan(\mathrm{phi}))$
end if;

$$Hdrained := 23690.7360!$$

Calculation of sliding resistance for undrained conditions [kN]

> **if** $driane d = n$ **then** $Hundrained := Aeff\cdot cud$ **end if**;

>

10. Relation water depth and wind speed for forces on the structure

Water depth	15 m				25 m				35 m			
Wind speed	30	35	40	45	30	35	40	45	30	35	40	45
	1	2	3	4	5	6	7	8	9	10	11	12
Wind Forces												
Force on the blades	575,919	783,89	1023,86	1295,82	575,919	783,89	1023,86	1295,82	575,919	783,89	1023,86	1295,82
Moment on foot due to blades	85446,2	116302	151904	192254	93221,1	126884	165726	209748	100996	137467	179549	227241
Force on the tower	372,137	506,52	661,577	837,309	372,137	506,52	661,577	837,309	372,137	506,52	661,577	837,309
Moment on foot due to tower	29622,1	40319	52661,5	66649,7	34646	47157	61592,8	77953,4	39669,8	53995	70524,1	89257,1
Force on the nacelle	19,1889	26,1183	34,1137	43,1751	19,1889	26,1183	34,1137	43,1751	19,1889	26,1183	34,1137	43,1751
Moment on foot due to nacelle	2846,97	3875,04	5061,27	6405,68	3106,02	4227,63	5521,81	6988,54	3365,07	4580,23	5982,34	7571,4
------------	0	0	0	0	0	0	0	0	0	0	0	0
------------	0	0	0	0	0	0	0	0	0	0	0	0
------------	0	0	0	0	0	0	0	0	0	0	0	0
------------	0	0	0	0	0	0	0	0	0	0	0	0
Wave forces	0	0	0	0	0	0	0	0	0	0	0	0
Forces on shaft due to waves	1096,78	1096,78	1096,78	1096,78	1276,57	1276,57	1276,57	1276,57	1383,48	1383,48	1383,48	1383,48
Forces on base due to waves	2568,72	2568,72	2568,72	2568,72	1623,02	1623,02	1623,02	1623,02	1080,71	1080,71	1080,71	1080,71
Moment on foot due to waves on shaft	12860,2	12860,2	12860,2	12860,2	22770,5	22770,5	22770,5	22770,5	34008,4	34008,4	34008,4	34008,4
Moment on foot due to waves on base	3863,4	3863,4	3863,4	3863,4	2439,14	2439,14	2439,14	2439,14	1623,66	1623,66	1623,66	1623,66
------------	0	0	0	0	0	0	0	0	0	0	0	0
------------	0	0	0	0	0	0	0	0	0	0	0	0
------------	0	0	0	0	0	0	0	0	0	0	0	0
------------	0	0	0	0	0	0	0	0	0	0	0	0
Ice forces	0	0	0	0	0	0	0	0	0	0	0	0
Horizontal force	343,862	343,862	343,862	343,862	343,862	343,862	343,862	343,862	343,862	343,862	343,862	343,862
Vertical force	244,776	244,776	244,776	244,776	244,776	244,776	244,776	244,776	244,776	244,776	244,776	244,776
Moments on foot due to ice loading	5157,93	5157,93	5157,93	5157,93	8596,56	8596,56	8596,56	8596,56	12035,2	12035,2	12035,2	12035,2
------------	0	0	0	0	0	0	0	0	0	0	0	0

------------	0	0	0	0	0	0	0	0	0	0	0	0
------------	0	0	0	0	0	0	0	0	0	0	0	0
Accidental loadings	0	0	0	0	0	0	0	0	0	0	0	0
Bow forces due to vessel collision	341,201	341,201	341,201	341,201	341,201	341,201	341,201	341,201	341,201	341,201	341,201	341,201
------------	0	0	0	0	0	0	0	0	0	0	0	0
------------	0	0	0	0	0	0	0	0	0	0	0	0
------------	0	0	0	0	0	0	0	0	0	0	0	0
------------	0	0	0	0	0	0	0	0	0	0	0	0
Bearing capacity	0	0	0	0	0	0	0	0	0	0	0	0
Bearing capacity drained conditions	834,085	834,085	834,085	834,085	834,085	834,085	834,085	834,085	834,085	834,085	834,085	834,085
Bearing capacity undrained conditions	0	0	0	0	0	0	0	0	0	0	0	0
Sliding resistance drained conditions	23690,7	23690,7	23690,7	23690,7	23690,7	23690,7	23690,7	23690,7	23690,7	23690,7	23690,7	23690,7
Sliding resistance undrained conditions	0	0	0	0	0	0	0	0	0	0	0	0
------------	0	0	0	0	0	0	0	0	0	0	0	0
------------	0	0	0	0	0	0	0	0	0	0	0	0
------------	0	0	0	0	0	0	0	0	0	0	0	0
------------	0	0	0	0	0	0	0	0	0	0	0	0
------------	0	0	0	0	0	0	0	0	0	0	0	0
------------	0	0	0	0	0	0	0	0	0	0	0	0
------------	0	0	0	0	0	0	0	0	0	0	0	0
------------	0	0	0	0	0	0	0	0	0	0	0	0
	0	0	0	0	0	0	0	0	0	0	0	0
Total horizontal forces [kN]	4976,62	5325,9	5728,92	6185,67	4210,7	4559,98	4963	5419,75	3775,3	4124,58	4527,6	4984,35
Total moments on footing [MNm]	139,797	182,377	231,509	287,191	164,779	212,075	266,647	328,496	191,698	243,709	303,722	371,737

11. Relation wave height, wind speed and water depth for forces acting on turbine foundation

Water depth	**15**		**25**		**35**		**15**		**25**		**35**	
Wind speed	**30**	**40**	**30**	**40**	**30**	**40**	**30**	**40**	**30**	**40**	**30**	**40**
Wave height	**9**	**9**	**9**	**9**	**9**	**9**	**10**	**10**	**10**	**10**	**10**	**10**
	1	**2**	**3**	**4**	**5**	**6**	**7**	**8**	**9**	**10**	**11**	**12**
Wind Forces												
Force on the blades	575,919	1023,86	575,919	1023,86	575,919	1023,86	575,919	1023,86	575,919	1023,86	575,919	1023,86
Moment on foot due to blades	85446,2	151904	93221,1	165726	100996	179549	85446,2	151904	93221,1	165726	100996	179549
Force on the tower	372,137	661,577	372,137	661,577	372,137	661,577	372,137	661,577	372,137	661,577	372,137	661,577
Moment on foot due to tower	29622,1	52661,5	34646	61592,8	39669,8	70524,1	29622,1	52661,5	34646	61592,8	39669,8	70524,1
Force on the nacelle	19,1889	34,1137	19,1889	34,1137	19,1889	34,1137	19,1889	34,1137	19,1889	34,1137	19,1889	34,1137
Moment on foot due to nacelle	2846,97	5061,27	3106,02	5521,81	3365,07	5982,34	2846,97	5061,27	3106,02	5521,81	3365,07	5982,34
------------	0	0	0	0	0	0	0	0	0	0	0	0
------------	0	0	0	0	0	0	0	0	0	0	0	0
------------	0	0	0	0	0	0	0	0	0	0	0	0
------------	0	0	0	0	0	0	0	0	0	0	0	0
Wave forces	0	0	0	0	0	0	0	0	0	0	0	0
Forces on shaft due to waves	1286,63	1286,63	1480,12	1480,12	1596,74	1596,74	1489,66	1489,66	1694,57	1694,57	1819,96	1819,96
Forces on base due to waves	2889,82	2889,82	1825,9	1825,9	1215,8	1215,8	3210,91	3210,91	2028,78	2028,78	1350,89	1350,89
Moment on foot due to waves on shaft	15483,2	15483,2	26903,3	26903,3	39842,4	39842,4	18390	18390	31379,8	31379,8	46090	46090
Moment on foot due to waves on base	4346,32	4346,32	2744,04	2744,04	1826,62	1826,62	4829,24	4829,24	3048,93	3048,93	2029,57	2029,57
------------	0	0	0	0	0	0	0	0	0	0	0	0
------------	0	0	0	0	0	0	0	0	0	0	0	0
------------	0	0	0	0	0	0	0	0	0	0	0	0
------------	0	0	0	0	0	0	0	0	0	0	0	0
Ice forces	0	0	0	0	0	0	0	0	0	0	0	0
Horizontal force	125,341	125,341	125,341	125,341	125,341	125,341	125,341	125,341	125,341	125,341	125,341	125,341
Vertical force	218,916	218,916	218,916	218,916	218,916	218,916	218,916	218,916	218,916	218,916	218,916	218,916
Moments on foot due to ice loading	1880,11	1880,11	3133,52	3133,52	4386,93	4386,93	1880,11	1880,11	3133,52	3133,52	4386,93	4386,93

------------	0	0	0	0	0	0	0	0	0	0	0	0
------------	0	0	0	0	0	0	0	0	0	0	0	0
------------	0	0	0	0	0	0	0	0	0	0	0	0
Accidental loadings	0	0	0	0	0	0	0	0	0	0	0	0
Bow forces due to vessel collision	341,201	341,201	341,201	341,201	341,201	341,201	341,201	341,201	341,201	341,201	341,201	341,201
------------	0	0	0	0	0	0	0	0	0	0	0	0
------------	0	0	0	0	0	0	0	0	0	0	0	0
------------	0	0	0	0	0	0	0	0	0	0	0	0
------------	0	0	0	0	0	0	0	0	0	0	0	0
Bearing capacity	0	0	0	0	0	0	0	0	0	0	0	0
Bearing capacity drained conditions	834,085	834,085	834,085	834,085	834,085	834,085	834,085	834,085	834,085	834,085	834,085	834,085
Bearing capacity undrained conditions	0	0	0	0	0	0	0	0	0	0	0	0
Sliding resistance drained conditions	23690,7	23690,7	23690,7	23690,7	23690,7	23690,7	23690,7	23690,7	23690,7	23690,7	23690,7	23690,7
Sliding resistance undrained conditions	0	0	0	0	0	0	0	0	0	0	0	0
------------	0	0	0	0	0	0	0	0	0	0	0	0
------------	0	0	0	0	0	0	0	0	0	0	0	0
------------	0	0	0	0	0	0	0	0	0	0	0	0
------------	0	0	0	0	0	0	0	0	0	0	0	0
------------	0	0	0	0	0	0	0	0	0	0	0	0
------------	0	0	0	0	0	0	0	0	0	0	0	0
------------	0	0	0	0	0	0	0	0	0	0	0	0
------------	0	0	0	0	0	0	0	0	0	0	0	0
	0	0	0	0	0	0	0	0	0	0	0	0
Total horizontal forces [kN]	5269,03	6021,33	4398,61	5150,91	3905,13	4657,43	5793,15	6545,45	4815,93	5568,23	4263,43	5015,74
Total moments on footing [MNm]	139,625	231,337	163,754	265,622	190,087	302,111	143,015	234,727	168,535	270,403	196,537	308,562

Table 30, Relations for varying wave heigt, wind speed and water depth

	Horizontal forces in kN				Moments on footing in kNm			
	15 m				**15 m**			
	30 m/s	**35 m/s**	**40 m/s**	**45 m/s**	**30 m/s**	**35 m/s**	**40 m/s**	**45 m/s**
wind	967	1.317	1.720	2.176	117.915	160.496	209.627	265.309
wave	3.666	3.666	3.666	3.666	16.724	16.724	16.724	16.724
	25 m				**25 m**			
	30 m/s	**35 m/s**	**40 m/s**	**45 m/s**	**30 m/s**	**35 m/s**	**40 m/s**	**45 m/s**
wind	967	1.317	1.720	2.176	130.973	178.269	232.841	294.690
wave	2.900	2.900	2.900	2.900	25.210	25.210	25.210	25.210
	35 m				**35 m**			
	30 m/s	**35 m/s**	**40 m/s**	**45 m/s**	**30 m/s**	**35 m/s**	**40 m/s**	**45 m/s**
wind	967	1.317	1.720	2.176	144.031	196.042	256.055	324.070
wave	2.464	2.464	2.464	2.464	35.632	35.632	35.632	35.632

Table 31, Calculation outcomes vor variance in water depth and wind speed

Ratios for horizontal forces on shaft and water depth

15 m		25 m		35 m
	x 1,16		x 1,08	

Ratios for moments on shaft and water depth

15 m		25 m		35 m
	x 1,77		x 1,49	

Ratios for horizontal forces on base and water depth

15 m		25 m		35 m
	x 0,63		x 0,67	

Ratios for moments on base and water depth

15 m		25 m		35 m
	x 0,63		x 0,67	

Table 32, Ratios for forces and moments on foundation shaft and base

Ratios for total horizontal forces on foundation for varying water depths

15 m		25 m		35 m
	x 0,79		x 0,85	

Ratios for total moments on foundation for varying water depths

15 m		25 m		35 m
	x 1,51		x 1,41	

Table 33, Ratios for total wave forces and moments on foundation

Horizontal forces on foundation in kN

Hmax	**9 m**		**9 m**		**9 m**	
d	**15 m**		**25 m**		**35 m**	
U	**30 m/s**	**40 m/s**	**30 m/s**	**40 m/s**	**30 m/s**	**40 m/s**
wind	967	1.720	967	1.720	967	1.720
wave	4.176	4.176	3.306	3.306	2.813	2.813
	10 m		**10 m**		**10 m**	
	15 m		**25 m**		**35 m**	
	30 m/s	**40 m/s**	**30 m/s**	**40 m/s**	**30 m/s**	**40 m/s**
wind	967	1.720	967	1.720	967	1.720
wave	4.701	4.701	3.723	3.723	3.171	3.171

Moments on foundation in kNm

Hmax	**9 m**		**9 m**		**9 m**	
d	**15 m**		**25 m**		**35 m**	
U	**30 m/s**	**40 m/s**	**30 m/s**	**40 m/s**	**30 m/s**	**40 m/s**
wind	117.915	209.627	130.973	232.841	144.031	256.055
wave	19.830	19.830	29.647	29.647	41.669	41.669
	10 m		**10 m**		**10 m**	
	15 m		**25 m**		**35 m**	
	30 m/s	**40 m/s**	**30 m/s**	**40 m/s**	**30 m/s**	**40 m/s**
wind	117.915	209.627	130.973	232.841	144.031	256.055
wave	23.219	23.219	34.429	34.429	48.120	48.120

Relation water depth and horizontal forces on foundation for 9 m wave height

9m

15 m		25 m		35 m
	0,79		0,85	

Relation water depth and horizontal forces on foundation for 10 m wave height

10m

15 m		25 m		35 m
	0,79		0,85	

Relation water depth and moment on foundation for 9 m wave height

9m

15 m		25 m		35 m
	1,50		1,41	

Relation water depth and moment on foundation for 10 m wave height

10m

15 m		25 m		35 m
	1,48		1,40	

Relation water depth and wave height for horizontal forces on foundation

15m			25m			35m		
9m		10m	9m		10m	9m		10m
	1,17			1,16			1,15	

Relation water depth and wave height for moments on foundation

15m			25m			35m		
9m		10m	9m		10m	9m		10m
	1,13			1,13			1,13	

12. Wave forces according to Morison Equation

When regarding the norm DNV-OS-J101 the parameters C_m and C_D need to be determined. According to page 49 of DNV-OS-J101 it can be red that this can be done using the formula's:

$$C_{DS} = \begin{cases} 0,65 & \dfrac{k}{D} < 10^{-4}(\text{smooth}) \\ \dfrac{29 + 4log_{10}\dfrac{k}{D}}{20} & 10^{-4} < \dfrac{k}{D} < 10^{-2} \\ 1,05 & \dfrac{k}{D} > 10^{-2}(\text{rough}) \end{cases}$$

$$C_D = C_{DS} \cdot \psi(C_{DS}, KC)$$

and

$$R_e = \frac{u_{max} D}{\nu}$$

$$KC = \frac{u_{max} T_i}{D}$$

where

u_{max} = horizontal particle velocity at still water level

ν = kinematic viscosity seawater

T_i = intrinsic period of the waves

For concrete surfaces it can be assumed that the value for $k = 0,003m$

The factor Ψ used to determine C_D can be obtained from figure 2 on page 49 from OS-J101:

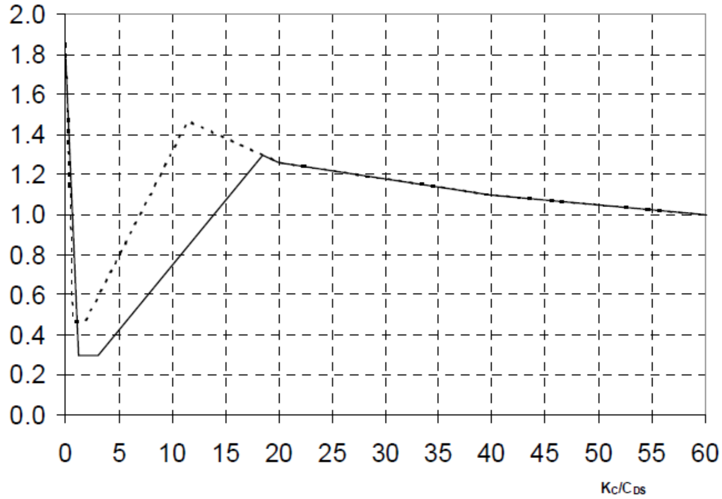

Figure 104, Determination of Psi for rough (dotted line) and smooth (solid line) surfaces

To determine C_M the following formula's can be used:

$$KC < 3 \Rightarrow C_M = 2,0$$

$$KC > 3 \Rightarrow C_M = max\begin{cases} 2,0 - 0,044(KC-3) \\ 1,6-(C_{DS}-0,65) \end{cases}$$

<u>Using the formula's to determine C_D and C_M</u>

With a foundation diameter of 6 meters the vaule for $\frac{k}{D}$ becomes $\frac{0.003}{6} = 5e^{-4}$. So the formula to be used to determine C_{DS} is: $\frac{29+4log_{10}\frac{k}{D}}{20} = \frac{29+4log_{10}5e^{-4}}{20} = 0,7898$

To determine KC the following parameters are used:

$u_{max} = 2,28m$ (for a water depth of 25m and a wave period of 9,7s)

$T_i = 9,7s$

KC then becomes: $KC = \frac{2,28 \cdot 9,7}{6} = 3,686$

$\frac{KC}{C_{DS}}$ now becomes $\frac{3,686}{0,7898} = 4,67$

When reading from the graph the value for Ψ can be found as $\Psi = 0,4$. With this value C_D then becomes $C_D = C_{DS} \cdot \Psi = 0,4 \cdot 0,7898 = 0,316$

For determination of C_M the parameters KC and C_{DS} are needed. With de before calculated values the value for C_M is the maximum value of $\begin{cases} 2,0 - 0,044(KC-3) \\ 1,6-(C_{DS}-0,65) \end{cases}$. This gives for C_M a value of

$$max\begin{cases} 2,0-0,044(3,686-3) \\ 1,6-(0,7898-0,65) \end{cases} = max\begin{cases} 1,97 \\ 1,46 \end{cases} = 1,97.$$

The formula for the total force on the structure hereby becomes as following:

$$dF = 1{,}97 \cdot 1027 \cdot \pi \cdot \frac{6^2}{4}\ddot{x}dz + 0{,}316 \cdot 1027\frac{6}{2}|\dot{x}|\dot{x}dz = 57204{,}35\ddot{x}dz + 973{,}60|\dot{x}|\dot{x}dz$$

Current forces

When no detailed measurements are available the following formula can be used to determine the wind generated current: $v_{wind0} = 0{,}01 \cdot U_0$ and $v_{wind}(z) = v_{wind0}\left(\frac{h_0 + z}{h_0}\right)$ for $-h_0 \le z \le 0$ where h_0 =water depth and z =water depth of evaluation. The value for U_0 should be taken as the one hourly averaged wind speed. For calculation of the tidal forces the following formula should be used:

$v_{tide}(z) = v_{tide0}\left(\frac{h+z}{h}\right)^{1/7}$ for $z \le 0$.

When for the calculation of the current loadings on the foundation the formula $q = \frac{1}{2} \cdot \rho \cdot v^2 \cdot C_{DS}$ and a foundation surface of $A_{found} = 188m^2$ is used for a foundation depth of 25m the current loadings can be calculated. The factor C_{DS} has been determined before at the declaration of parameters and is $C_{DS} = 0{,}7898$. The current loadings then become:

$$F_{\text{wind current}} = 188 \cdot \frac{1}{2} \cdot 1023 \cdot 0{,}4^2 \cdot 0{,}7898 = 12{,}15kN$$

$$F_{\text{tidal current}} = 188 \cdot \frac{1}{2} \cdot 1023 \cdot 1^2 \cdot 0{,}7898 = 75{,}95kN$$

13. Formula's used to calculate parameters for design conditions

The table below contains the formula's used for determining the parameters for the different models and states

Wind related parameters

NTM	$\sigma_{U,c} = I_{ref}(0,75V_{hub} + b); \quad b = 5,6 \text{ m/s}$
ETM	$\sigma_{U,c} = c \cdot I_{ref} \cdot \left(0,072 \cdot \left(\frac{U_{average}}{c} + 3\right) \cdot \left(\frac{U_{hub}}{c} - 4\right) + 10\right)$
ECD	$V_{cg} = 15 \text{ m/s}$, $V(z,t) = \begin{cases} u(z) & for \quad t < 0 \\ u(z) + 0,5V_{cg}(1 - \cos(\pi \cdot t / T)) & for \quad 0 \le t \le T \\ u(z) + V_{cg} & for \quad t > T \end{cases}$
EWS	$V(z,t) = \begin{cases} U_{10}(z) \pm \frac{z - z_{hub}}{D} \cdot \left(2,5 + 0,2\beta\sigma_{U,c}\left(\frac{D}{\Lambda_1}\right)^{1/4}\right) \cdot \left(1 - \cos(\frac{2\pi \cdot t}{T})\right) & for\ 0 \le t \le T \\ U_{10}(z) & \text{otherwise} \end{cases}$
EOG	$V_{gust} = \min\left\{1,35(U_{hub,1-yr} - U_{10,hub}); \frac{3,3\sigma_{U,c}}{1 + 0,1D/\Lambda_1}\right\}$ $V(z,t) = \begin{cases} u(z) - 0,37V_{gust}\sin(\frac{3\pi \cdot t}{T})(1 - \cos(\frac{2\pi \cot t}{T})) & for 0 \le t \le T \\ u(z) & \text{otherwise} \end{cases}$
NWP	$V(z) = V_{hub}\left(\frac{z}{z_{hub}}\right)^{\alpha}$ with the power law exponent $\alpha = 0.14$ for offshore locations
EDC	$\theta_e = \pm 4 \cdot \arctan\frac{\sigma_{U,c}}{U_{10,hub}(1 + 0,1D/\Lambda_1)}$ $\theta(t) = \begin{cases} 0 & for\ t < 0 \\ 0,5\theta_e(1 - \cos(\pi \cdot t / T)) & for\ 0 \le t \le T \\ 0 & for\ t \ge T \end{cases}$
EWM	$U_{hub,50-yr} = 1,4 \cdot U_{10,hub,50-yr}$ $U_{hub,1-yr} = 0,8 \cdot U_{hub,50-yr}$
RWM	$U_{RWM} = \psi \cdot U_{EWM}, \psi < 1$ $\psi = 0,79$

Wave related parameters

NSS	$H_{S,NSS}$
NWH	$H_{NWH} = H_{S,NSS}$ $11{,}1\sqrt{H_{S,NSS}(U_{10})/g} \leq T \leq 14{,}3\sqrt{H_{S,NSS}(U_{10})/g}$
SSS	$H_{S,SSS}(U_{10}) = H_{S,50-yr}$
SWH	$H_{SWH} = H_{S,SSS}$ $11{,}1\sqrt{H_{S,SSS}(U_{10})/g} \leq T \leq 14{,}3\sqrt{H_{S,SSS}(U_{10})/g}$
ESS	$H_{S,ESS}$
EWS	$H_{50-yr} = 1{,}86 \cdot H_{S,50-yr}$ $H_{1-yr} = 1{,}86 \cdot H_{S,1-yr}$
RWH	$H_{Red,50-yr} = 1{,}3 \cdot H_{S,50-yr}$ $H_{Red,1-yr} = 1{,}3 \cdot H_{S,1-yr}$

Design combination	Wind speed (±turulence) [m/s]	Wave height [m]	Wave period [s]	Current [m/s]	Sea level [m]	Remarks
1.1	25 ± 3,9	6	8,7	0,29		
1.2	25 ± 3,9	6	8,7		± 1	FLS
1.3	25 ± 3,9	6	8,7	0,29		Same as 1.1
1.4	25 ± 2	6	8,7	0,27		
1.5	25 ± 9	6	8,7	0,25		Calculation of RNA
1.6a	25 ± 3,9	7,2	9,5	0,29	± 1	
1.6b	25 ± 3,9	7,2	9,5		± 1	
2.1	25 ± 3,9	6	8,7	0,29	25 ± 3,9	Calculation for fault conditon
2.2	25 ± 3,9	6	8,7	0,29		Calculation for fault conditon
2.3	28	6	8,7	0,28		Calculation for fault conditon
2.4	25 ± 3,9	6	8,7	0,29	± 1	Calculation for fault conditon, FLS
3.1	5	6	8,7	0,25	± 1	Calculation for start up, low wind speed, FLS
3.2	5	6	8,7	0,25		Calculation for start up, low wind speed
3.3	5	6	8,7	0,25		Calculation for start up, low wind speed
4.1	25	6	8,7	0,25	± 1	FLS
4.2	28	6	8,7	0,28		
5.1	25 ± 3,9	6	8,7	0,29		
6.1a	35 ± 2,75	7,2	9,5	0,7	± 2	
6.1b	49	9,36	9,5	0,7	± 2	
6.1c	38,5	13,4	9,5	0,7	± 2	
6.2a	35 ± 2,75	7,2	9,5	0,7	± 2	
6.2b	49	9,36	9,5	0,7	± 2	Same as 6.1b
6.3a	28 ± 3	6	8,7	0,5	± 1	Calculation for Yaw misalingment
6.3b	39,2	6	8,7	0,5	± 1	Calculation for Yaw misalingment
6.4	24,5 ± 3,5	6	8,7	0,25	± 1	FLS
7.1a	28 ± 3	6	8,7	0,5	± 1	
7.1b	39,2	7,8	8,7	0,5	± 1	
7.1c	30,8	6	8,7	0,5	± 1	
7.2	24,5	6	8,7	0,25	± 1	FLS
8.2a	39,2	9,36	9,5	0,5	± 1	
8.2b	30,8	6	8,7	0,5	± 1	
8.3	24,5 ±3,5	6	8,7	0,25	± 1	FLS

14. Table with parameters used for 32 design conditions DNV-OS-J101

Table E1 Proposed load cases combining various environmental conditions

Design situation	*Load case*	*Wind condition: Wind climate ($U_{10,hub}$) or wind speed (U_{hub})*	*Wave condition: Sea state (H_S) or individual wave height (H) to combine with in simulations for simultaneous wind and waves (7)*	*Wind and wave directionality*	*Current*	*Water level*	*Other conditions*	*Limit state*
Power production	1.1	NTM $v_{in} < U_{10,hub} < v_{out}$	NSS $H_S = E[H_S \mid U_{10,hub}]$	Codirectional in one direction	Wind-generated current	MWL	For prediction of extreme loads on RNA and interface to tower	ULS
	1.2	NTM $v_{in} < U_{10,hub} < v_{out}$	NSS H_S according to joint probability distribution of H_S, T_P and $U_{10,hub}$	Codirectional in one direction (See F900)	(5)	Range between upper and lower 1-year water level		FLS
	1.3	ETM $v_{in} < U_{10,hub} < v_{out}$	NSS $H_S = E[H_S \mid U_{10,hub}]$	Codirectional in one direction	Wind-generated current	MWL		ULS
	1.4	ECD $U_{10hub} = v_r - 2$ m/s, v_r, v_r+2 m/s	NSS $H_S = E[H_S \mid U_{10,hub}]$ or NWH $H = E[H_S \mid U_{10,hub}]$ (3)	Misaligned	Wind-generated current	MWL		ULS
	1.5	EWS $v_{in} < U_{10,hub} < v_{out}$	NSS $H_S = E[H_S \mid U_{10,hub}]$ or NWH $H = E[H_S \mid U_{10,hub}]$ (3)	Codirectional in one direction	Wind-generated current	MWL		ULS
	1.6a	NTM $v_{in} < U_{10,hub} < v_{out}$	SSS $H_S = H_{S,50\text{-}yr}$ (See item F703)	Codirectional in one direction	Wind-generated current	1-year water level (4)		ULS
	1.6b	NTM $v_{in} < U_{10,hub} < v_{out}$	SWH $H = H_{50\text{-}yr}$ (See item F703)	Codirectional in one direction	Wind-generated current	1-year water level (4)		ULS
Power production plus occurrence of fault	2.1	NTM $v_{in} < U_{10,hub} < v_{out}$	NSS $H_S = E[H_S \mid U_{10,hub}]$	Codirectional in one direction	Wind-generated current	MWL	Control system fault or loss of electrical connection	ULS
	2.2	NTM $v_{in} < U_{10,hub} < v_{out}$	NSS $H_S = E[H_S \mid U_{10,hub}]$	Codirectional in one direction	Wind-generated current	MWL	Protection system fault or preceding internal electrical fault	ULS Abnormal
	2.3	EOG $U_{10,hub} = v_{out}$ and v_r **r** 2 m/s	NSS $H_S = E[H_S \mid U_{10,hub}]$ or NWH $H = E[H_S \mid U_{10,hub}]$ (3) (6)	Codirectional in one direction	Wind-generated current	MWL	External or internal electrical fault including loss of electrical network connection	ULS Abnormal
	2.4	NTM $v_{in} < U_{10,hub} < v_{out}$	NSS $H_S = E[H_S \mid U_{10,hub}]$	Codirectional in one direction (See F900)	(5)	Range between upper and lower 1-year water level	Control or protection system fault including loss of electrical network	FLS

Tables describing design conditions according to DNV-OS-J101

Table E1 Proposed load cases combining various environmental conditions (Continued)

Design situation	*Load case*	*Wind condition: Wind climate ($U_{10,hub}$) or wind speed (U_{hub})*	*Wave condition: Sea state (H_S) or individual wave height (H) to combine with in simulations for simultaneous wind and waves (7)*	*Wind and wave directionality*	*Current*	*Water level*	*Other conditions*	*Limit state*
Start up	3.1	NWP $v_{in} < U_{10,hub} < v_{out}$ + normal wind profile to find average vertical wind shear across swept area of rotor	NSS $H_S = E[H_S \mid U_{10,hub}]$ or NWH $H = E[H_S \mid U_{10,hub}]$ (3)	Codirectional in one direction (See F900)	(5)	Range between upper and lower 1-year water level		FLS
	3.2	EOG $U_{10,hub} = v_{in}, v_{out}$ and v_r **r** 2 m/s	NSS $H_S = E[H_S \mid U_{10,hub}]$ or NWH $H = E[H_S \mid U_{10,hub}]$ (3)	Codirectional in one direction	Wind-generated current	MWL		ULS
	3.3	EDC $U_{10,hub} = v_{in}, v_{out}$ and v_r **r** 2 m/s	NSS $H_S = E[H_S \mid U_{10,hub}]$ or NWH $H = E[H_S \mid U_{10,hub}]$ (3)	Misaligned	Wind-generated current	MWL		ULS
Normal shutdown	4.1	NWP $v_{in} < U_{10,hub} < v_{out}$ + normal wind profile to find average vertical wind shear across swept area of rotor	NSS $H_S = E[H_S \mid U_{10,hub}]$ or NWH $H = E[H_S \mid U_{10,hub}]$ (3)	Codirectional in one direction (See F900)	(5)	Range between upper and lower 1-year water level		FLS
	4.2	EOG $U_{10,hub} = v_{out}$ and v_r **r** 2 m/s	NSS $H_S = E[H_S \mid U_{10,hub}]$ or NWH $H = E[H_S \mid U_{10,hub}]$ (3)	Codirectional in one direction	Wind-generated current	MWL		ULS
Emergency shutdown	5.1	NTM $U_{10,hub} = v_{out}$ and v_r **r** 2 m/s	NSS $H_S = E[H_S \mid U_{10,hub}]$	Codirectional in one direction	Wind-generated current	MWL		ULS

Table E1 Proposed load cases combining various environmental conditions (Continued)

Design situation	*Load case*	*Wind condition: Wind climate ($U_{10,hub}$) or wind speed (U_{hub})*	*Wave condition: Sea state (H_S) or individual wave height (H) to combine with in simulations for simultaneous wind and waves (7)*	*Wind and wave directionality*	*Current*	*Water level*	*Other conditions*	*Limit state*
Parked (standing still or idling)	6.1a	EWM Turbulent wind $U_{10,hub} = U_{10,50\text{-}yr}$ (characteristic standard deviation of wind speed $V_{U,c} = 0.11 \cdot U_{10hub}$)	ESS $H_S = H_{S,50\text{-}yr}$ (1)	Misaligned Multiple directions	50-year current	50-year water level		ULS
	6.1b	EWM Steady wind $U_{hub} = 1.4 \cdot U_{10,50\text{-}yr}$	RWH $H = \setminus \cdot H_{50\text{-}yr}$ (2)	Misaligned Multiple directions	50-year current	50-year water level		ULS
	6.1c	RWM Steady wind $U_{hub} = 1.1 \cdot U_{10,50\text{-}yr}$	EWH $H = H_{50\text{-}yr}$	Misaligned Multiple directions	50-year current	50-year water level		ULS
	6.2a	EWM Turbulent wind $U_{10,hub} = U_{10,50\text{-}yr}$ (characteristic standard deviation of wind speed $V_{U,c} = 0.11 \cdot U_{10hub}$)	ESS $H_S = H_{S,50\text{-}yr}$ (1)	Misaligned Multiple directions	50-year current	50-year water level	Loss of electrical network connection	ULS Abnormal
	6.2b	EWM Steady wind $U_{hub} = 1.4 \cdot U_{10,50\text{-}yr}$	RWH $H = \setminus \cdot H_{50\text{-}yr}$ (2)	Misaligned Multiple directions	50-year current	50-year water level	Loss of electrical network connection	ULS Abnormal
	6.3a	EWM Turbulent wind $U_{10,hub} = U_{10,1\text{-}yr}$ (characteristic standard deviation of wind speed $V_{U,c} = 0.11 \cdot U_{10hub}$)	ESS $H_S = H_{S,1\text{-}yr}$ (1)	Misaligned Multiple directions	1-year current	1-year water level	Extreme yaw misalignment	ULS
	6.3b	EWM Steady wind $U_{hub} = 1.4 \cdot U_{10,1\text{-}yr}$	RWH $H = \setminus \cdot H_{1\text{-}yr}$ (2)	Misaligned Multiple directions	1-year current	1-year water level	Extreme yaw misalignment	ULS
	6.4	NTM $U_{10,hub} < 0.7 U_{10,50\text{-}yr}$	NSS H_S according to joint probability distribution of H_S, T_P and $U_{10,hub}$	Codirectional in multiple direction (See F900)	(5)	Range between upper and lower 1-year water level		FLS
Parked and fault conditions	7.1a	EWM Turbulent wind $U_{10,hub} = U_{10,1\text{-}yr}$ (characteristic standard deviation of wind speed $V_{U,c} = 0.11 \cdot U_{10hub}$)	ESS $H_S = H_{S,1\text{-}yr}$ (1)	Misaligned Multiple directions	1-year current	1-year water level		ULS Abnormal

	7.1b	EWM Steady wind $U_{hub} = 1.4 \cdot U_{10,1\text{-}yr}$	RWH $H = \setminus \cdot H_{1\text{-}yr}$ (2)	Misaligned Multiple directions	1-year current	1-year water level		ULS Abnormal
	7.1c	RWM Steady wind $U_{hub} = 0.88 \cdot U_{10,50\text{-}yr}$	EWH $H = H_{1\text{-}yr}$	Misaligned Multiple directions	1-year current	1-year water level		ULS Abnormal
	7.2	NTM $U_{10,hub} < 0.7U_{10,50\text{-}yr}$	NSS H_S according to joint probability distribution of H_S, T_P and $U_{10,hub}$	Codirectional in multiple direction (See F900)	(5)	Range between upper and lower 1-year water level		FLS

Table E1 Proposed load cases combining various environmental conditions (Continued)

Design situation	*Load case*	*Wind condition: Wind climate ($U_{10,hub}$) or wind speed (U_{hub})*	*Wave condition: Sea state (H_S) or individual wave height (H) to combine with in simulations for simultaneous wind and waves (7)*	*Wind and wave directionality*	*Current*	*Water level*	*Other conditions*	*Limit state*
Transport, assembly, maintenance and repair	8.2a	EWM Steady wind $U_{hub} = 1.4 \cdot U_{10,1\text{-yr}}$	RWH $H = \setminus \cdot H_{1\text{-yr}}$ (2)	Codirectional in one direction	1-year current	1-year water level		ULS Abnormal
	8.2b	RWM Steady wind $U_{hub} = 0.88 \cdot U_{10,50\text{-yr}}$	EWH $H = H_{1\text{-yr}}$	Codirectional in one direction	1-year current	1-year water level		ULS Abnormal
	8.3	NTM $U_{10,hub} < 0.7U_{10,50\text{-yr}}$	NSS H_S according to joint probability distribution of H_S, T_P and $U_{10,hub}$	Codirectional in multiple direction (See F900)	(5)	Range between upper and lower 1-year water level		FLS

1) In cases where load and response simulations are to be performed and the simulation period is shorter than the reference period for the significant wave height H_S, the significant wave height needs to be converted to a reference period equal to the simulation period, see 3C202. Moreover, an inflation factor on the significant wave height needs to be applied in order to make sure that the shorter simulation period captures the maximum wave height when the original reference period does. When the reference period is 3 hours and the simulation period is 1 hour, the combined conversion and inflation factor is 1.09 provided the wave heights are Rayleigh-distributed and the number of waves in 3 hours is 1000. Likewise, if the simulation period is longer than the averaging period for the mean wind speed, a deflation factor on U_{10} may be applied. When the simulation period is 1 hour and the averaging period is 10 minutes, the deflation factor may be taken as 0.95.

2) It is practice for offshore structures to apply $\setminus = H_{5\text{-yr}}/H_{50\text{-yr}}$, where $H_{5\text{-yr}}$ and $H_{50\text{-yr}}$ denote the individual wave heights with 5- and 50-year return period, respectively. The shallower the water depth, the larger is usually the value of $\setminus$.

3) The load case is not driven by waves and it is optional whether the wind load shall be combined with an individual wave height or with a sea state.

4) The water level shall be taken as the upper-tail 50-year water level in cases where the extreme wave height will become limited by the water depth.

5) In principle, current acting concurrently with the design situation in question needs to be included, because the current influences the hydrodynamic coefficients and thereby the fatigue loading relative to the case without current. However, in many cases current will be of little importance and can be ignored, e.g. when the wave loading is inertia-dominated or when the current speed is small.

6) In the case that the extreme operational gust is combined with an individual wave height rather than with a sea state, the resulting load shall be calculated for the most unfavourable location of the profile of the individual wave relative to the temporal profile of the gust.

7) Whenever the wave loading associated with a specific load case refers to a wave train or a time series of wave loads, the sought-after combined load effect shall be interpreted as the maximum resulting load effect from the time series of load effects which is produced by the simulations.

15. Graphs used to determine parameters used for calculating design conditions

The graphs presented here are originating from the DOWEC report Wind and Wave Conditions.

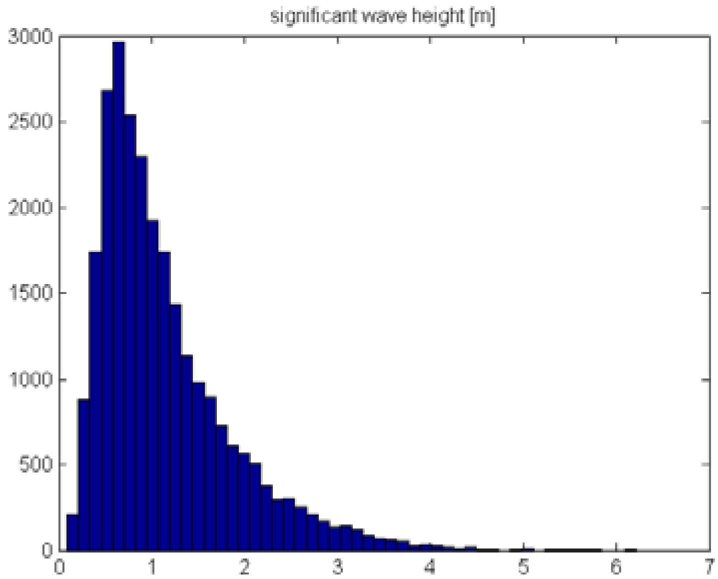

Figure 105, DOWEC significant wave height

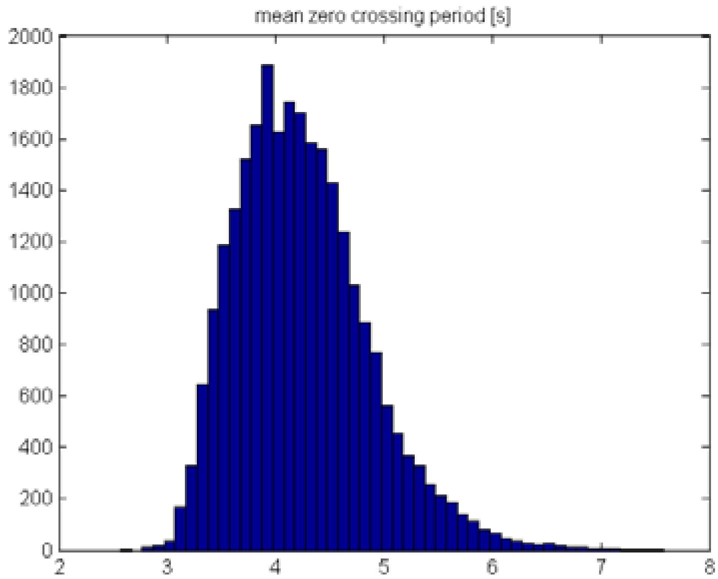

Figure 106, DOWEC mean zero crossing period

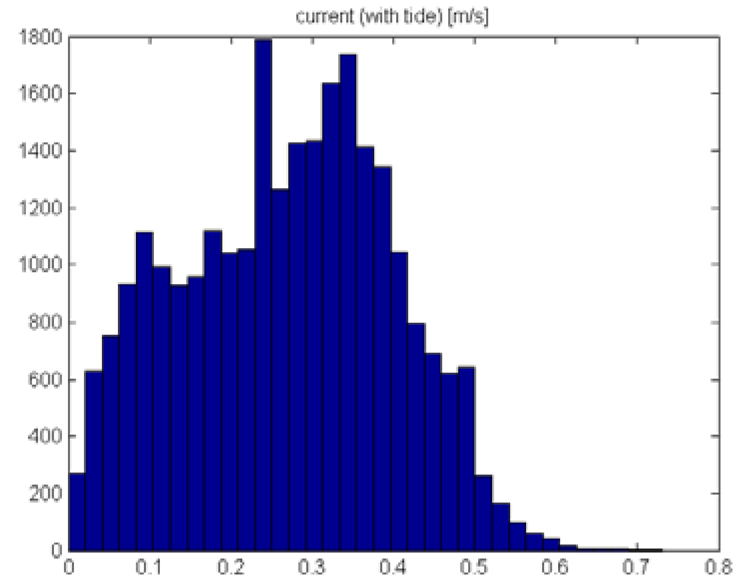

Figure 107, DOWEC current with tide

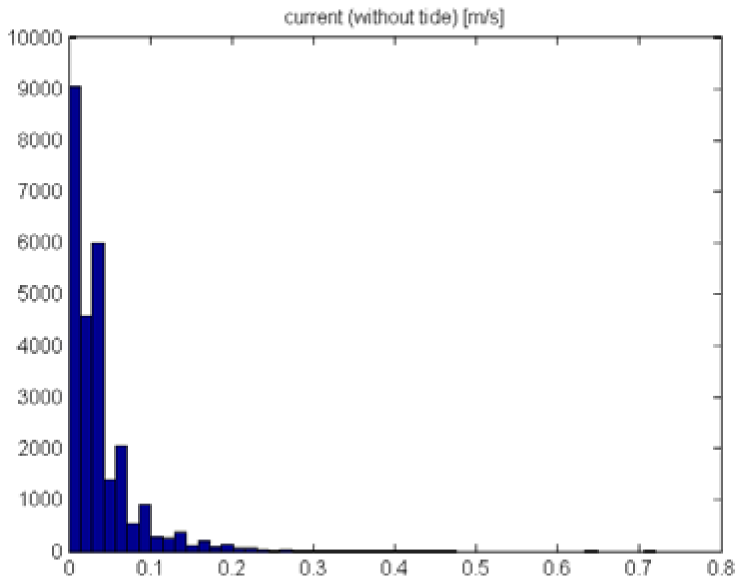

Figure 108, DOWEC current without tide

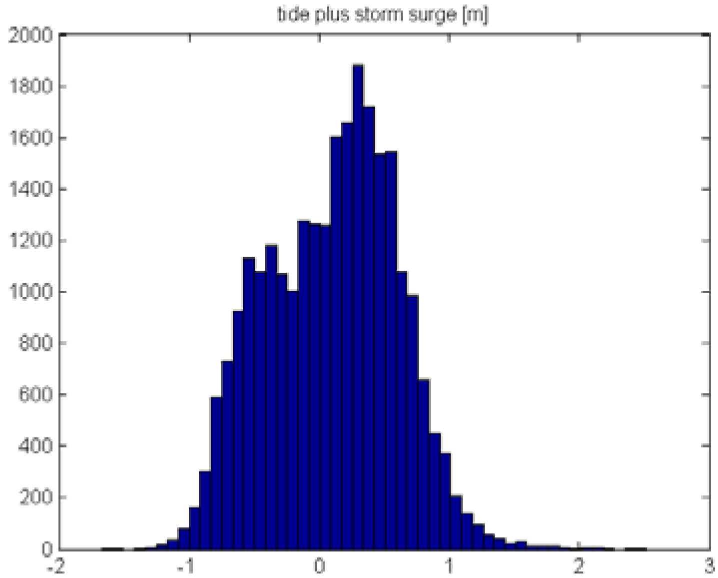

Figure 109, DOWEC tide plus storm surge

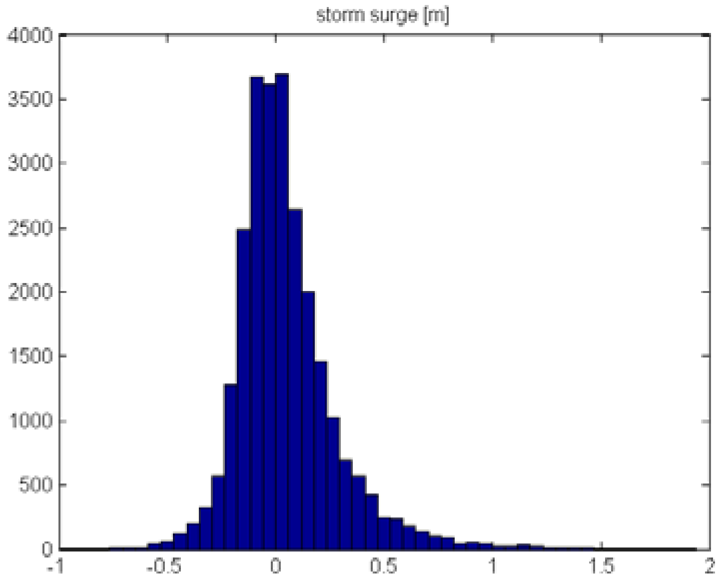

Figure 110, DOWEC storm surge

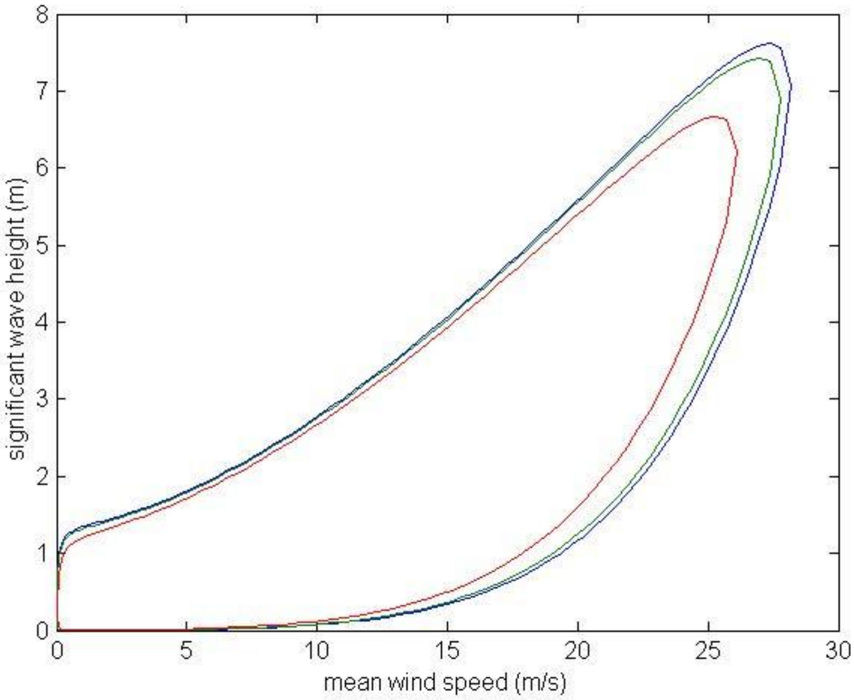

Figure 111, DOWEC contour plot of joint density function of the mean wind speed and significant wave height

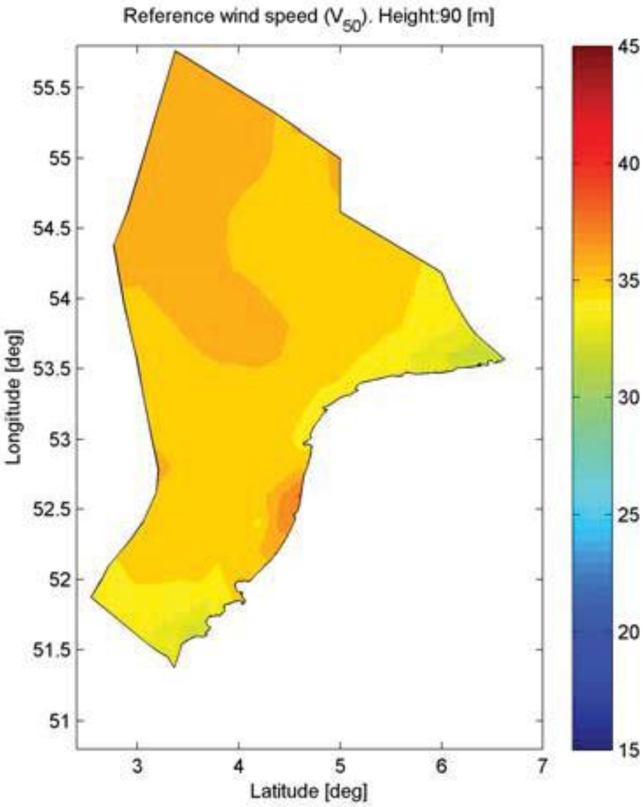

Figure 112, ECN Wind Atlas, Reference wind speed at hub height with return period of 50 years

16. Results calculations design conditions for a water depth of 15m

Design conditions	2.3	6.1a	6.1b	6.1c	6.2a	6.3b	7.1b	8.2a
Wind Forces								
Force on the blades	278,2639	505,7953	852,1833	526,09277	505,7953	545,3973	545,3973	545,39733
Moment on foot due to blades	40383,05	73403,54	123673,1	76349,213	73403,54	79150,79	79150,79	79150,788
Force on the tower	219,1169	398,2848	671,0455	414,26787	398,2848	429,4691	429,4691	429,4691
Moment on foot due to tower	17112,26	31104,64	52406,29	32352,86	31104,64	33540,02	33540,02	33540,023
Force on the nacelle	11,60812	21,09987	35,54988	21,946607	21,09987	22,75192	22,75192	22,751921
Moment on foot due to nacelle	1684,629	3062,119	5159,176	3185,0014	3062,119	3301,872	3301,872	3301,8725
------------	0	0	0	0	0	0	0	0
------------	0	0	0	0	0	0	0	0
------------	0	0	0	0	0	0	0	0
------------	0	0	0	0	0	0	0	0
Wave forces	0	0	0	0	0	0	0	0
Forces on shaft due to waves	1319,969	1599,489	2262,366	3768,9128	1599,489	1656,91	2372,085	2225,623
Forces on base due to waves	2006,722	2105,248	2736,822	3918,0998	2105,248	1864,549	2423,914	2878,8944
Moment on foot due to waves on shaft	14891,6	20299,95	30260,07	55357,204	20299,95	20611,45	31038,24	28434,33
Moment on foot due to waves on base	3020,69	3165,992	4115,79	5892,2634	3165,992	2814,23	3658,498	4329,9417
------------	0	0	0	0	0	0	0	0
------------	0	0	0	0	0	0	0	0
------------	0	0	0	0	0	0	0	0
------------	0	0	0	0	0	0	0	0
Ice forces	0	0	0	0	0	0	0	0
Horizontal force	123,4412	123,4412	123,4412	123,44124	123,4412	123,4412	123,4412	123,44124
Vertical force	163,9737	163,9737	163,9737	163,9737	163,9737	163,9737	163,9737	163,9737
Moments on foot due to ice loading	1851,619	2098,501	2098,501	2098,5011	2098,501	1975,06	1975,06	1975,0599
------------	0	0	0	0	0	0	0	0

------------	0	0	0	0	0	0	0	0
------------	0	0	0	0	0	0	0	0
Accidental loadings	0	0	0	0	0	0	0	0
Bow forces due to vessel collision	341,2007	341,2007	341,2007	341,20068	341,2007	341,2007	341,2007	341,20068
------------	0	0	0	0	0	0	0	0
------------	0	0	0	0	0	0	0	0
------------	0	0	0	0	0	0	0	0
------------	0	0	0	0	0	0	0	0
Bearing capacity	0	0	0	0	0	0	0	0
Bearing capacity drained conditions	834,085	834,085	834,085	834,085	834,085	834,085	834,085	834,085
Bearing capacity undrained conditions	0	0	0	0	0	0	0	0
Sliding resistance drained conditions	23690,74	23690,74	23690,74	23690,736	23690,74	23690,74	23690,74	23690,736
Sliding resistance undrained conditions	0	0	0	0	0	0	0	0
------------	0	0	0	0	0	0	0	0
------------	0	0	0	0	0	0	0	0
------------	0	0	0	0	0	0	0	0
------------	0	0	0	0	0	0	0	0
------------	0	0	0	0	0	0	0	0
------------	0	0	0	0	0	0	0	0
------------	0	0	0	0	0	0	0	0
------------	0	0	0	0	0	0	0	0
	0	0	0	0	0	0	0	0
Total horizontal forces [kN]	3959,121	4753,358	6681,407	8772,7611	4753,358	4642,519	5917,058	6225,577
Total moments on footing [MNm]	78,94385	133,1347	217,7129	175,23504	133,1347	141,3934	152,6645	150,73201

17. Results calculations design conditions for a water depth of 25m

Design conditions	2.3	6.1a	6.1b	6.1c	6.2a	6.3b	7.1b	8.2a
Wind Forces								
Force on the blades	278,2639	505,7953	852,1833	526,09277	505,7953	545,3973	545,3973	545,39733
Moment on foot due to blades	44139,62	80231,78	135177,6	83451,466	80231,78	86513,65	86513,65	86513,652
Force on the tower	219,1169	398,2848	671,0455	414,26787	398,2848	429,4691	429,4691	429,4691
Moment on foot due to tower	20070,33	36481,48	61465,4	37945,476	36481,48	39337,86	39337,86	39337,856
Force on the nacelle	11,60812	21,09987	35,54988	21,946607	21,09987	22,75192	22,75192	22,751921
Moment on foot due to nacelle	1841,338	3346,967	5639,099	3481,2806	3346,967	3609,023	3609,023	3609,0234
------------	0	0	0	0	0	0	0	0
------------	0	0	0	0	0	0	0	0
------------	0	0	0	0	0	0	0	0
------------	0	0	0	0	0	0	0	0
Wave forces	0	0	0	0	0	0	0	0
Forces on shaft due to waves	1546,655	1835,268	2543,179	4094,072	1835,268	1835,858	2586,227	2521,1512
Forces on base due to waves	1181,323	1336,948	1738,032	2488,2082	1336,948	862,4502	1121,185	1814,1117
Moment on foot due to waves on shaft	27294,93	34797,95	50137,34	86600,07	34797,95	36435,03	53245,22	48030,312
Moment on foot due to waves on base	1776,601	2009,286	2612,071	3739,5039	2009,286	1300,513	1690,667	2726,5171
------------	0	0	0	0	0	0	0	0
------------	0	0	0	0	0	0	0	0
------------	0	0	0	0	0	0	0	0
------------	0	0	0	0	0	0	0	0
Ice forces	0	0	0	0	0	0	0	0
Horizontal force	123,4412	123,4412	123,4412	123,44124	123,4412	123,4412	123,4412	123,44124
Vertical force	163,9737	163,9737	163,9737	163,9737	163,9737	163,9737	163,9737	163,9737
Moments on foot due to ice loading	3086,031	3332,914	3332,914	3332,9135	3332,914	3209,472	3209,472	3209,4723
------------	0	0	0	0	0	0	0	0

------------	0	0	0	0	0	0	0	0
------------	0	0	0	0	0	0	0	0
Accidental loadings	0	0	0	0	0	0	0	0
Bow forces due to vessel collision	341,2007	341,2007	341,2007	341,20068	341,2007	341,2007	341,2007	341,20068
------------	0	0	0	0	0	0	0	0
------------	0	0	0	0	0	0	0	0
------------	0	0	0	0	0	0	0	0
------------	0	0	0	0	0	0	0	0
Bearing capacity	0	0	0	0	0	0	0	0
Bearing capacity drained conditions	834,085	834,085	834,085	834,085	834,085	834,085	834,085	834,085
Bearing capacity undrained conditions	0	0	0	0	0	0	0	0
Sliding resistance drained conditions	23690,74	23690,74	23690,74	23690,736	23690,74	23690,74	23690,74	23690,736
Sliding resistance undrained conditions	0	0	0	0	0	0	0	0
------------	0	0	0	0	0	0	0	0
------------	0	0	0	0	0	0	0	0
------------	0	0	0	0	0	0	0	0
------------	0	0	0	0	0	0	0	0
------------	0	0	0	0	0	0	0	0
------------	0	0	0	0	0	0	0	0
------------	0	0	0	0	0	0	0	0
------------	0	0	0	0	0	0	0	0
	0	0	0	0	0	0	0	0
Total horizontal forces [kN]	3360,408	4220,836	5963,431	7668,0287	4220,836	3819,367	4828,472	5456,3224
Total moments on footing [MNm]	98,20885	160,2004	258,3644	218,55071	160,2004	170,4055	187,6059	183,42683

18. Results calculations design conditions for a water depth of 35m

Design conditions	2.3	6.1a	6.1b	6.1c	6.2a	6.3b	7.1b	8.2a
Wind Forces								
Force on the blades	278,2639	505,7953	852,1833	526,09277	505,7953	545,3973	545,3973	545,39733
Moment on foot due to blades	47896,18	87060,02	146682,1	90553,718	87060,02	93876,52	93876,52	93876,515
Force on the tower	219,1169	398,2848	671,0455	414,26787	398,2848	429,4691	429,4691	429,4691
Moment on foot due to tower	23028,41	41858,33	70524,51	43538,093	41858,33	45135,69	45135,69	45135,689
Force on the nacelle	11,60812	21,09987	35,54988	21,946607	21,09987	22,75192	22,75192	22,751921
Moment on foot due to nacelle	1998,048	3631,816	6119,022	3777,5598	3631,816	3916,174	3916,174	3916,1743
------------	0	0	0	0	0	0	0	0
------------	0	0	0	0	0	0	0	0
------------	0	0	0	0	0	0	0	0
------------	0	0	0	0	0	0	0	0
Wave forces	0	0	0	0	0	0	0	0
Forces on shaft due to waves	1664,269	1971,384	2709,248	4299,5981	1971,384	1903,96	2670,571	2696,4227
Forces on base due to waves	718,6119	879,5532	1143,419	1636,9463	879,5532	390,2426	507,3154	1191,9407
Moment on foot due to waves on shaft	41331,27	51079,52	72428,92	121668,91	51079,52	53989,2	77896,46	70107,511
Moment on foot due to waves on base	1080,393	1321,544	1718,008	2459,5409	1321,544	588,3382	764,8396	1790,9415
------------	0	0	0	0	0	0	0	0
------------	0	0	0	0	0	0	0	0
------------	0	0	0	0	0	0	0	0
------------	0	0	0	0	0	0	0	0
Ice forces	0	0	0	0	0	0	0	0
Horizontal force	123,4412	123,4412	123,4412	123,44124	123,4412	123,4412	123,4412	123,44124
Vertical force	163,9737	163,9737	163,9737	163,9737	163,9737	163,9737	163,9737	163,9737
Moments on foot due to ice loading	4320,443	4567,326	4567,326	4567,3259	4567,326	4443,885	4443,885	4443,8847
------------	0	0	0	0	0	0	0	0

------------	0	0	0	0	0	0	0	0
------------	0	0	0	0	0	0	0	0
Accidental loadings	0	0	0	0	0	0	0	0
Bow forces due to vessel collision	341,2007	341,2007	341,2007	341,20068	341,2007	341,2007	341,2007	341,20068
------------	0	0	0	0	0	0	0	0
------------	0	0	0	0	0	0	0	0
------------	0	0	0	0	0	0	0	0
------------	0	0	0	0	0	0	0	0
Bearing capacity	0	0	0	0	0	0	0	0
Bearing capacity drained conditions	834,085	834,085	834,085	834,085	834,085	834,085	834,085	834,085
Bearing capacity undrained conditions	0	0	0	0	0	0	0	0
Sliding resistance drained conditions	23690,74	23690,74	23690,74	23690,736	23690,74	23690,74	23690,74	23690,736
Sliding resistance undrained conditions	0	0	0	0	0	0	0	0
------------	0	0	0	0	0	0	0	0
------------	0	0	0	0	0	0	0	0
------------	0	0	0	0	0	0	0	0
------------	0	0	0	0	0	0	0	0
------------	0	0	0	0	0	0	0	0
------------	0	0	0	0	0	0	0	0
------------	0	0	0	0	0	0	0	0
------------	0	0	0	0	0	0	0	0
	0	0	0	0	0	0	0	0
Total horizontal forces [kN]	3015,311	3899,558	5534,887	7022,2929	3899,558	3415,262	4298,946	5009,4231
Total moments on footing [MNm]	119,6547	189,5185	302,0398	266,56515	189,5185	201,9498	226,0336	219,27072

19. Calculation sheet bending resistance

> *restart*;

xu<1664mm otherwise change formula demerine hls!!

> $xu := 1461;$

$$xu := 1461$$

> $MedULS := 2.134\text{e}11;\ MedSLS := \frac{MedULS}{1.35};\ fcd := \frac{45}{1.5};$

$$MedULS := 2.134\ 10^{11}$$

$$MedSLS := 1.580740741\ 10^{11}$$

$$fcd := 30.00000000$$

> $d := 4500;\ Diam := 6000;\ dm := \frac{(d + Diam)}{2};$

$$d := 4500$$

$$Diam := 6000$$

$$dm := 5250$$

> $y := 3000 - xu;$

$$y := 1539$$

> $theta1 := evalf\left(2 \cdot \arctan\left(\frac{\text{sqrt}\left(\frac{Diam^2}{4} - y^2\right)}{y}\right)\right);$
$theta2 := evalf\left(2 \cdot \arctan\left(\frac{\text{sqrt}\left(\frac{d^2}{4} - y^2\right)}{y}\right)\right);$

$$\theta 1 := 2.064240502$$

$$\theta 2 := 1.635128693$$

> $Aa := \frac{0.5 \cdot Diam^2}{4} \cdot (theta1 - \sin(theta1)) - \frac{0.5 \cdot d^2}{4} \cdot (theta2 - \sin(theta2));$

$$Aa := 3.712996383\ 10^{6}$$

> $bardiam := 32;\ spacing := 150;\ number\_row := 2;\ fyd := \frac{500}{1.15};$

$$bardiam := 32$$

$$spacing := 150$$

$$number\_row := 2$$

$$fyd := 434.7826087$$

> $As := \frac{0.25 \cdot evalf(\text{Pi}) \cdot \text{bardiam}^2 \cdot number\_row \cdot 1000}{spacing};$

$$As := 10723.30293$$

> $Acs := Aa;$

$$Acs := 3.712996383\ 10^{6}$$

> $ys := x;$

$$ys := x$$

> $theta1s := evalf\left(2 \cdot \arctan\left(\frac{\operatorname{sqrt}\left(\frac{Diam^2}{4} - ys^2\right)}{ys}\right)\right);$
$theta2s := evalf\left(2 \cdot \arctan\left(\frac{\operatorname{sqrt}\left(\frac{d^2}{4} - ys^2\right)}{ys}\right)\right);$

$$theta1s := 2.\ \arctan\left(\frac{\sqrt{-1.\ x^2 + 9.000000\ 10^{6}}}{x}\right)$$
$$theta2s := 2.\ \arctan\left(\frac{\sqrt{-1.\ x^2 + 5.062500\ 10^{6}}}{x}\right)$$

> $Aas := \frac{0.5 \cdot Diam^2}{4} \cdot (theta1s - \sin(theta1s));$

$$Aas := 9.000000000\ 10^{6} \arctan\left(\frac{\sqrt{-1.\ x^2 + 9.000000\ 10^{6}}}{x}\right) - 4.500000000\ 10^{6} \sin\left(2.\ \arctan\left(\frac{\sqrt{-1.\ x^2 + 9.000000\ 10^{6}}}{x}\right)\right)$$

>

> $eq1 := solve\left(Aas = \frac{Acs}{2}, x\right);$

$eq1 := -3349.879943 - 580.7602712\,\mathrm{I},\ -2296.850942,\ -3349.879943 + 580.7602712\,\mathrm{I},\ 2296.850942$

> $hls := eq1[4];$

$$hls := 2296.850942$$

> $hls\_old := 1849.494560;$

$$hls\_old := 1849.494560$$

Length of Aas

> $thetadm := evalf\left(2 \cdot \arctan\left(\frac{\operatorname{sqrt}\left(\frac{dm^2}{4} - y^2\right)}{y}\right)\right);$

$$thetadm := 1.888660164$$

> $LengthAas := \dfrac{evalf\left(\left(thetadm \cdot \frac{dm}{2}\right)\right)}{1000};$

$$LengthAas := 4.957732930$$

> $Ns := LengthAas \cdot As \cdot fyd$

$$Ns := 2.311446611\ 10^7$$

> $Ns\_old := evalf\left(\dfrac{0.5 \cdot dm \cdot \mathrm{Pi}}{1000}\right) \cdot As \cdot fyd;$

$$Ns\_old := 3.844854587\ 10^7$$

>

> $\mathrm{y1} := \dfrac{Diam}{2} - 0.5 \cdot xu;$

$$y1 := 2269.5$$

> $theta11 := evalf\left(2 \cdot \arctan\left(\dfrac{\mathrm{sqrt}\left(\frac{Diam^2}{4} - y1^2\right)}{y1}\right)\right);$
$theta21 := evalf\left(2 \cdot \arctan\left(\dfrac{\mathrm{sqrt}\left(\frac{d^2}{4} - y1^2\right)}{y1}\right)\right);$

$$\theta 11 := 1.425703280$$
$$\theta 21 := 0.2631224352\ \mathrm{I}$$

> $Aa1 := \dfrac{0.5 \cdot Diam^2}{4} \cdot (theta11 - \sin(theta11));$

$$Aa1 := 1.962948704\ 10^6$$

>

> $\mathrm{y2} := \dfrac{Diam}{2} - xu;$

$$y2 := 1539$$

> $theta12 := evalf\left(2 \cdot \arctan\left(\dfrac{\mathrm{sqrt}\left(\frac{Diam^2}{4} - y2^2\right)}{y2}\right)\right);$
$theta22 := evalf\left(2 \cdot \arctan\left(\dfrac{\mathrm{sqrt}\left(\frac{d^2}{4} - y2^2\right)}{y2}\right)\right);$

$$\theta 12 := 2.064240502$$
$$\theta 22 := 1.635128693$$

> $Aa2 := \dfrac{0.5 \cdot Diam^2}{4} \cdot (theta12 - \sin(theta12)) - \dfrac{0.5 \cdot d^2}{4} \cdot (theta22 - \sin(theta22));$

$$Aa2 := 3.712996383\ 10^6$$

> $Aa3 := Aa2 - Aa1;$

$$Aa3 := 1.750047679\ 10^6$$

>

> $hlc := \frac{Diam}{2} - \frac{Aa1 + \frac{Aa3}{2}}{Aa2} \cdot xu;$

$$hlc := 1883.306780$$

> $Nc := Aa1 \cdot fcd + (Aa2 - Aa1) \cdot 0.5 \cdot fcd;$

$$Nc := 8.513917630\ 10^7$$

>

> $xu := \mathrm{xu};\ MedULS;\ \mathrm{MrdULS} := evalf(\,Nc \cdot hlc + Ns \cdot hls);$

$$xu := 1461$$

$$2.134\ 10^{11}$$

$$MrdULS := 2.134336713\ 10^{11}$$

20. Drawings foundation side view and top view

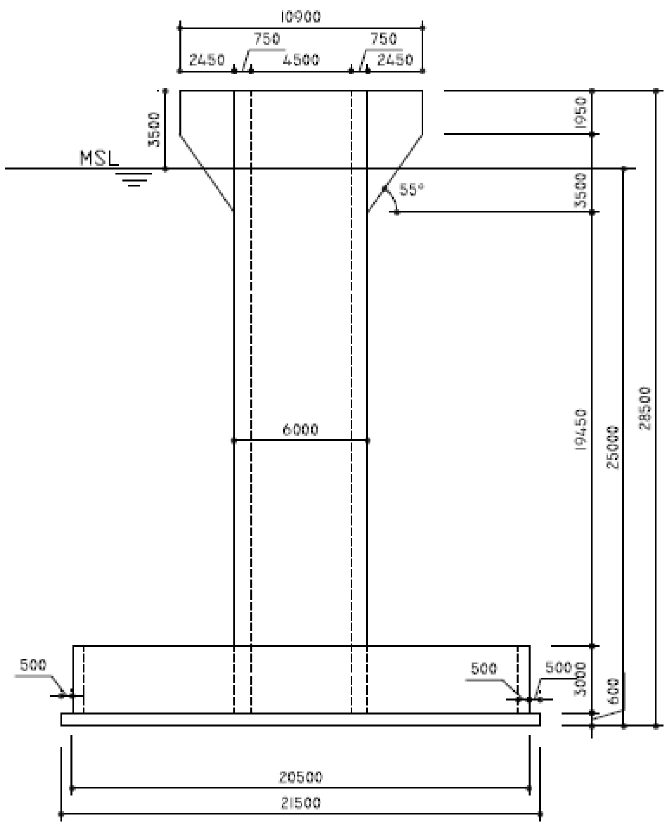

Figure 113, Sketch foundation with dimensions on large scale

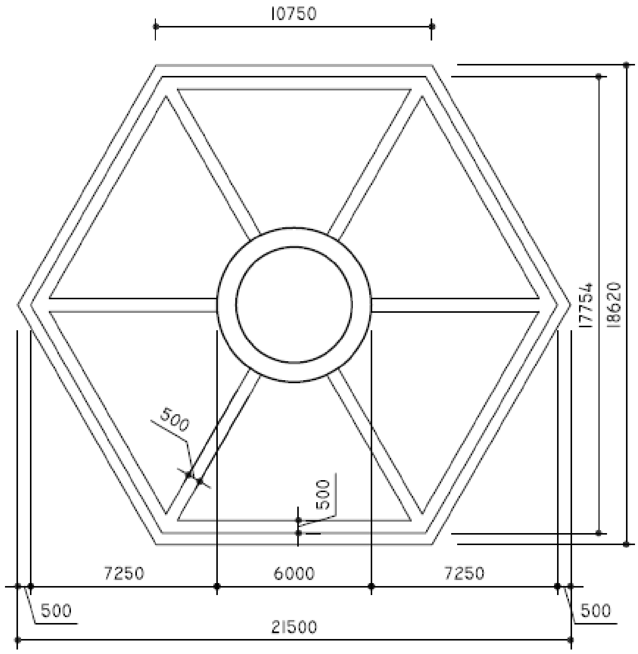

Figure 114, Dimensions foundation base large scale

21. Appendix, NEN 6740 table 1

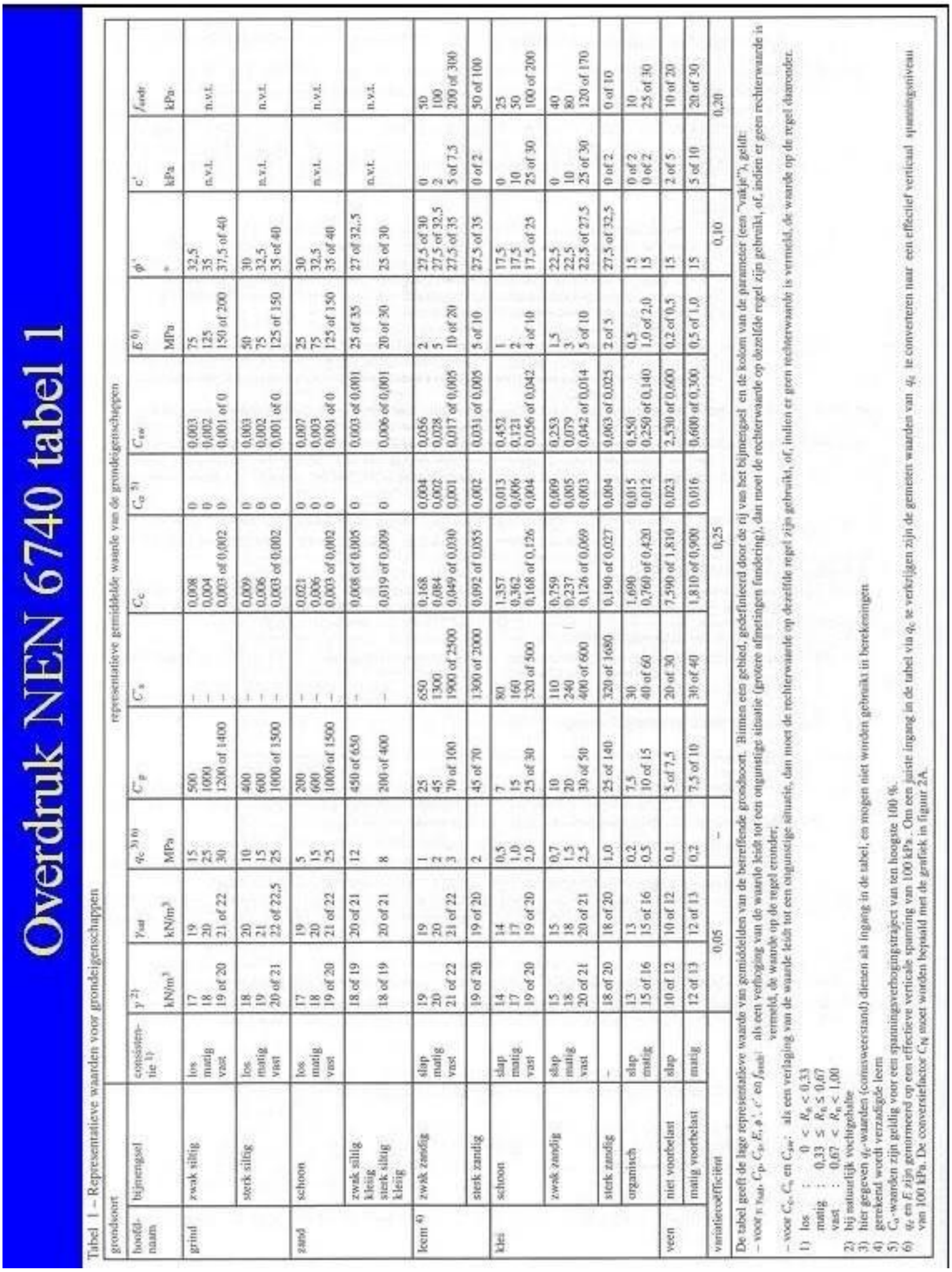

Overdruk NEN 6740 tabel 1

Tabel 1 – Representatieve waarden voor grondeigenschappen

grondsoort			representatieve gemiddelde waarde van de grondeigenschappen											
hoofdnaam	bijmengsel	consistentie [1]	γ [2] kN/m³	γ_{sat} kN/m³	q_c [3] [6] MPa	C'_p	C'_s	C_c	C_α [5]	C_{sw}	E [6] MPa	ϕ' °	c' kPa	f_{undr} kPa
grind	zwak siltig	los matig vast	17 18 19 of 20	19 20 21 of 22	15 25 30	500 1000 1200 of 1400	– – –	0,008 0,004 0,003 of 0,002	0 0 0	0,003 0,002 0,001 of 0	75 125 150 of 200	32,5 35 37,5 of 40	n.v.t.	n.v.t.
	sterk siltig	los matig vast	18 19 20 of 21	20 21 22 of 22,5	10 15 25	400 600 1000 of 1500	– – –	0,009 0,006 0,003 of 0,002	0 0 0	0,003 0,002 0,001 of 0	50 75 125 of 150	30 32,5 35 of 40	n.v.t.	n.v.t.
zand	schoon	los matig vast	17 18 19 of 20	19 20 21 of 22	5 15 25	200 600 1000 of 1500	– – –	0,021 0,006 0,003 of 0,002	0 0 0	0,007 0,003 0,001 of 0	25 75 125 of 150	30 32,5 35 of 40	n.v.t.	n.v.t.
	zwak siltig kleiig sterk siltig kleiig		18 of 19 18 of 19	20 of 21 20 of 21	12 8	450 of 650 200 of 400	– –	0,008 of 0,005 0,019 of 0,009	0 0	0,003 of 0,001 0,006 of 0,001	25 of 35 20 of 30	27 of 32,,5 25 of 30	n.v.t.	n.v.t.
leem [4]	zwak zandig	slap matig vast	19 20 21 of 22	19 20 21 of 22	1 2 3	25 45 70 of 100	650 1300 1900 of 2500	0,168 0,084 0,049 of 0,030	0,004 0,002 0,001	0,056 0,028 0,017 of 0,005	2 5 10 of 20	27,5 of 30 27,5 of 32,5 27,5 of 35	0 2 5 of 7,5	50 100 200 of 300
	sterk zandig		19 of 20	19 of 20	2	45 of 70	1300 of 2000	0,092 of 0,055	0,002	0,031 of 0,005	5 of 10	27,5 of 35	0 of 2	50 of 100
klei	schoon	slap matig vast	14 17 19 of 20	14 17 19 of 20	0,5 1,0 2,0	7 15 25 of 30	80 160 320 of 500	1,357 0,362 0,168 of 0,126	0,013 0,006 0,004	0,452 0,121 0,056 of 0,042	1 2 4 of 10	17,5 17,5 17,5 of 25	0 10 25 of 30	25 50 100 of 200
	zwak zandig	slap matig vast	15 18 20 of 21	15 18 20 of 21	0,7 1,5 2,5	10 20 30 of 50	110 240 400 of 600	0,759 0,237 0,126 of 0,069	0,009 0,005 0,003	0,253 0,079 0,042 of 0,014	1,5 3 5 of 10	22,5 22,5 22,5 of 27,5	0 10 25 of 30	40 80 120 of 170
	sterk zandig	–	18 of 20	18 of 20	1,0	25 of 140	320 of 1680	0,190 of 0,027	0,004	0,063 of 0,025	2 of 5	27,5 of 32,5	0 of 2	0 of 10
	organisch	slap matig	13 15 of 16	13 15 of 16	0,2 0,5	7,5 10 of 15	30 40 of 60	1,690 0,760 of 0,420	0,015 0,012	0,550 0,250 of 0,140	0,5 1,0 of 2,0	15 15	0 of 2 0 of 2	10 25 of 30
veen	niet voorbelast	slap	10 of 12	10 of 12	0,1	5 of 7,5	20 of 30	7,590 of 1,810	0,023	2,530 of 0,600	0,2 of 0,5	15	2 of 5	10 of 20
	matig voorbelast	matig	12 of 13	12 of 13	0,2	7,5 of 10	30 of 40	1,810 of 0,900	0,016	0,600 of 0,300	0,5 of 1,0	15	5 of 10	20 of 30
variatiecoëfficiënt			0,05		–	0,25						0,10	0,20	

De tabel geeft de lage representatieve waarde van gemiddelden van de betreffende grondsoort. Binnen een gebied, gedefinieerd door de rij van het bijmengsel en de kolom van de parameter (een "vakje"), geldt:

– voor γ, γ_{sat}, C_p, C_s, E, ϕ', c' en f_{undr}: als een verhoging van de waarde leidt tot een ongunstige situatie (grotere afmetingen fundering), dan moet de rechterwaarde op dezelfde regel zijn gebruikt, of, indien er geen rechterwaarde is vermeld, de waarde op de regel eronder;

– voor C_c, C_α en C_{sw}: als een verlaging van de waarde leidt tot een ongunstige situatie, dan moet de rechterwaarde op dezelfde regel zijn gebruikt, of, indien er geen rechterwaarde is vermeld, de waarde op de regel daaronder.

1) los : $0 < R_e < 0,33$
matig : $0,33 \leq R_e \leq 0,67$
vast : $0,67 < R_e < 1,00$

2) bij natuurlijk vochtgehalte

3) hier gegeven q_c-waarden (conusweerstand) dienen als ingang in de tabel, en mogen niet worden gebruikt in berekeningen

4) gerekend wordt verzadigde leem

5) C_α-waarden zijn geldig voor een spanningsverhogingstraject van ten hoogste 100 %.

6) q_c en E zijn genormeerd op een effectieve verticale spanning van 100 kPa. Om een juiste ingang in de tabel via q_c te verkrijgen zijn de gemeten waarden van q_c te converteren naar een effectief verticaal spanningsniveau van 100 kPa. De conversiefactor C_N moet worden bepaald met de grafiek in figuur 2A.

Figure 115, NEN6740 Table 1

22. Dimensions and parameters used for undrained calculations Brinch Hansen

Calculating the eccentricity of the foundation loadings

With the design vertical load V_d and the design bending moment M_d the eccentricity of the loading centre can be calculated as $e = \frac{M_d}{V_d}$. Using the calculated values for $V_d = 7.467 \text{ tonnes}$ and $M_d = 2,40 \cdot 10^{11} Nmm$. The eccentricity hereby becomes $e = \frac{2,40 \cdot 10^{11}}{7,647 \cdot 10^{7}} = 3134mm$.

Calculating the effective foundation area

With the calculated eccentricity of $e = 3.134mm$ and the known dimensions of the foundation the effective foundation area can be calculated. For the radius of the foundation the inner radius should be taken according to the DNV-OS-J101 calculation examples. This is because this radius is the largest radius that falls completely inside the foundation area. This inner radius is illustrated in the figure.

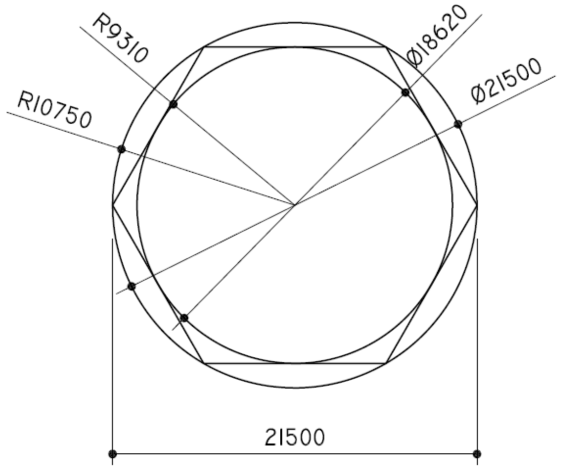

Figure 116, Inner and outer radius of foundation

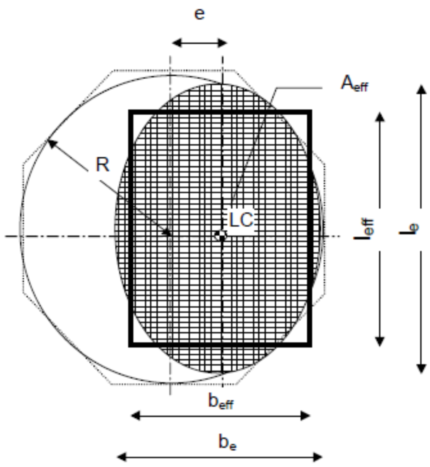

Figure 117, Effective foundation area from DNV-OS-J101

As can be seen the internal diameter of the foundation is 18.620mm and thus the radius of the inner circle is 9.310mm. According to the DNV the effective foundation area, as visible in the figure, can be calculated using the following formula: $A_{eff} = 2\left[R^2 \arccos\left(\frac{e}{R}\right) - e\sqrt{R^2 - e^2}\right]$.

With this effective foundation area the major axis of A_{eff} can be calculated as $b_e = 2(R - e)$ and $l_e = 2R\sqrt{1 - \left(1 - \frac{b_e}{2R}\right)^2}$. With these major axes the effective area A_{eff} can be represented by $l_{eff} = \sqrt{A_{eff} \frac{l_e}{b_e}}$ and $b_{eff} = \frac{l_{eff}}{l_e} b_e$. Using the values for $e = 3.134mm$ and $R = 9.310mm$ the outcomes of the formulas are:

$b_e = 12,4m$
$l_e = 17,5m$
$b_{eff} = 10,5m$
$l_{eff} = 15,0m$
$A_{eff} = 157,8m^2$

These outcomes serve as the input for the bearing capacity calculation for the foundation.

Calculation bearing capacity foundation soil for drained conditions[28]

With the calculated effective foundation area and the known vertical load of the foundation the bearing capacity of the foundation subsoil can be calculated. The formulas in this paragraph are only valid for drained conditions for the subsoil.

The formula used is a variation on the Prandtl formula by Brinch Hansen. The formula consists of three parts. The first part incorporates the bearing capacity of the soil itself, the second the bearing capacity due to an effective overburden pressure by the adjacent soil and the last part incorporates the bearing capacity due to the cohesion of the soil. The formula also takes into account a possible inclination of the load and the shape of the loaded area. The total formula stated by Hansen is:

$q_d = \frac{1}{2}\gamma' b_{eff} N_\gamma s_\gamma i_\gamma + p_0^{'} N_q s_q i_q + c_d N_c s_c i_c$ where $N = \text{bearing capacity factor, } s = \text{shape factor and } i = \text{inclination factor}$. The formulas for determining these factors can be found below.

The bearing capacity factors can be determined using the formula's:

$N_\gamma = 2\cdot(N_q - 1)\cdot\tan\phi_d$, $N_q = e^{\pi\tan\phi_d}\cdot\frac{1+\sin\phi_d}{1-sin\phi_d}$ and $N_c = (N_q - 1)\cdot\cot\phi_d$.

As can be seen the bearing capacity factors are only depending on one soil parameter being the internal angle of friction ϕ of the soil. The formulas for the shape factors are:

$s_\gamma = 1 - 0,4\cdot\frac{b_{eff}}{L_{eff}}$ and $s_q = s_c = 1 + 0,2\cdot\frac{b_{eff}}{l_{eff}}$. For the shape factors it can be noticed that they are only depending on the dimensions of the effective foundation area. The inclination factors incorporate the loading in two directions, being a vertical and a horizontal load. These inclination factors can be calculated using the following formula's:

$i_\gamma = i_q^2$ and $i_q = i_c = \left(1 - \frac{H_d}{V_d + A_{eff}\cdot c_d\cdot\cot\phi_d}\right)$

With the previously assumed soil conditions and the calculated forces acting on the foundation the effective bearing capacity of the foundation can be calculated using the presented formula for q_d. The outcomes for the bearing capacity factor, the inclination factor and the shape factors are calculated with an internal angle of friction of the soil of 32,5° and an inner foundation radius of 9.310mm and are:

[28] Values used for calculating the bearing capacity are according to DNV-OS-J101 October 2010, Appendix G.

$\phi = 32,5^o$

$\phi_d = \dfrac{\phi_d}{\gamma_\phi} = \dfrac{32,5}{1,25} = 27,0^o$

$N_q = 13,208 \quad s_q = 1,141 \quad i_q = 0,7$
$N_c = 23,953 \quad s_c = 1,141 \quad i_c = 0,7$
$N_\gamma = 12,443 \quad s_\gamma = 0,718 \quad i_\gamma = 0,5$

The other values needed for the calculation of q_d are γ', b_{eff}, p_0' and c_d. Since the assumed soil type is cohesionless soil and there is no overburden pressure at the foundation (the foundation is not embedded in soil) the factors $p_{o'}$ and c_d are 0. The values for γ' and b_{eff} are:
$\gamma' = \gamma_{soil} - \gamma_{water} = 18 - 9,81 = 8,2 kN/m^3$ and $b_{eff} = 10,5m$ as calculated before. Therefore the calculation for the value of q_d becomes:

$$q_d = \frac{1}{2}\gamma' b_{eff} N_\gamma s_\gamma i_\gamma + p_0' N_q s_q i_q + c_d N_c s_c i_c$$ [29]

$$= \frac{1}{2} \cdot 8,2 \cdot 10,5 \cdot 12,443 \cdot 0,718 \cdot 0,5 + 0 \cdot 13,208 \cdot 1,141 \cdot 0,7 + 0 \cdot 23,953 \cdot 1,141 \cdot 0,7 = 209 kN/m^2$$

To calculate the total bearing capacity of the foundation the value found for q_d has to be multiplied by the effective foundation area A_{eff}. This gives a total bearing capacity of $R_d = q_d \cdot A_{eff} = 209 \cdot 157,8 = 32.944 kN$. This is smaller than the effective vertical force of $V_d = 76.470 kN$ and thus the soil is not able to bear the foundation with the given foundation diameter.

[29] This value found for q_d is calculated with the values found in the DNV-OS-J101. When the slightly different formula's presented in the book Grondmechanica by A. Verruijt p.243 are used the value found for $q_d = 168,6 kN/m^2$ which is lower than found according to the DNV Formula's.

23. Material input D-Geo Stability

The material properties as inserted in the software D-Geo Stability

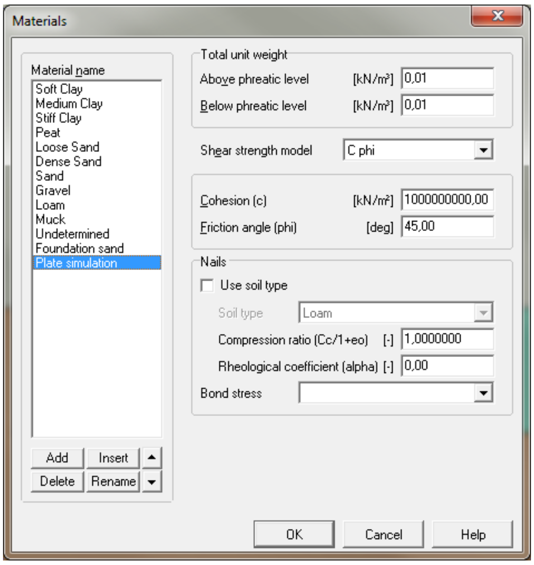

Figure 118, Plate material properties

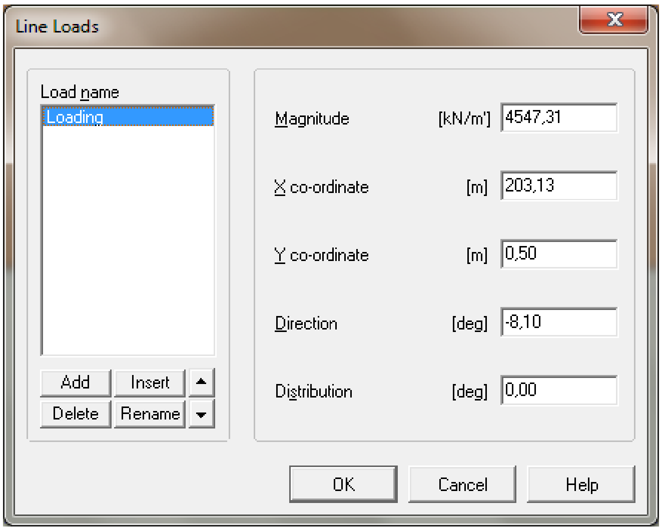

Figure 119, Line load modulation

The stiff plate is modelled in the program as an object with a thickness of 0,5m. An image of the modelled stiff plate can be seen in the figure below.

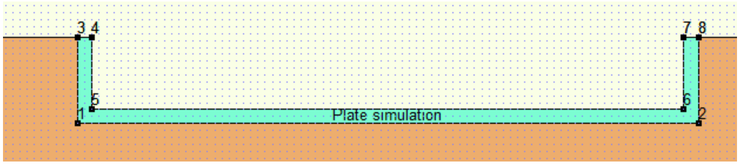

Figure 120, Stiff plate as modelled in D-Geo Stability

24. Validation Uplift Van calculation

Validating Uplift Van module

To validate the model calculations of the D-Geo Stability software different situations are evaluated. This is done by modelling 7 different situations which are varying with respect to the calculation grid and 6 situations which are varying with respect to the soil layout. The variations regarding the grid size are summarized in the table below. The sketches of the results are placed at the appendix at the end of this document. As can be seen in the table it is attempted to concentrate the grid points of the slip circles around the final positions found by the D-Geo Stability software. After 7 attempts is was found that the location of the grids was close enough to the final points found with the software.

Situation	Left circle						Right circle						Tangent lines		
	X-left	X-right	Nr	Y-top	Y-bot	Nr	X-left	X-right	Nr	Y-top	Y-bot	Nr	Y-top	Y-bot	Nr
1	180	200	15	20	3.1	10	200	220	15	20	3.1	10	0	-15	15
2	190	200	15	5	1	15	200	210	15	5	1	15	0	-10	15
3	190	200	10	5	1	10	200	210	10	2	1	10	0	-10	10
4	190	200	5	5	2	5	200	210	5	5	2	5	0	-10	10
5	195	200	7	5	2	7	200	205	7	5	2	7	0	-10	10
6	195	200	7	5	2	7	200	205	7	5	2	7	-2.5	-10	10
7	199	200	7	5	4	7	199	200	7	8	7	7	-2.5	-10	10

Table 34, Variations for grid size. Coordinates are in meters.

Form the table above it was found that for the 7th situation the modelled grid locations were having great resemblance with the finally found slip circle locations. Therefore it was chosen to use this situation as the basis for the variations with respect to the soil layout. The only difference for the modelling of this situation is the tangent line configuration. For the calculations made for the soil layout variation the tangent line is modelled from -2,5m to -22,5m using 21 lines.
This means that every 1,0m a tangent line is modelled. In the table on the next page it is visible which situations are modelled for the soil layer variation.

Situation	Depth of clay layer [m]	Thickness of clay layer [m]
1	5	2,5
2	5	5,0
3	5	7,5
4	10	2,5
5	10	5,0
6	10	7,5

Table 35, Variation in soil layout

Results of model calculations

For the variation in the grid size the results are presented below. From the results the following data is presented: The safety factor, active driving moment and active resisting moment. The results of the variation in soil layout are only presented in safety factors.
For all the calculation made the results are added in the appendix at the end of this document.

Situation	Safety factor	Driving moment {kNm]	Resisting moment [kNm]
1	0,805	-14.496.41	3345.86
2	0,749	-13.624,99	2878,89
3	0,653	-13.597,59	2615,88

4	0,912	-26.494,32	5943,94
5	0,733	-19.813,43	3895,36
6	0,798	-15.839,70	3800,78
7	0,575	-11.284,45	2161,64

Table 36, Results for variation in grid size

The results for the variations in the soil layout are, as mentioned before, based on situation 7. The results for the model calculations for the soil variations are summarized in the table below.

Situation	Safety factor
5-2,5	0,59
5-5,0	0,59
5-7,5	0,59
10-2,5	1,09
10-5,0	1,09
10-7,5	Not performed

Table 37, Results for variations in soil layout

As can be seen from the results presented in the table above the thickness of the clay layer has no influence on the safety factor. Because of this finding, and the conclusion that the results are not correct the last calculation for the 10-7,5 calculation was not performed. The results are found not correct because it is quite remarkable that the safety factor is not changing when the layer thickness is increased. It is namely expected that the thickness should have an influence on the safety of the model.
Because of this remarked behaviour and it is decided to perform a validation to check whether the program D-Geo Stability is able to calculate the models as described before. This is done by checking with the aid of calculations if the stress increment in the soil by the point loads is correctly incorporated in the model calculations. If this is not the case the program is not able to calculate the correct safety factors and thus not usable for this study.

Validation of D-Geo Stability Uplift Van calculations

To check whether the D-Geo Stability program takes the increase of the stress in the subsoil due to the point loads adequately into account two different models are evaluated. The first model uses a weightless foundation plate and has the combined force (Horizontal, bending moment and self-weight) applied at a distance of 3,13m from the centre of the foundation. The second model has placed the combined force at 8,75m from the centre of the foundation. Because by doing so not all the vertical force of the foundation is incorporated also a mass is given to the stiff foundation plate which will be explained later on.
For both the models only the forces and on the plate and the mass of the plate are varied. The calculation grid and other model parameters are held constant.

<u>Calculation of force for 8,75m eccentricity model</u>

The force to be applied for this model is calculated as follows: $\frac{M_D}{e} = \frac{239.640}{8,75} = 27.387 kN$. When combined with the horizontal force this results in a inclined force of $F_{res} = \sqrt{10.890^2 + 27.387^2} = 29.473 kN$. The angle of this force is $\tan^{-1}\left(\frac{27.387}{10.890}\right) = 68,32^o$ with respect to the horizontal axis.

To use the resulting force in the model the force has to be converted to kN/m'. This is done by dividing the force by the foundation surface and multiplying it with the model width:
$F_{res'} = \frac{29.473}{0,25 \cdot \pi \cdot 21,5^2} = 81,18 kN/m^2 \cdot 21,5 = 1.745,41 kN/m'$.

Since not the total vertical force ($76.470kN$) is incorporated in the resulting force the resulting part of the vertical force is included in the weight of the stiff plate. The resulting vertical force is $76.470 - 27.387 = 49.083kN$. Since the maximum soil weight for the program is $100kN/m^3$ the thickness of the stiff plate is adjusted to $\frac{49.083}{0,25 \cdot \pi \cdot 21,5^2 \cdot 100} = 1,352m$. The mass of the foundation plate is thus $100kN/m^3$

Evaluation model with force at 3,13m eccentricity

The model with an eccentricity of 3,13m for the vertical force gives an output which is similar to the calculations made before. The outcomes of this calculation are a safety factor of 0,67 and moments of:

Active moments
Driving moment [kNm] : -13275.39
Resisting moment [kNm] : 2264.86
Passive moments
Driving moment [kNm] : 1787.57
Resisting moment [kNm] : 4817.86

Evaluation model with force at 8,75m eccentricity

For this second model the eccentricity of the force is increased to be able to study the behaviour of the model with respect to the stresses in the subsoil. The outcomes of this calculation are giving other results than for the first model. The safety factor for this model now is 1,25 and the moments are:

Active moments
Driving moment [kNm] : -21503.74
Resisting moment [kNm] : 9259.92
Passive moments
Driving moment [kNm] : 3282.40
Resisting moment [kNm] : 6729.37

The images of the results for both calculations are placed in the appendix at the end of this document.

Validation outcomes

It can be seen that the differences with the first model (3,13m eccentricity) are significant. Since the total loads applied at the foundation are equal for both the evaluated models it is expected to have more or less comparable calculation outcomes. Since this is not the case for the presented calculations it is stated that the program used, D-Geo Stability, is not sufficient capable in incorporating the stress increases in the soil due to point loads and thus unsuitable for performing the calculations for the Gravity Base Foundation models. The model setup and the images of the results are placed in the next Appendix.
Besides the possible lack in the capability of the software in incorporating the stress increases in the soil there is a second possible explanation for the differences in the safety factors for the two

evaluated models. By modelling the stiff plate it is tried to model a stiff plate that remains stiff under the applied loadings. Because the eccentricity of the applied force and the thickness of the modelled plate are varying for the two evaluated models it could be, that when the behaviour of the stiff plate is not completely stiff, differences in safety factor outcomes are occurring. For example the thickness of the stiff plate for the 3,13m eccentricity model is modelled as 0,5m. For the 8,75m eccentricity model the thickness of the plate is changed to 1,35m. This could have as a result, when the plate is not behaving completely stiff, that the stiffness of the thicker plate is higher than it is for the 0,5m thick plate. This possible difference in stiffness of the plate could have could result in the observed differences of the calculated safety factors.
When it indeed is the case that the stiffness of the plate is not as stiff as it is tried to model it is also indicates that the program D-Geo Stability is not suitable for performing the calculations for the Gravity Base Foundation. Since there are no other possibilities found in the software to model a stiff plate it is not possible to apply the eccentric forces on the foundation slab correctly.

Taking the above into account it was justified to make a switch to a different geotechnical software package.

25. Calculation results Uplift Van calculations

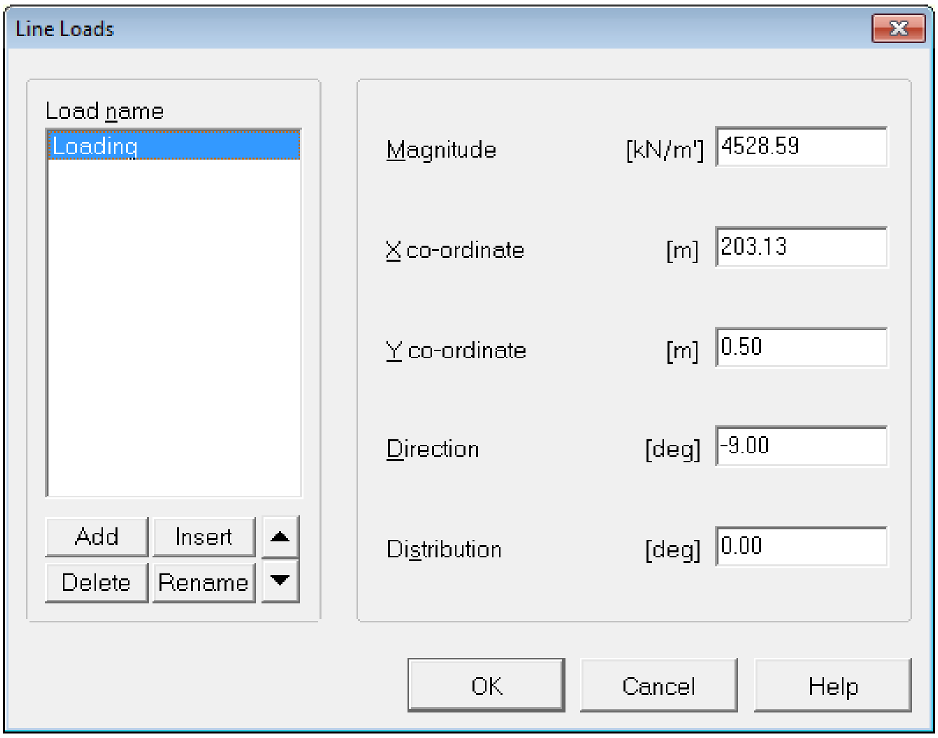

Figuur 1, Line load

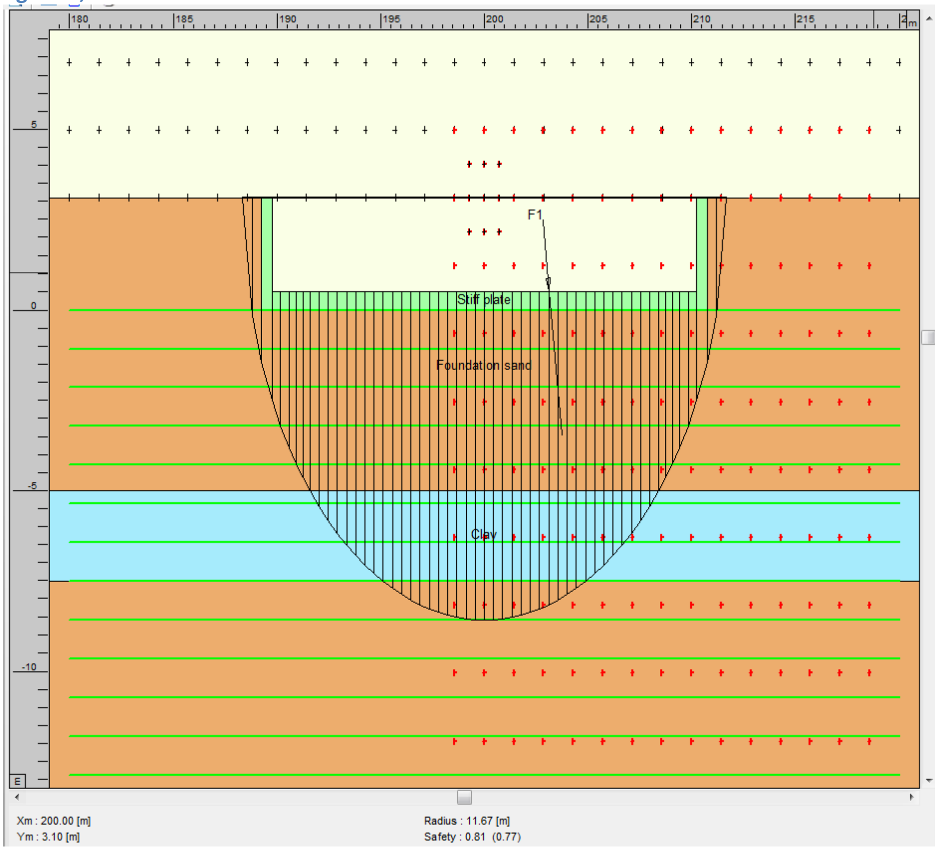

Figure 121, Situation 1

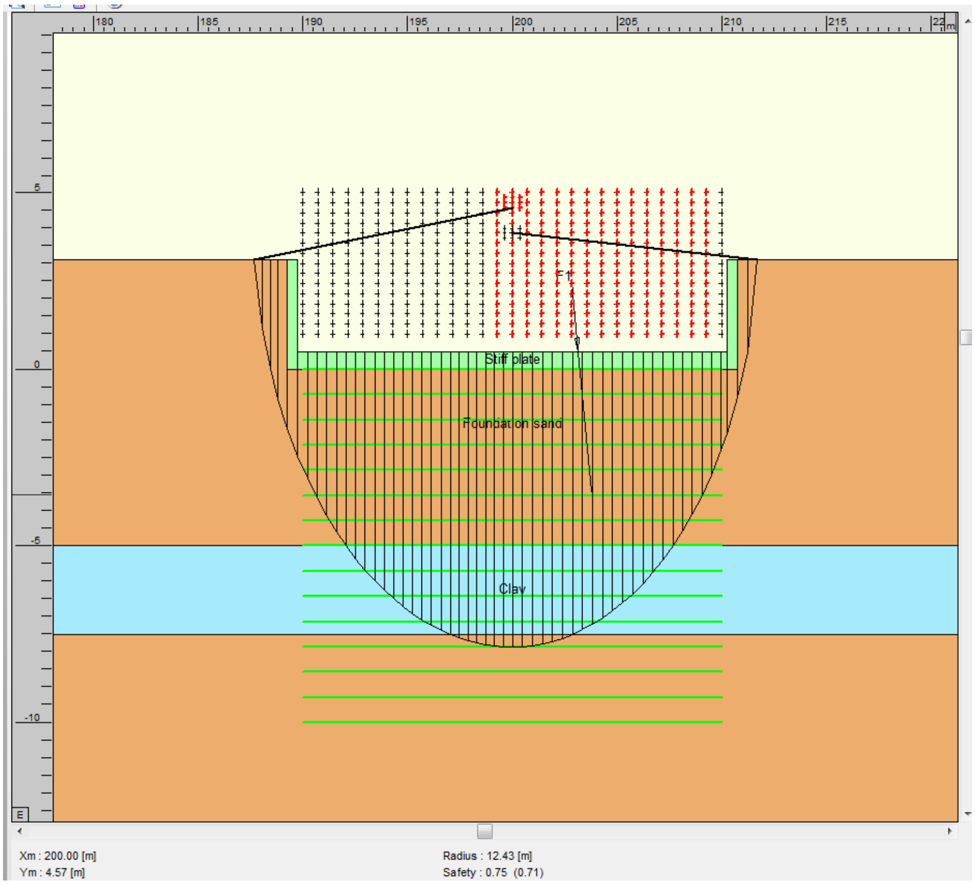

Figure 122, Situation 2

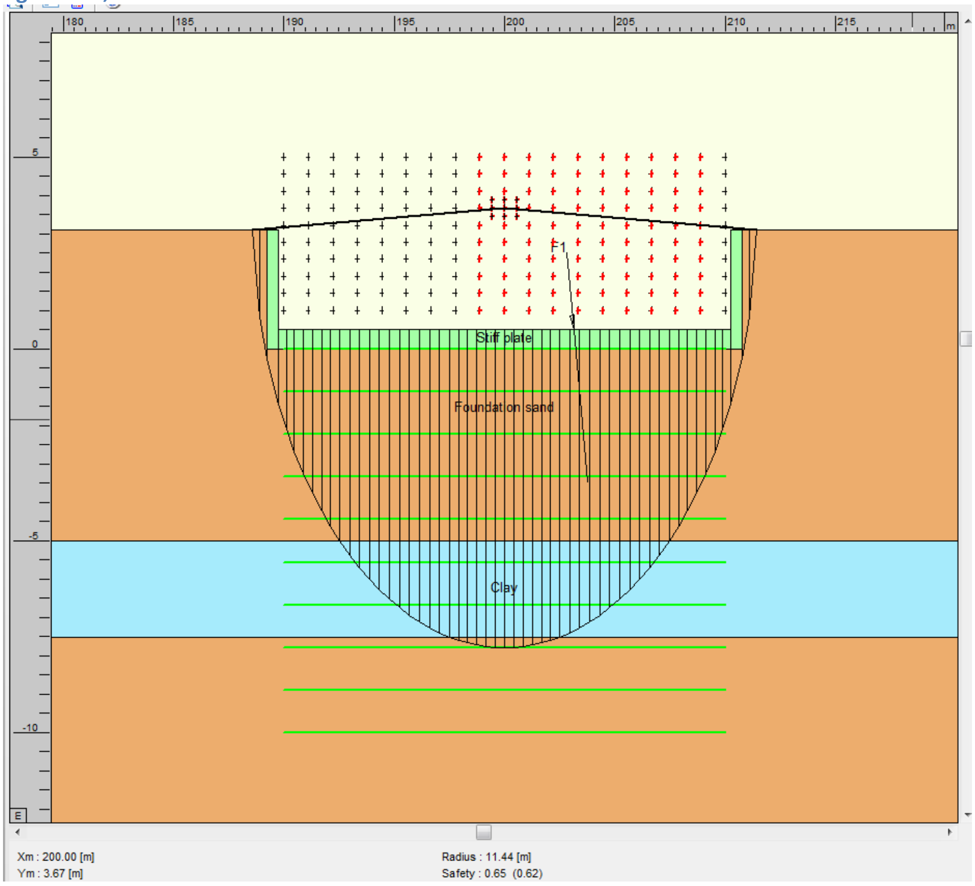

Figure 123, Situation 3

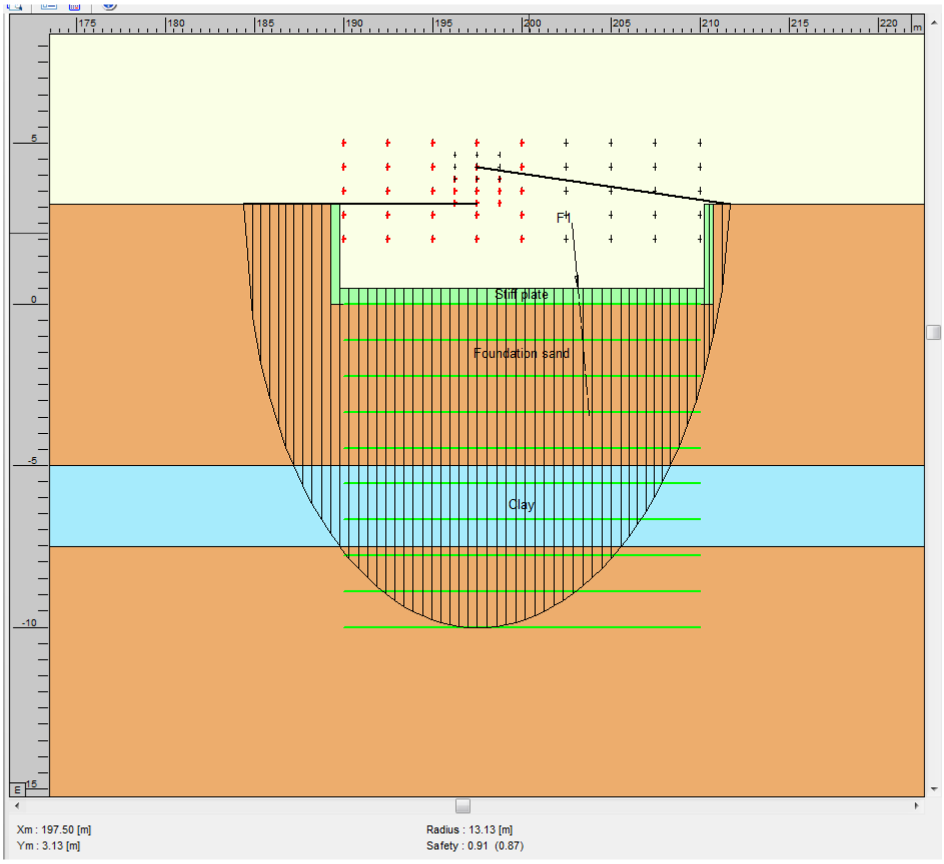

Figure 124, Situation 4

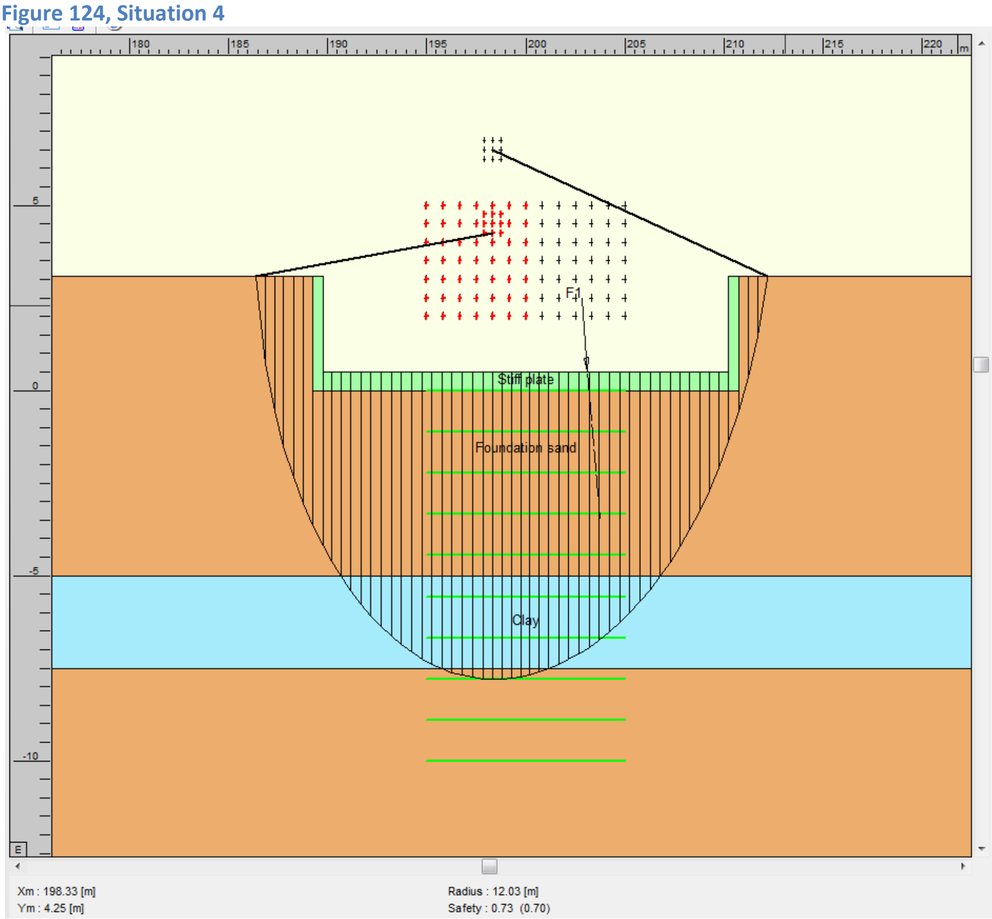

Figure 125, Situation 5

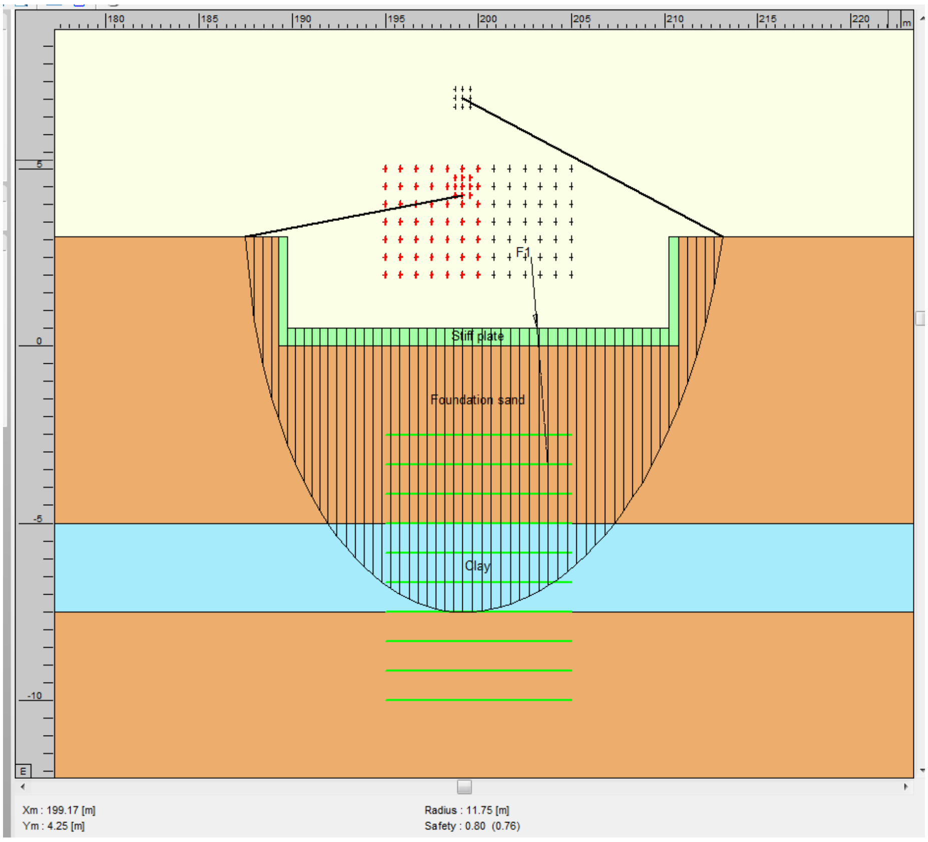

Figure 126, Situation 6

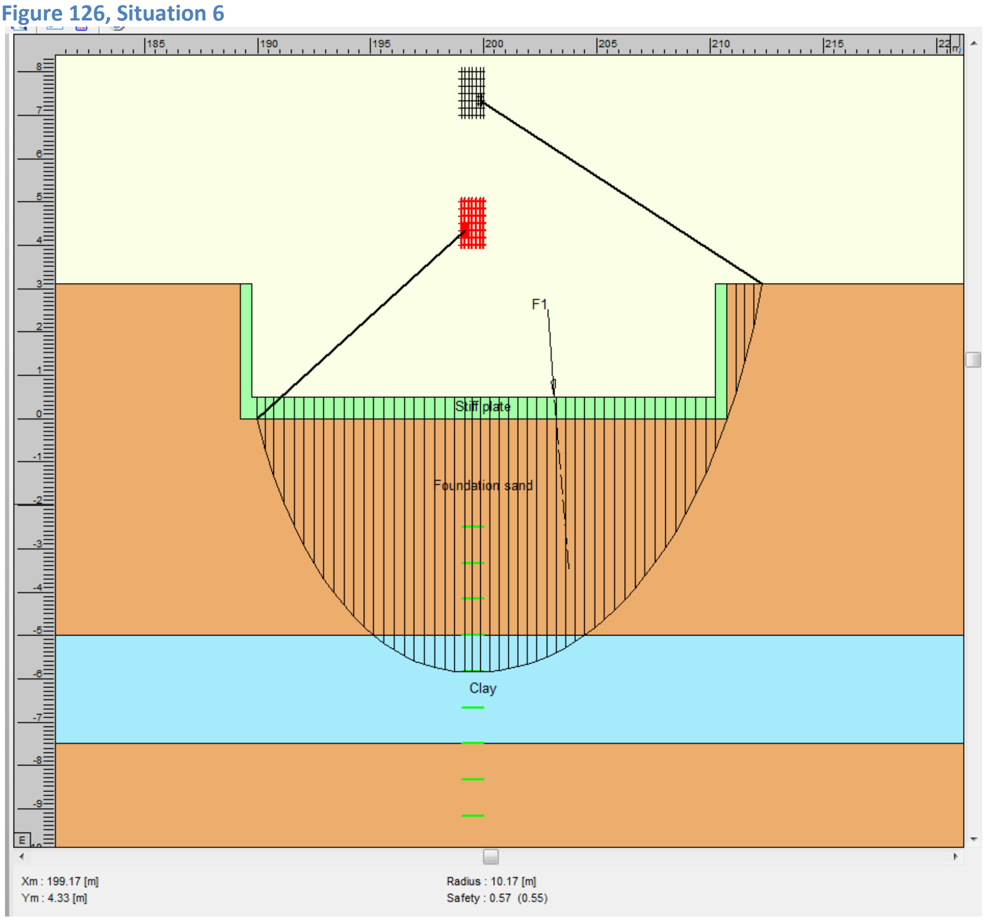

Figure 127, Situation 7

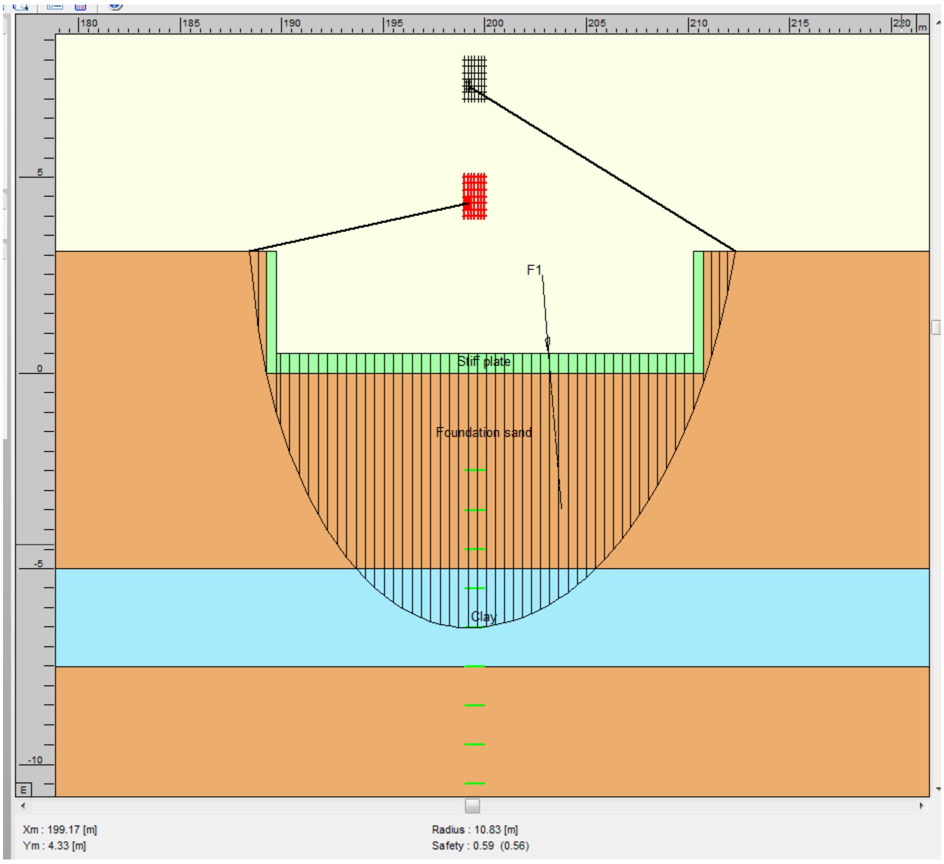

Figure 128, Clay at 5m depth, 2,5m thickness

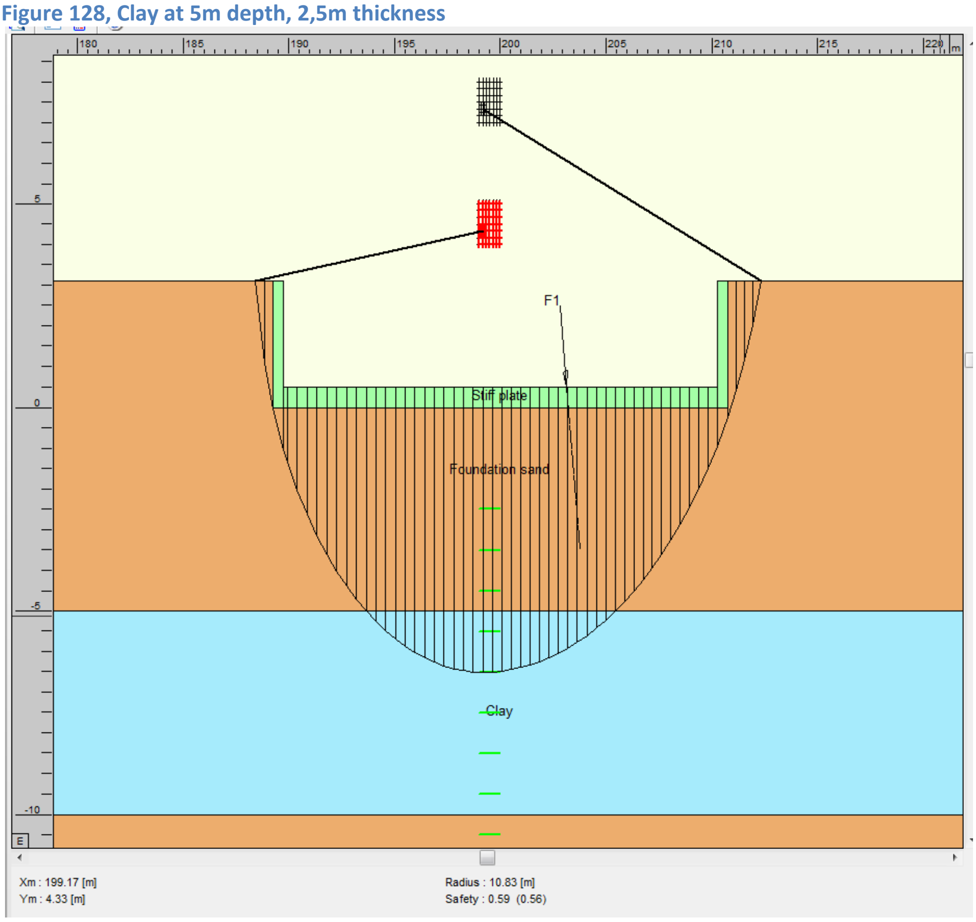

Figure 129, Clay at 5m depth, 5,0m thickness

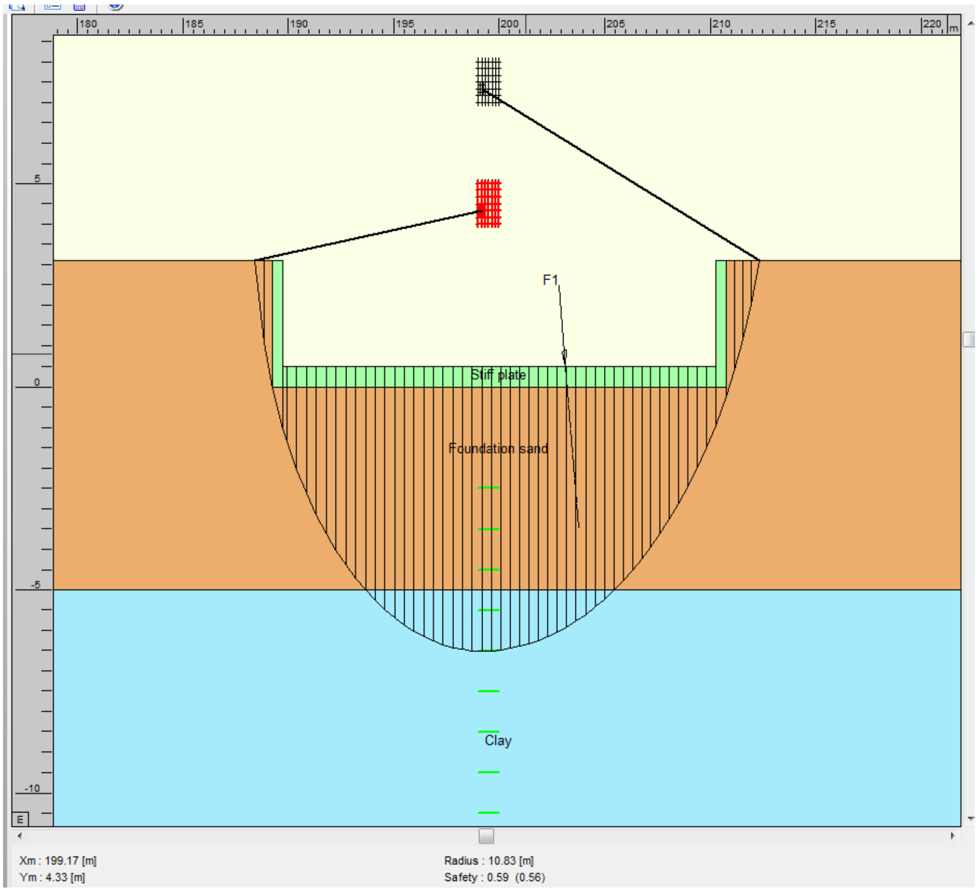

Figure 130, Clay at 5m depth, 7,5m thickness

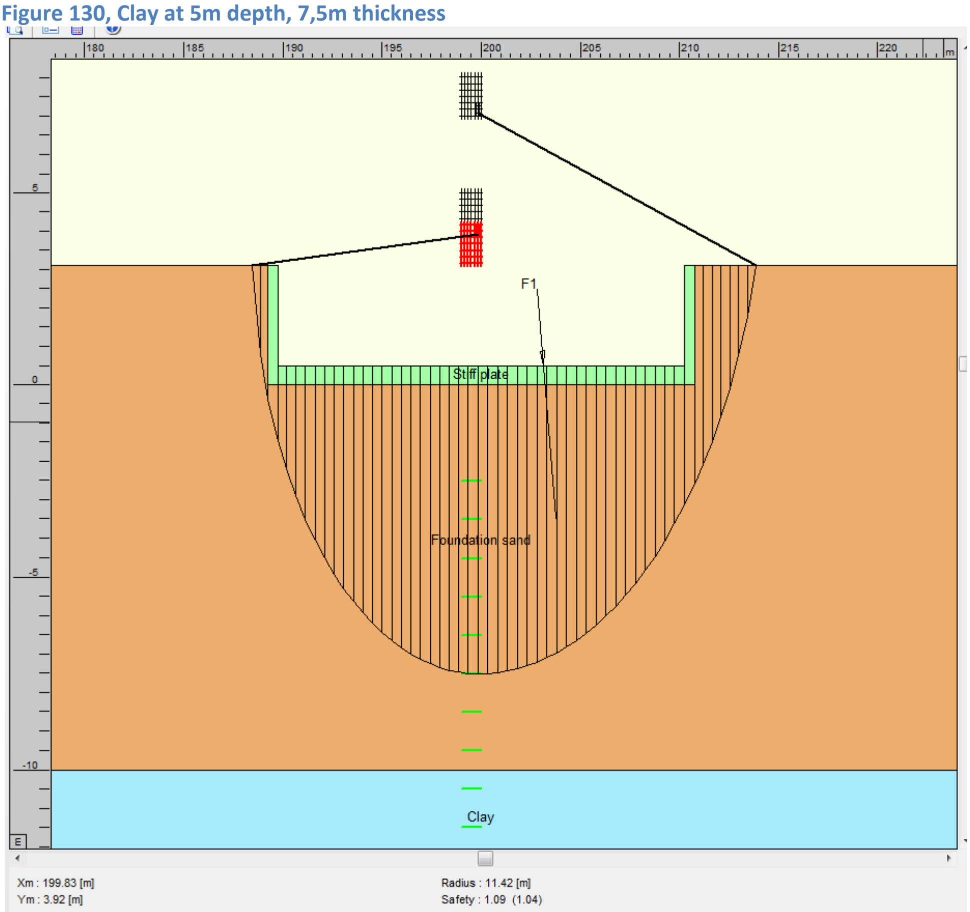

Figure 131, Clay at 10m depth, 2,5m thickness

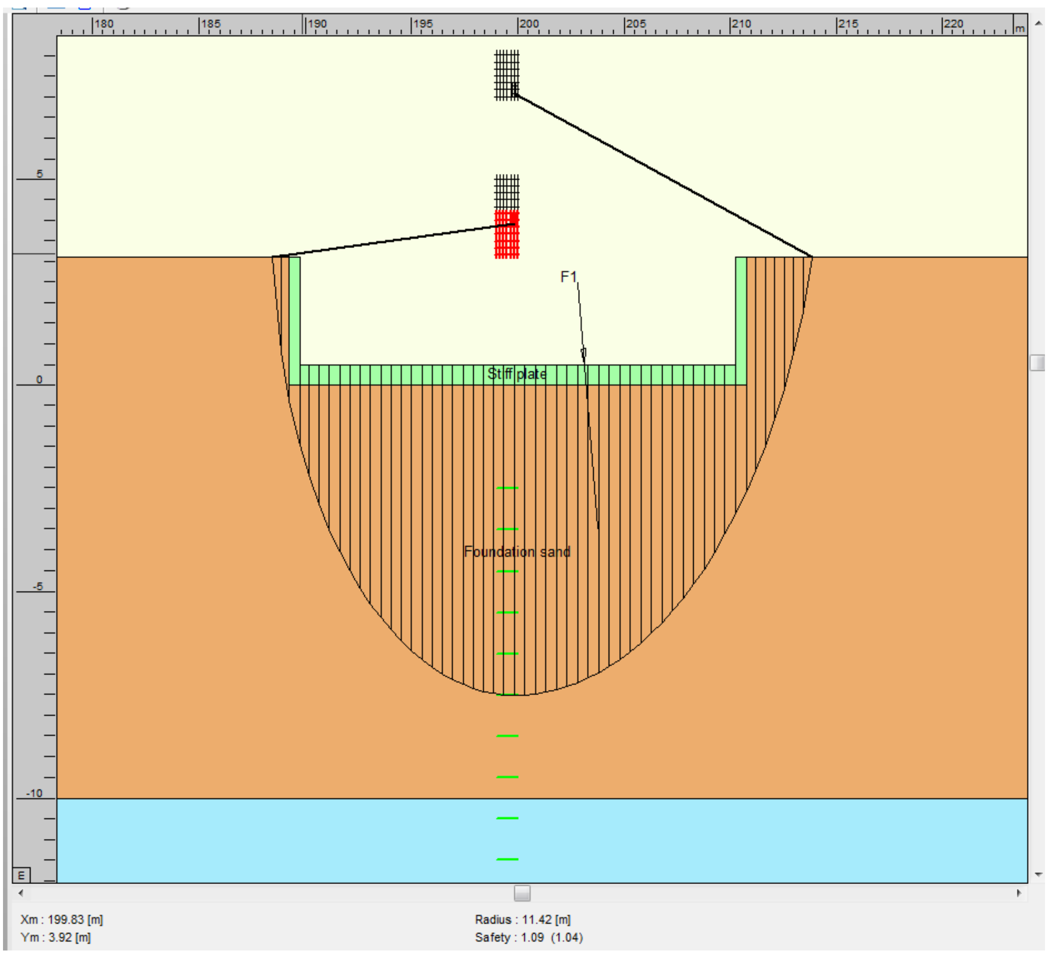

Figure 132, Clay at 10m depth, 5,0m thickness

```
 LEFT GRID                  CENTER POINT GRID AND TANGENT LINES
============                ===================================

 X co-ordinate grid left                      :  180.00 [m]
 X co-ordinate grid right                     :  200.00 [m]
 Number of grid points in X - direction       :    15

 Y co-ordinate grid bottom                    :    3.10 [m]
 Y co-ordinate grid top                       :   20.00 [m]
 Number of grid points in Y - direction       :    10

 RIGHT GRID                 CENTER POINT GRID AND TANGENT LINES
============                ===================================

 X co-ordinate grid left                      :  200.00 [m]
 X co-ordinate grid right                     :  220.00 [m]
 Number of grid points in X - direction       :    15

 Y co-ordinate grid bottom                    :    3.10 [m]
 Y co-ordinate grid top                       :   20.00 [m]
 Number of grid points in Y - direction       :    10

 Y co-ordinate tangent line                   :  -15.00 [m]
 Y co-ordinate tangent line                   :  -13.93 [m]
 Y co-ordinate tangent line                   :  -12.86 [m]
 Y co-ordinate tangent line                   :  -11.79 [m]
Y co-ordinate tangent line                   :  -10.71 [m]
Y co-ordinate tangent line                   :   -9.64 [m]
Y co-ordinate tangent line                   :   -8.57 [m]
Y co-ordinate tangent line                   :   -7.50 [m]
Y co-ordinate tangent line                   :   -6.43 [m]
Y co-ordinate tangent line                   :   -5.36 [m]
Y co-ordinate tangent line                   :   -4.29 [m]
Y co-ordinate tangent line                   :   -3.21 [m]
Y co-ordinate tangent line                   :   -2.14 [m]
Y co-ordinate tangent line                   :   -1.07 [m]
Y co-ordinate tangent line                   :    0.00 [m]

Total number of lift slide planes in the grid : 22500
 Information on the critical plane    : Fmin =      0.805          0.766 model
factor included
 Calculation method used              : Uplift Van - C phi
 ==============================================================================

 X co-ordinate left center point     :       200.00 [m]
 Y co-ordinate left center point     :         3.10 [m]
 Left radius of critical circle      :        11.67 [m]

 X co-ordinate right center point    :       200.00 [m]
 Y co-ordinate right center point    :         3.10 [m]
 Right radius of critical circle     :        11.67 [m]

 Non iterated values
 Force Ia   [kN]           :      1271.74
 Force Ip   [kN]           :       978.44
 Force Fs   [kN]           :         0.00

 Iterated values           :
 Force Ia   [kN]           :      1195.39
 Force Ip   [kN]           :      1195.59
 Force Fs   [kN]           :         0.00

 Active moments
 Driving moment    [kNm]   :    -14496.41
 Resisting moment  [kNm]   :      3345.86
 Passive moments
 Driving moment    [kNm]   :      2338.35
 Resisting moment  [kNm]   :      6436.13
```

```
 LEFT GRID                  CENTER POINT GRID AND TANGENT LINES
============                ===================================

 X co-ordinate grid left                     :  190.00 [m]
 X co-ordinate grid right                    :  200.00 [m]
 Number of grid points in X - direction      :    15

 Y co-ordinate grid bottom                   :    1.00 [m]
 Y co-ordinate grid top                      :    5.00 [m]
 Number of grid points in Y - direction      :    15

 RIGHT GRID                 CENTER POINT GRID AND TANGENT LINES
============                ===================================

 X co-ordinate grid left                     :  200.00 [m]
 X co-ordinate grid right                    :  210.00 [m]
 Number of grid points in X - direction      :    15

 Y co-ordinate grid bottom                   :    1.00 [m]
 Y co-ordinate grid top                      :    5.00 [m]
 Number of grid points in Y - direction      :    15

 Y co-ordinate tangent line                  : -10.00 [m]
 Y co-ordinate tangent line                  :  -9.29 [m]
 Y co-ordinate tangent line                  :  -8.57 [m]
 Y co-ordinate tangent line                  :  -7.86 [m]
 Y co-ordinate tangent line                  :  -7.14 [m]
 Y co-ordinate tangent line                  :  -6.43 [m]
 Y co-ordinate tangent line                  :  -5.71 [m]
 Y co-ordinate tangent line                  :  -5.00 [m]
 Y co-ordinate tangent line                  :  -4.29 [m]
 Y co-ordinate tangent line                  :  -3.57 [m]
 Y co-ordinate tangent line                  :  -2.86 [m]
 Y co-ordinate tangent line                  :  -2.14 [m]
 Y co-ordinate tangent line                  :  -1.43 [m]
 Y co-ordinate tangent line                  :  -0.71 [m]
 Y co-ordinate tangent line                  :   0.00 [m]


 Total number of lift slide planes in the grid : 50625

Information on the critical plane    : Fmin =      0.749         0.713 model factor included
Calculation method used              : Uplift Van - C phi
==============================================================================

X co-ordinate left center point      :       200.00 [m]
Y co-ordinate left center point      :         4.57 [m]
Left radius of critical circle       :        12.43 [m]

X co-ordinate right center point     :       200.00 [m]
Y co-ordinate right center point     :         3.86 [m]
Right radius of critical circle      :        11.71 [m]

Non iterated values
Force Ia   [kN]          :      1185.32
Force Ip   [kN]          :       847.32
Force Fs   [kN]          :         0.00

Iterated values          :
Force Ia   [kN]          :      1096.11
Force Ip   [kN]          :      1094.44
Force Fs   [kN]          :         0.00

Active moments
Driving moment    [kNm]  :    -13624.99
Resisting moment  [kNm]  :      2878.89
Passive moments
Driving moment    [kNm]  :      2367.92
Resisting moment  [kNm]  :      6139.60
```

```
 LEFT GRID                 CENTER POINT GRID AND TANGENT LINES
============               ==================================

 X co-ordinate grid left                   :  190.00 [m]
 X co-ordinate grid right                  :  200.00 [m]
 Number of grid points in X - direction    :    10

 Y co-ordinate grid bottom                 :    1.00 [m]
 Y co-ordinate grid top                    :    5.00 [m]
 Number of grid points in Y - direction    :    10

 RIGHT GRID                CENTER POINT GRID AND TANGENT LINES
============               ==================================

 X co-ordinate grid left                   :  200.00 [m]
 X co-ordinate grid right                  :  210.00 [m]
 Number of grid points in X - direction    :    10

 Y co-ordinate grid bottom                 :    1.00 [m]
 Y co-ordinate grid top                    :    5.00 [m]
 Number of grid points in Y - direction    :    10

 Y co-ordinate tangent line                :  -10.00 [m]
 Y co-ordinate tangent line                :   -8.89 [m]
 Y co-ordinate tangent line                :   -7.78 [m]
 Y co-ordinate tangent line                :   -6.67 [m]
 Y co-ordinate tangent line                :   -5.56 [m]
 Y co-ordinate tangent line                :   -4.44 [m]
 Y co-ordinate tangent line                :   -3.33 [m]
 Y co-ordinate tangent line                :   -2.22 [m]
 Y co-ordinate tangent line                :   -1.11 [m]
 Y co-ordinate tangent line                :    0.00 [m]

 Total number of lift slide planes in the grid : 10000

Information on the critical plane    : Fmin =      0.653        0.622 model factor included
Calculation method used              : Uplift Van - C phi
==============================================================================

X co-ordinate left center point      :        200.00 [m]
Y co-ordinate left center point      :          3.67 [m]
Left radius of critical circle       :         11.44 [m]

X co-ordinate right center point     :        200.00 [m]
Y co-ordinate right center point     :          3.67 [m]
Right radius of critical circle      :         11.44 [m]

Non iterated values
Force Ia   [kN]          :      1238.69
Force Ip   [kN]          :       747.78
Force Fs   [kN]          :         0.00

Iterated values          :
Force Ia   [kN]          :      1104.29
Force Ip   [kN]          :      1104.45
Force Fs   [kN]          :         0.00

Active moments
Driving moment    [kNm]  :    -13597.59
Resisting moment  [kNm]  :      2615.88
Passive moments
Driving moment    [kNm]  :      1840.97
Resisting moment  [kNm]  :      5060.83
```

```
 LEFT GRID                  CENTER POINT GRID AND TANGENT LINES
============                ===================================

 X co-ordinate grid left                         :  190.00 [m]
 X co-ordinate grid right                        :  200.00 [m]
 Number of grid points in X - direction          :     5

 Y co-ordinate grid bottom                       :    2.00 [m]
 Y co-ordinate grid top                          :    5.00 [m]
 Number of grid points in Y - direction          :     5

 RIGHT GRID                 CENTER POINT GRID AND TANGENT LINES
============                ===================================

 X co-ordinate grid left                         :  200.00 [m]
 X co-ordinate grid right                        :  210.00 [m]
 Number of grid points in X - direction          :     5

 Y co-ordinate grid bottom                       :    2.00 [m]
 Y co-ordinate grid top                          :    5.00 [m]
 Number of grid points in Y - direction          :     5

 Y co-ordinate tangent line                      :  -10.00 [m]
 Y co-ordinate tangent line                      :   -8.89 [m]
 Y co-ordinate tangent line                      :   -7.78 [m]
 Y co-ordinate tangent line                      :   -6.67 [m]
 Y co-ordinate tangent line                      :   -5.56 [m]
 Y co-ordinate tangent line                      :   -4.44 [m]
 Y co-ordinate tangent line                      :   -3.33 [m]
 Y co-ordinate tangent line                      :   -2.22 [m]
 Y co-ordinate tangent line                      :   -1.11 [m]
 Y co-ordinate tangent line                      :    0.00 [m]


 Total number of lift slide planes in the grid :   625


Information on the critical plane    : Fmin =      0.912         0.869 model factor included
Calculation method used              : Uplift Van - C phi
============================================================================

X co-ordinate left center point     :       197.50 [m]
Y co-ordinate left center point     :         3.13 [m]
Left radius of critical circle      :        13.13 [m]

X co-ordinate right center point    :       197.50 [m]
Y co-ordinate right center point    :         4.25 [m]
Right radius of critical circle     :        14.25 [m]

Non iterated values
Force Ia   [kN]           :      1901.44
Force Ip   [kN]           :      1713.27
Force Fs   [kN]           :         0.00

Iterated values           :
Force Ia   [kN]           :      1859.12
Force Ip   [kN]           :      1857.06
Force Fs   [kN]           :         0.00

Active moments
Driving moment    [kNm]   :    -26494.32
Resisting moment [kNm]    :      5943.94
Passive moments
Driving moment    [kNm]   :      4843.41


Resisting moment [kNm]    :     11899.93
```

```
 LEFT GRID                  CENTER POINT GRID AND TANGENT LINES
============                ===================================

 X co-ordinate grid left                    :  195.00 [m]
 X co-ordinate grid right                   :  200.00 [m]
 Number of grid points in X - direction     :      7

 Y co-ordinate grid bottom                  :    2.00 [m]
 Y co-ordinate grid top                     :    5.00 [m]
 Number of grid points in Y - direction     :      7

 RIGHT GRID                 CENTER POINT GRID AND TANGENT LINES
============                ===================================

 X co-ordinate grid left                    :  200.00 [m]
 X co-ordinate grid right                   :  205.00 [m]
 Number of grid points in X - direction     :      7

 Y co-ordinate grid bottom                  :    2.00 [m]
 Y co-ordinate grid top                     :    5.00 [m]
 Number of grid points in Y - direction     :      7

 Y co-ordinate tangent line                 :  -10.00 [m]
 Y co-ordinate tangent line                 :   -8.89 [m]
 Y co-ordinate tangent line                 :   -7.78 [m]
 Y co-ordinate tangent line                 :   -6.67 [m]
 Y co-ordinate tangent line                 :   -5.56 [m]
 Y co-ordinate tangent line                 :   -4.44 [m]
 Y co-ordinate tangent line                 :   -3.33 [m]
 Y co-ordinate tangent line                 :   -2.22 [m]
 Y co-ordinate tangent line                 :   -1.11 [m]
 Y co-ordinate tangent line                 :    0.00 [m]


 Total number of lift slide planes in the grid :  2401


Information on the critical plane   : Fmin =      0.733         0.698 model factor included
Calculation method used             : Uplift Van - C phi
==============================================================================

X co-ordinate left center point     :       198.33 [m]
Y co-ordinate left center point     :         4.25 [m]
Left radius of critical circle      :        12.03 [m]

X co-ordinate right center point    :       198.33 [m]
Y co-ordinate right center point    :         6.50 [m]
Right radius of critical circle     :        14.28 [m]

Non iterated values
Force Ia  [kN]           :      1362.67
Force Ip  [kN]           :       954.84
Force Fs  [kN]           :         0.00

Iterated values          :


Force Ia  [kN]           :      1258.41
Force Ip  [kN]           :      1258.64
Force Fs  [kN]           :         0.00

Active moments
Driving moment    [kNm]  :    -19813.43
Resisting moment  [kNm]  :      3895.36
Passive moments
Driving moment    [kNm]  :      2640.00
Resisting moment  [kNm]  :      6610.75
```

```
 LEFT GRID                 CENTER POINT GRID AND TANGENT LINES
============               ===================================

 X co-ordinate grid left                      :  195.00 [m]
 X co-ordinate grid right                     :  200.00 [m]
 Number of grid points in X - direction       :     7

 Y co-ordinate grid bottom                    :    2.00 [m]
 Y co-ordinate grid top                       :    5.00 [m]
 Number of grid points in Y - direction       :     7

 RIGHT GRID                CENTER POINT GRID AND TANGENT LINES
============               ===================================

 X co-ordinate grid left                      :  200.00 [m]
 X co-ordinate grid right                     :  205.00 [m]
 Number of grid points in X - direction       :     7

 Y co-ordinate grid bottom                    :    2.00 [m]
 Y co-ordinate grid top                       :    5.00 [m]
 Number of grid points in Y - direction       :     7

 Y co-ordinate tangent line                   :  -10.00 [m]
 Y co-ordinate tangent line                   :   -9.17 [m]
 Y co-ordinate tangent line                   :   -8.33 [m]
 Y co-ordinate tangent line                   :   -7.50 [m]
 Y co-ordinate tangent line                   :   -6.67 [m]
 Y co-ordinate tangent line                   :   -5.83 [m]
 Y co-ordinate tangent line                   :   -5.00 [m]
 Y co-ordinate tangent line                   :   -4.17 [m]
 Y co-ordinate tangent line                   :   -3.33 [m]
 Y co-ordinate tangent line                   :   -2.50 [m]


 Total number of lift slide planes in the grid :  2401

Information on the critical plane   : Fmin =      0.798          0.760 model factor included
Calculation method used             : Uplift Van - C phi
=============================================================================

X co-ordinate left center point     :       199.17 [m]
Y co-ordinate left center point     :         4.25 [m]
Left radius of critical circle      :        11.75 [m]

X co-ordinate right center point    :       199.17 [m]
Y co-ordinate right center point    :         7.00 [m]
Right radius of critical circle     :        14.50 [m]

Non iterated values
Force Ia  [kN]            :      1012.02
Force Ip  [kN]            :       776.77
Force Fs  [kN]            :         0.00

Iterated values           :
Force Ia  [kN]            :       944.93
Force Ip  [kN]            :       944.15
Force Fs  [kN]            :         0.00

Active moments
Driving moment    [kNm]   :    -15939.70
Resisting moment [kNm]    :      3800.78
Passive moments
Driving moment    [kNm]   :      2108.01


Resisting moment [kNm]    :      5166.69
```

```
 LEFT GRID                 CENTER POINT GRID AND TANGENT LINES
============               ==================================

 X co-ordinate grid left                     :  199.00 [m]
 X co-ordinate grid right                    :  200.00 [m]
 Number of grid points in X - direction      :     7

 Y co-ordinate grid bottom                   :    4.00 [m]
 Y co-ordinate grid top                      :    5.00 [m]
 Number of grid points in Y - direction      :     7

 RIGHT GRID                CENTER POINT GRID AND TANGENT LINES
============               ==================================

 X co-ordinate grid left                     :  199.00 [m]
 X co-ordinate grid right                    :  200.00 [m]
 Number of grid points in X - direction      :     7

 Y co-ordinate grid bottom                   :    7.00 [m]
 Y co-ordinate grid top                      :    8.00 [m]
 Number of grid points in Y - direction      :     7

 Y co-ordinate tangent line                  :  -10.00 [m]
 Y co-ordinate tangent line                  :   -9.17 [m]
 Y co-ordinate tangent line                  :   -8.33 [m]
 Y co-ordinate tangent line                  :   -7.50 [m]
 Y co-ordinate tangent line                  :   -6.67 [m]
 Y co-ordinate tangent line                  :   -5.83 [m]
 Y co-ordinate tangent line                  :   -5.00 [m]
 Y co-ordinate tangent line                  :   -4.17 [m]
 Y co-ordinate tangent line                  :   -3.33 [m]
 Y co-ordinate tangent line                  :   -2.50 [m]


 Total number of lift slide planes in the grid :  2401


Information on the critical plane   : Fmin =      0.575         0.547 model factor included
Calculation method used             : Uplift Van - C phi
==========================================================================

X co-ordinate left center point     :       199.17 [m]
Y co-ordinate left center point     :         4.33 [m]
Left radius of critical circle      :        10.17 [m]

X co-ordinate right center point    :       199.83 [m]
Y co-ordinate right center point    :         7.33 [m]
Right radius of critical circle     :        13.17 [m]

Non iterated values
Force Ia  [kN]          :       802.30
Force Ip  [kN]          :       382.72
Force Fs  [kN]          :        15.50

Iterated values         :
Force Ia  [kN]          :       680.65
Force Ip  [kN]          :       653.37
Force Fs  [kN]          :        26.96

Active moments
Driving moment    [kNm]   :    -11284.45
Resisting moment [kNm]    :      2161.64
Passive moments
Driving moment    [kNm]   :       737.77
Resisting moment [kNm]    :      2602.10
```

26. Validation output for D-Geo Stability

Results first model with eccentricity of 3,13m

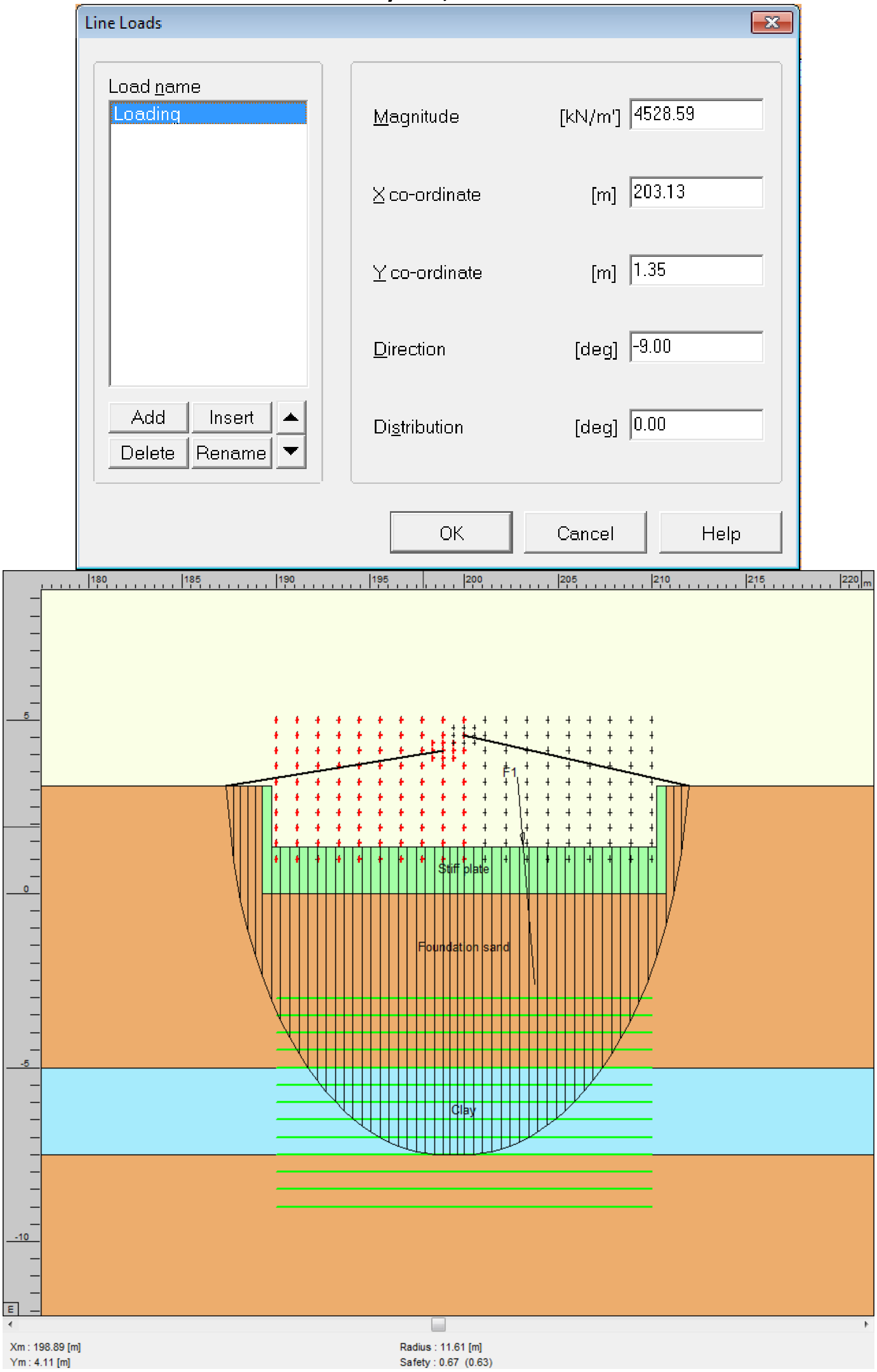

Results for second model with eccentricity of 8,75m

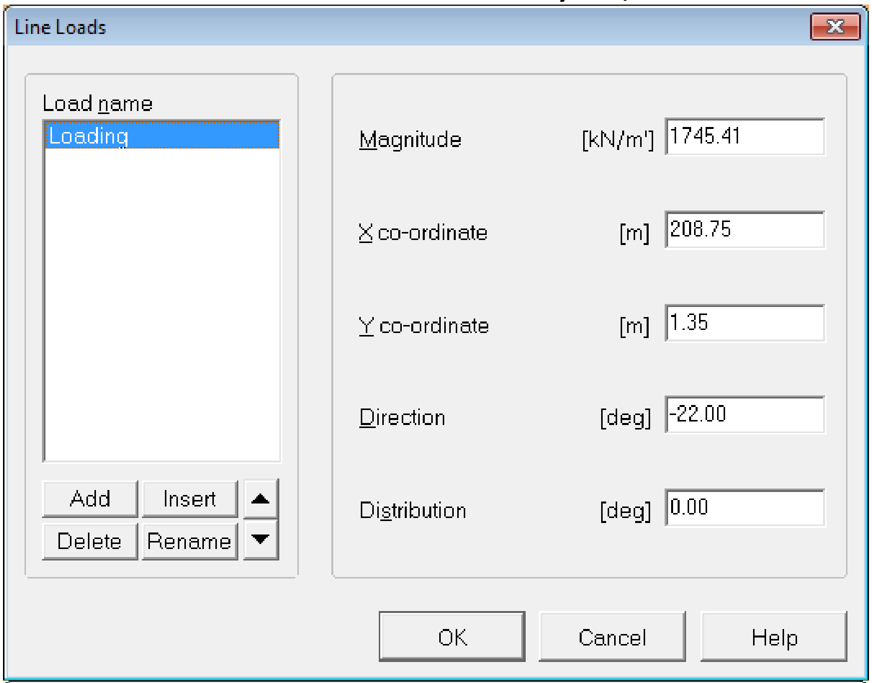

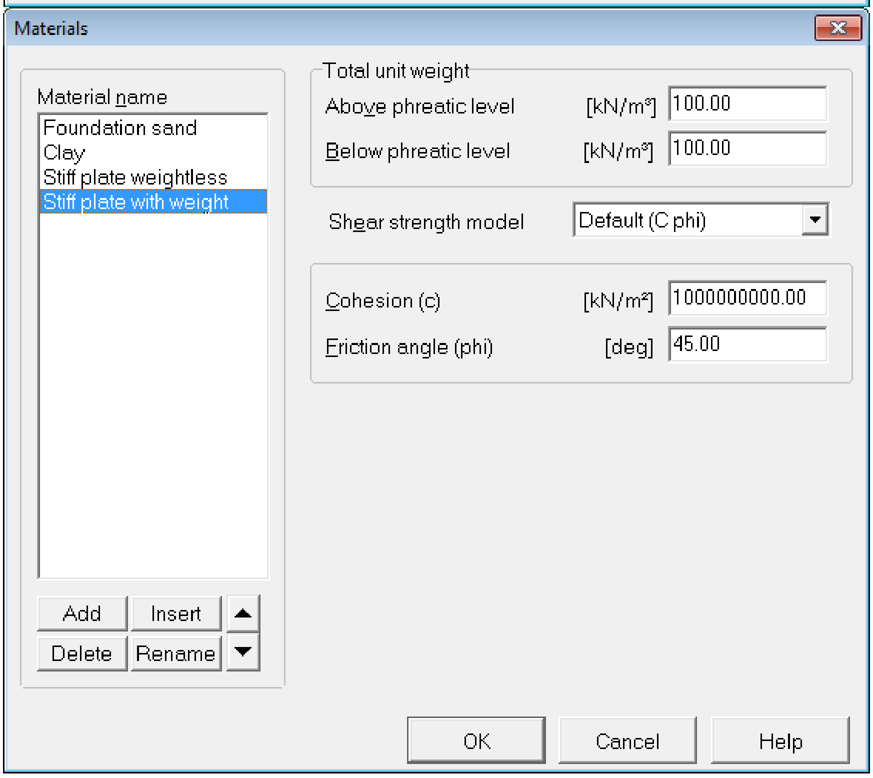

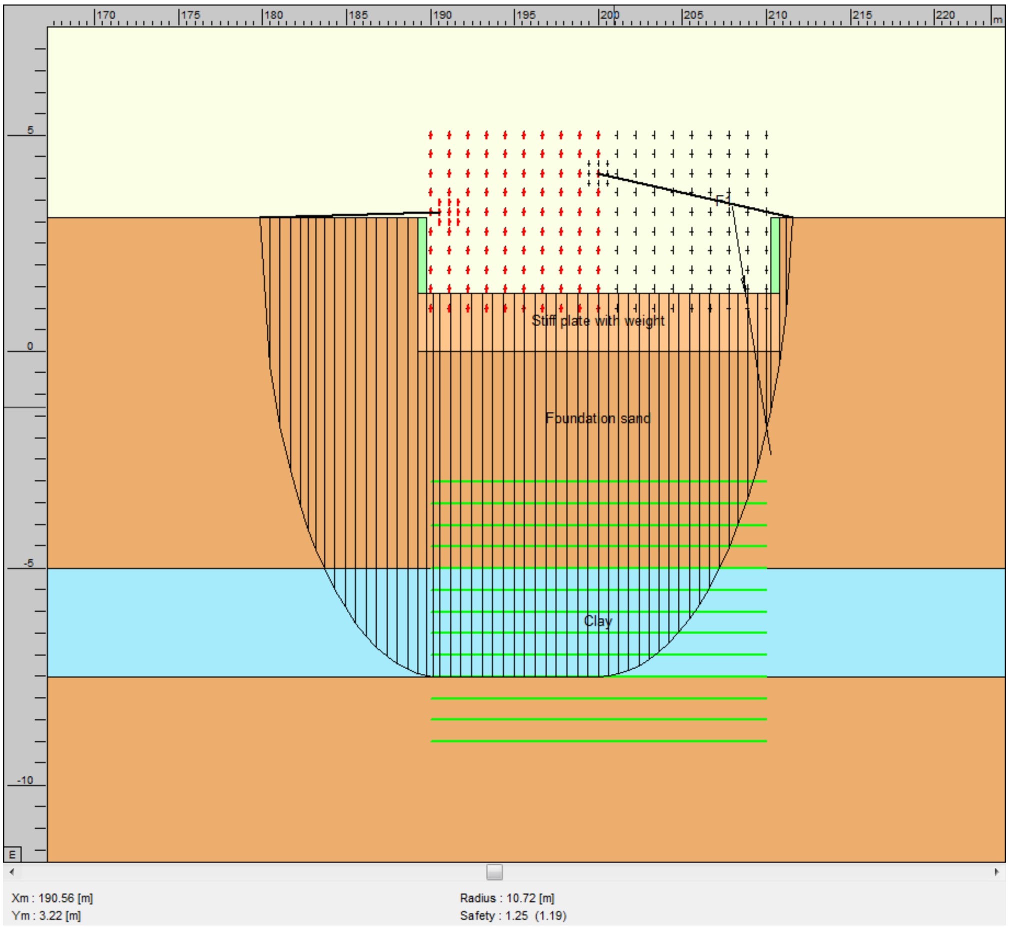
170
175
180
185
190
195
200
205
210
215
220
m
5
0
-5
-10
Stiff plate with weight
Foundation sand
Clay
Xm : 190.56 [m]
Ym : 3.22 [m]
Radius : 10.72 [m]
Safety : 1.25 (1.19)

27. Plaxis 3D model properties

The model values are entered in the model as can be seen in the figures below.

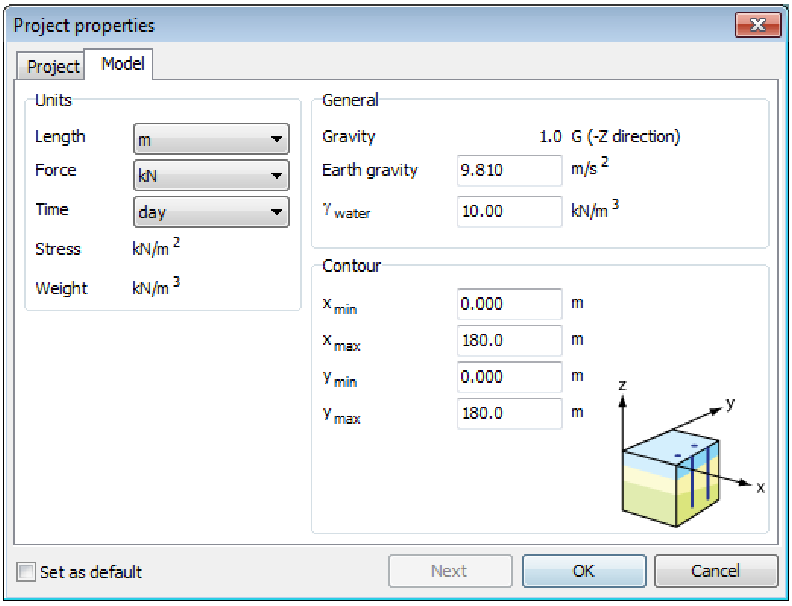

Figure 133, Model dimensions for x and y direction

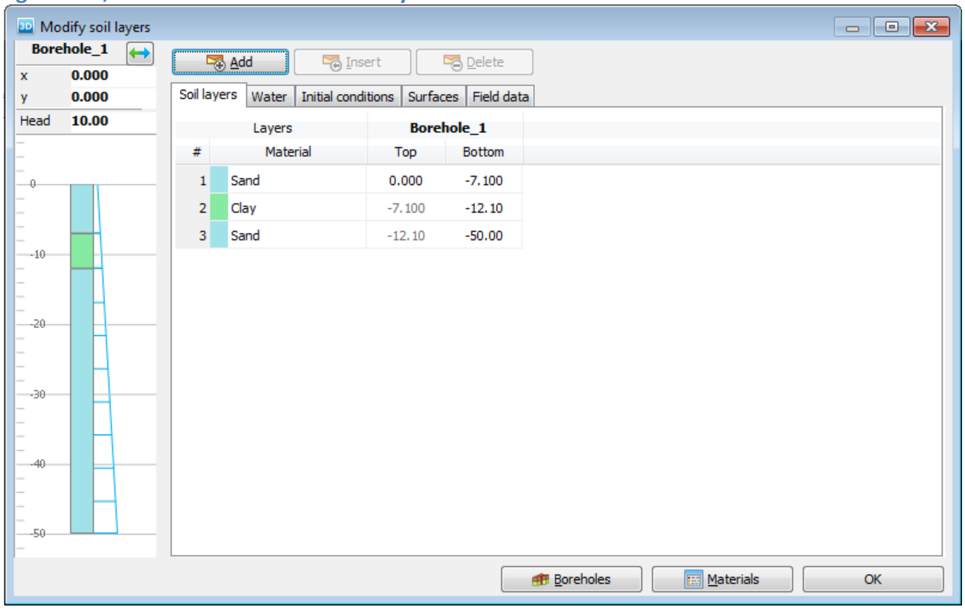

Figure 134, Model dimensions for z direction including the definition of a clay layer and phreatic level

Material properties sand and clay

Material set		
Identification		Sand
Material model		Hardening soil
Drainage type		Drained
Colour		RGB 161, 226, 232
Comments		
General properties		
γ_{unsat}	kN/m³	18.00
γ_{sat}	kN/m³	20.00
Advanced		
Void ratio		
Dilatancy cut-off		☐
e_{init}		0.5000
e_{min}		0.000
e_{max}		999.0
Damping		
Rayleigh α		0.000
Rayleigh β		0.000

Figure 135, Material properties for sand (1)

Stiffness		
E_{50}^{ref}	kN/m²	43.00E3
E_{oed}^{ref}	kN/m²	43.00E3
E_{ur}^{ref}	kN/m²	129.0E3
power (m)		0.5000
Alternatives		
Use alternatives		☐
C_c		8.023E-3
C_s		2.407E-3
e_{init}		0.5000
Strength		
c'_{ref}	kN/m²	0.1000
φ' (phi)	°	32.50
ψ (psi)	°	2.500
Advanced		
Set to default values		☑
Stiffness		
ν'_{ur}		0.2000
p_{ref}	kN/m²	100.0
K_0^{nc}		0.4627
Strength		
c'_{inc}	kN/m²/m	0.000
z_{ref}	m	0.000
R_f		0.9000
Tension cut-off		☑
Tensile strength	kN/m²	0.000

Figure 136, Material properties for sand (2)

Material set		
Identification		Clay
Material model		Hardening soil
Drainage type		Drained
Colour		RGB 134, 234, 162
Comments		
General properties		
γ_{unsat}	kN/m³	17.00
γ_{sat}	kN/m³	17.00
Advanced		
Void ratio		
Dilatancy cut-off		☐
e_{init}		0.5000
e_{min}		0.000
e_{max}		999.0
Damping		
Rayleigh α		0.000
Rayleigh β		0.000

Figure 137, Material properties for clay (1)

Stiffness		
E_{50}^{ref}	kN/m²	10.00E3
E_{oed}^{ref}	kN/m²	10.00E3
E_{ur}^{ref}	kN/m²	30.00E3
power (m)		0.8000
Alternatives		
Use alternatives		☐
C_c		0.03450
C_s		0.01035
e_{init}		0.5000
Strength		
c'_{ref}	kN/m²	10.00
φ' (phi)	°	17.50
ψ (psi)	°	0.000
Advanced		
Set to default values		☑
Stiffness		
ν'_{ur}		0.2000
p_{ref}	kN/m²	100.0
K_0^{nc}		0.6993
Strength		
c'_{inc}	kN/m²/m	0.000
z_{ref}	m	0.000
R_f		0.9000
Tension cut-off		☑
Tensile strength	kN/m²	0.000

Figure 138, Material properties for clay (2)

Declaration of soil parameters in model

Since the declaration of the soil parameters is important for the behaviour of the model and influences the calculation outcomes the chosen values for the soil parameters are explained. When using the Plaxis 3D software it is chosen to only use two different types of soil. Since the goal of the calculations is to investigate the influence of weaker soil layers in a sand stratum it is chosen to model a relative strong soil material, sand, and a relative weak soil material, clay. By evaluating only two types of soil the complexity and time consumption of creating the models is reduced even though the possibility to study the effect of weak soil layers is maintained.
For both the sand and clay soil material the Hardening Soil model is selected. The hardening Soil model is an advanced model for the simulation of soil behaviour. This model has some advantages over the Mohr-Coulomb model, which is recommended to use for a first analysis. For example the Hardening Soil model describes the soil stiffness much more accurately by using three different input stiffnesses: E_{50}, E_{ur} and E_{oed}. In contrast to the Mohr-Coulomb model the Hardening Soil model also accounts for stress-dependency of stiffness moduli. This means that all stiffnesses increase with pressure.[30]
For the general properties and the strength parameters according to the Mohr-Coulomb model for both the sand and clay soil the representative values for the lower bound soil parameters are taken as described in table 1 from the NEN 6740[31]. For the Sand material parameter c'_{ref} a value of 0,1kN/m3 is taken. This is done to eliminate the possible numerical errors that could occur if the cohesion is set to 0,0. The dilatancy angle ψ is defined as $\varphi - 30° \text{ (for } \varphi > 30°)$. This gives the following values for the sand and clay material:

	Sand	Clay
$\gamma_{unsat}\ [kN/m^3]$	18	17
$\gamma_{sat}\ [kN/m^3]$	20	17
$c'_{ref}\ [kN/m^2]$	0,1	10
φ' [°]	32,5	17,5
ψ [°]	2,5	0

Table 38, General and strength properties sand and clay

Besides these general and strength properties the Hardening Soil model also requires the stiffness parameters $E_{50}{}^{ref}$, $E_{oed}{}^{ref}$, $E_{ur}{}^{ref}$ and the stress dependent stiffness power m. These values are accepted standard values for both sand and soil materials. As average values the default settings for the stiffness parameters are suggested as $E_{oed} \approx E_{50}$ and $E_{ur} \approx 3 \cdot E_{50}$.

	Sand	Clay
$E_{50}{}^{ref}\ [kN/m^2]$	43.000	10.000
$E_{oed}{}^{ref}\ [kN/m^2]$	43.000	10.000
$E_{ur}{}^{ref}\ [kN/m^2]$	129.000	30.000
Power (m)	0,5	0,9

Table 39, Stiffness properties for Hardening Soil model

All the parameters described in this paragraph are set as input for the Plaxis 3D model as can be viewed in the soil material figures presented before.

[30] Plaxis-GiD Material Models Manual – Version 1
[31] “Representatieve waarden voor grondparameters in de Geotechniek”, Geotechniek, April (2008): 24-29

Phreatic level

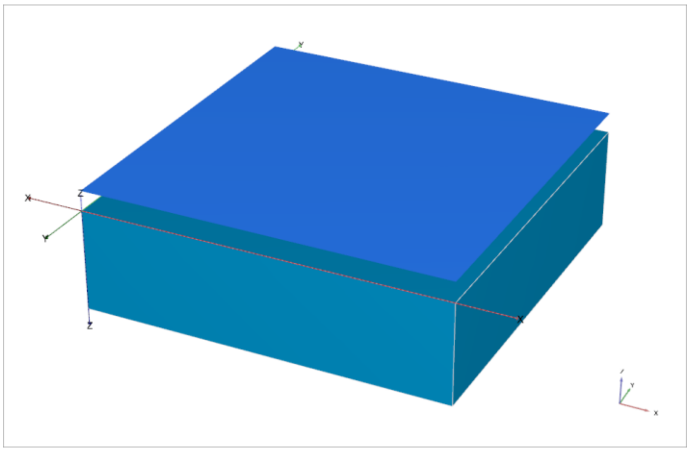

Figure 139, Soil stratum and phreatic level modelled in Plaxis 3D

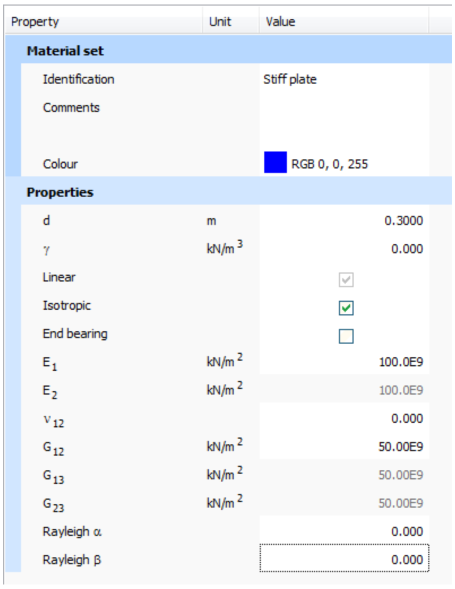

Property	Unit	Value
Material set		
Identification		Stiff plate
Comments		
Colour		RGB 0, 0, 255
Properties		
d	m	0.3000
γ	kN/m³	0.000
Linear		☑
Isotropic		☑
End bearing		☐
E_1	kN/m²	100.0E9
E_2	kN/m²	100.0E9
ν_{12}		0.000
G_{12}	kN/m²	50.00E9
G_{13}	kN/m²	50.00E9
G_{23}	kN/m²	50.00E9
Rayleigh α		0.000
Rayleigh β		0.000

Figure 140, Properties for stiff plate

Input of the load in Plaxis 3D

Converting bending moment to vertical force

The governing bending moment action on the foundation is $M_{ED} = 239.640kNm$ as has been calculated in the first part of this study. Since it is not possible to model bending moments in the program Plaxis 3D the bending moment is converted in a vertical force. This is done in the same way as it was done for the calculation of the D-Geo Stability forces. Therefore only the results of the calculations made in this previous chapter are presented. The magnitude of the vertical force is $76.470kN$ with a calculated eccentricity of 3,13m. This vertical force and it's eccentricity are input for the Plaxis 3D model.

Horizontal force component

Besides the self weight and the bending moment also a horizontal force is acting on the foundation. The magnitude of this horizontal force is $H_D = 10.890kN$. In Plaxis 3D it is possible to model a single point load with both a horizontal and vertical component. The program automatically calculates the resulting force and the angle in which it is acting. The input of the force components in the model and the result of the force modelling are visible in following figures.

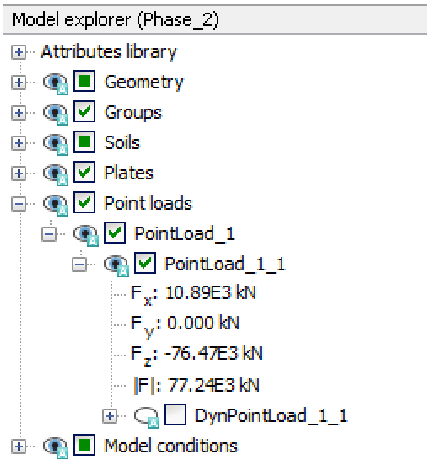

Figure 141, Forces as entered in Plaxis 3D

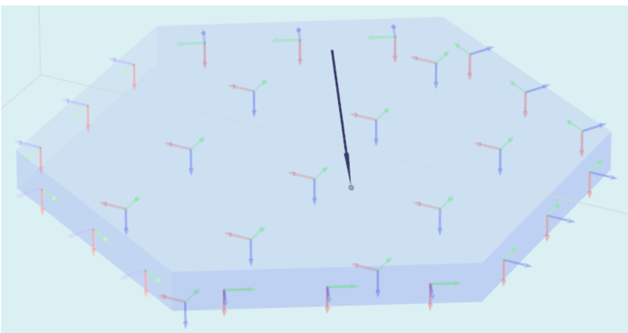

Figure 142, 3D view of applied point load on foundation plate

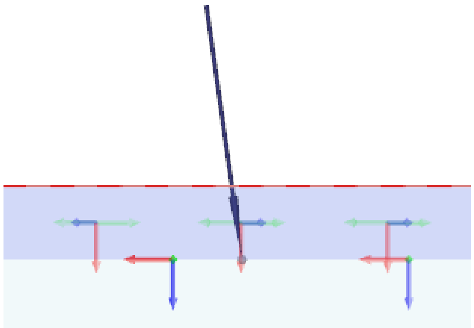

Figure 143, Side view of inclined resulting force

Determine the safety factor using calculation phase Load_10

The input of the Load_10 loads is visible in the figure below.

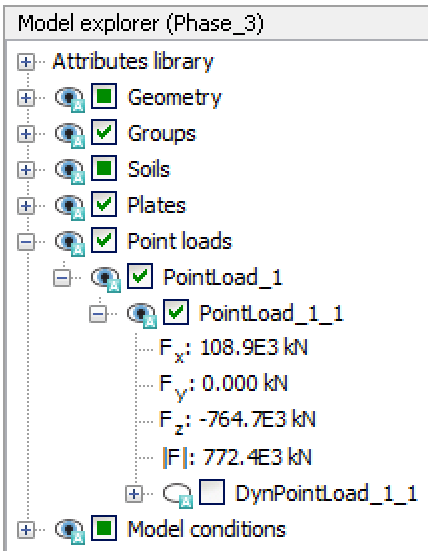

Figure 144, Loads entered in model for Load_10 calculation phase

Variations in soil layout

To investigate this influence the Plaxis model for the foundation is varied. The basis of this geotechnical study is a subsoil of sand only. For this variation a clay layer is added to the sand subsoil. This clay layer is subsequently varied in depth and thickness. In total 15 different clay layer configurations are calculated (5 variations in layer depths and 3 in layer thickness). The depth of the clay layer is varied with steps of 2m from 2 to 10m depth with respect to the bottom of the foundation plate (2m, 4m, 6m, 8m and 10m). Since the foundation is embedded 3,1m into the subsoil the coordinate of the 2m depth layer starts at -5,1m (3,1m overburden depth + 2m layer depth).
The thickness of the clay layer is varied in two steps of 2,5m (2,5m, 5,0m and 7,5m layer thickness). As a result the following 15 soil configuration models are investigated:

Layer depth [m]	Layer thickness [m]	Z-Coordinate top [m]	Z-Coordinate bottom [m]
2,0 meter	2,5	-5,1	-7,6
	5,0	-5,1	-10,1
	7,5	-5,1	-12,6
4,0 meter	2,5	-7,1	-9,6
	5,0	-7,1	-12,1
	7,5	-7,1	-14,6
6,0 meter	2,5	-9,1	-11,6
	5,0	-9,1	-14,1
	7,5	-9,1	-16,6
8,0 meter	2,5	-11,1	-13,6
	5,0	-11,1	-16,1
	7,5	-11,1	-18,6
10,0 meter	2,5	-13,1	-15,6
	5,0	-13,1	-18,1
	7,5	-13,1	-20,6

Table 40, Investigated soil configurations with their layer coordinates

Calculation outcomes

After the meshing of the model and defining the calculation phases the calculations of the model are performed. As a result of the calculations the deformation of the soil and the safety factor of the model can be viewed. Since this study mainly focuses on the safety of the model, the settlements and displacements of the foundation are of minor importance. Although some remarkable phenomena can be observed in the displacement contour plots the plots are placed in the appendix. An image of a deformed model containing a clay layer after calculations is visible in the figure below. In this figure it can be seen that the foundation will lean to the side at which the force is applied.

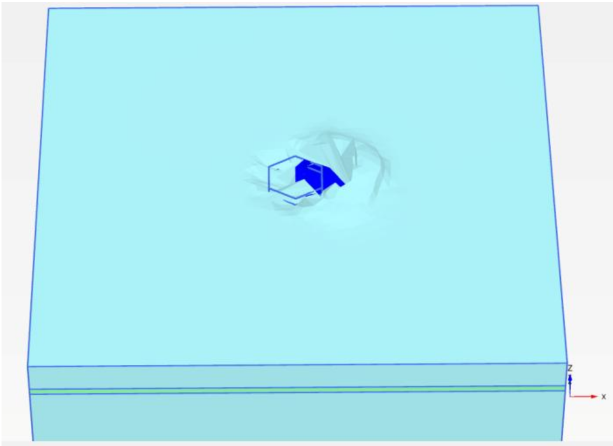

Figure 145, Soil deformations results for Plaxis 3D calculations

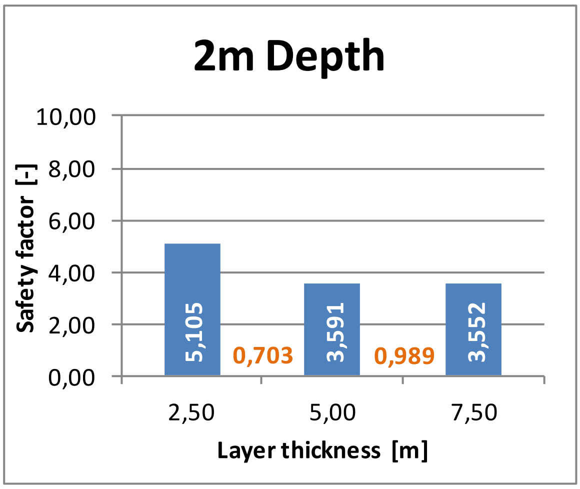

Figure 146, Safety factors for 2m clay layer depth

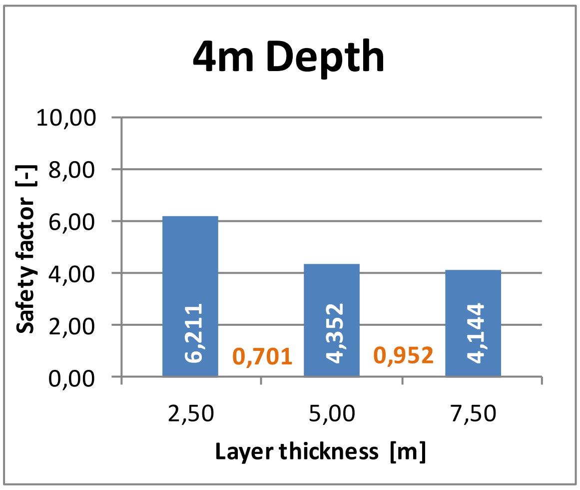

Figure 147, Safety factors for 4m clay layer depth

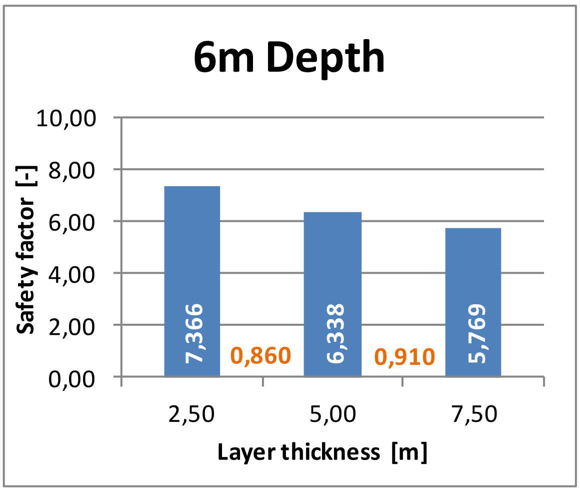

Figure 148, Safety factors for 6m clay layer depth

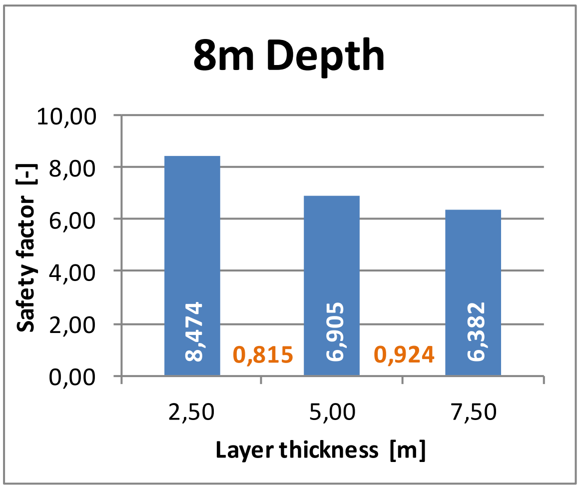

Figure 149, Safety factors for 8m clay layer depth

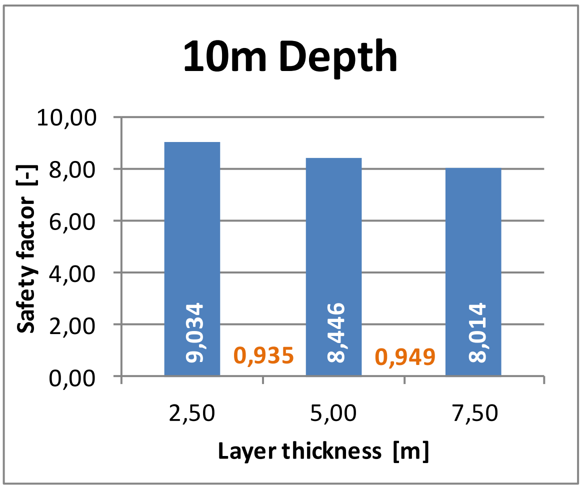

Figure 150, Safety factors for 10m clay layer depth

Evaluation of principal stresses

In the output files of the calculations also the principal stresses and the settlements of the soil are obtained. As stated before the displacements are not regarded as a main topic in this study and are discussed in the appendix. For the principal stresses the same holds, but also for these plots it holds that interesting phenomena can be observed when regarding the plot. For all 15 soil variation calculations the principal stress plots are also displayed in the next chapter of this appendix. For one situation the principal stress plot is displayed below. This plot is for the calculation phase where the normal force is present (phase 2). In this graph it can be clearly seen that a failure mechanism is developing underneath the foundation. The global shape of this failure mechanism is well explainable with the slip circle theory which was also regarded when the D-Geo Stability software was used. The a-symmetric loading of the foundation will results in failure of the shear capacity of the soil along the perimeter of the slip circle which is clearly visible in the figure. The presence of this slip circle pattern in the principal stress plot indicates that the program is developing a credible failure mechanism. When the plots in the appendix are regarded the influence of the clay layer depth an thicknesses on the principal stresses can be observed as well as the influence on the displacements.

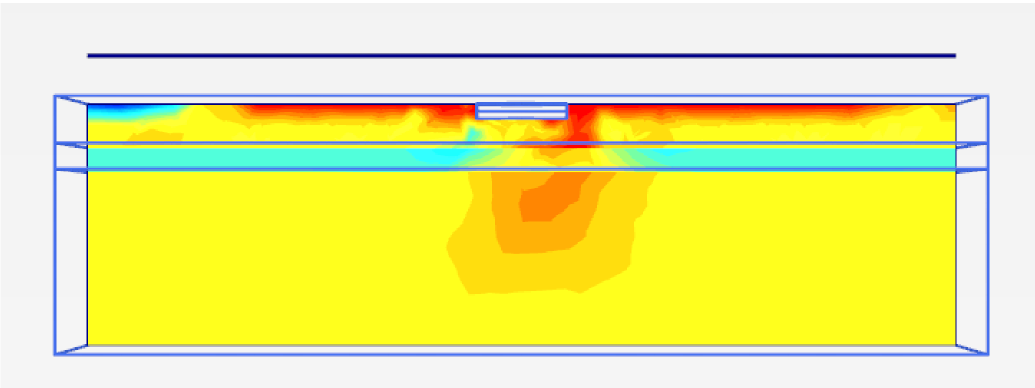

Figure 151, Principal stress plot from Plaxis 3D output, 5,0m thick clay layer at 6m depth

Analysis of clay layer depth calculation outcomes

For all three the layer thicknesses used in this model a graph is presented displaying the ratios between the safety factors. The graphs are added on the next page.

From the increment safety factor graphs for 2,5m layer depth it can be seen that the influence of the layer depth increase is decreasing for the larger layer depths. This can be seen by the decrease of the increment factors displayed in orange in the graph. This increment factors is decreasing from 20% for the layer at 2m depth to around 10% for the deeper layers at 8m and 10m depth.
For the increment safety factor graphs for the 5,0m and 7,5m layer depth this consistent behaviour is not clearly visible as it is for the 2,5m thick layers. For these graphs the relation between the increment factors shows no constant decrease of the increment factors.

This phenomena can also be explained when regarding the slip circles. For the thin clay layers the reduction in the average angle of internal friction and the part of the slip circle that lies within the clay layer is relatively small. Therefore the slip circle passes the thin clay layer without being strongly influenced. It is observed that the depth of the clay layer positively influences the safety factor. This influence on the slip circle is larger for the shallow layers than for the deeper layers as can be seen in the ratios between the safety factors for the 2,5m thick clay layers.
But when the thickness of the clay layers is increased the influence of the clay layer becomes larger. The average angle of internal friction will decrease further and a larger part of the slip circle will be located inside the weaker clay layer. Also the reduction of the internal angle of friction results in shifting the bottom of the slip circle more upwards. Therefore an increase of the clay layer depth has a larger influence on the slip circle for the thicker clay layers than for the thin clay layer. This can also be observed in the larger ratios between the safety factors for the 5,0 and 7,5m thick clay layers.
On the other hand it is noticed that for the deeper clay layers the differences between the safety factors are reducing. This may indicate that the influence of the thickness of the clay layer on the slip circle is reducing when the depth of the layer is increased.

Eventually it is stated that the thickness of the clay layers is significantly influencing the safety factors for the shallow clay layers, but that the influence of the clay layer thickness reduces when the layer is located at larger depths. On the larger depths the thickness of the layer is of minor importance and the proximity of the slip circle is having a larger influence. This change from the safety factor sensitivity from the clay layer thickness to the clay layer depth may also explain the inconsistent behaviour of the safety factors for the thicker clay layers.

It should be noticed that the findings presented are partly based on the slip circle theory and partly on the principal stress plots presented in this appendix. The exact location and shape of the slip circles is not known and it is thus mentioned that the findings are not based on the exact slip circles. When plots could be created of the exact shape and location of the slip circles it is possible to validate the findings presented.

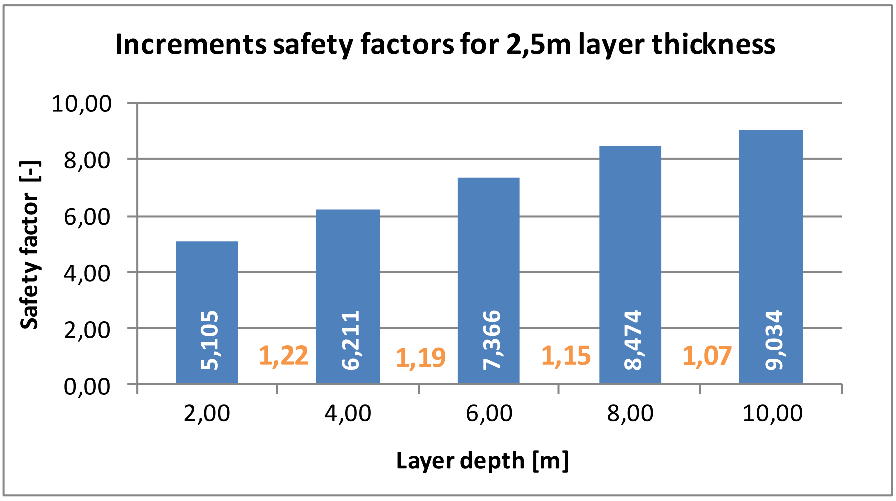

Figure 152, Ratios between safety factors for 2,5m clay layer thickness

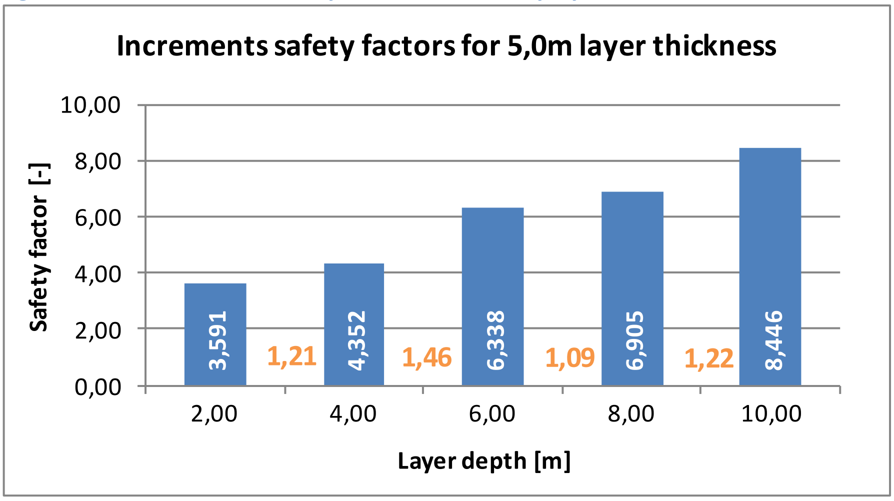

Figure 153, Ratios between safety factors for 5,0m clay layer thickness

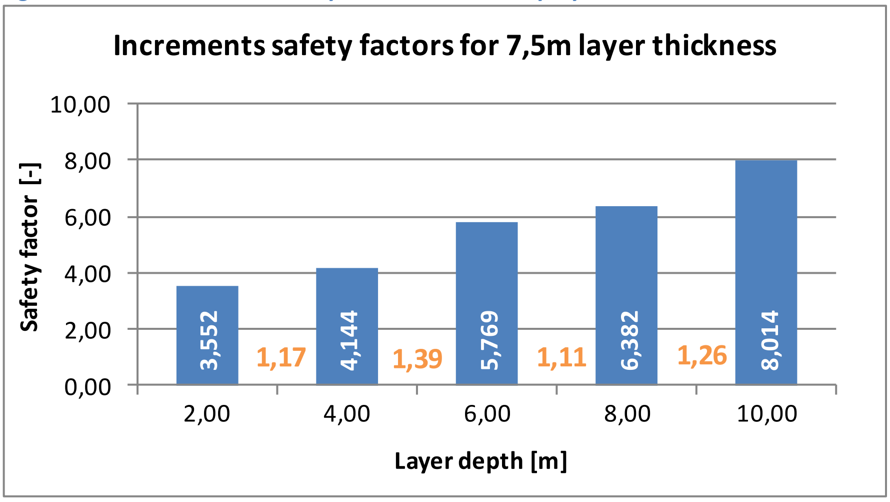

Figure 154, Ratios between safety factors for 7,5m clay layer thickness

Model properties and calculation outcomes for clay layer parameter variation

The used soil parameters for the 7 calculated models are listed in the table below.

	Cohesion c [kN/m²]	Specific soil weight γ [kN/m³]	Internal angle of friction φ [°]	Calculated safety factor [-]
1	0,1	17	17,5	5,912
2	20	17	17,5	6,825
3	10	13	17,5	6,229
4	10	21	17,5	6,504
5	10	17	12,5	4,659
6	10	17	15,0	5,474
7	10	17	20,0	7,408
Reference value	10	17	17,5	6,338

Table 41, Clay parameter variations and calculated safety factors, changed parameters are marked grey

Safety factor calculation outcomes

In the table presented above the calculated safety factors for all 7 variations and the reference model are presented. Form this table it can be seen that the variation in the safety factors is quite large when compared to the differences in the safety factors found for the clay layer depth and thickness variations. The safety factor for the reference model, a 5,0m thick clay layer at 6m depth, is 6,338 as calculated before. The situation with a low internal angle of friction, model 5 in the table, results in a much lower safety factor of only 4,659. On the other hand the situation with a slightly higher internal angle of friction results in a safety factor that is higher than was found for the reference value. The percentage difference for all 7 variations can be found in the table below. Here it can be seen that the difference between the safety factors of the reference value is the largest for the variations of the internal angle of friction. For these variations differences of -26,5% and +16,9% are found. For the other parameters the differences are much smaller where the difference for specific soil weight has the least influence on the safety factor.

Although the differences in the parameters values are realistic, but not equal for the three varied soil characteristics, the variation of c=0,1 to c=20 is much higher than the variation from φ=12,5 to φ=20, the outcome of the calculations clearly indicates that a difference in the internal angle has the most influence on the safety factor, and thus the bearing capacity of the model.

All the calculated safety factors are also visible in the graph presented below. Here the reference value is indicated red.

Calculated model	Calculated safety factor [-]	Difference with reference factor (6,338)
1 (c=0,1)	5,912	- 6,7%
2 (c=20)	6,825	+ 7,7%
3 (γ=13)	6,229	- 1,7%
4 (γ=21)	6,504	+ 2,6%
5 (φ=12,5)	4,659	- 26,5%
6 (φ=15,0)	5,474	- 13,6%
7 (φ=20,0)	7,408	+16,9%

Table 42, Percentage difference for safety factors with respect to reference value

28. Appendix: Displacements and principal stresses for foundation foot for different soil configurations

Since this study mainly focuses on the safety of the foundation structure and not on the settlements and displacements the settlements are not quantitatively investigated. But since it is interesting how the settlement of the foundation is distributed over the different soil layers here the cross sections are presented which show the settlement of the soil for the different configurations. From these cross sections it can be seen that when the thickness of the clay layer is increased the settlements of the foundation are more located within the weaker clay layer. Also it can be seen that for a larger clay layer depth the settlements of the foundation are reaching to a larger depth.

For the principal stresses obtained with the calculation results of Plaxis 3D the same effect holds for the variation in clay layer thickness. Here it is also visible that for thicker clay layers the plot shows that the extreme principal stresses are shifting towards the clay layer. This means that the slip circle is shifting towards the weaker layers.
When the depth of the clay layer is regarded it can be seen that the shape of the principal stress plot is not changing significantly for the thin 2,5m clay layer, this in contrast to the displacement plots where it is visible that the displacement is primarily located in the weaker clay layer. This means that the depth of the clay layer has little influence on the principal stresses in the subsoil for the thinner clay layer. For the thicker clay layers the shift of the principal stresses is more visible and thus indicates that the thickness of the clay layer is playing an important role in the location of the extreme principal stresses.

Soil displacements for configuration with clay layer at 2m depth

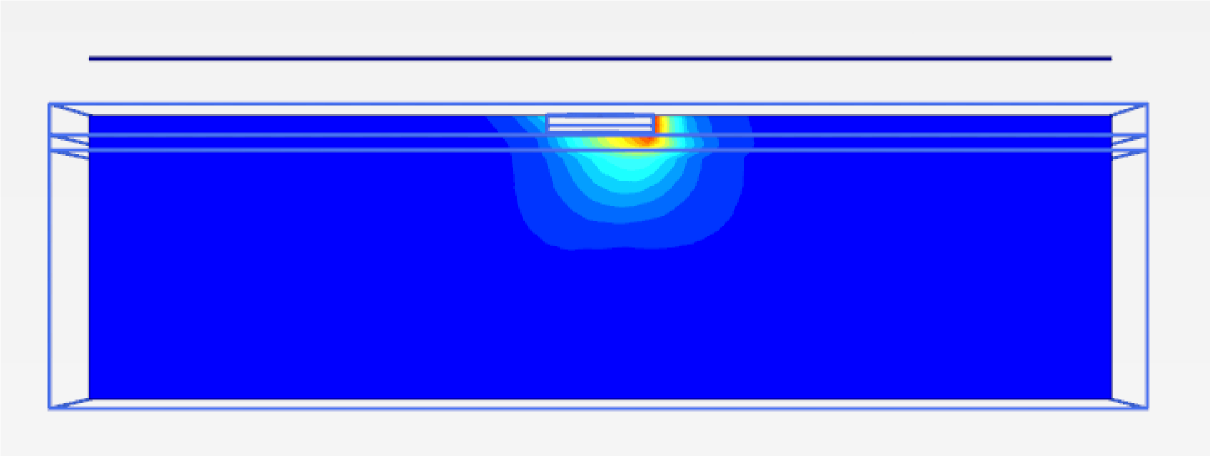

Figure 155, Displacement of foundation for configuration with clay layer at 2m depth and 2,5m thickness

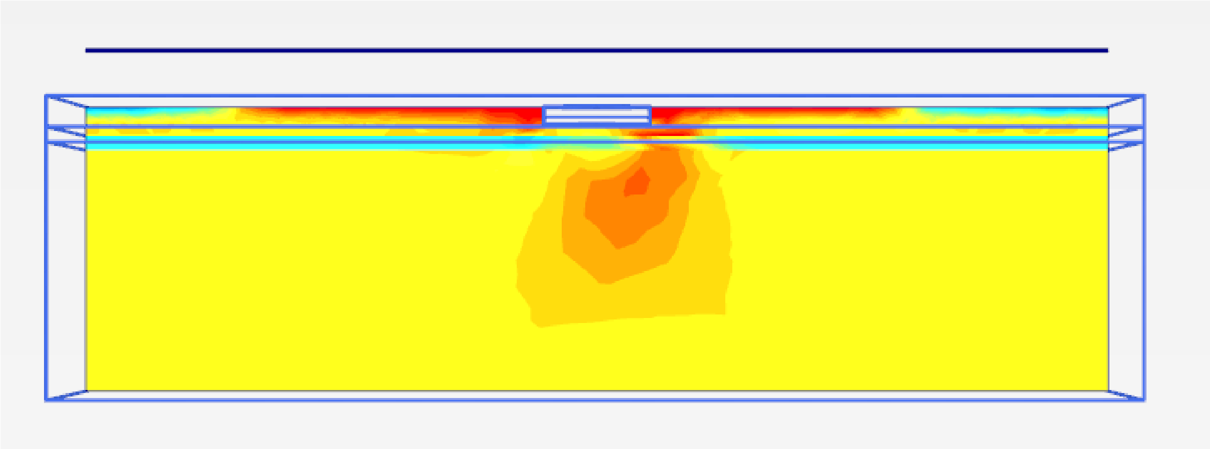

Figure 156, Principal stresses in foundation sub soil for configuration with clay layer at 2m depth and 2,5m thickness

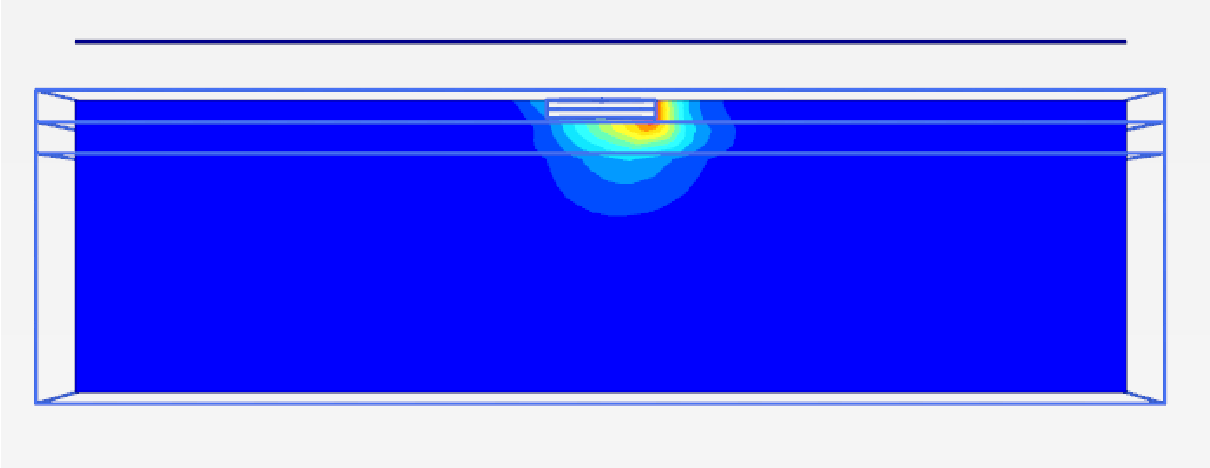

Figure 157, Displacement of foundation for configuration with clay layer at 2m depth and 5,0m thickness

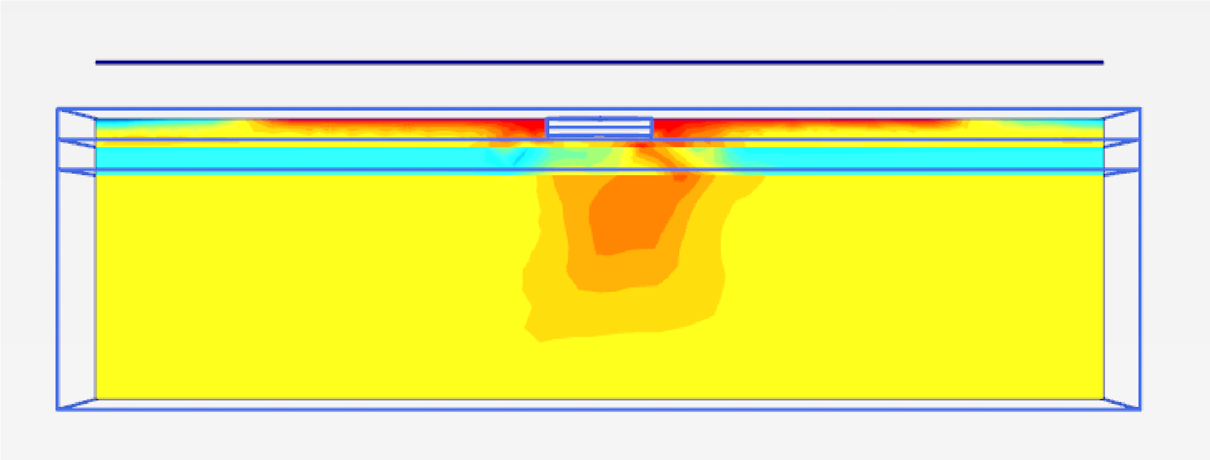

Figure 158, Principal stresses in foundation sub soil for configuration with clay layer at 2m depth and 5,0m thickness

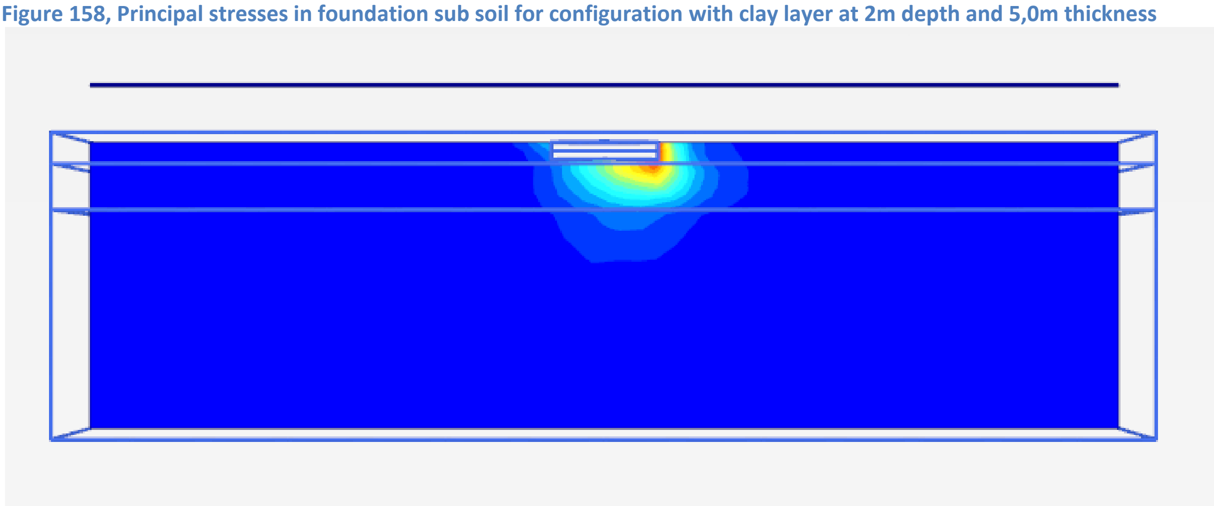

Figure 159, Displacement of foundation for configuration with clay layer at 2m depth and 7,5m thickness

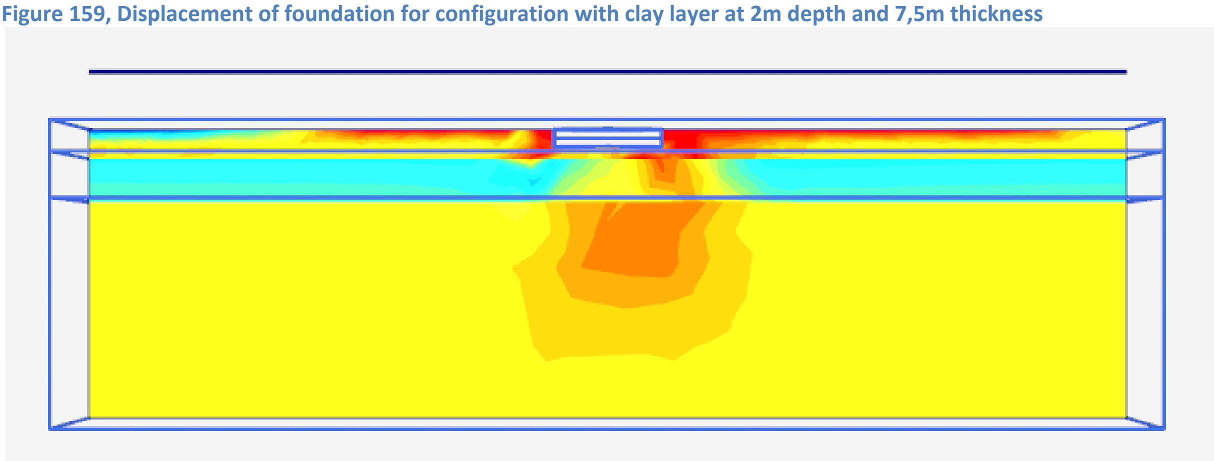

Figure 160, Principal stresses in foundation sub soil for configuration with clay layer at 2m depth and 7,5m thickness

Soil displacements for configuration with clay layer at 4m depth

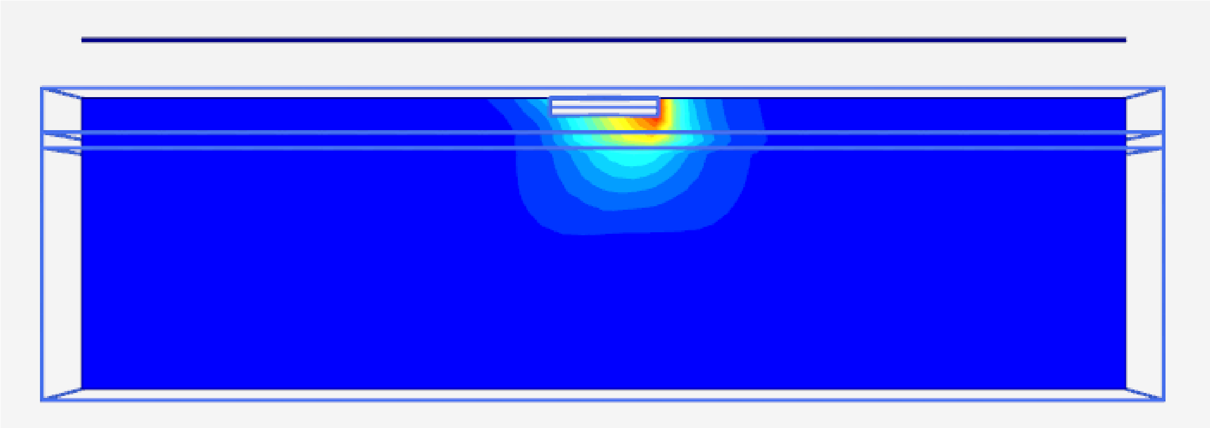

Figure 161, Displacement of foundation for configuration with clay layer at 4m depth and 2,5m thickness

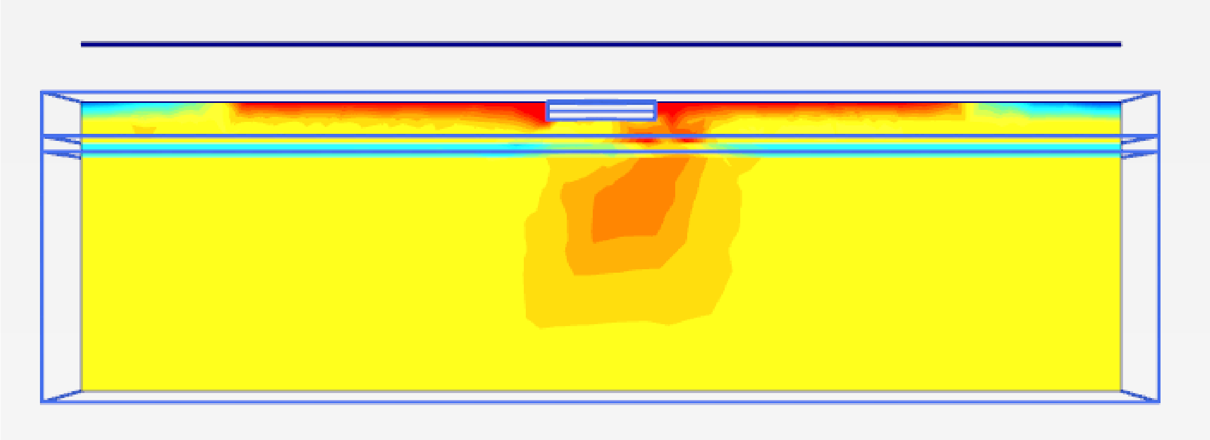

Figure 162, Principal stresses in foundation sub soil for configuration with clay layer at 4m depth and 2,5m thickness

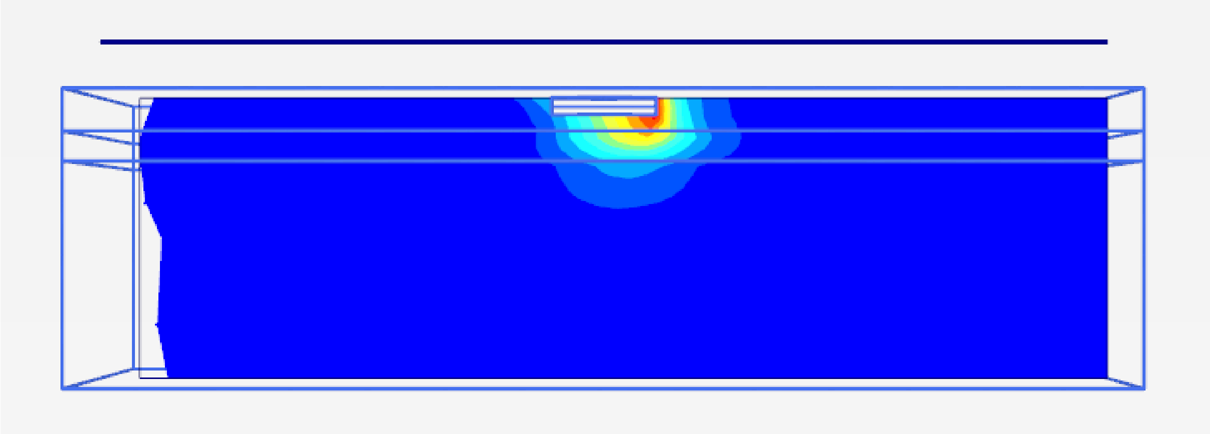

Figure 163, Displacement of foundation for configuration with clay layer at 4m depth and 5,0m thickness

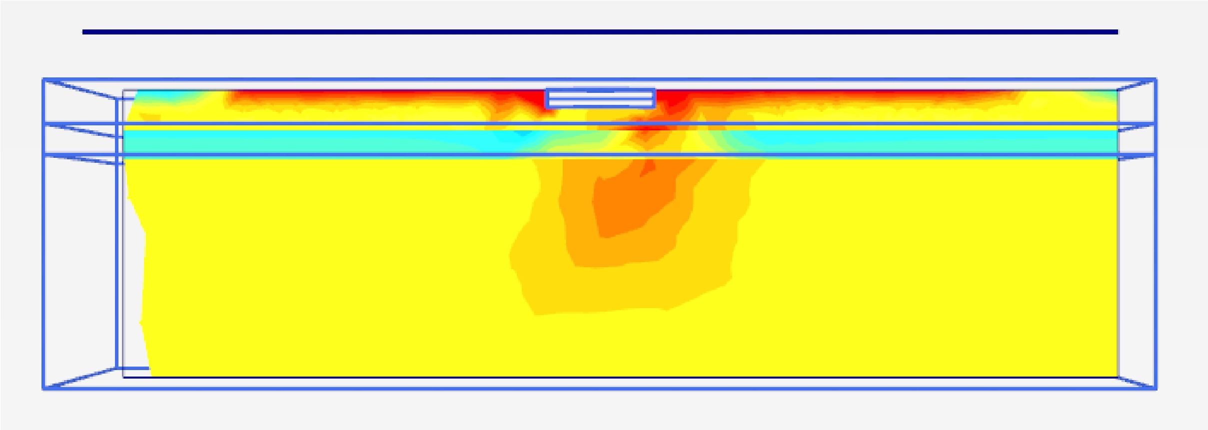

Figure 164, Principal stresses in foundation sub soil for configuration with clay layer at 4m depth and 5,0m thickness

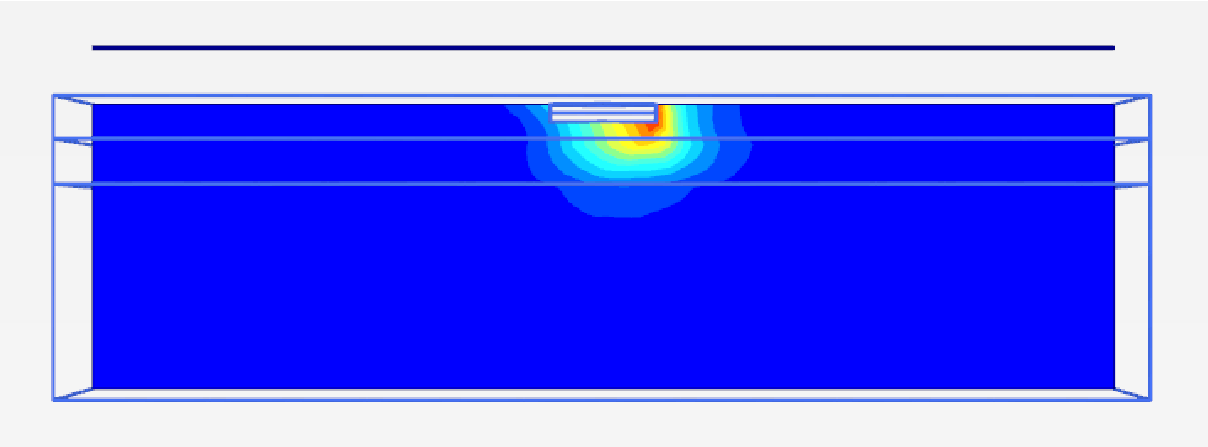

Figure 165, Displacement of foundation for configuration with clay layer at 4m depth and 7,5m thickness

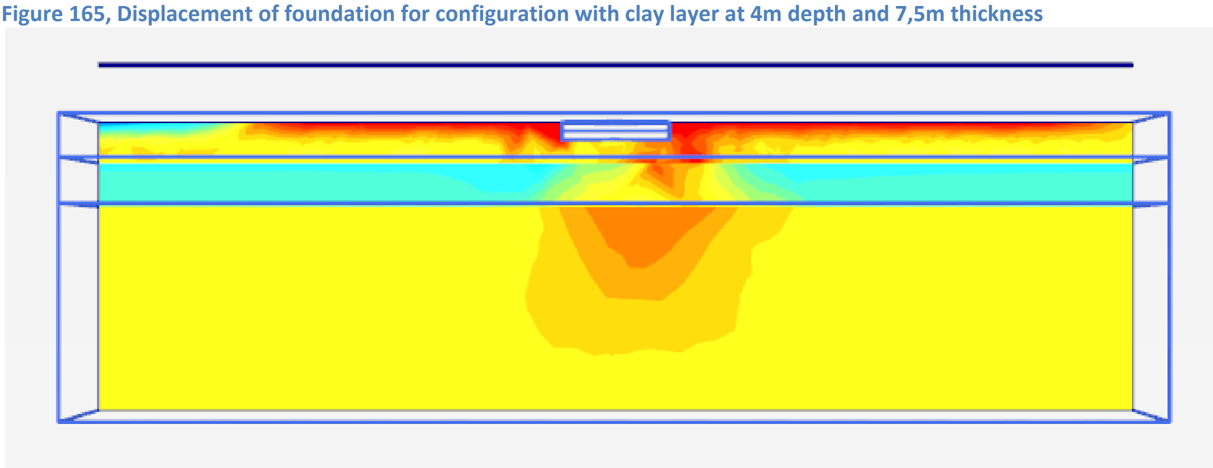

Figure 166, Principal stresses in foundation sub soil for configuration with clay layer at 4m depth and 7,5m thickness

Soil displacements for configuration with clay layer at 6m depth

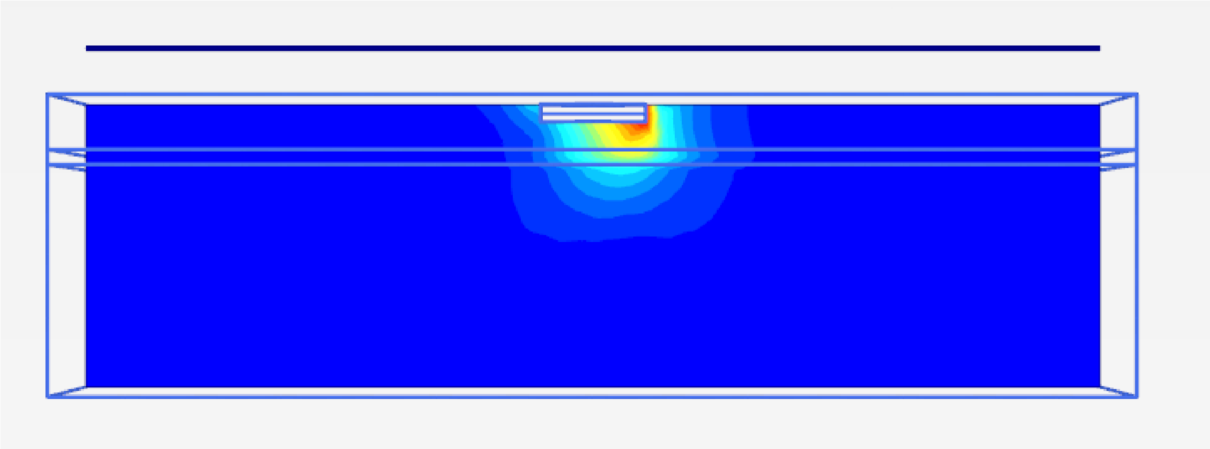

Figure 167, Displacement of foundation for configuration with clay layer at 6m depth and 2,5m thickness

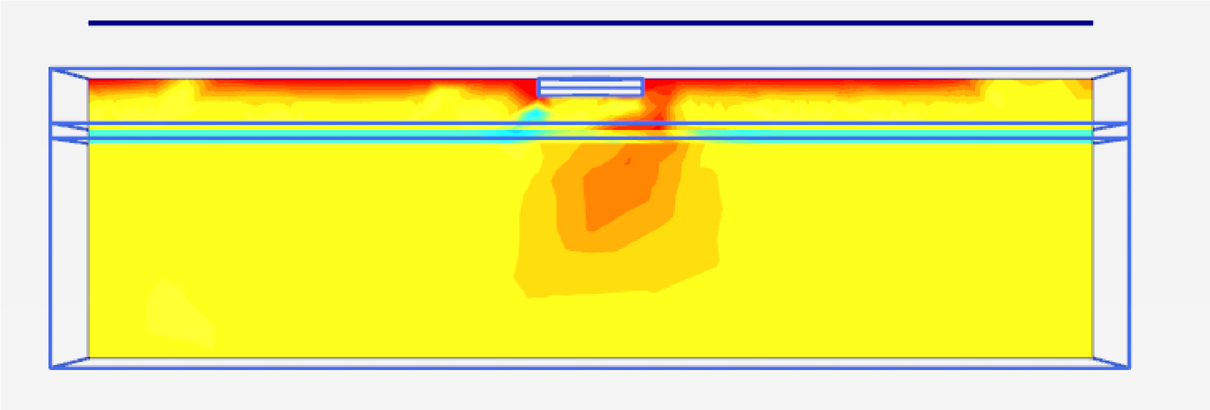

Figure 168, Principal stresses in foundation sub soil for configuration with clay layer at 6m depth and 2,5m thickness

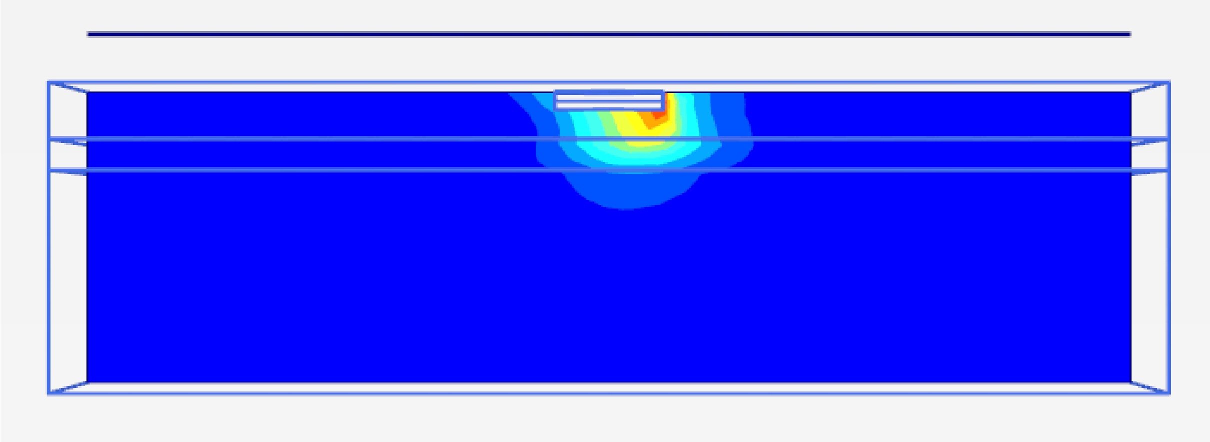

Figure 169, Displacement of foundation for configuration with clay layer at 6m depth and 5,0m thickness

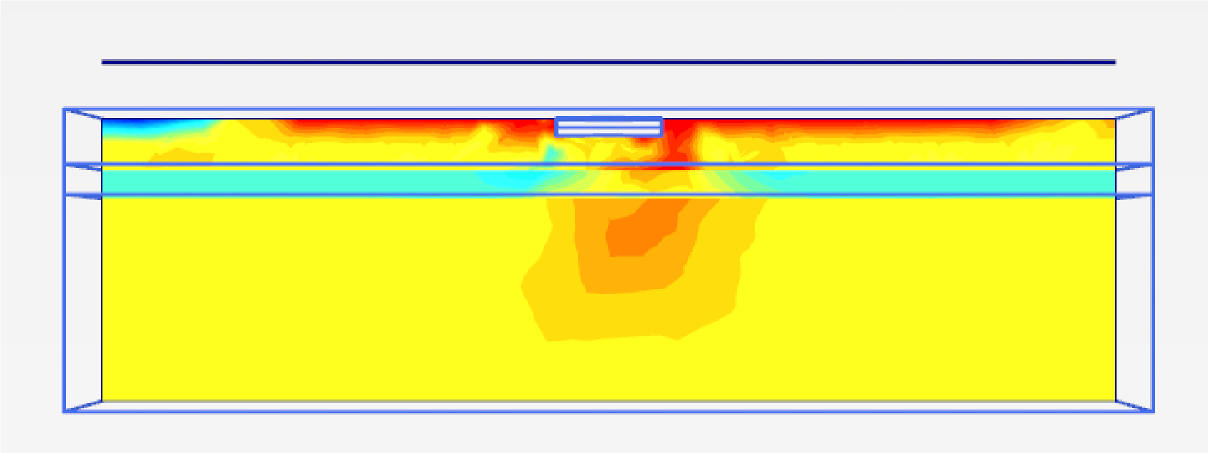

Figure 170, Principal stresses in foundation sub soil for configuration with clay layer at 6m depth and 5,0m thickness

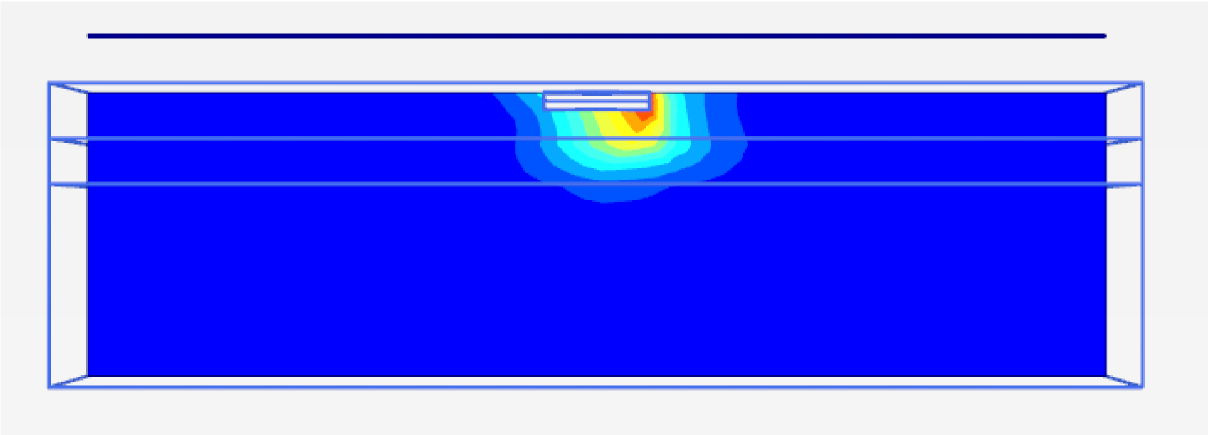

Figure 171, Displacement of foundation for configuration with clay layer at 6m depth and 7,5m thickness

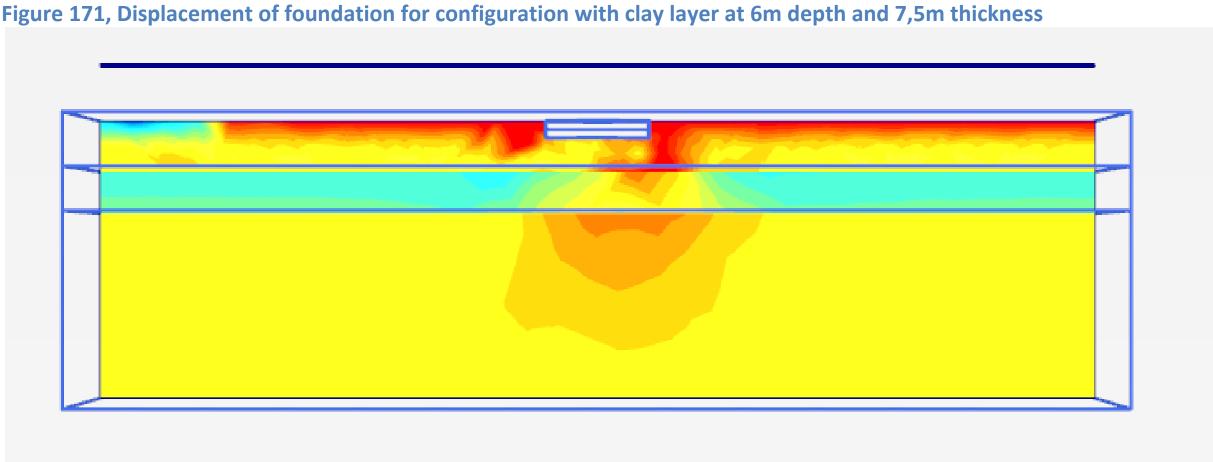

Figure 172, Principal stresses in foundation sub soil for configuration with clay layer at 6m depth and 7,5m thickness

Soil displacements for configuration with clay layer at 8m depth

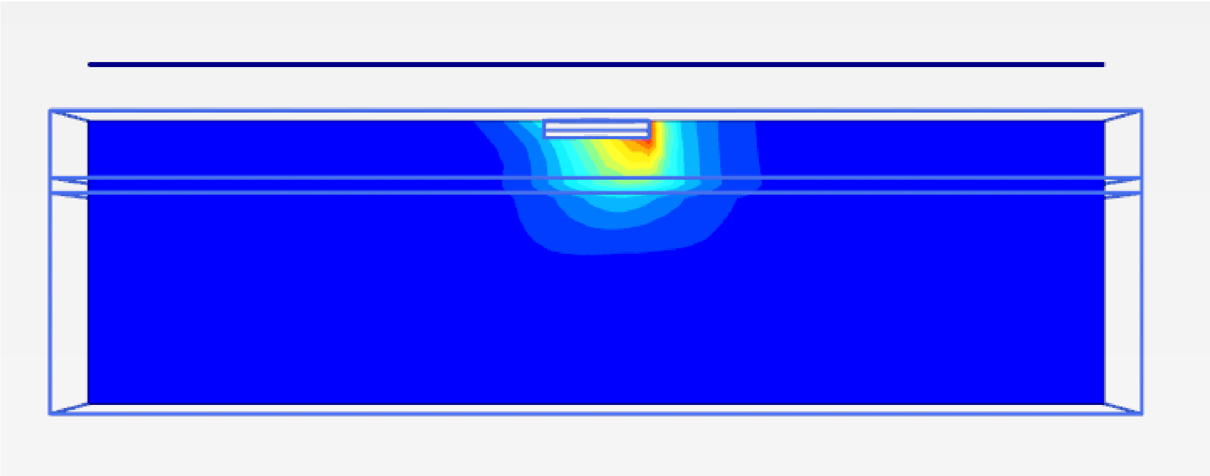

Figure 173, Displacement of foundation for configuration with clay layer at 8m depth and 2,5m thickness

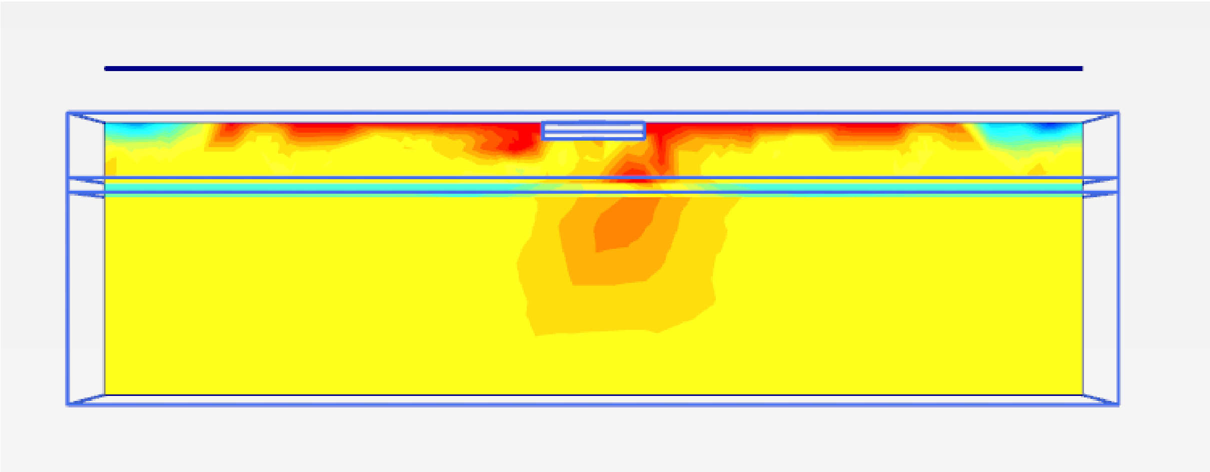

Figure 174, Principal stresses in foundation sub soil for configuration with clay layer at 8m depth and 2,5m thickness

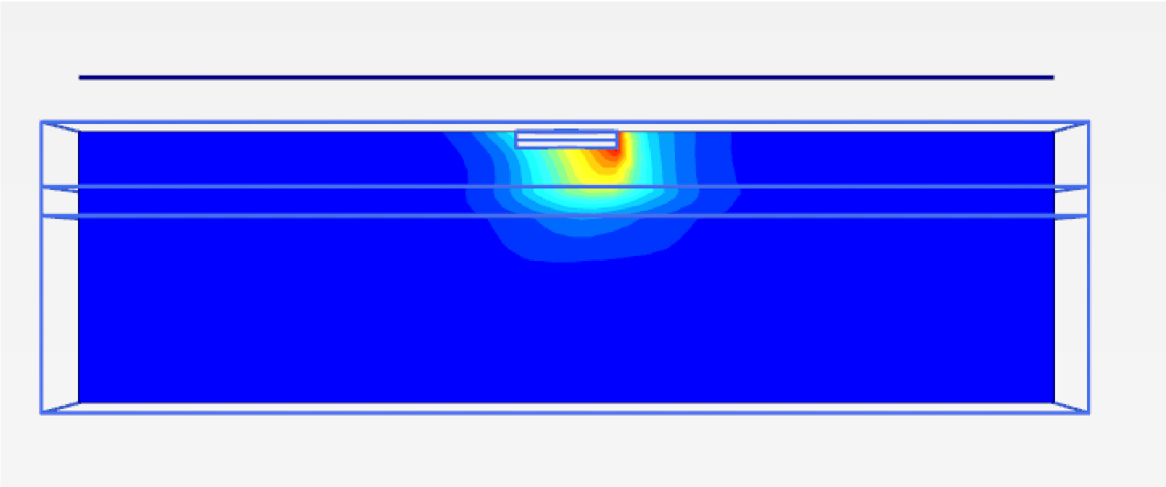

Figure 175, Displacement of foundation for configuration with clay layer at 8m depth and 5,0m thickness

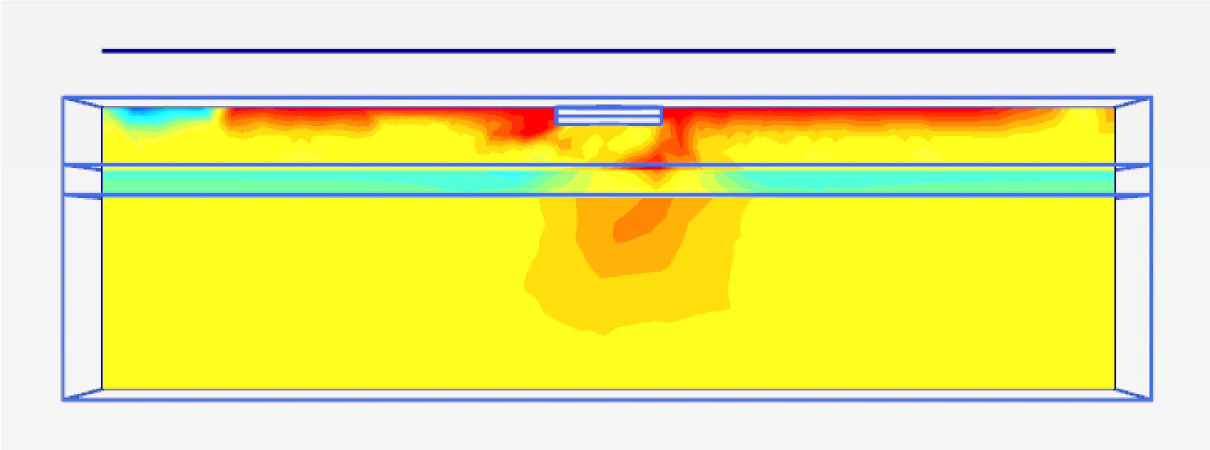

Figure 176, Principal stresses in foundation sub soil for configuration with clay layer at 8m depth and 5,0m thickness

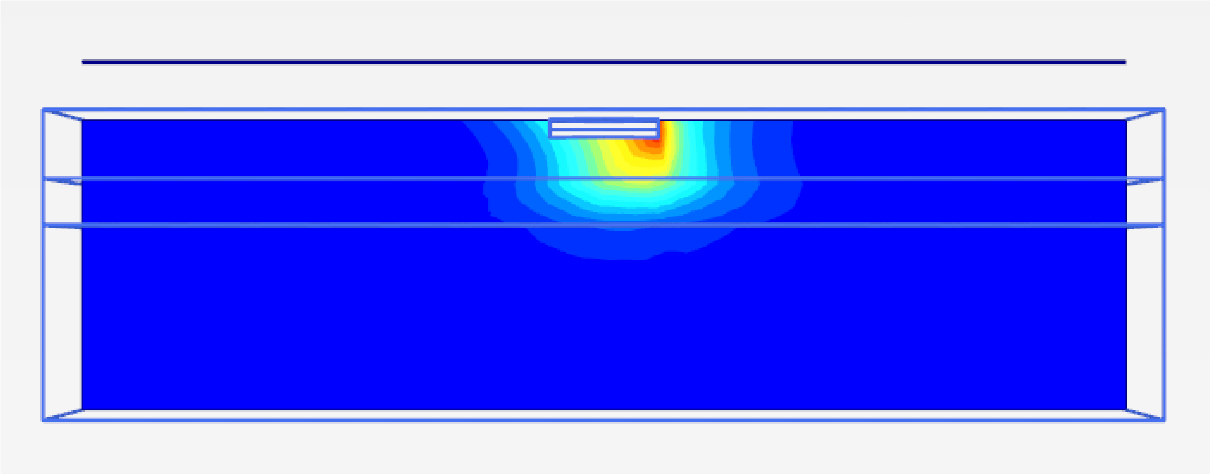

Figure 177, Displacement of foundation for configuration with clay layer at 8m depth and 7,5m thickness

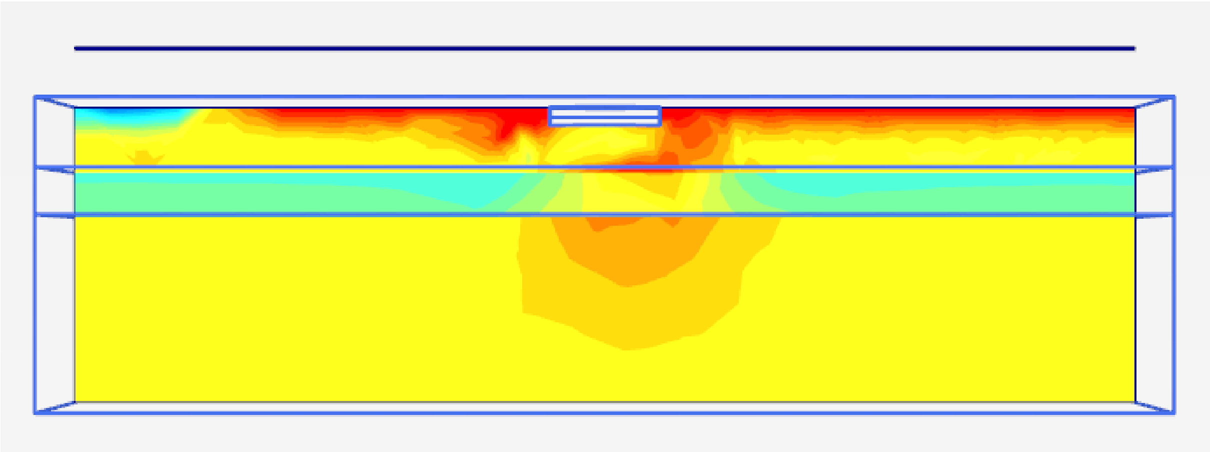

Figure 178, Principal stresses in foundation sub soil for configuration with clay layer at 8m depth and 7,5m thickness

Soil displacements for configuration with clay layer at 10m depth

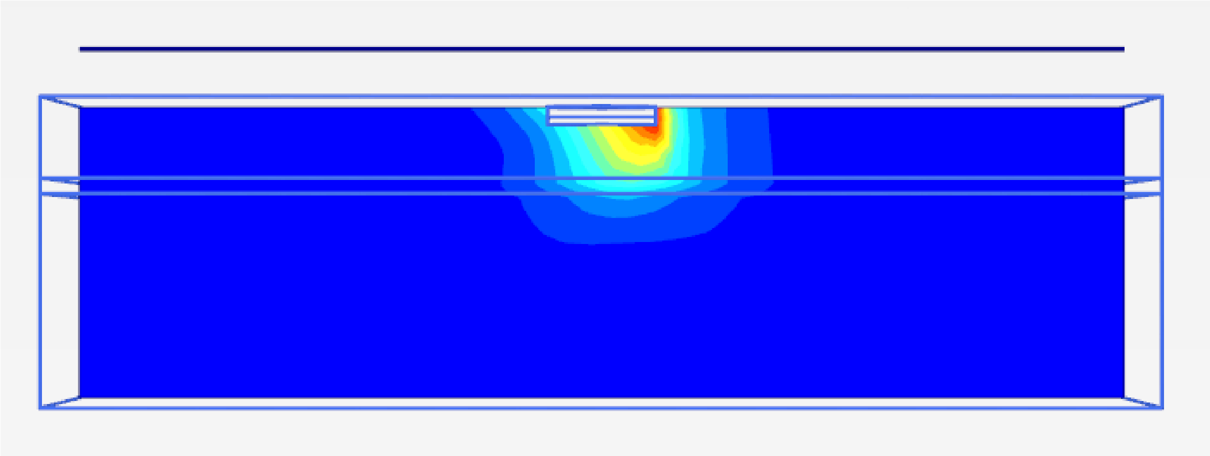

Figure 179, Displacement of foundation for configuration with clay layer at 10m depth and 2,5m thickness

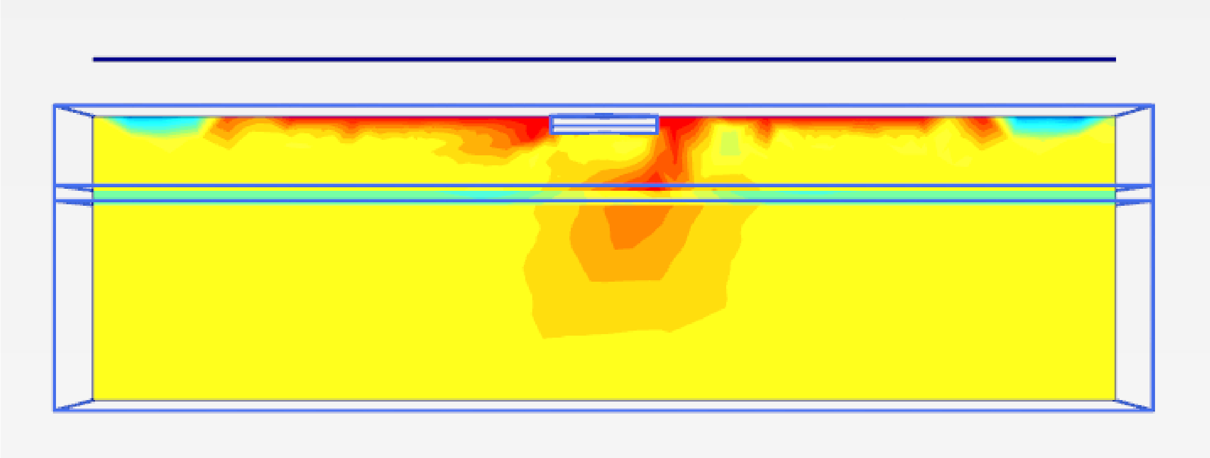

Figure 180, Principal stresses in foundation sub soil for configuration with clay layer at 10m depth and 2,5m thickness

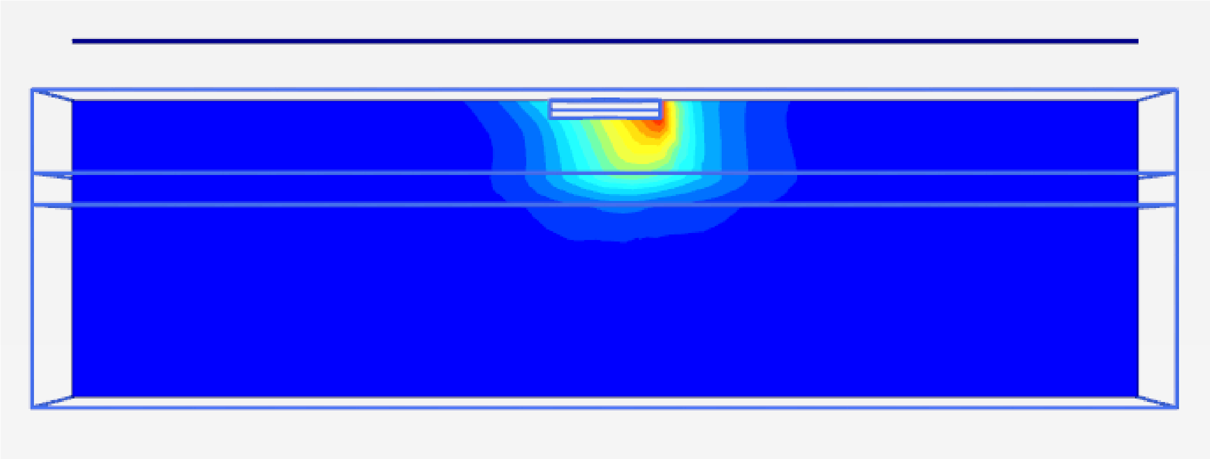

Figure 181, Displacement of foundation for configuration with clay layer at 10m depth and 5,0m thickness

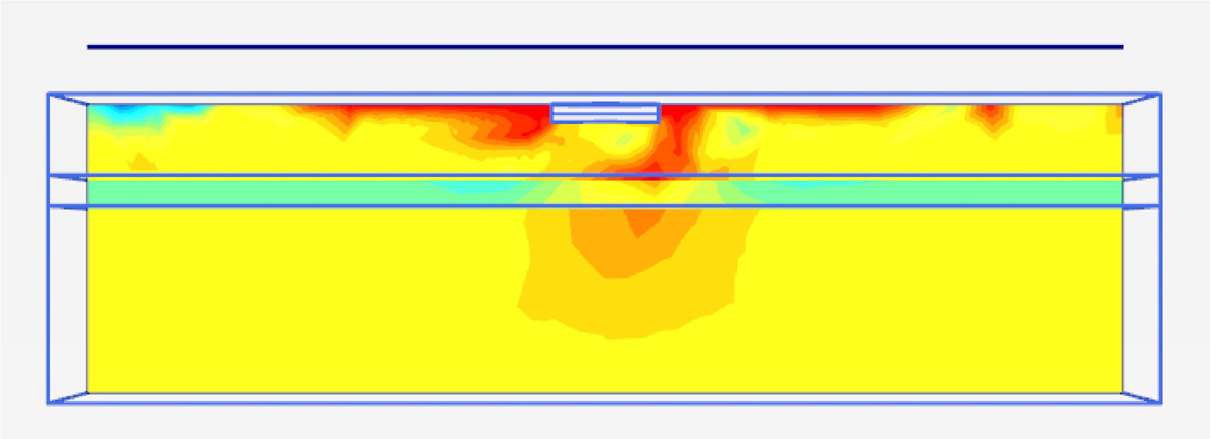

Figure 182, Principal stresses in foundation sub soil for configuration with clay layer at 10m depth and 5,0m thickness

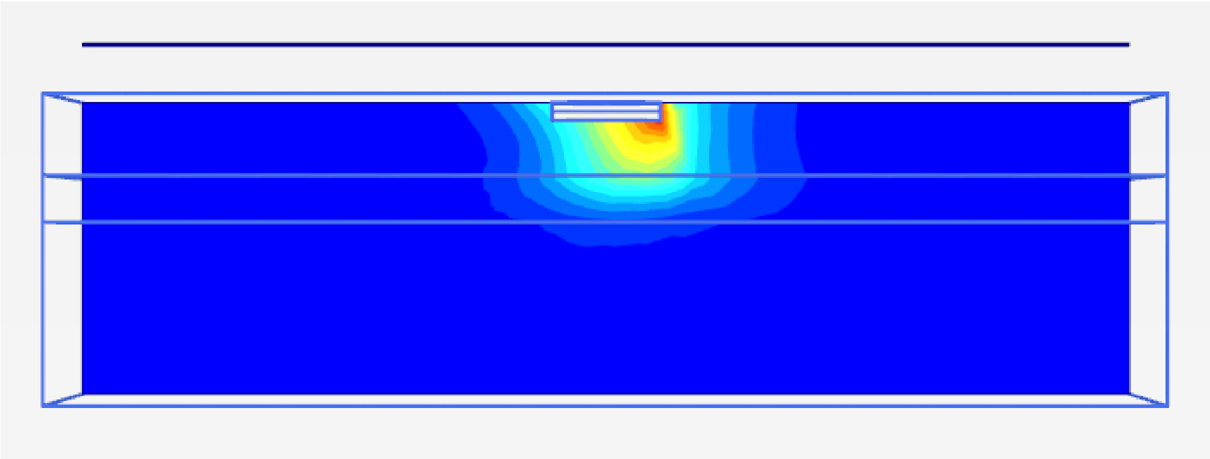

Figure 183, Displacement of foundation for configuration with clay layer at 10m depth and 7,5m thickness

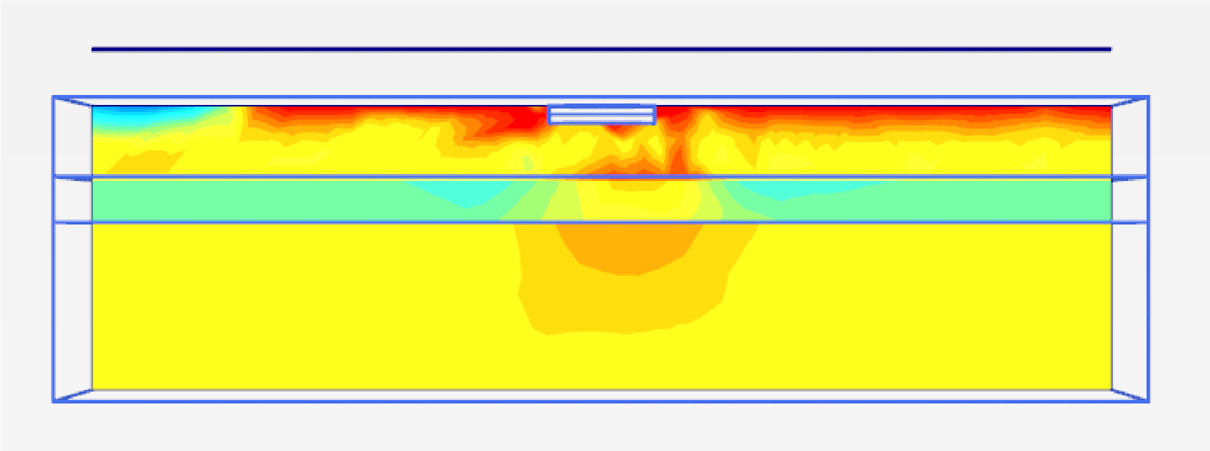

Figure 184, Principal stresses in foundation sub soil for configuration with clay layer at 10m depth and 7,5m thickness

29. Formulas to determine depth of slip circle

In the copied page placed below (in German) some hand calculation formula's are shown to calculate the depth of a formed slip circle. It can be seen that the formula's are only depending on the angle of internal friction.

8/7 **Grundbruchgleitlinie**

bei lotrecht-mittiger Last

a) Bruchfuge nach PRANDTL [26]

Für die Grundbruchgleitlinie sind die Grenzneigungen ϑ_a^* und ϑ_p^* der MOHR-/COULOMBschen Bruchbedingung maßgebend. Als Übergangskurve vom aktiven zum passiven Erdkeil wird eine logarithmische Spirale gewählt, deren Radiusstrahl gemäß dem Reibungsgesetz unter φ zur Normalen geneigt ist. Der theoretisch beidseitige Bruch tritt praktisch nur einseitig auf, da durch Unregelmäßigkeiten bei Untergrund und Laststellung eine der beiden Seiten schwächeren Widerstand leisten wird.

Skizze für $\varphi = 30°$:

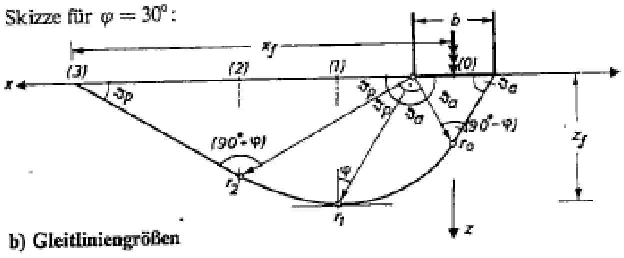

b) Gleitliniengrößen

Gleitflächenwinkel: $\vartheta_a = \vartheta_a^* = (45° + \frac{1}{2}\varphi)$; $\vartheta_p = \vartheta_p^* = (45° - \frac{1}{2}\varphi)$.

Log. Spirale: $r = r_0 \cdot e^{\hat{\vartheta} \cdot \tan\varphi}$ s. T. 8/13.

Aktiver Erdkeil: $r_0 = \frac{1}{2} \cdot \frac{b}{\cos\vartheta_a}$; $x_0 = 0$; $z_0 = \frac{1}{2} b \cdot \tan\vartheta_a$.

Bruchtiefe: $r_1 = r_0 \cdot e^{\vartheta_a \cdot \tan\varphi}$; $x_1 = \frac{1}{2} b + r_1 \cdot \sin\varphi$; $z_f = z_1 = r_1 \cdot \cos\varphi$.

Passiver Keil: $r_2 = \cancel{r_0 \cdot e^{\frac{\pi}{2} \cdot \tan\varphi}}$; $r_0 \cdot e^{\frac{\pi}{2} \tan\varphi}$ $x_2 = \frac{1}{2} b + r_2 \cdot \cos\vartheta_p$; $z_2 = r_2 \cdot \sin\vartheta_p$.

Bruchlänge: $x_f = x_3 = \frac{1}{2} b + 2 \cdot r_2 \cdot \cos\vartheta_p$; $z_3 = 0$.

c) Tabelle

φ	0°	15°	20°	25°	27,5°	30°	32,5°	35°	37,5°	40°	45°
ϑ_a ϑ_p	45° 45°	52,5° 37,5°	55° 35°	57,5° 32,5°	58,75° 31,25°	60° 30°	61,25° 28,75°	62,5° 27,5°	63,75° 26,25°	65° 25°	67,5° 22,5°
r_0/b z_0/b	0,71 0,50	0,82 0,65	0,87 0,71	0,93 0,79	0,96 0,83	1 0,87	1,04 0,91	1,08 0,96	1,13 1,01	1,18 1,07	1,31 1,21
r_1/b x_1/b z_1/b	0,71 0,50 0,71	1,04 0,57 1,01	1,24 0,92 1,16	1,48 1,13 1,35	1,64 1,26 1,46	1,83 1,42 1,59	2,05 1,60 1,73	2,32 1,83 1,90	2,66 2,12 2,11	3,06 2,47 2,35	4,25 3,00 3,00
r_2/b x_2/b z_2/b	0,71 1 0,50	1,25 1,49 0,76	1,54 1,76 0,89	1,94 2,13 1,04	2,18 2,36 1,13	2,48 2,65 1,24	2,83 2,98 1,36	3,25 3,38 1,50	3,77 3,88 1,67	4,42 4,51 1,87	6,29 6,31 2,41
x_3/b	1,50	2,48	3,03	3,76	4,23	4,79	5,46	6,27	7,27	8,51	12,1

104

Figure 185, Hand calculation method to determine the depth of slip circle for uniform soil

30. Dynamic loadings in Plaxis 3D

Representation of load fluctuations for an offshore wind turbine

The frequency for the dynamic loading is different per origin. The frequency of the waves has a value of around 0,2-0,1hz (5-10sec per period). The excitations of the wind are having a higher frequency which is different per situation. The blade passing frequency of the tower is much higher than both the wind and wave frequencies namely in the order of 1-2Hz (0,5-1sec per period). A representation of the load fluctuations of a offshore wind turbine during a non production phase can be seen in the table[32] and figure below.

	Configuration of turbine		
	Blades: In normal position		Blades: 90° pitched
Mode shape	Freq. [Hz]	Damp. (%)	Freq. [Hz]
1st tower transversal	0.418	6.0	0.417
1st tower longitudinal	0.419	6.0	0.420
1st rotor torsion	0.805	5.0	0.704
1st rotor torsion	0.979		1.002
1st asymmetric rotor (yaw)	1.000		1.064
1st symmetric rotor (flap)	1.067	3.1	1.769
1st edgewise mode	1.857	3.1	1.032
2nd edgewise mode			1.045

Table 43, Dynamic properties of 1,8MW reference wind turbine

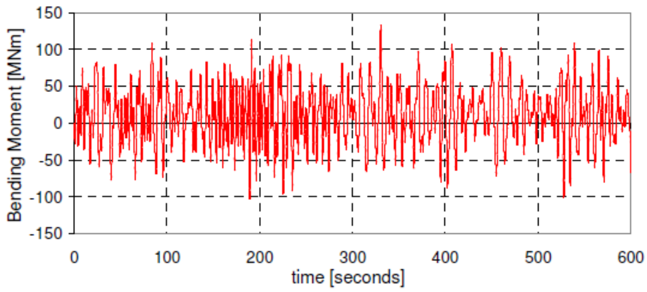

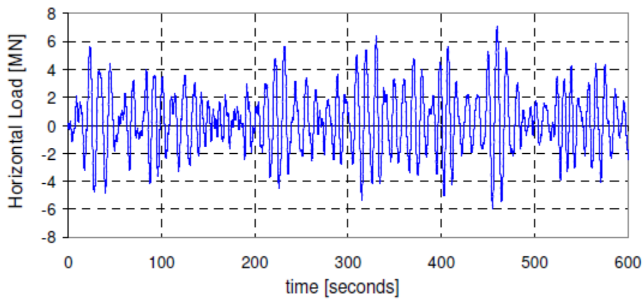

Figure 186, Typical load sequence acting on foundation for offshore wind turbine during a non production phase

[32] Analysis of Gravity Base Foundation for Offshore Wind Turbine under Cyclic Loads, S. Safinus, G. Sedlacek, and U. Hartwig 2011

Material properties used for undrained Plaxis 3D calculations

Sand

Property	Unit	Value
Material set		
Identification		Sand
Material model		Hardening soil
Drainage type		Undrained (A)
Colour		RGB 161, 226, 232
Comments		
General properties		
γ_{unsat}	kN/m^3	18,00
γ_{sat}	kN/m^3	20,00
Advanced		
Void ratio		
Dilatancy cut-off		☐
e_{init}		0,5000
e_{min}		0,000
e_{max}		999,0
Damping		
Rayleigh α		0,000
Rayleigh β		0,000

Figure 187, General properties undrained sand

Property	Unit	Value
Stiffness		
E_{50}^{ref}	kN/m^2	43,00E3
E_{oed}^{ref}	kN/m^2	43,00E3
E_{ur}^{ref}	kN/m^2	129,0E3
power (m)		0,5000
Alternatives		
Use alternatives		☐
C_c		8,023E-3
C_s		2,407E-3
e_{init}		0,5000
Strength		
c'_{ref}	kN/m^2	0,1000
φ' (phi)	°	32,50
ψ (psi)	°	2,500
Advanced		
Set to default values		☑
Stiffness		
ν'_{ur}		0,2000
p_{ref}	kN/m^2	100,0
K_0^{nc}		0,4627
Strength		
c'_{inc}	$kN/m^2/m$	0,000
z_{ref}	m	0,000
R_f		0,9000
Tension cut-off		☑
Tensile strength	kN/m^2	0,000
Undrained behaviour		
Undrained behaviour		Standard
Skempton-B		0,9866
ν_u		0,4950
$K_{w,ref}$ / n	kN/m^2	5,285E6

Figure 188, Parameters undrained sand

Property	Unit	Value
Model		
Data set		Standard
Soil		
Type		Coarse
< 2 µm	%	10,00
2 µm - 50 µm	%	13,00
50 µm - 2 mm	%	77,00
Parameters		
Set to default values		☐
k_x	m/day	0,000
k_y	m/day	0,000
k_z	m/day	0,000
$-\Psi_{unsat}$	m	10,00E3
e_{init}		0,5000
Change of permeability		
c_k		1,000E15

Figure 189, Flow parameters undrained sand

Property	Unit	Value
Strength		
Strength		Manual
R_{inter}		0,9000
Consider gap closure		☑
Real interface thickness		
δ_{inter}		0,000

Figure 190, Interface properties undrained sand

Property	Unit	Value
K0 settings		
K_0 determination		Automatic
Overconsolidation		
OCR		1,000
POP	kN/m^2	10,00

Figure 191, Initial properties undrained sand

Clay

Property	Unit	Value
Material set		
Identification		Clay
Material model		Hardening soil
Drainage type		Undrained (A)
Colour		RGB 134, 234, 162
Comments		
General properties		
γ_{unsat}	kN/m ^{3}	17,00
γ_{sat}	kN/m ^{3}	17,00
Advanced		
Void ratio		
Dilatancy cut-off		☐
e_{init}		0,5000
e_{min}		0,000
e_{max}		999,0
Damping		
Rayleigh α		0,000
Rayleigh β		0,000

Figure 192, General properties undrained clay

Property	Unit	Value
Stiffness		
$E_{50}{}^{ref}$	kN/m ^{2}	10,00E3
$E_{oed}{}^{ref}$	kN/m ^{2}	10,00E3
$E_{ur}{}^{ref}$	kN/m ^{2}	30,00E3
power (m)		0,8000
Alternatives		
Use alternatives		☐
C_c		0,03450
C_s		0,01035
e_{init}		0,5000
Strength		
c'_{ref}	kN/m ^{2}	10,00
φ' (phi)	°	17,50
ψ (psi)	°	0,000
Advanced		
Set to default values		☑
Stiffness		
ν'_{ur}		0,2000
p_{ref}	kN/m ^{2}	100,0
$K_0{}^{nc}$		0,6993
Strength		
c'_{inc}	kN/m ^{2}/m	0,000
z_{ref}	m	0,000
R_f		0,9000
Tension cut-off		☑
Tensile strength	kN/m ^{2}	0,000
Undrained behaviour		
Undrained behaviour		Standard
Skempton-B		0,9866
ν_u		0,4950
$K_{w,ref}$ / n	kN/m ^{2}	1,229E6

Figure 193, Parameters undrained clay

Property	Unit	Value
Model		
Data set		Standard
Soil		
Type		Coarse
< 2 µm	%	10,00
2 µm - 50 µm	%	13,00
50 µm - 2 mm	%	77,00
Parameters		
Set to default values		☐
k_x	m/day	0,000
k_y	m/day	0,000
k_z	m/day	0,000
$-\psi_{unsat}$	m	10,00E3
e_{init}		0,5000
Change of permeability		
c_k		1,000E15

Figure 194, Flow parameters undrained clay

Property	Unit	Value
Strength		
Strength		Manual
R_{inter}		0,9000
Consider gap closure		☑
Real interface thickness		
δ_{inter}		0,000

Figure 195, Interface properties undrained clay

Property	Unit	Value
K0 settings		
K_0 determination		Automatic
Overconsolidation		
OCR		1,000
POP	kN/m^2	10,00

Figure 196, Initial properties undrained clay

31. Appendix A, Calculation outcomes for undrained 3D calculations

Reached values	
Reached total time	0.000 day
CSP - Relative stiffnes	0.04962
ForceX - Reached total	0.000 kN
ForceY - Reached total	0.000 kN
ForceZ - Reached total	0.000 kN
Pmax - Reached max p	-2110 kN/m^2
ΣM_{stage} - Reached pha	0.2334
ΣM_{weight} - Reached w	1.000
ΣM_{sf} - Reached safety	1.000

Figure 197, Calculation outcomes for 2-2,5 model

Reached values	
Reached total time	0.000 day
CSP - Relative stiffnes	0.02495
ForceX - Reached total	0.000 kN
ForceY - Reached total	0.000 kN
ForceZ - Reached total	0.000 kN
Pmax - Reached max p	-1618 kN/m^2
ΣM_{stage} - Reached pha	0.1831
ΣM_{weight} - Reached w	1.000
ΣM_{sf} - Reached safety	1.000

Figure 198, Calculation outcomes for 4-2,5 model

Reached values	
Reached total time	0.000 day
CSP - Relative stiffnes	1.023E-3
ForceX - Reached total	0.000 kN
ForceY - Reached total	0.000 kN
ForceZ - Reached total	0.000 kN
Pmax - Reached max p	-1559 kN/m^2
ΣM_{stage} - Reached pha	0.1926
ΣM_{weight} - Reached w	1.000
ΣM_{sf} - Reached safety	1.000

Figure 199, Calculation outcomes for 2-5,0 model

Reached values	
Reached total time	0.000 day
CSP - Relative stiffnes	1.051
ForceX - Reached total	0.000 kN
ForceY - Reached total	0.000 kN
ForceZ - Reached total	0.000 kN
Pmax - Reached max p	-1126 kN/m^2
ΣM_{stage} - Reached pha	0.1225
ΣM_{weight} - Reached w	1.000
ΣM_{sf} - Reached safety	1.000

Figure 200, Calculation outcomes for 4-5,0 model

Reached values	
Reached total time	0.000 day
CSP - Relative stiffnes	0.9590
ForceX - Reached total	0.000 kN
ForceY - Reached total	0.000 kN
ForceZ - Reached total	0.000 kN
Pmax - Reached max p	-1598 kN/m^2
ΣM_{stage} - Reached pha	0.1038
ΣM_{weight} - Reached w	1.000
ΣM_{sf} - Reached safety	1.000

Figure 201, Calculation outcomes for 2-7,5 model

Reached values	
Reached total time	0.000 day
CSP - Relative stiffness	0.8461
ForceX - Reached total force X	0.000 kN
ForceY - Reached total force Y	0.000 kN
ForceZ - Reached total force Z	0.000 kN
Pmax - Reached max pp	-1416 kN/m^2
ΣM_{stage} - Reached phase propc	0.1331
ΣM_{weight} - Reached weight pro	1.000
ΣM_{sf} - Reached safety factor	1.000

Figure 202, Calculation outcomes for 4-7,5 model

Reached values	
Reached total time	0.000 day
CSP - Relative stiffness	1.037
ForceX - Reached total force X	0.000 kN
ForceY - Reached total force Y	0.000 kN
ForceZ - Reached total force Z	0.000 kN
Pmax - Reached max pp	-2856 kN/m 2
ΣM_{stage} - Reached phase propc	0.1330
ΣM_{weight} - Reached weight pro	1.000
ΣM_{sf} - Reached safety factor	1.000

Figure 203, Calculation outcomes for 6-2,5 model

Reached values	
Reached total time	0.000 day
CSP - Relative stiffness	0.01739
ForceX - Reached total	0.000 kN
ForceY - Reached total	0.000 kN
ForceZ - Reached total	0.000 kN
Pmax - Reached max p	-2327 kN/m 2
ΣM_{stage} - Reached pha	0.3797
ΣM_{weight} - Reached w	1.000
ΣM_{sf} - Reached safety	1.000

Figure 204, Calculation outcomes for 8-2,5 model

Reached values	
Reached total time	0.000 day
CSP - Relative stiffness	0.3995
ForceX - Reached total force X	0.000 kN
ForceY - Reached total force Y	0.000 kN
ForceZ - Reached total force Z	0.000 kN
Pmax - Reached max pp	-3042 kN/m 2
ΣM_{stage} - Reached phase propc	0.2901
ΣM_{weight} - Reached weight pro	1.000
ΣM_{sf} - Reached safety factor	1.000

Figure 205, Calculation outcomes for 8-5,0 model

Reached values	
Reached total time	0.000 day
CSP - Relative stiffness	0.1411
ForceX - Reached total force X	0.000 kN
ForceY - Reached total force Y	0.000 kN
ForceZ - Reached total force Z	0.000 kN
Pmax - Reached max pp	-2419 kN/m 2
ΣM_{stage} - Reached phase propc	0.2085
ΣM_{weight} - Reached weight pro	1.000
ΣM_{sf} - Reached safety factor	1.000

Figure 206, Calculation outcomes for 6-7,5 model

Reached values	
Reached total time	0.000 day
CSP - Relative stiffness	0.01103
ForceX - Reached total	0.000 kN
ForceY - Reached total	0.000 kN
ForceZ - Reached total	0.000 kN
Pmax - Reached max p	-2377 kN/m 2
ΣM_{stage} - Reached pha	0.4519
ΣM_{weight} - Reached w	1.000
ΣM_{sf} - Reached safety	1.000

Figure 207, Calculation outcomes for 8-7,5 model

Reached values

Reached total time	0.000 day
CSP - Relative stiffness	0.9929
ForceX - Reached total	0.000 kN
ForceY - Reached total	0.000 kN
ForceZ - Reached total	0.000 kN
Pmax - Reached max p	-1612 kN/m ^{2}
ΣM_{stage} - Reached pha	0.1897
ΣM_{weight} - Reached w	1.000
ΣM_{sf} - Reached safety	1.000

Figure 208, Calculation outcomes for 10-2,5 model

Reached values

Reached total time	0.000 day
CSP - Relative stiffness	0.5697
ForceX - Reached total force X	0.000 kN
ForceY - Reached total force Y	0.000 kN
ForceZ - Reached total force Z	0.000 kN
Pmax - Reached max pp	-2639 kN/m ^{2}
ΣM_{stage} - Reached phase propc	0.1396
ΣM_{weight} - Reached weight pro	1.000
ΣM_{sf} - Reached safety factor	1.000

Figure 209, Calculation outcomes for 10-5,0 model

Reached values

Reached total time	0.000 day
CSP - Relative stiffness	0.01151
ForceX - Reached total	0.000 kN
ForceY - Reached total	0.000 kN
ForceZ - Reached total	0.000 kN
Pmax - Reached max p	-3718 kN/m ^{2}
ΣM_{stage} - Reached pha	0.5342
ΣM_{weight} - Reached w	1.000
ΣM_{sf} - Reached safety	1.000

Figure 210, Calculation outcomes for 10-7,5 model

32. Calculation outcomes drained 2D analyses

Analysis and calculation outcomes for 2D drained models with interface

An overview of the calculation outcomes for both the drained 2D calculations with and without active interface elements is presented in the figures on the next page.

Firstly the calculation results with the interface active are discussed. In the table presenting the drained safety factors for the models including the interface some safety factors are highlighted in yellow or red. The values marked yellow were giving errors during the calculation and the values marked red are questioned by its correctness.

The calculation of the 8-2,5 model presented an error with the message: "Load advancement error" and the calculation of the 10-2,5 model presented an error with the message "Accuracy not met".

For the red marked questioned safety factors it holds that the calculation outcome is not in line with the pattern that is expected to occur. For the calculation of the drained model it was showed that an increase of the layer thickness would result in a lower safety factor. Furthermore it is also expected, according to the 3D drained calculation outcomes, that an increase of the depth of the clay layer will lead to an increase of the safety factor. For the questioned values one of these expected relations is not observed.

Depth [m]	Thickness [m] 2,50	5,00	7,50
Clay only	1,331	1,331	1,331
2,00	3,972	1,784	1,937
4,00	2,632	2,110	2,004
6,00	3,035	2,394	2,313
8,00	2,646	2,826	2,520
10,00	3,211	2,601	2,498
Sand only	4,449	4,449	4,449

Table 44, Safety factors for drained calculations for models with interface

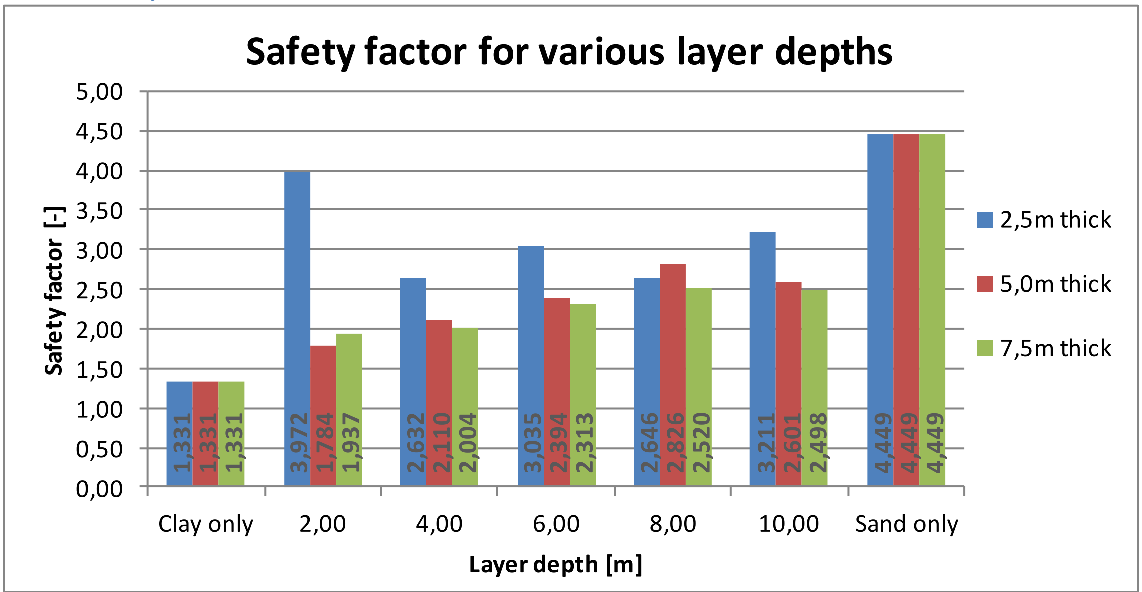

Figure 211, Graph safety factors for drained calculations with interface

Analysis and calculation outcomes for drained 2D models with inactive interface

Depth [m]	Thickness [m] 2,50	5,00	7,50
Clay only	1,322	1,322	1,322
2,00	3,970	2,286	1,937
4,00	3,717	2,449	2,194
6,00	3,493	2,583	2,330
8,00	3,364	2,922	2,625
10,00	3,695	2,959	2,609
Sand only	4,338	4,338	4,338

Table 45, Safety factors for drained calculations for models without interface

Reliability of Plaxis 2D calculation outcomes

As can be seen from the presented safety factor outcomes there are numerous questionable outcomes for the 2D drained calculations. Therefore it is concluded that with the obtained safety factors for the 2D analyses are not usable to investigate a reliable ratio between the calculated drained safety factors of the 2D and 3D models.
When the calculation outcomes of the drained 2D models with interface are regarded it can be seen that the ratios between the safety factors are not as expected for the models with clay layers at 2 and 10 meters depth. The safety factors for the 2m layer depth are questioned because the value for the 2-2,5m is too high. The values for 2-5,0 and 2-7,5 are questioned because the value for the 7,5m thick layer is higher than for the 5,0m thick layer.
For the questioned values for the 10m deep clay layers it can be seen that the values for the 5,0 and 7,5m thick layers are meeting the requirements by the safety factor of the 7,5m thick layer being lower than the 5,0m thick layer, but both values are lower than the values for the layers at 8m deep. Since this does not meets the expectations of the safety factors being higher when the layer depth is increased the values are questioned.

When regarding the safety factors for the models with the interface turned off it is noticed that the ratios within the same clay layer depth are meeting the previous stated expectations. But for the ratios between the different clay layer depths it can be seen that the values for all 2,5m thick clay layers are not according to the expected ratios. When the clay layer depth is increased it can be seen that the safety factors are decreasing. This is opposite to what is expected to happen.
All other safety factors are meeting the requirements but one. This is the safety factor for the 10-7,5 model. Here it can be seen that the calculated safety factor is slightly lower than the one calculated for the clay layer at 8m depth.

Possible explanations for relations not meeting expectations

As noticed before the relations between the safety factors are not as consistent as expected. On the beforehand it was expected that the ratios of the safety factors would be more or less the same as the ratios obtained for the 3D analyses. Since this is not the case it is asked what possible explanations could be found for this behaviour.
Firstly it is mentioned that the values being questioned are not the same for both the models with interface and without interface. For the models with interface the questioned values are for the most shallowest and deepest layer. It could therefore be said that the program is not able to calculate clay layers near to the surface when interface elements are applied. It could be that the number and size of the meshed elements between the foundation bottom and the top of the shallow clay layer is not sufficient. At the mesh plots of the models it is visible that the amount of mesh elements between the foundation and the top for the 2m deep clay layer is only 1 row of elements. For the other clay layers it holds that the number of elements between the foundation and the clay layer increases

when the layer depth increases. Since the meshes used for the 2D analysis already are meshed with the largest fineness a method should be found to increase the number of mesh elements between the foundation bottom and the top of the soil layer.
When the calculation outcomes of the models without interface are regarded it is seen that the calculation outcomes for the models with a clay layer of 2,5m thick are questioned. It looks like that the program is not able to accurately calculate the influence of thin clay layers. It is seen that how lower the clay layer is located how more the safety factors for the 2,5m thick layer are decreasing to a more expected value. From the values for the 8m deep layer it is noticed that the calculated safety factors are more meeting the expected values as obtained at the 3D calculations.

In short is can be concluded that for the models with an active interface the problems are occurring for the shallow clay layers. This may be resolved by meshing more elements between the bottom of the foundation and the top of the clay layer. How this will improve the calculation outcomes for the layers at 10m depth is not sure. When the mesh plots for the 8m and 10m deep clay layers are compared it is visible that there is an difference between the number of mesh elements, but this is also visible for the other clay layer thickness variations. Therefore it is not possible to conclude that this change in the amount of mesh elements is causing the inconsistency in the relation between the 8m and 10m safety factors.

For the drained models without the interface it is seen that the program has problems with the shallow clay layers of 2,5m thick. This could also have to do with the number or size of the meshed elements inside the clay layer. But when the mesh plots of the 2,5m thick clay layer is compared with the 5,0m thick clay layer it is seen that the number of mesh elements is equal for both 2,5 and 5,0m thick clay layers. Only for the 7,5m thick clay layer the number of mesh elements changes. Therefore it is unlikely that the number of elements within the clay layer is causing the inconsistency in the relations between the safety factor outcomes for the 2,5m thick clay layers.

Graphs for 2D drained models with interfaces

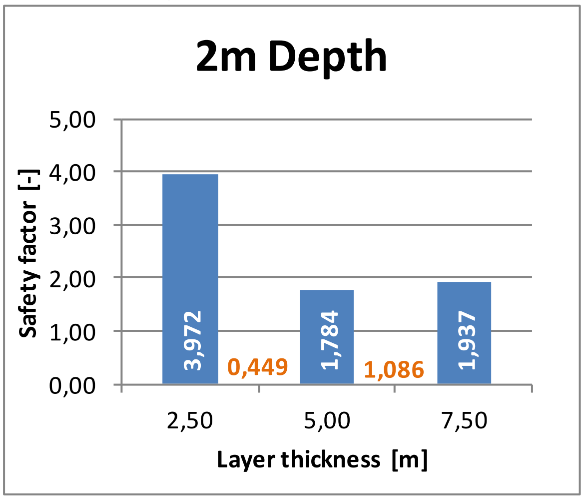

Figure 212, Safety factors for 2m deep 2D models with interface

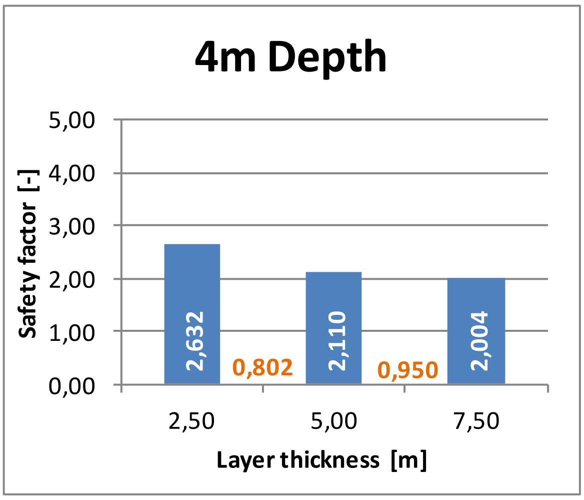

Figure 213, Safety factors for 4m deep 2D models with interface

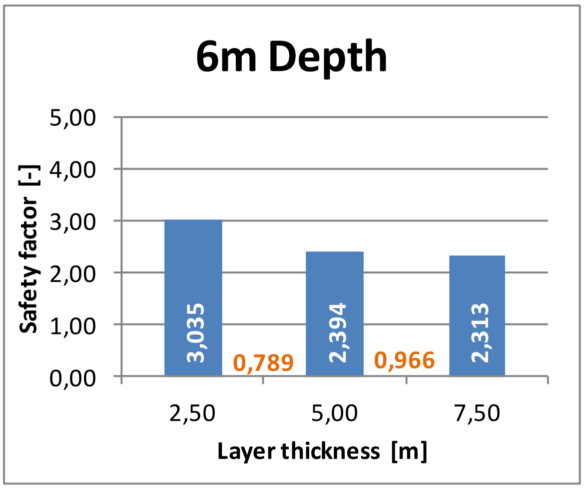

Figure 214, Safety factors for 6m deep 2D models with interface

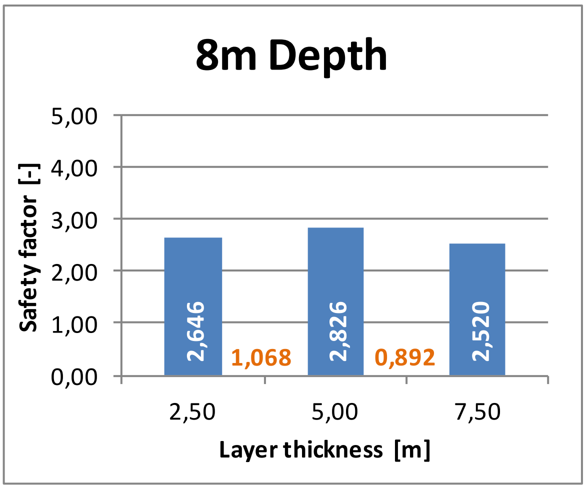

Figure 215, Safety factors for 8m deep 2D models with interface

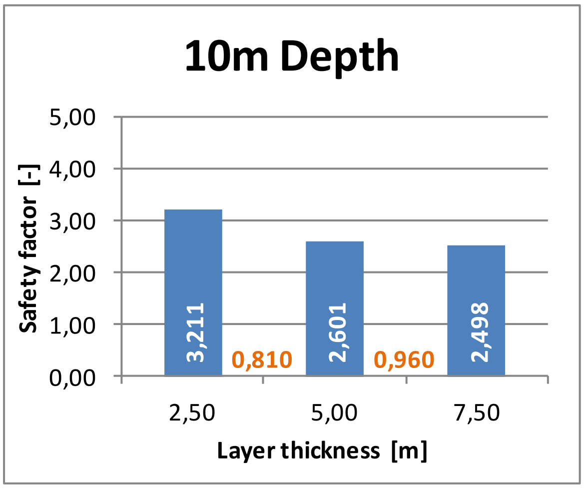

Figure 216, Safety factors for 10m deep 2D models with interface

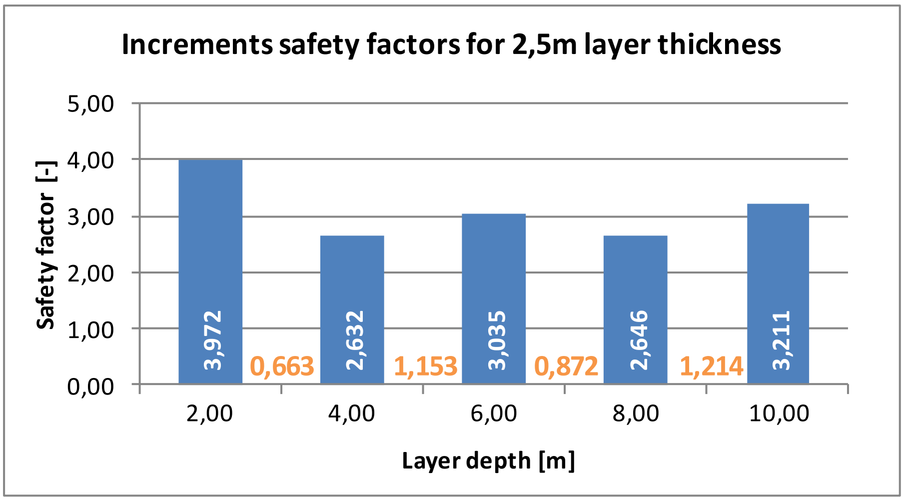

Figure 217, Relation safety factors for 2,5m thick layers for 2D models with interface

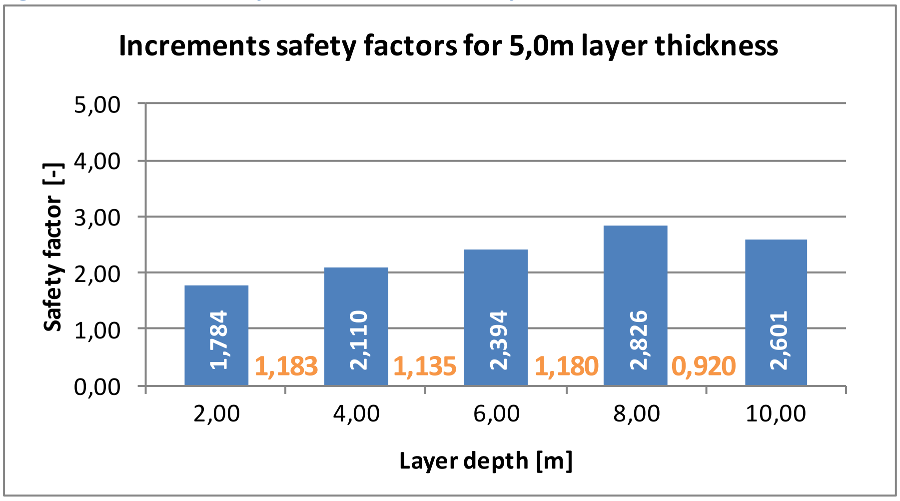

Figure 218, Relation safety factors for 5,0m thick layers for 2D models with interface

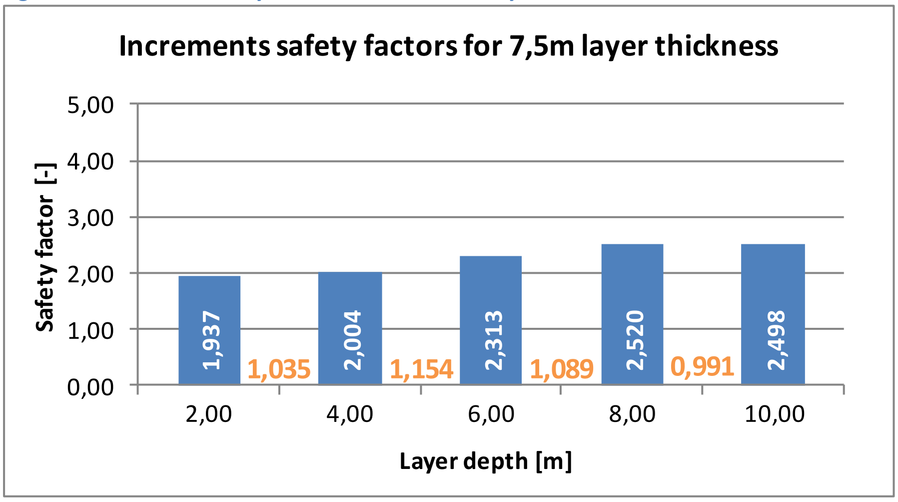

Figure 219, Relation safety factors for 7,5m thick layers for 2D models with interface

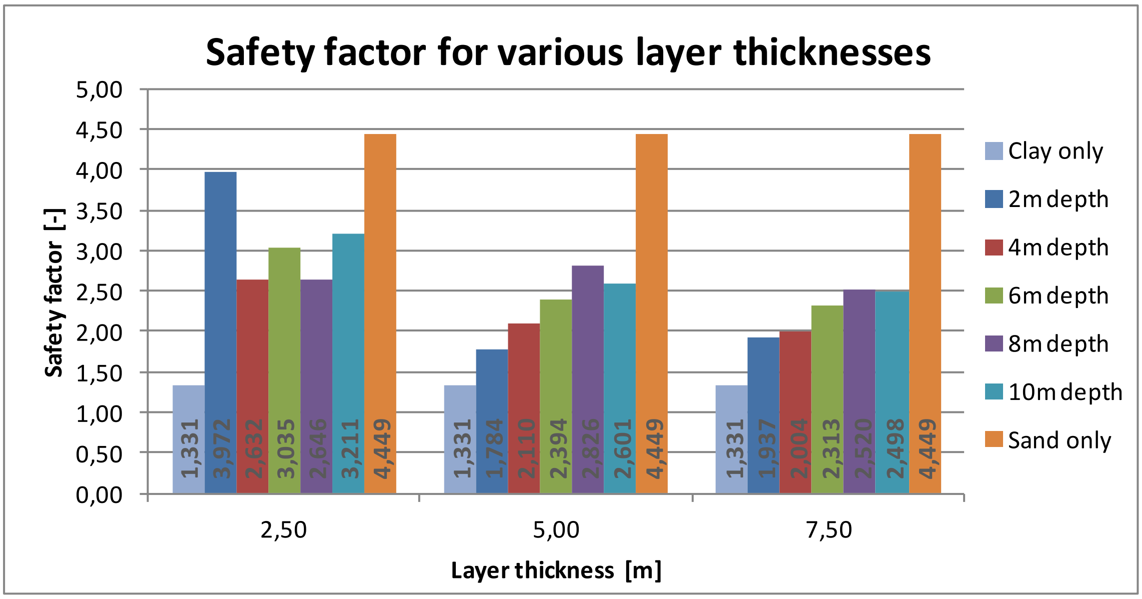

Figure 220, Safety factors for various layer thicknesses for 2D models with interface

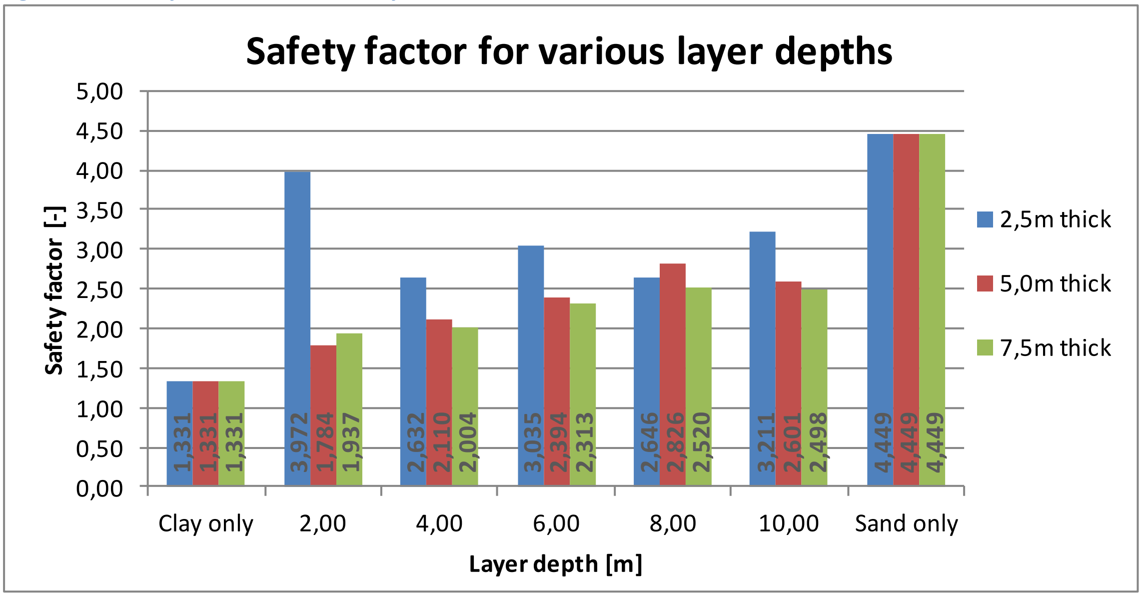

Figure 221, Safety factors for various layer depths for 2D models with interface

Graphs for 2D drained models without interfaces

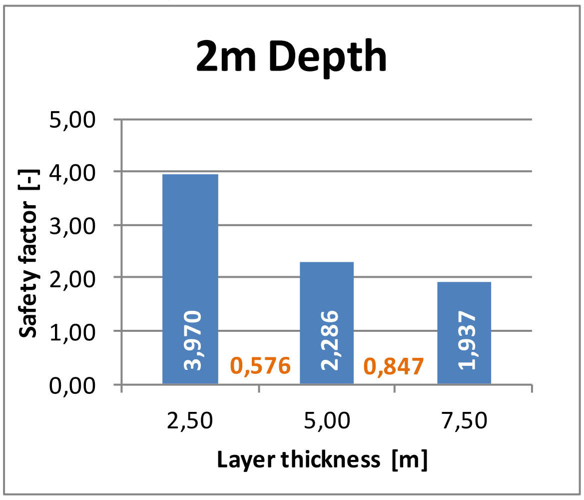

Figure 222, Safety factors for 2m deep 2D models without interface

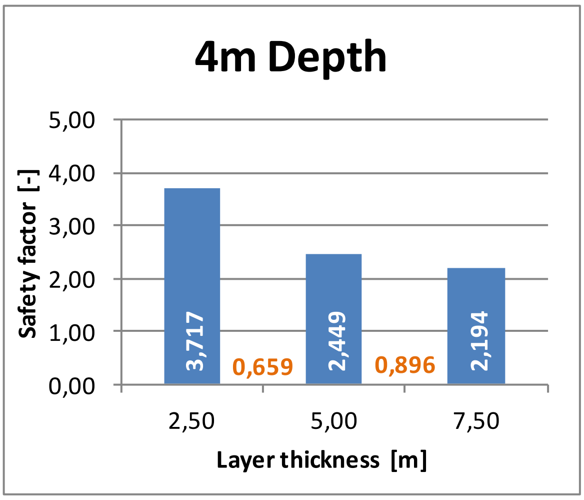

Figure 223, Safety factors for 4m deep 2D models without interface

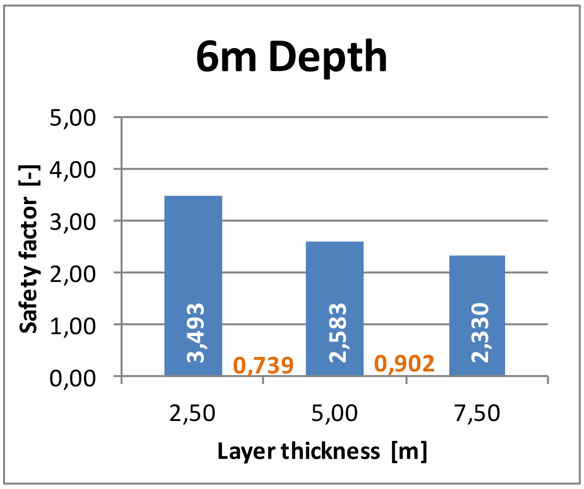

Figure 224, Safety factors for 6m deep 2D models without interface

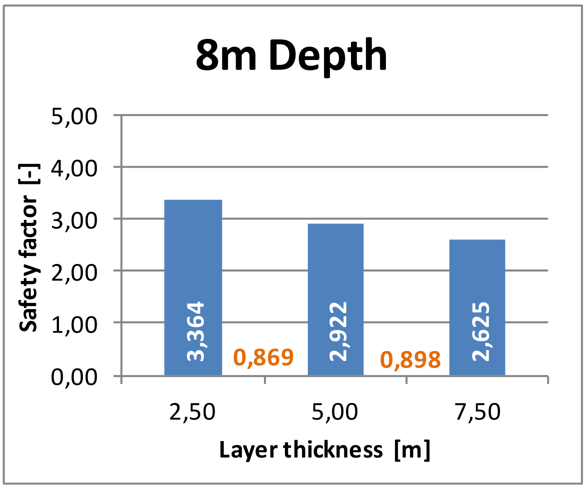

Figure 225, Safety factors for 8m deep 2D models without interface

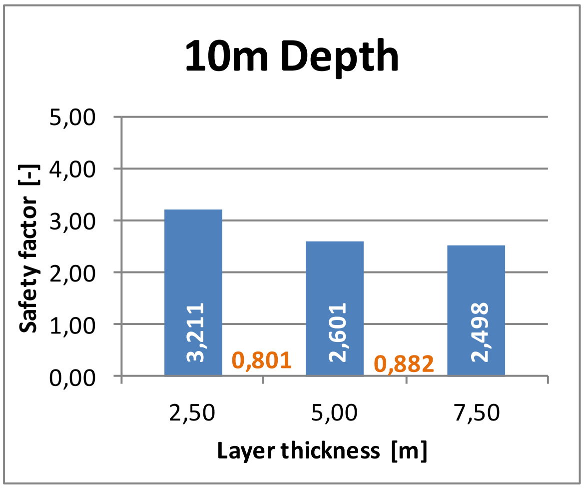

Figure 226, Safety factors for 10m deep 2D models without interface

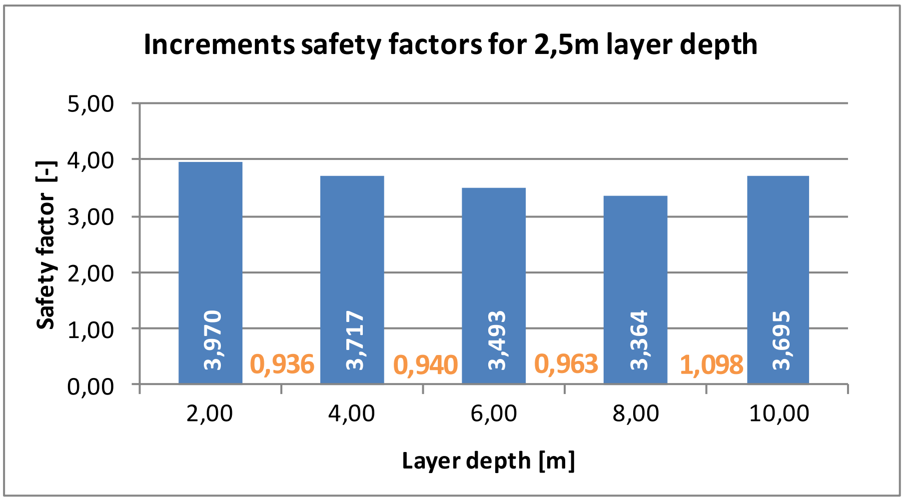

Figure 227, Relation safety factors for 2,5m thick layers for 2D models without interface

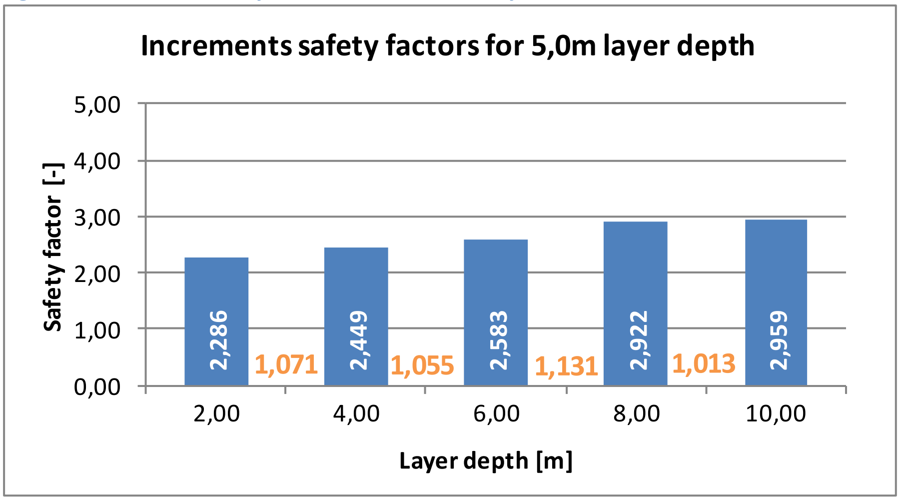

Figure 228, Relation safety factors for 5,0m thick layers for 2D models without interface

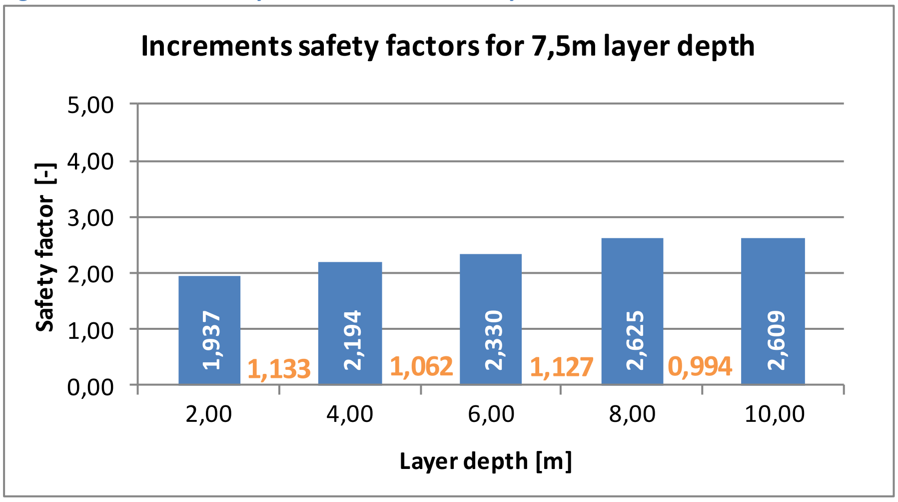

Figure 229, Relation safety factors for 7,5m thick layers for 2D models without interface

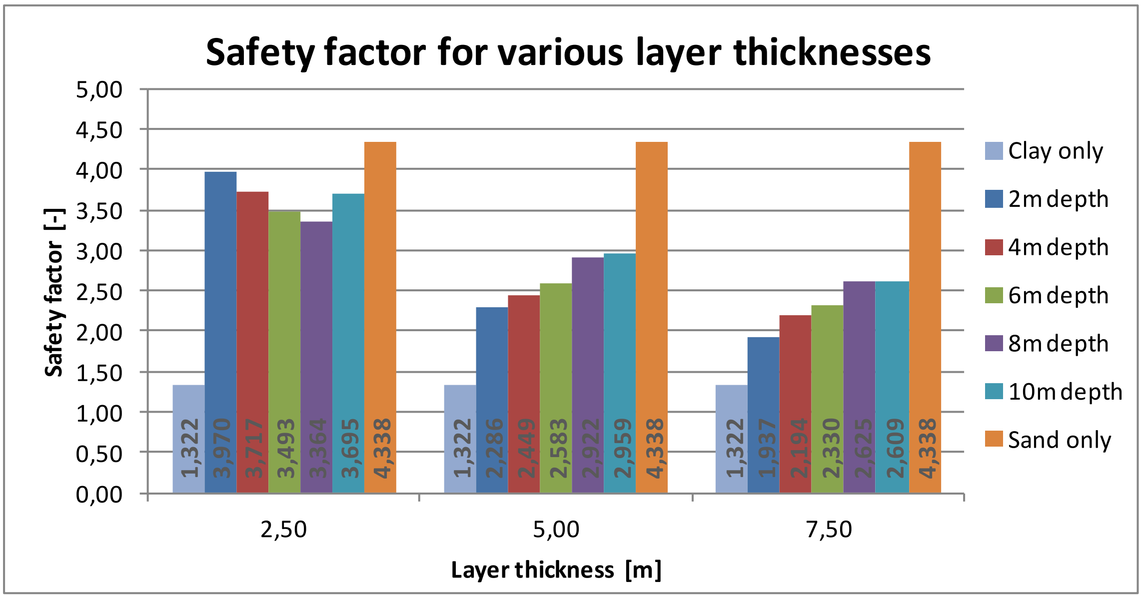

Figure 230, Safety factors for various layer thicknesses for 2D models without interface

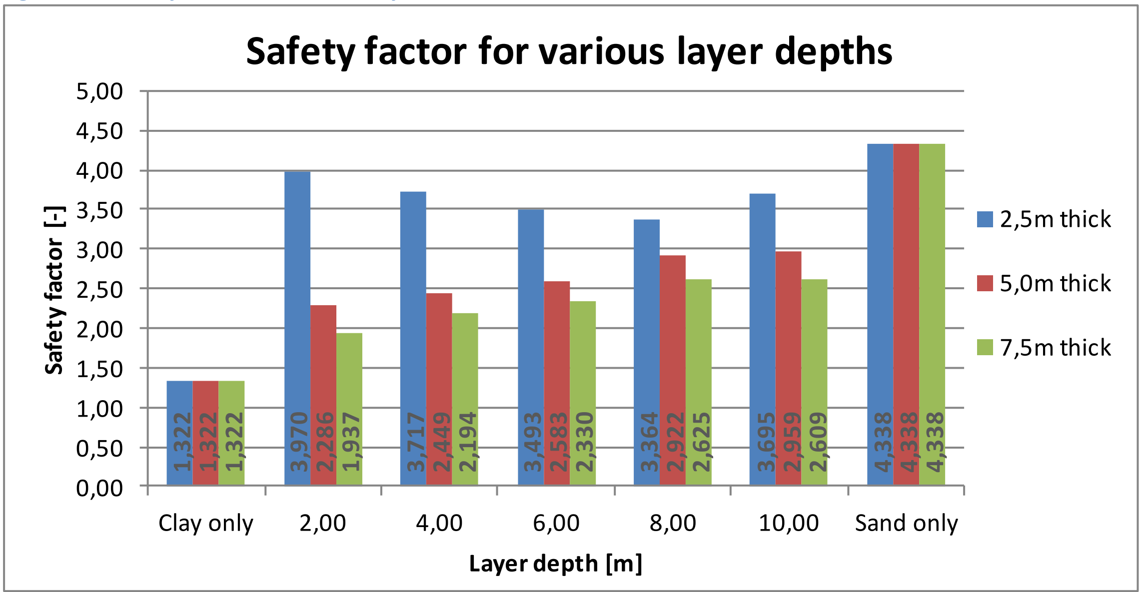

Figure 231, Safety factors for various layer depths for 2D models without interface

33. Soil material properties for undrained models for Plaxis 2D

Undrained properties for sand as used in Plaxis 2D

Property	Unit	Value
Material set		
Identification		Sand
Material model		Hardening soil
Drainage type		Undrained (A)
Colour		RGB 161, 226, 232
Comments		
General properties		
γ_{unsat}	kN/m^3	18,00
γ_{sat}	kN/m^3	20,00
Advanced		
Void ratio		
Dilatancy cut-off		☐
e_{init}		0,5000
e_{min}		0,000
e_{max}		999,0
Damping		
Rayleigh α		0,000
Rayleigh β		0,000

Figure 232, General properties for undrained sand

Property	Unit	Value
Stiffness		
$E_{50}{}^{ref}$	kN/m^2	43,00E3
$E_{oed}{}^{ref}$	kN/m^2	43,00E3
$E_{ur}{}^{ref}$	kN/m^2	129,0E3
power (m)		0,5000
Alternatives		
Use alternatives		☐
C_c		8,023E-3
C_s		2,407E-3
e_{init}		0,5000
Strength		
c'_{ref}	kN/m^2	0,1000
φ' (phi)	°	32,50
ψ (psi)	°	2,500
Advanced		
Set to default values		☑
Stiffness		
ν'_{ur}		0,2000
p_{ref}	kN/m^2	100,0
$K_0{}^{nc}$		0,4627
Strength		
c'_{inc}	kN/m^2/m	0,000
y_{ref}	m	0,000
R_f		0,9000
Tension cut-off		☑
Tensile strength	kN/m^2	0,000
Undrained behaviour		
Undrained behaviour		Standard
Skempton-B		0,9866
ν_u		0,4950
$K_{w,ref}$ / n	kN/m^2	5,285E6

Figure 233, Parameters for undrained sand

Property	Unit	Value
Model		
Data set		Standard
Soil		
Type		Coarse
< 2 µm	%	10,00
2 µm - 50 µm	%	13,00
50 µm - 2 mm	%	77,00
Parameters		
Set to default values		☐
k_x	m/day	0,000
k_y	m/day	0,000
$-\psi_{unsat}$	m	10,00E3
e_{init}		0,5000
Change of permeability		
c_k		1,000E15

Figure 234, Flow parameters for undrained sand

Property	Unit	Value
Strength		
Strength		Rigid
R_{inter}		1,000
Real interface thickness		
δ_{inter}		0,000

Figure 235, Interface properties for undrained sand

Property	Unit	Value
K0 settings		
K_0 determination		Automatic
$K_{0,x}$		0,4627
Overconsolidation		
OCR		1,000
POP	kN/m^2	0,000

Figure 236, Initial properties for undrained sand

Undrained properties for clay used in Plaxis 2D

Property	Unit	Value
Material set		
Identification		Clay
Material model		Hardening soil
Drainage type		Undrained (A)
Colour		RGB 134, 234, 162
Comments		
General properties		
γ_{unsat}	kN/m³	17,00
γ_{sat}	kN/m³	17,00
Advanced		
Void ratio		
Dilatancy cut-off		☐
e_{init}		0,5000
e_{min}		0,000
e_{max}		999,0
Damping		
Rayleigh α		0,000
Rayleigh β		0,000

Figure 237, General properties for undrained clay

Property	Unit	Value
Stiffness		
E_{50}^{ref}	kN/m²	10,00E3
E_{oed}^{ref}	kN/m²	10,00E3
E_{ur}^{ref}	kN/m²	30,00E3
power (m)		0,8000
Alternatives		
Use alternatives		☐
C_c		0,03450
C_s		0,01035
e_{init}		0,5000
Strength		
c'_{ref}	kN/m²	10,00
φ' (phi)	°	17,50
ψ (psi)	°	0,000
Advanced		
Set to default values		☑
Stiffness		
ν'_{ur}		0,2000
p_{ref}	kN/m²	100,0
K_0^{nc}		0,6993
Strength		
c'_{inc}	kN/m²/m	0,000
y_{ref}	m	0,000
R_f		0,9000
Tension cut-off		☑
Tensile strength	kN/m²	0,000
Undrained behaviour		
Undrained behaviour		Standard
Skempton-B		0,9866
ν_u		0,4950
$K_{w,ref} / n$	kN/m²	1,229E6

Figure 238, Parameters for undrained clay

Property	Unit	Value
Model		
Data set		Standard
Soil		
Type		Coarse
< 2 µm	%	10,00
2 µm - 50 µm	%	13,00
50 µm - 2 mm	%	77,00
Parameters		
Set to default values		☐
k_x	m/day	0,000
k_y	m/day	0,000
$-\Psi_{unsat}$	m	10,00E3
e_{init}		0,5000
Change of permeability		
c_k		1,000E15

Figure 239, Flow parameters for undrained clay

Property	Unit	Value
Strength		
Strength		Manual
R_{inter}		0,9000
Real interface thickness		
δ_{inter}		0,000

Figure 240, Interface properties for undrained clay

Property	Unit	Value
K0 settings		
K_0 determination		Automatic
Overconsolidation		
OCR		1,000
POP	kN/m^2	10,00

Figure 241, Initial properties for undrained clay

34. Calculation outcomes undrained 2D analyses

Load1 graphs for 2D undrained models with interfaces

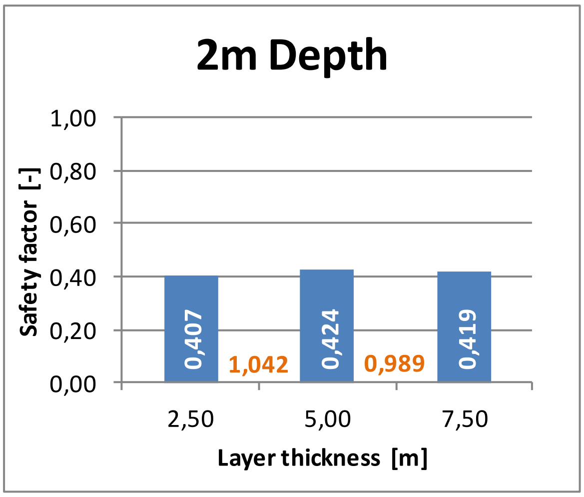

Figure 242, Load1 safety factors for 2m deep 2D models with interface

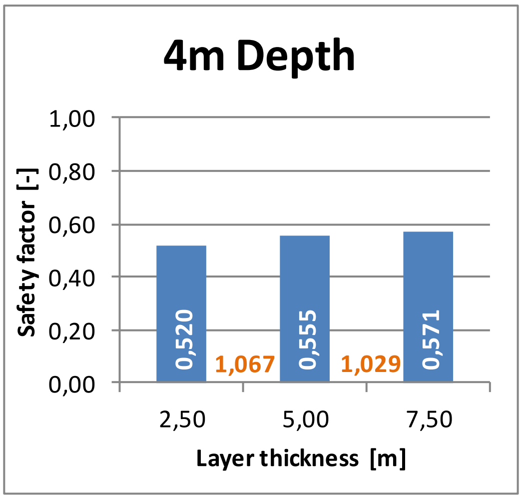

Figure 243, Load1 safety factors for 4m deep 2D models with interface

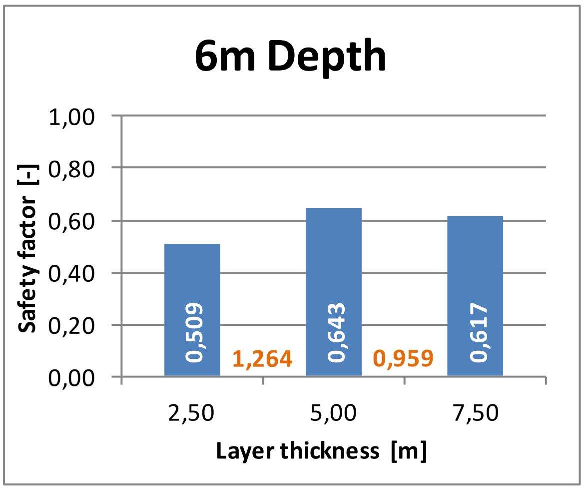

Figure 244, Load1 safety factors for 6m deep 2D models with interface

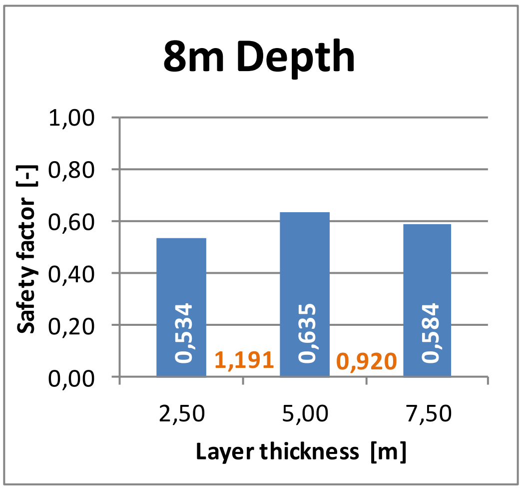

Figure 245, Load1 safety factors for 8m deep 2D models with interface

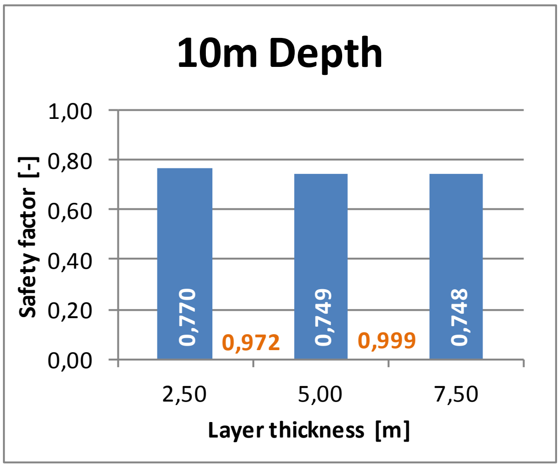

Figure 246, Load1 safety factors for 10m deep 2D models with interface

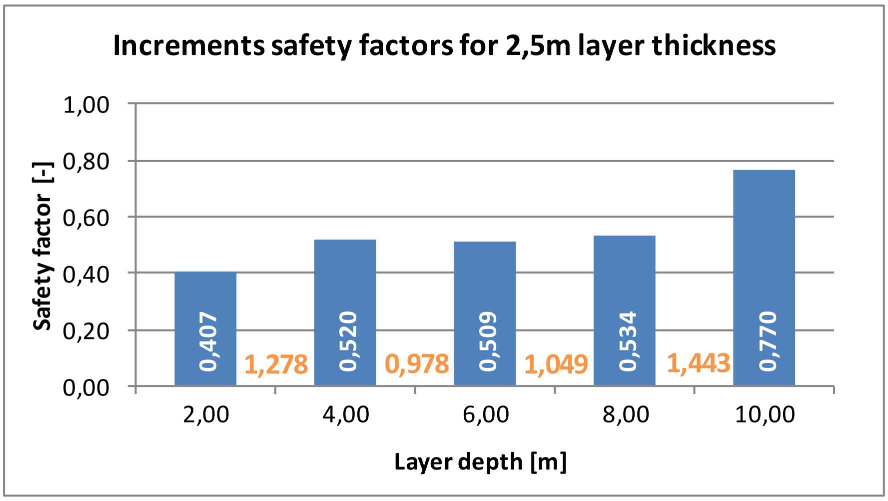

Figure 247, Load1 relation safety factors for 2,5m thick layers for 2D models with interface

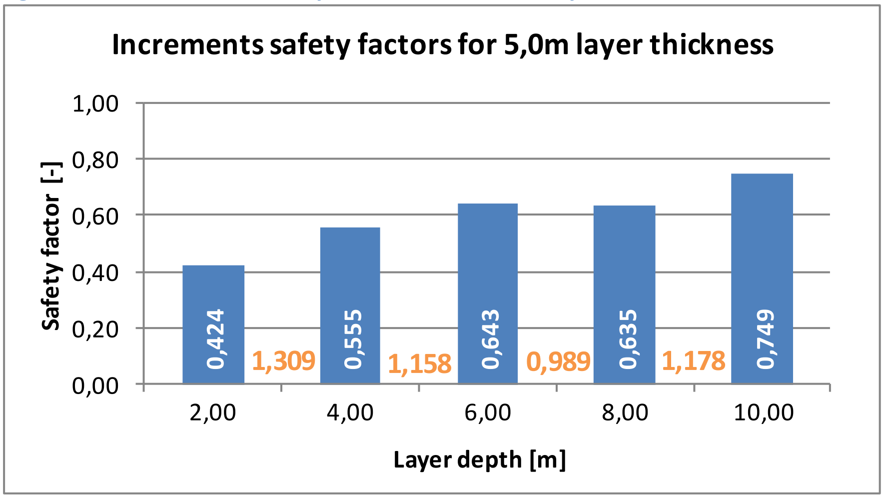

Figure 248, Load1 relation safety factors for 5,0m thick layers for 2D models with interface

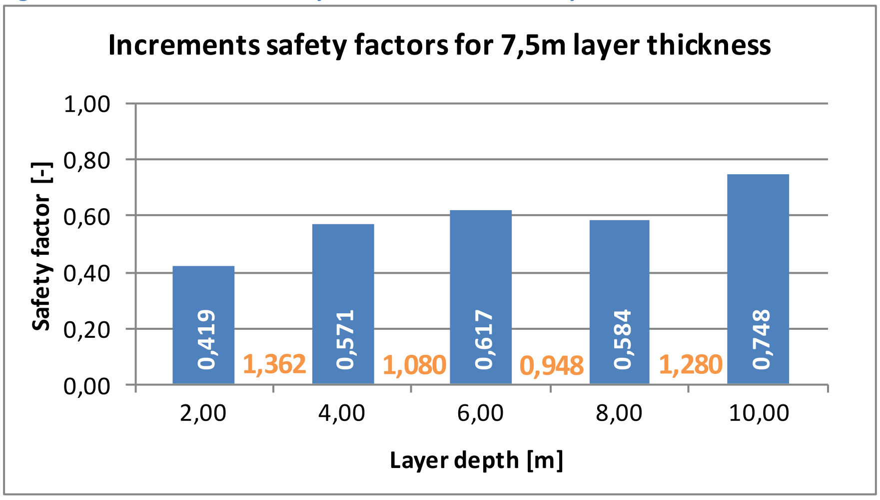

Figure 249, Load1 relation safety factors for ,5m thick layers for 2D models with interface

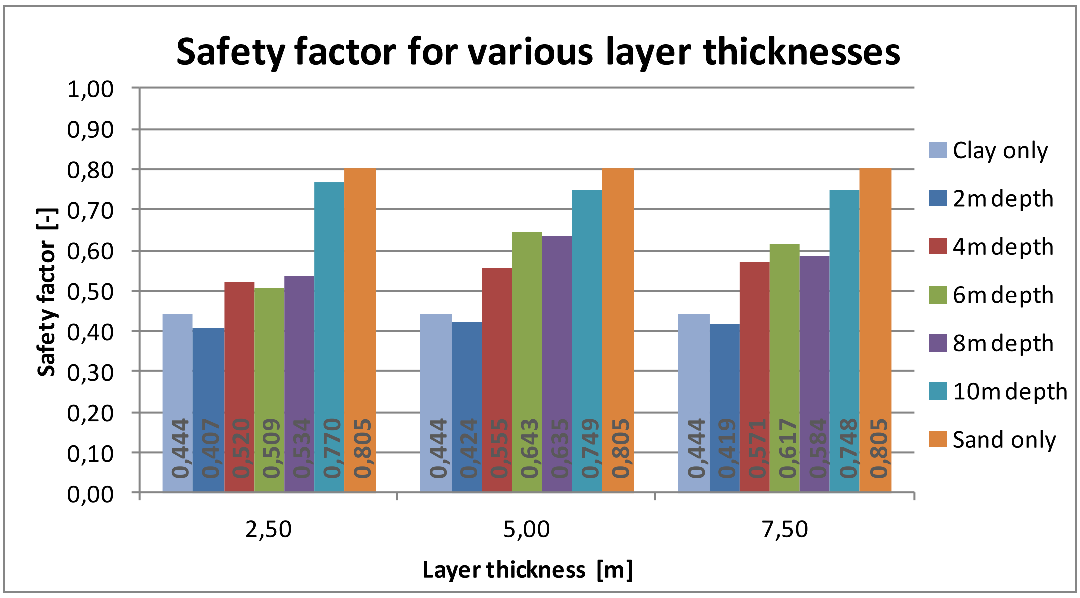

Figure 250, Load1 safety factors for various layer thicknesses for 2D models with interface

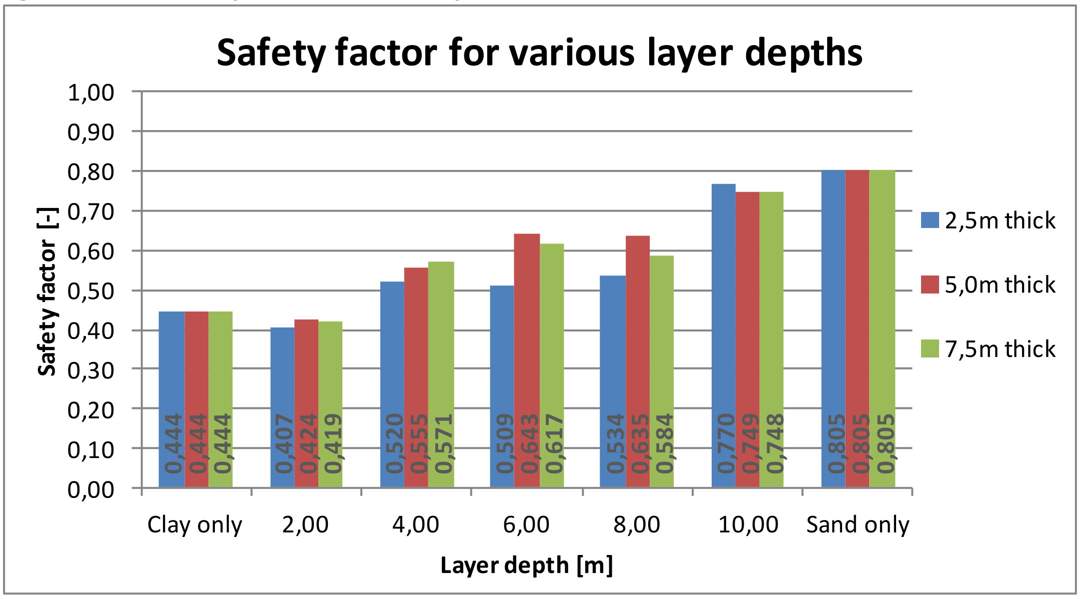

Figure 251, Load1 safety factors for various layer depths for 2D models with interface

In the graphs presented below the calculation outcomes for the undrained models with interface are presented. In the table it can be seen that some values are marked green. These marked values are indicating the calculation outcomes where the soil did collapse.

		Thickness [m]		
		2,50	5,00	7,50
Depth [m]	Clay only	0,444	0,444	0,444
	2,00	0,407	0,424	0,419
	4,00	0,520	0,555	0,571
	6,00	0,509	0,643	0,617
	8,00	0,534	0,635	0,584
	10,00	0,770	0,749	0,748
	Sand only	0,805	0,805	0,805

Table 46, Load1 safety factors for undrained 2D models with interface

Load10 graphs for 2D undrained models with interfaces

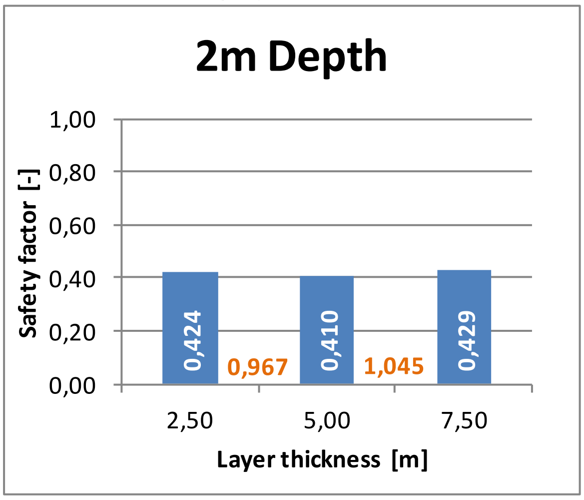

Figure 252, Load10 safety factors for 2m deep 2D models with interface

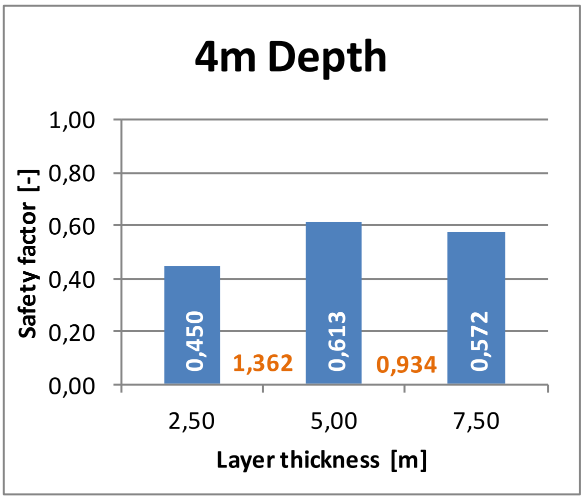

Figure 253, Load10 safety factors for 4m deep 2D models with interface

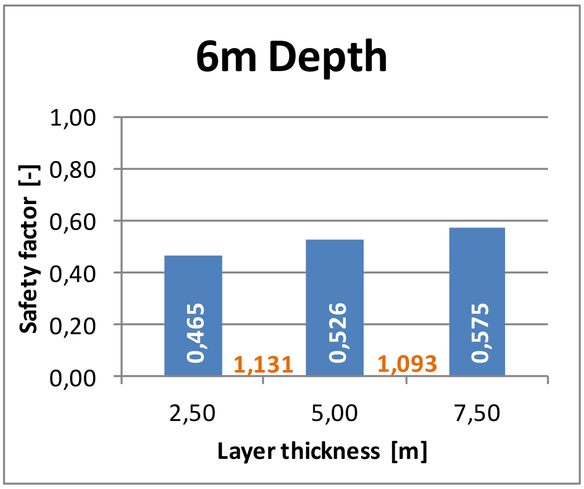

Figure 254, Load10 safety factors for 6m deep 2D models with interface

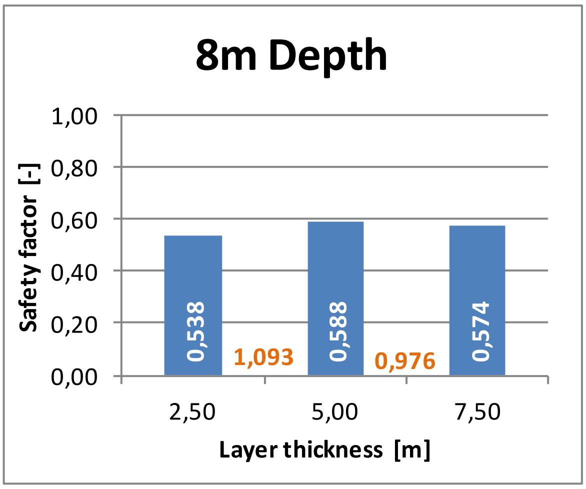

Figure 255, Load10 safety factors for 8m deep 2D models with interface

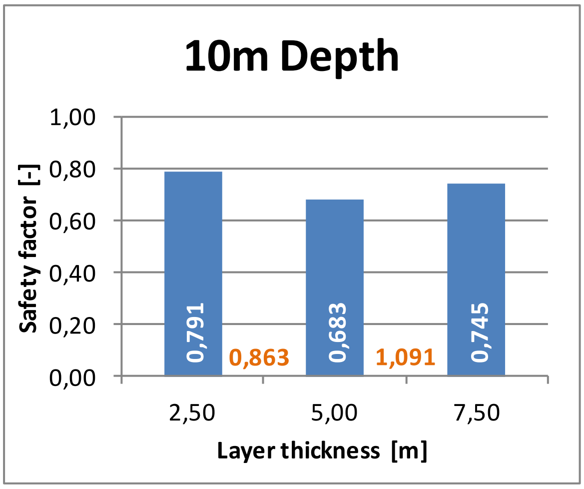

Figure 256, Load10 safety factors for 10m deep 2D models with interface

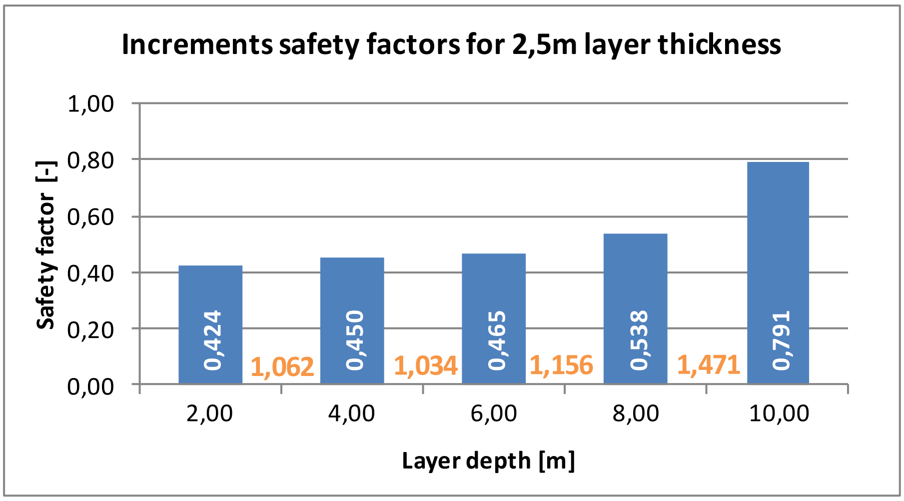

Figure 257, Load10 relation safety factors for 2,5m thick layers for 2D models with interface

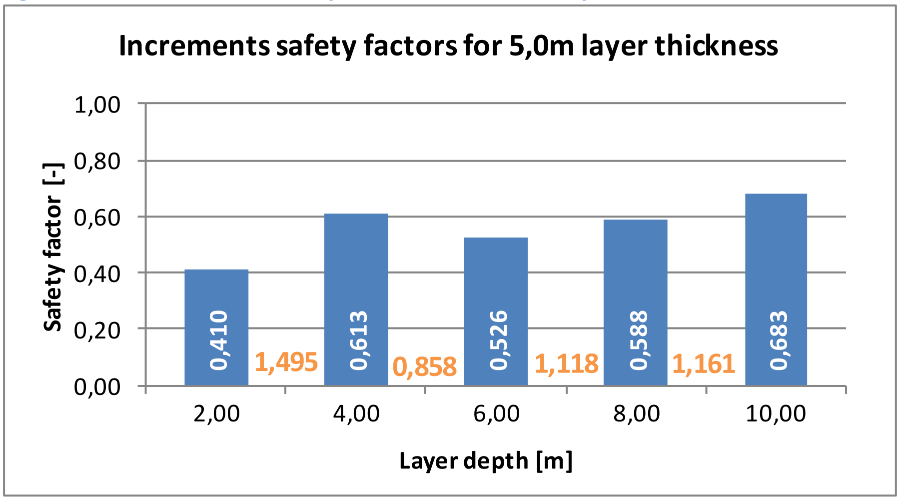

Figure 258, Load10 relation safety factors for 5,0m thick layers for 2D models with interface

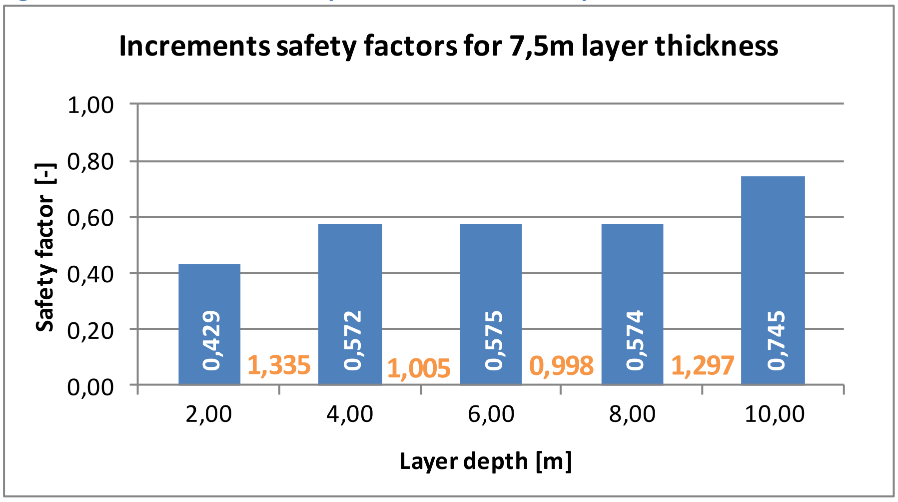

Figure 259, Load10 relation safety factors for 7,5m thick layers for 2D models with interface

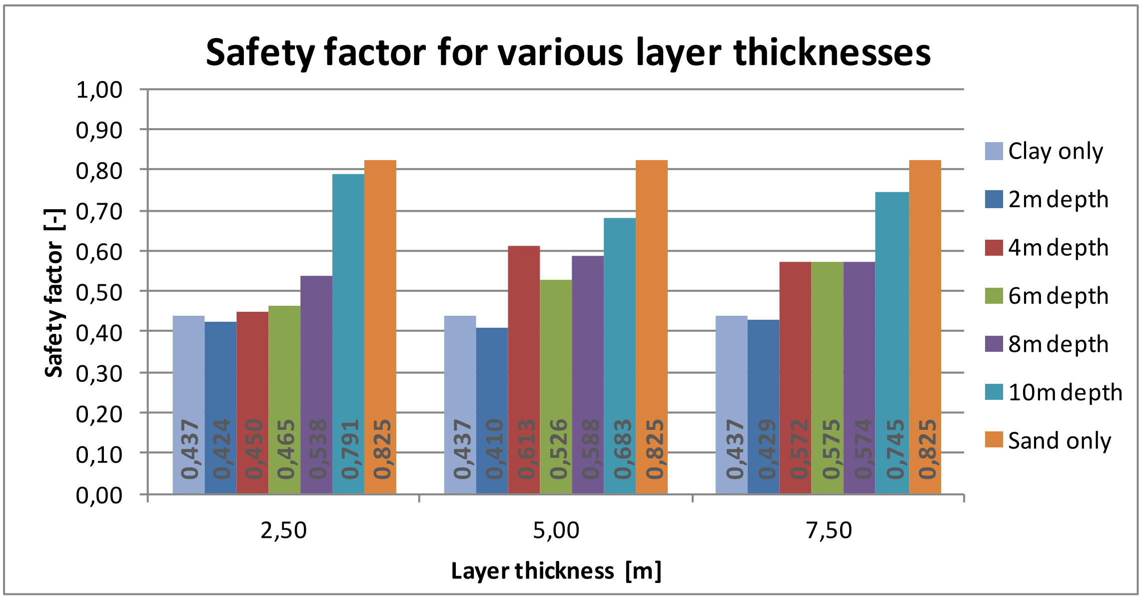

Figure 260, Load10 safety factors for various layer thicknesses for 2D models with interface

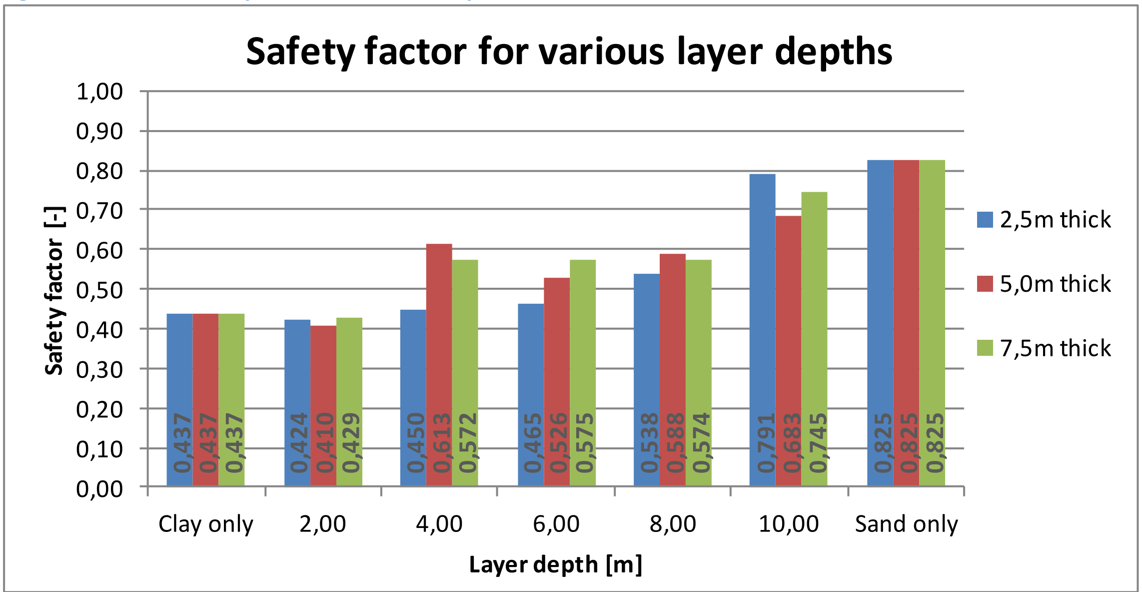

Figure 261, Load10 safety factors for various layer depths for 2D models with interface

		Thickness [m]		
		2,50	5,00	7,50
Depth [m]	Clay only	0,437	0,437	0,437
	2,00	0,424	0,410	0,429
	4,00	0,450	0,613	0,572
	6,00	0,465	0,526	0,575
	8,00	0,538	0,588	0,574
	10,00	0,791	0,683	0,745
	Sand only	0,825	0,825	0,825

Table 47, Load10 safety factors for undrained 2D models with interface

Graphs for 2D undrained models without interfaces

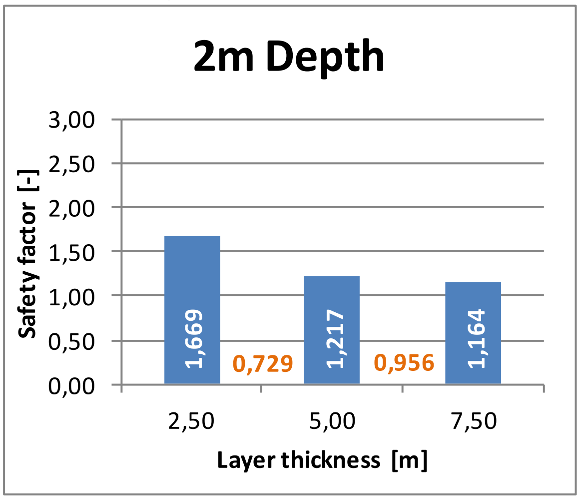

Figure 262, Safety factors for 2m deep 2D models without interface

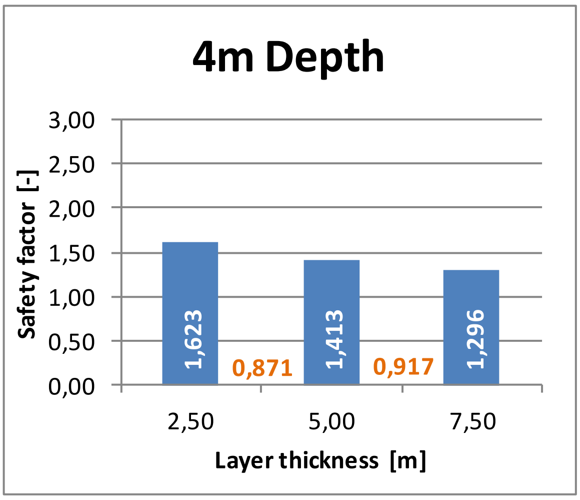

Figure 263, Safety factors for 4m deep 2D models without interface

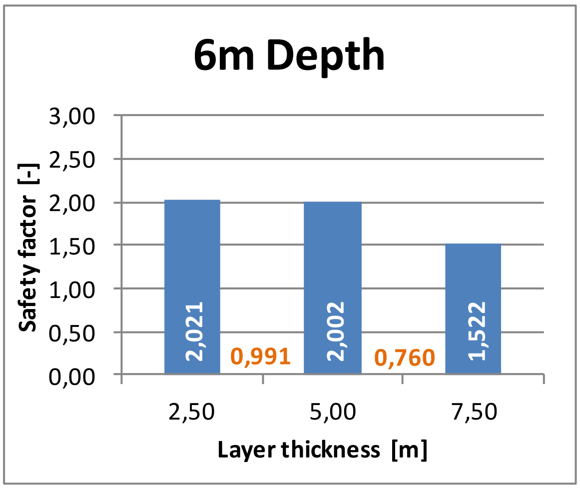

Figure 264, Safety factors for 6m deep 2D models without interface

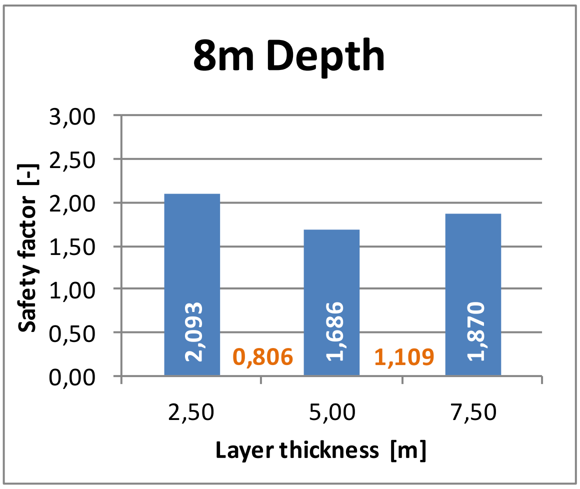

Figure 265, Safety factors for 8m deep 2D models without interface

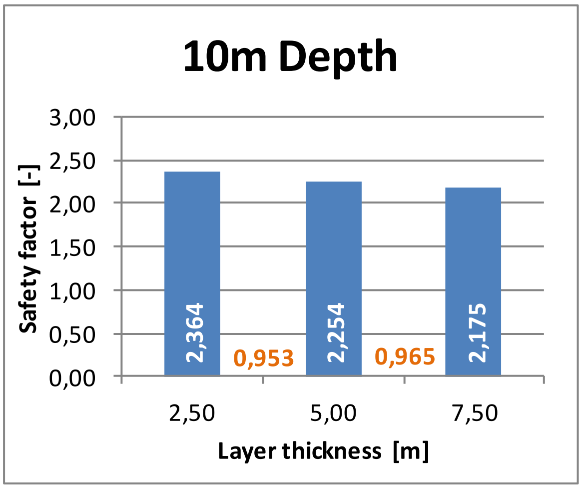

Figure 266, Safety factors for 10m deep 2D models without interface

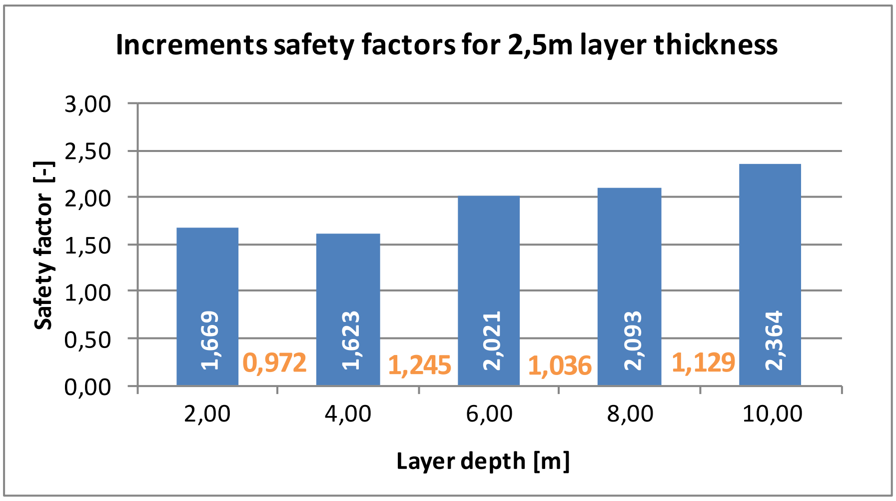

Figure 267, Relation safety factors for 2,5m thick layers for 2D models without interface

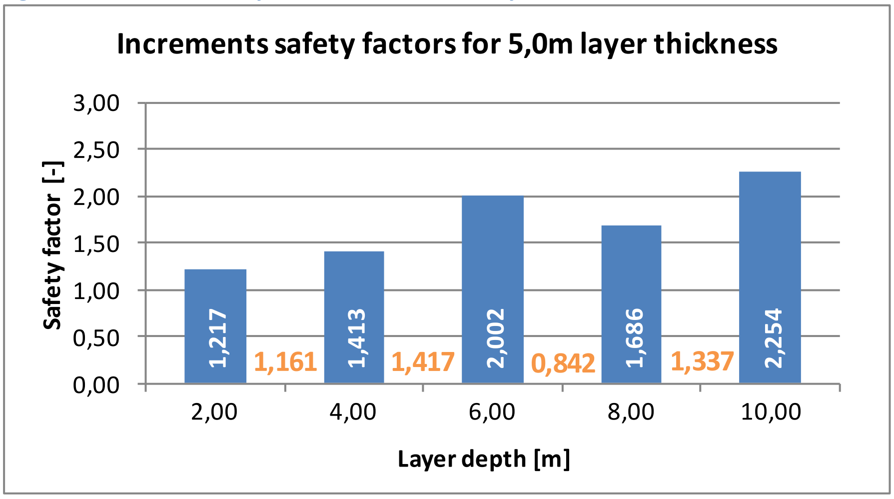

Figure 268, Relation safety factors for 5,0m thick layers for 2D models without interface

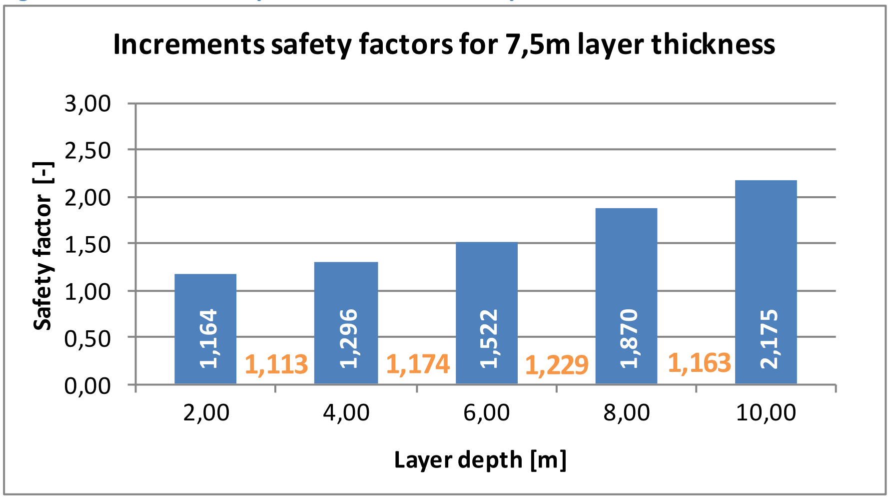

Figure 269, Relation safety factors for 7,5m thick layers for 2D models without interface

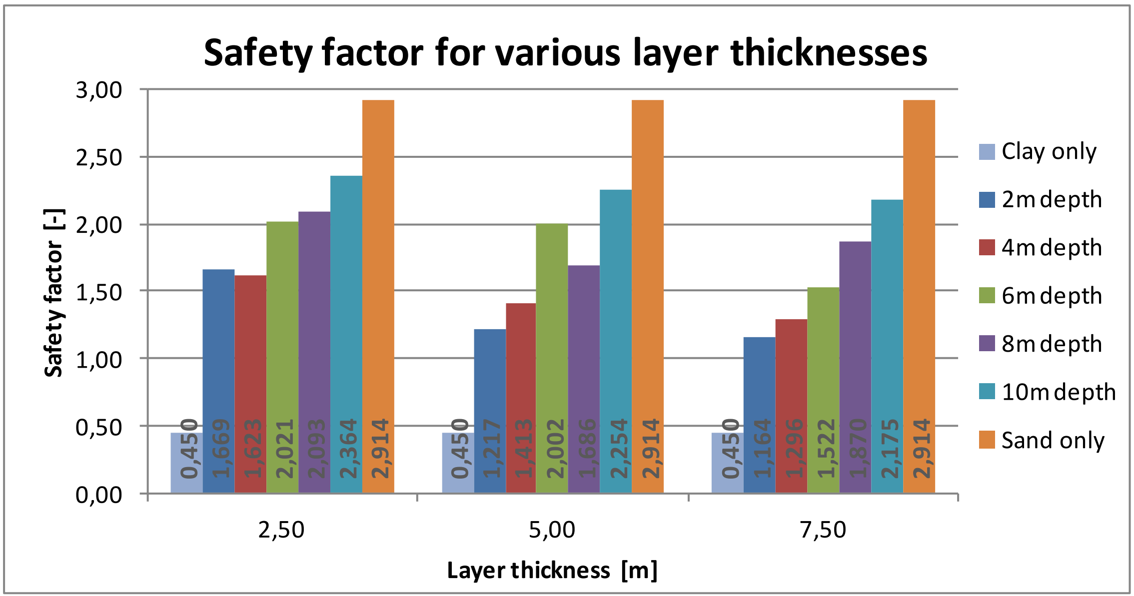

Figure 270, Safety factors for various layer thicknesses for 2D models without interface

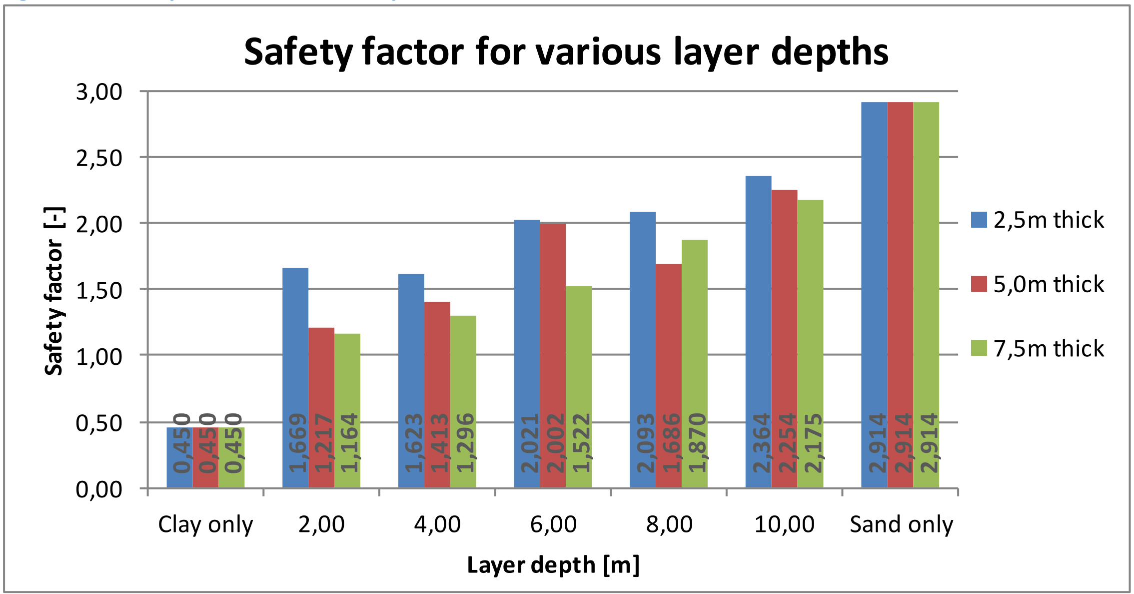

Figure 271, Safety factors for various layer depths for 2D models without interface

Depth [m]	Thickness [m] 2,50	5,00	7,50
Clay only	0,450	0,450	0,450
2,00	1,669	1,217	1,164
4,00	1,623	1,413	1,296
6,00	2,021	2,002	1,522
8,00	2,093	1,686	1,870
10,00	2,364	2,254	2,175
Sand only	2,914	2,914	2,914

Table 48, Load10 safety factors for undrained 2D models without interface

35. List of figures

36. List of tables